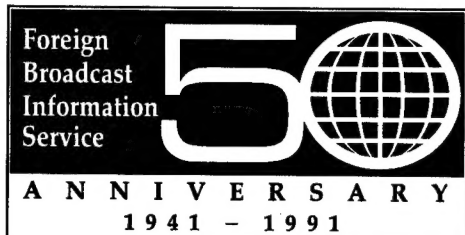


JPRS-JST-91-028
3 SEPTEMBER 1991

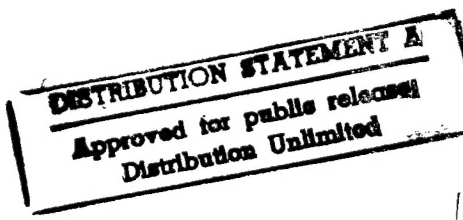


JPRS Report

1990107 089
680

Science & Technology

Japan
International Symposium on Ultra-High Temperature Materials



DTIC QUALITY INSPECTED 3

REPRODUCED BY
U.S. DEPARTMENT OF COMMERCE
NATIONAL TECHNICAL
INFORMATION SERVICE
SPRINGFIELD, VA 22161

Science & Technology

Japan

International Symposium on Ultra-High Temperature Materials

JPRS-JST-91-028

CONTENTS

3 September 1991

[Selected papers and abstracts of papers presented at the International Symposium on Ultra-High Temperature Materials held 15-16 Mar 91 in Ube, sponsored by the New Energy and Industrial Technology Development Organization (NEDO), Chugoku Economic Federation, Yamaguchi Prefectural Government, the Faculty of Engineering of Yamaguchi University, and Japan Ultra-High Temperature Materials Research Center (JUTEM).]

Present, Future of Ultra-High Temperature Materials

[Ryohei Tanaka; CHO KO-ON ZAIRYO KOKUSAI SHINPOJIUMU, 15 Mar 91] 1

Role of Japan Ultra-High Temperature Materials Research Center

[Toshio Hiraki; CHO KO-ON ZAIRYO KOKUSAI SHINPOJIUMU, 15 Mar 91] 9

Advanced Materials for Aircraft Gas Turbine Engines

[Yukiya Nakagawa; CHO KO-ON ZAIRYO KOKUSAI SHINPOJIUMU, 15 Mar 91] 15

Trends of Research, Development in Carbon/Carbon Composites

[Shiushichi Kimura, Eiichi Yasuda; CHO-KO-ON ZAIRYO KOKUSAI SHINPOJIUMU, 15 Mar 91] 28

Future of Thermal Plasma Processing Discussed

[Toyonobu Yoshida; CHO KO-ON ZAIRYO KOKUSAI SHINPOJIUMU, 16 Mar 91] 39

Nanocomposite Technology of Structural Ceramics

[Koichi Niihara; CHO KO-ON ZAIRYO KOKUSAI SHINPOJIUMU, 16 Mar 91] 46

Functionally Gradient Materials as Nanocomposites

[Toshio Hirai; CHO KO-ON ZAIRYO KOKUSAI SHINPOJIUMU, 16 Mar 91] 51

Analysis of Deformation, Strength of Engineering Ceramics at Elevated Temperatures, Its Further Development

[Kenji Hatanaka; CHO KO-ON ZAIRYO KOKUSAI SHINPOJIUMU, 16 Mar 91] 56

The Activities of Japan Ultra-High Temperature Materials Research Center (JUTEM) and Japan Ultra-High Temperature Materials Research Institute (JUTEMI)

[Koh Miyamura, Toshio Yarii; CHO KO-ON ZAIRYO KOKUSAI SHINPOJIUMU, 15 Mar 91] 67

Development of a New Nickel-Base Single Crystal Superalloy by an Alloy Designing Method

*[Takehiro Ohno, Rikizo Watanabe, et al.; CHO KO-ON ZAIRYO KOKUSAI SHINPOJIUMU
in Japanese 15 Mar 91]* 71

Hydrogen Embrittlement of Ni-Base Superalloys

*[Seiji Fukuyama, Kiyoshi Yokogawa, et al.; CHO KO-ON ZAIRYO KOKUSAI SHINPOJIUMU,
15 Mar 91]* 76

Development of W/Cu Composite With Gradient Structure

*[Yoshiyasu Itoh, Masashi Takahashi, et al.; CHO KO-ON ZAIRYO KOKUSAI SHINPOJIUMU,
15 Mar 91]* 76

Amorphous FeSi₂ Alloys as a New Thermoelectric Material Developed by Plasma Ion Processing

*[Kakuei Matsubara, Norimichi Minerura, et al.; CHO KO-ON ZAIRYO KOKUSAI SHINPOJIUMU,
15 Mar 91]* 80

Effects of Microstructure on Mechanical Properties and Fracture of γ-Base Titanium Aluminides

[S. Tsuyama, S. Mitao, et al.; CHO KO-ON ZAIRYO KOKUSAI SHINPOJIUMU, 15 Mar 91] 80

Phase Structure and Properties of Nb-Al-X Intermetallics by Rapid Solidification or Sintering

[Tetsuo Fujiwara, Ken Yasuda, et al.; CHO KO-ON ZAIRYO KOKUSAI SHINPOJIUMU, 15 Mar 91] .. 84

An Advanced Technique of X-Ray Diffractometry for in Situ Observation at High Temperatures—Application for Intermetallic Compounds

*[Masao Kimura, Keizo Hashimoto, et al.; CHO KO-ON ZAIRYO KOKUSAI SHINPOJIUMU,
15 Mar 91]* 89

Thermal Plasma Processing of High Temperature Materials in a Low Pressure Plasma Jet

*[Satoshi Sakiyama, Tetsuya Hirabaru, et al.; CHO KO-ON ZAIRYO KOKUSAI SHINPOJIUMU,
15 Mar 91]* 94

Magnesia Ceramics—Effect of Microstructure on Bending Strength of Sintered Magnesia

[Shinji Fukuda, Akio Nishida, et al.; CHO KO-ON ZAIRYO KOKUSAI SHINPOJIUMU, 15 Mar 91] .. 98

Properties and Application of SiC Produced by Chemical Vapor Deposition [Kazuhisu Matsumoto, Fusao Fujita, et al.; <i>CHO KO-ON ZAIRYO KOKUSAI SHINPOJIUMU</i> , 15 Mar 91]	98
Development of High Performance Carbon-Carbon Composites for Space Vehicles [Tadashi Matsushita, Hidehiko Mitsuma, et al.; <i>CHO KO-ON ZAIRYO KOKUSAI SHINPOJIUMU</i> , 15 Mar 91]	104

Present, Future of Ultra-High Temperature Materials

916C0035A Ube CHO KO-ON ZAIRYO KOKUSAI SHINPOJIUMU in Japanese 15 Mar 91 pp 2-12

[Article by Ryohei Tanaka, Yokohama National University]

[Text] [English Abstract]: The purpose of this paper is to review the current status and future trends of the research and development of so-called ultra-high temperature materials. As for the former, the prospective needs of the materials are described, focusing on the fields of space and aviation, energy and materials manufacturing. Superalloys will have only a limited increase in temperature in the future, while such advanced materials as intermetallic compounds, metallic and ceramic matrix composites, refractory metals and their alloys, ceramics and carbon/carbon composites, with their higher melting points, will be highlighted in the fields of higher temperature applications. Among these, carbon/carbon composites have the most potential for use in ultra supersonic aircraft and space planes. The problems that need to be resolved with respect to these materials are also discussed.

1. Introduction

On 19 November 1989, newspapers and television stations reported news to the effect that MITI was "scheduled to initiate 'R&D on a supersonic airplane transportation system' over an 8-year period, starting in FY89, under a total budget of ¥ 28 billion, with the anticipated participation of a total of seven companies, including four companies in Europe and the United States," as a large-scale project. This supersonic airplane transportation system would connect Tokyo and New York in 3 hours at Mach 5, that is, at a speed of 6,000 km/hour.

In February 1986, three years before the above news, President Reagan, in his annual State of the Union address to Congress, announced the national aerospace plane (NASP) project, aimed at the development of a new "Orient Express." Occasioned by that, a space plane investigation meeting was established in Japan as well, the object of discussion of which was the space transportation system, and a report was prepared in June 1987.

The space plane is currently being described in Japan as follows: "a horizontal take-off and landing type hypersonic manned transportation airplane which accelerates itself by means of air suction engines in the atmosphere and propels itself by means of rocket engines outside of the atmosphere."

Such a space plane is being planned not only in the United States and Japan, but also in France, the United Kingdom, Germany and the USSR.

High temperature-related fields that are expected to make rapid advancements toward the 21st Century are not limited to the aerospace field, but include such

diverse fields as energy technology and material processing, with various plans and ideas being examined in detail, and there are many that have already made some progress.

Now, in order to realize such plans, materials that support them are indispensable. In particular, new materials are demanded that will satisfy various required performances that have been impossible to realize with conventional materials, such as heat resistance, heat-resistant impact characteristics, high specific strength, high specific rigidity and resistance to oxidation under limiting environments of temperature, pressure, atmosphere, etc. Above all, the development of structural materials of light weight and high strength that can withstand the high temperatures of 1,000 to 2,000°C, i.e., "ultra-high temperature materials," is necessary.

Under these circumstances, the idea surfaced of establishing an ultra-high temperature material research center as a research infrastructure facility of the New Energy and Technology Development Organization (NEDO), which is a MITI-related organization. Toward the realization of this idea, the Committee for the Investigation of Ultra-High Temperature Material Technology was organized in September 1988 in order to clarify the current status, tasks, needs, etc., of R&D related to ultra-high temperature materials, as well as to examine the basic thoughts regarding the structure of the proposed facility. A report summarizing the results of the discussion was prepared in March 1989. At about the same time as the above, a report was also prepared which investigated the facilities and technology involving ultra-high temperature materials. In the following, we will present the research trends with regard to ultra-high temperature materials, based principally on the main contents of the former report, but with some personal opinions added.

2. Demand for Ultra-High Temperature Materials

The prefix "high" or "ultra" is used almost at will in various fields, as in the case of "high temperature" superconductivity in spite of the fact that the actual temperature involved is below room temperature. However, what is meant by "ultra-high temperature materials" in this article implies advanced materials that can be used under severe environments of oxidation and corrosion in the ultra-high temperature range of up to about 2000°C, as was mentioned in the previous section. In this section, we will touch upon the needs for ultra-high temperature materials in the main fields of aerospace, energy and material manufacturing.

2.1 Aerospace Field

The operating temperature of a jet engine is represented by the temperature at the turbine inlet. It is said that the output can be increased by 4 percent if the temperature at the inlet is increased by 56°C (100°F). In recent years, the temperature has reached 1300 to 1400°C at the most, even for engines of civil passenger aircraft as shown in

Figure 1. On the other hand, regarding supersonic aircraft or the so-called space shuttle which will fly between the future space station and earth, the aircraft will fly at a high speed, reaching Mach 2 to 25, and thus will be subjected to the aerodynamic heat generated by collision or friction with the air where the engines are exposed to the combustion gas which is at a still higher temperature. Because of this, the body and the engine of the aircraft are expected to reach the temperatures shown in Table 1(a). In particular, reusable manned crafts, such as the above-mentioned winged and horizontal take-off/landing type, should be developed rather than the "dispensable" type which includes ordinary rockets. Accordingly, the materials are required to be durable, resistant to thermal fatigue, etc., in order to permit repeated use. The turbo-jet engine that is currently in widespread use in military aircraft can be used only up to about Mach 3. However, an air-turbo-ram (ATR) jet engine, indicated in the footnote to Table 1(a), can be used up to about Mach 6, and a scram-jet engine is said to exhibit excellent specific thrust for the range of from Mach 6 to 12. However, under such high speeds, portions that are heated to surface temperatures of from 1200 to 1600°C occur even in the aircraft body, and the

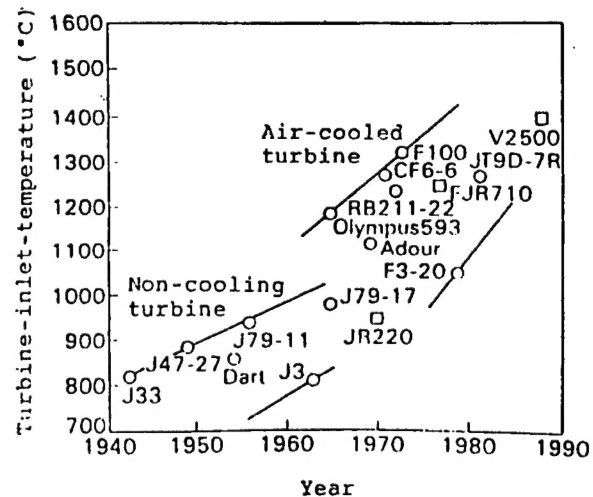


Figure 1. Increasing Tendency of Turbine-Inlet Temperature for Aircraft Engines

maximum engine temperature is expected to approach 3000°C.

Table 1. Estimated Temperature Conditions Required for Various Future Technologies

(a) Fields Involving Supersonic Aircraft and Next Generation Space Planes			
Supersonic Aircraft (M 2-6)		Next Generation Space Planes (approx. M 25)	
Body	Engine*	Body	Engine**
(Surface temperature) approx. 1200°C	(Intake) approx. 1500°C	(Surface temperature) approx. 1800°C	(Intake) approx. 1700°C
	(Combustion chamber)*** approx. 2800°C		(Combustion chamber) approx. 3000°C

* Air-turbo-ram-jet engine
** Scram-jet engine
*** Application of cooling system for parts made of ultra-high temperature materials
(b) Fields in Energy Technology

Kinds of Energy Technology	Components	Temperature
Fusion reactor	First wall, blanket, etc.	1000-2000°C*
Coal gasification	Furnace, heat exchanger, etc.	1300-1800°C
High performance gas turbine	Turbine blades, etc.	1300-1600°C

* Instantaneously, it will reach 3500-4000°C
(c) Fields in Materials Manufacturing Equipment

Materials Manufacturing Process	Components and Parts	Temperature
High temperature furnace	Heater, reflector, heat insulator, etc.	2000-3000°C
Melting furnace	Fire brick, nozzle, etc.	approx. 2000°C
Hot press	Die, refractories, etc.	2000-2500°C
HIP	Heater, material case, heat insulator, etc.	approx. 2000°C

The turbo-jet engine that is currently in widespread use in military aircraft can be used only up to about Mach 3. However, an air-turbo-ram (ATR) jet engine, indicated in the footnote to Table 1(a), can be used up to about Mach 6, and a scram-jet engine is said to exhibit excellent

specific thrust (Thrust generated per unit flowrate of the propellant, having the unit of "second.") The specific thrust is larger for higher temperatures of the combustion gas and for smaller molecular weights of the fuel.) for the range of from Mach 6 to 12. However, under such high speeds,

portions that are heated to surface temperatures of from 1200 to 1600°C occur even in the aircraft body, and the maximum engine temperature is expected to approach 3000°C.

2.2 Energy Technology Field

In thermal power generation employing the steam turbine, even in the ultra super critical (USC) power generation which has been actively researched and developed lately and has begun operation with actual equipment, although the goal is about 650°C, temperatures exceed 1100°C during gas turbine power generation. In particular, the operating temperature has been demonstrating a continuing upward trend aimed mainly at reducing the power generation cost by improving the thermal efficiency. Recently, however, the global environmental problems, referred to as warming or the greenhouse effect, have been attracting worldwide attention, making it important to reduce the amount of carbon dioxide generated per unit energy and supplying another reason for raising the temperature. Table 1(b) shows the temperature environment for principal energy technology fields. Of them, the high performance gas turbine is used for compound cycle power generation which generates power, from the standpoint of the effective use of heat, by operating a boiler using the residual heat of the exhaust gas of the gas turbine and by rotating the turbine with steam from the boiler. This system has already been put into practical use, but the extent to which the overall heat efficiency can be raised may well depend on the gas temperature at the gas turbine inlet.

On the other hand, in coal gasification, the highest temperature obtainable depends on the type of gasification method used. While, in the fixed floor furnace, it approaches 1800°C, in any case there is the possibility of severely deteriorating the materials by the H₂S gas resulting from the sulfur in the coal.

As for the nuclear fusion furnace, among the many developmental tasks needed for its realization, so far as the materials go, the most important development is that of the protective wall, i.e., the so-called first wall, of the vacuum vessel to stably confine the plasma. Along with encountering a substantial heat load from the plasma, the furnace is subjected to collisions with a large number of neutrons and to wear and tear due to interaction with the plasma, and since the impurity particles produced contaminate the plasma, it is desirable to use compounds consisting of elements with small atomic numbers, such as graphite, TiC and SiC. In order for the furnace to be able to withstand such an environment over a long period of time, it may be said that the compounding of the materials is indispensable.

2.3 Material Manufacturing Processes

High melting metals with melting points exceeding 2000°C (refractory metals) include W (3387°C), Ta (2996°C), Mo (2610°C), Nb (2470°C), etc. (noble metals rhenium, osmium, iridium, etc., also have melting points higher than 2000°C). In addition, there exist more than

200 substances of single body ceramic compounds that have melting points exceeding 2000°C, and this number can be increased further if those having melting points approaching 2000°C are included.

In the processes which handle these materials or which manufacture them as industrial materials, ultra-high temperature materials are required for use in such equipment as fusion furnaces, hot presses, hot isostatic presses (HIP's), various kinds of heat treatment furnaces, molten glass transporting apparatuses, heat exchangers for chemical plants, etc., and their active use is expected to enhance the reliability of the apparatus and provide a significant effect on the reliability enhancement and cost reduction of the material manufacturing processes through the prolongation of the working life. Examples of the temperature environments of the main items mentioned above are shown in Table 1(c).

The high temperature facilities in the manufacturing processes related to iron and steel are constructed mainly by making maximum use of refractory materials and water cooling. The refractory materials suffer from wear and tear due to slug corrosion, etc., but techniques for controlling the environment so as to allow self-coating are being examined rather than changing the materials. Accordingly, the needs for ultra-high temperature materials are mostly for parts related to the heating furnace and for working tools used at high temperatures.

In particular, a technique called the semi-solidified working process, or rheocasting, is drawing attention as a material manufacturing process of the future, and its technical development is under way. In this process, a slurry (the so-called rheometal), in which fine metallic particles and liquid coexist, is produced by breaking the dendritic crystals formed by the vigorous stirring of a coexisting mixture of solid and liquid phases, and a material close to the final product is obtained by the direct molding of the slurry. For iron and steel materials, materials are needed for mechanical stirring at about 1100°C. In addition, for the working stage, roll materials are required that have strength at high temperatures and heat insulating properties since rolling is involved in the semi-molten state.

2.4 Other Needs

Regarding gas turbines for automobiles, if it is possible to raise the turbine inlet temperature to 1350°C, the fuel consumption will become fully competitive with that of the diesel engine, and it will become possible to reduce the environmental contamination caused by exhaust gas. In automobiles as well, if the air cooling system employed by jet engines is adopted, it will be possible to use gas turbines for super heat resistant alloys. However, if compact gas turbines are to be used in automobiles, it will be necessary to employ ceramics because the fuel consumption will deteriorate and the structure will become complex, even when air cooling is attempted. In this field, a developmental project (100 kW) centered around MITI is in progress in Japan, while the Advanced

Turbine Technology Application Project (ATTAP) is under way in the United States.

In addition, as future technologies that will require ultra-high temperature materials, one may mention high efficiency discharge lamps and the extraction of underground magma energy.

3. R&D on Super-High Temperature Materials—Current Status and Future Outlook

As mentioned in the previous section, the development of ultra-high temperature materials is eagerly awaited, as is their practical use as structural materials under limiting environments. In recent years, R&D on ultra-high temperature materials has been very active in Japan, Europe and the United States. In this section, the current status and future outlook of R&D will be briefly surveyed for metallic systems, ceramic systems, compound materials, etc., with regard to ultra-high temperature materials that can be used in the temperature range of from 1000 to 2000°C.

3.1 Super Heat Resistant Alloys

The full-scale development of super heat resistant alloys, the so-called super alloys, was initiated in the 1940's at about the same time that the jet engine development race was begun in the United States, United Kingdom, etc. Super heat resistant alloys can generally be roughly divided into three groups—iron-based alloys which contain iron as the principal component, nickel-based alloys, and cobalt-based alloys. During the initial period of development, the Co-based alloys demonstrated excellent strength to withstand high temperatures, but then the Ni-based alloys, which utilize the precipitation strength of the so-called γ' -phase $Ni_3(Al, Ti)$ advanced rapidly, and it has been a long time since the Co-based alloys were pulled down from the throne.

Figure 2 shows the developmental trend of the super heat resistant alloys since the initial period with respect to changes in the usable surface temperature of materials. The Ni-based alloys achieved rapid advancement to the present state through the application of vacuum melting and precision casting, the advancement of hollow blade manufacturing technology supported by ceramic core material development, the development of alloy design and texture control techniques, and the realization of single crystal gas turbine moving blades from columnar crystals by the adoption of the unidirectional solidification method. Currently, nearly one-half of the mass of jet engines is occupied by Ni-based alloys.

On the other hand, since Co-based alloys generally have excellent castability and resistance to oxidation and thermal fatigue, etc., they are widely used for the stationary blades of jet engines. Moreover, since Fe-based alloys have advantages such as sufficient strength at temperatures below 700°C, although their strength is

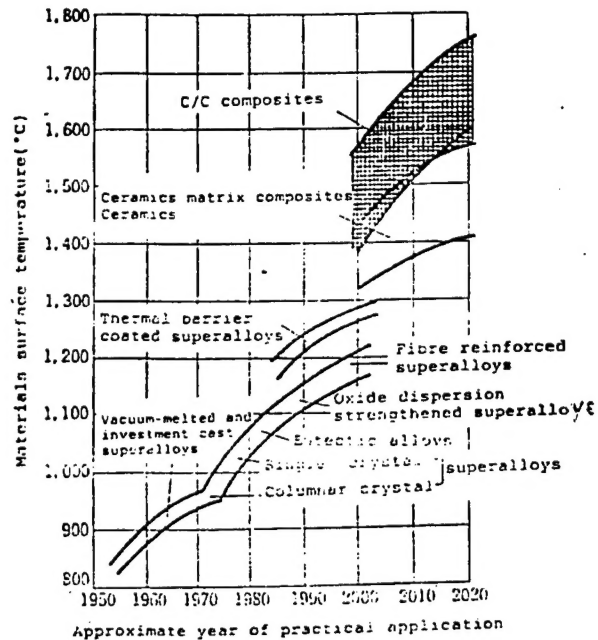


Figure 2. Developmental Trends of Heat-Resistant Materials

inferior to that of Ni- and Co-based alloys at temperatures above 700°C, and are inexpensive, they are still finding widespread use in the rotors and disks of gas turbines.

As for the Ni-based alloys which are forming the mainstream of current super heat resistant alloys, the melting point of Ni, their principal component, is 1455°C. Therefore, it may be difficult to achieve 1300°C, as can be seen from Figure 2, even if an attempt is made to improve heat insurability and resistance to oxidation and corrosion by means of reinforcement through the addition of alloying elements, reinforcement with W fibers (see Section 3.4.3 below) and thermal barrier coating (TBC) by the plasma spraying of ceramics.

As materials which are expected to have superior heat resistance when compared to the super heat resistant alloys, one may mention intermetallic compounds and alloys of high melting point metals among the metallic materials, and carbon/carbon (C/C) composite materials, ceramic matrix composite (CMC) materials, metallic matrix composite (MMC) materials, and others among the composite materials. In addition, as for ceramics, the nonoxide systems such as sialon, silicon carbide (SiC) and silicon nitride (Si_3N_4) may be said to represent the main compounds.

3.2 Intermetallic Compounds

Compounds in which metallic elements are combined in relative simple atomic ratios are called intermetallic compounds (IMC's, sometimes also referred to as intermetallics) and have crystal structures that differ from

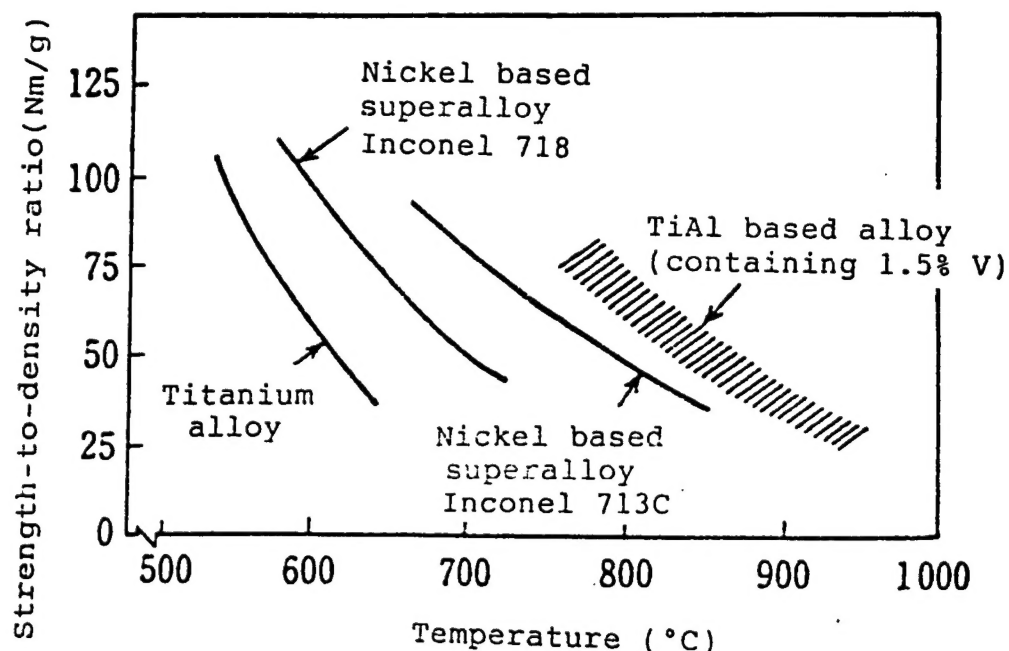


Figure 3. Comparison of Strength-to-Density Ratio of TiAl Alloy Containing Vanadium with Nickel-Based Superalloys and Titanium Alloy. The strength-to-density ratio is based on 100 h creep-rupture strength.

those of the component metals. The number of kinds of these compounds approaches 150, even when limited to the binary system, and among them more than 100 kinds have melting points of above 1500°C.

The fact that the melting point is so high generally means that the binding force between the atoms is strong, and that the hardness and strength at high temperatures are accordingly large. In particular, attention is being attracted by the fact that so many of the compounds that have the $L1_2$ type of face-centered cubic system crystal structure, including the above-mentioned γ' -phase $Ni_3(Al, Ti)$, exhibit the so-called reverse temperature dependence of strength in which the strength becomes greater for high temperatures within a certain temperature range. As for heat resistant structural materials, the iron group metals (Fe, Ni and Co) and aluminides of Mo, etc., are the objects of research, and many studies on $NiAl$, $TiAl$, Ti_3Al , etc., are being conducted since the balance between strength and resistance to oxidation is ideal. Figure 3 shows that the creep-rupture strength of $TiAl$ is superior to that of super heat resistant alloys.

There are still many unsolved problems with intermetallic compounds with regard to tenacity, workability, resistance to oxidation, etc., and it seems that only some of them are being used for the trial manufacture of gas turbines and turbo chargers. However, much improvement is expected in the future based on the fact that substantial ductility can be obtained by adding a trace amount of boron to Ni_3Al , as well as due to the discovery of the super-plasticity phenomenon in $TiAl$.

In addition, aluminides or silicides of high melting point metals, such as Nb and Mo, are promising since they have high melting points comparable to those of the high melting point metals themselves, and also have excellent lightness and resistance to oxidation. As candidates for ultra-high temperature materials, one may mention $C11b$ -type compounds, such as $TaSi_2$, $CrSi_2$, etc., as well as $A15$ -type compounds such as Nb_3Al . However, note that the compounds of high melting point metals have so far been studied only as superconducting materials for the most part and electric heating materials to some extent, and not many studies have been yet been found that deal with them as heat resistant structural materials.

3.3 High Melting Point Metals and Their Alloys

The high melting point metals W, Mo, Nb, Ta, etc., and their alloys have heat conductivity which is two to six times higher than that of super heat resistant alloys and have physical properties favorable for heat resistance. However, the greatest defect is their lack of resistance to oxidation, and Ta and W also have high densities and are disadvantageous with regard to specific strength. In addition, although Nb and Ta have satisfactory low temperature ductility, Mo and W exhibit brittleness at low temperatures. Therefore, the biggest problem involves determining whether it is possible to develop alloys which possess both strength and resistance to oxidation by improving the resistance to oxidation without impairing their ductility, for Nb and Ta, and exploring alloying elements which can lower, even a little, the transition temperature at which the ductility

deteriorates, for Mo and W. Regarding the increase in strength, solid solutions of W, Ta, Hf, Re, etc., and the precipitation of HfC, ZrC, etc., seem to be available. As for isothermal forging in which the superplasticity used in the powder metallurgical process of a Ni-based super heat resistant alloy is applied, Mo alloys to which a small amount of Ti and Zr have been added and TZM (Mo - 0.5 percent Ti - 0.08 percent Zr) are already in widespread use as dies. However, they must be used in the atmosphere of an inert gas. Therefore, if a material with excellent resistance to oxidation is developed which can be used in the atmosphere, then it is expected that the cost for facilities and forging can be reduced considerably.

As the material for the first wall of the nuclear fusion furnace, an Mo-5 percent Re alloy is considered promising.

3.4 Composite Materials

So that composite materials can be used for ultra high temperature materials, improvement in the strength at high temperatures of the matrix materials is aimed at by principally using high strength fibers.

In general, fiber reinforced composite materials are divided according to the kind of matrix into resin system (fiber reinforced plastics (FRPs) or polymer matrix composites (PMCs)), metallic system (fiber reinforced metals (FRMs) or metal matrix composites (MMCs)), ceramic system (fiber reinforced ceramics (FRCs) or ceramic matrix composites (CMCs)) or carbon system (carbon/carbon (C/C) composite). The C/C composite materials are companions of ceramic-based composite materials (CMCs), but in most cases they are given separately from the CMCs. In Figure 4, the relationship between the limiting temperatures of use and the time of introduction to engine use of these composite materials is shown in comparison to those of metallic materials and super heat resistant alloys. It is well-known that the FRPs were developed first and are already approaching maturity, while the development of CMCs was initiated most recently. It can be seen from the figure that the later the time of development and introduction to engine use, the greater the possibility, in general, of being used at higher temperatures.

Recently, studies on the heat resistant materials referred to as functionally gradient materials (FGMs) have been active in Japan. In the following, various composite materials will be surveyed briefly regarding their inclusion in composite materials.

3.4.1 Carbon/Carbon (C/C) Composite Materials

C/C composite materials are a new type of composite material that employs carbon fibers of high elasticity or high strength, with carbon as the base. As is clear from Figures 2 and 4, they are materials with excellent heat resistance and, with their densities having extremely low values, i.e., less than 2.0, their specific strengths are quite dominant, as can be seen in Figure 5. In particular, the

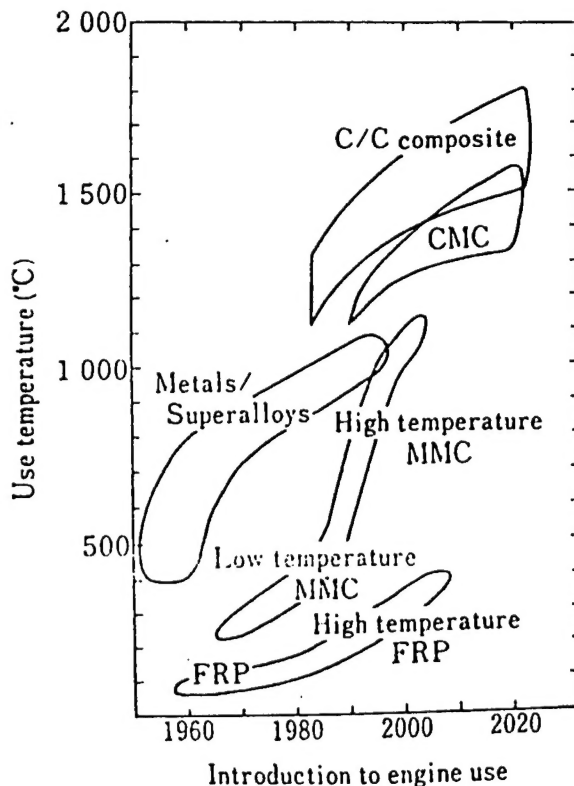


Figure 4. Relationship Between Temperature of Use and Introduction to Engine Use for Various Composite Systems

significant feature is that, when compared to other materials, their specific strengths do not diminish when approaching the high temperature region. They are employed as brake materials for the supersonic passenger airplane Concorde, the F15 fighter, etc., as well as for the nose cone and the leading edge of the space shuttle. Current C/C composite materials are compound body structures employing carbon fibers that are ingeniously oriented as the reinforcing material, and carbonized layers of pitch or resin, or CVD carbon, as the matrix material, and it is becoming possible to manufacture materials demonstrating excellent performance. However, there is one big defect in that oxidation starts around 600°C if even a small amount of oxygen exists. Accordingly, for the case of short time use, such as for the space shuttle, it is acceptable since it is semi-expendable. However, for the case of reuse or use for a long period under high temperature oxidation conditions, a method is being employed in which it is coated with a ceramic.

With the advances in fields related to space development, strength and resistance to oxidation are required in the ultra-high temperature range around 2000°C, and C/C composite materials are very promising as representing the so-called advanced composites. However, the

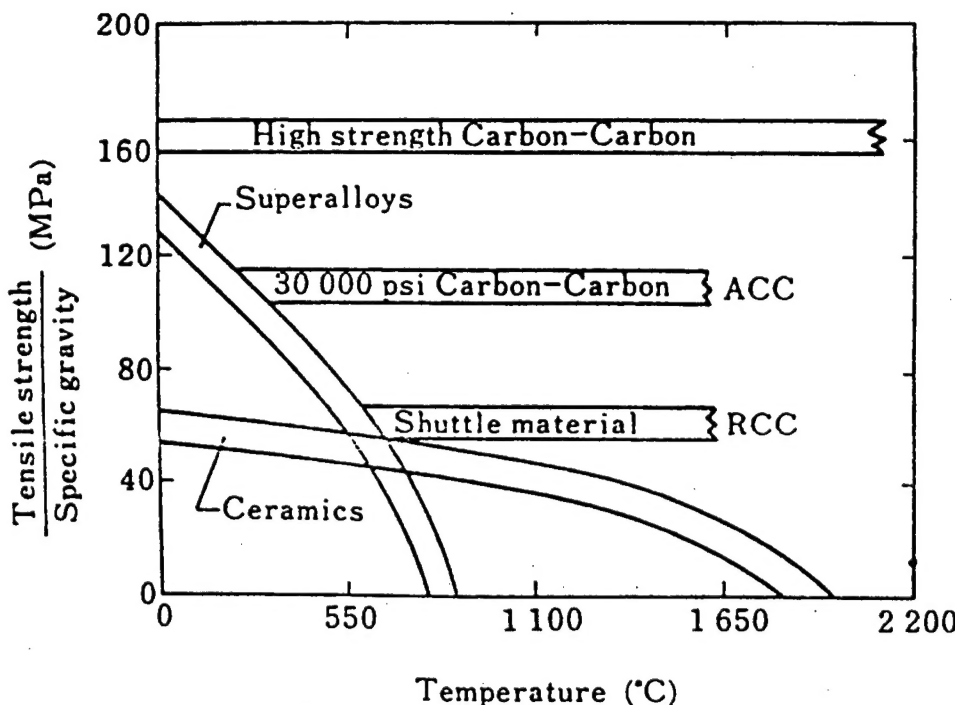


Figure 5. Temperature Dependence of Specific Strength of Superalloys, Ceramics and Various Carbon/Carbon Composites

history of research on C/C composite materials in Japan is short, and it is still at the stage where the relationship between the basis of the manufacturing method and their properties is being examined, with scarcely any data available concerning the properties at high temperatures. Since such problems as material cost exist in addition to the resistance to oxidation, the early establishment of the manufacturing method, including the carbon raw material and surface processing, is desired, as is the resulting cost reduction.

3.4.2 Ceramic-Based Composite Materials (CMCs)

Representative ceramic fibers expected to be employed as reinforcing materials include, in addition to carbon fibers, alumina, SiC_{PC} (obtained by calcining organic fibers that contain Si in the form of SiC as the so-called precursor fiber), SiC_{CVD} (obtained by using CVD to attach SiC, employing carbon fibers as the core lines), etc. The heat resistant temperature for materials other than carbon fiber is considered to be about 1200°C.

As examples of CMCs, one thinks of glass ceramic or oxide ceramic systems, but these can be used only up to 1100°C at the most. On the other hand, those materials that employ, for example, SiC and Si_3N_4 as the matrices can be used up to 1200 and 1700°C, respectively, and yet are able to maintain a level of strength that is comparable to that at room temperature. In the future, there will be a demand for developments that will further

improve the rupture tenacity and strength of the ceramics, and yet allow them to maintain these properties at high temperatures.

3.4.3 Metal-Based Composite Materials (MMCs and FRMs)

MMCs are said to be indispensable materials for use in the construction of space stations because of their excellent properties against heat deterioration and ultraviolet deterioration, as well as for the heat resistant cycle and moisture absorbency. However, research is also in progress with regard to applying materials that are combinations of boron fibers and an Al or Ti alloy to aircraft engine parts and composite materials of W wires/super heat resistant alloys to turbines.

On the other hand, although some of the materials are being introduced to automobile engines, there are problems with the cost, etc., so it seems as if some more time will be required before they can be adopted on a full-scale basis.

However, materials whose use at temperatures exceeding 1000°C is expected, at least to some extent, are those employing a super heat resistant alloy or intermetallic compound as the matrix. The former is generally called a fiber reinforced superalloy (FRS), although those that employ W fibers are sometimes called tungsten FRSs (TFRSs). These materials have mainly been studied with turbine blades of complicated shapes for use in jet engines as the object. Although the study of the latter has

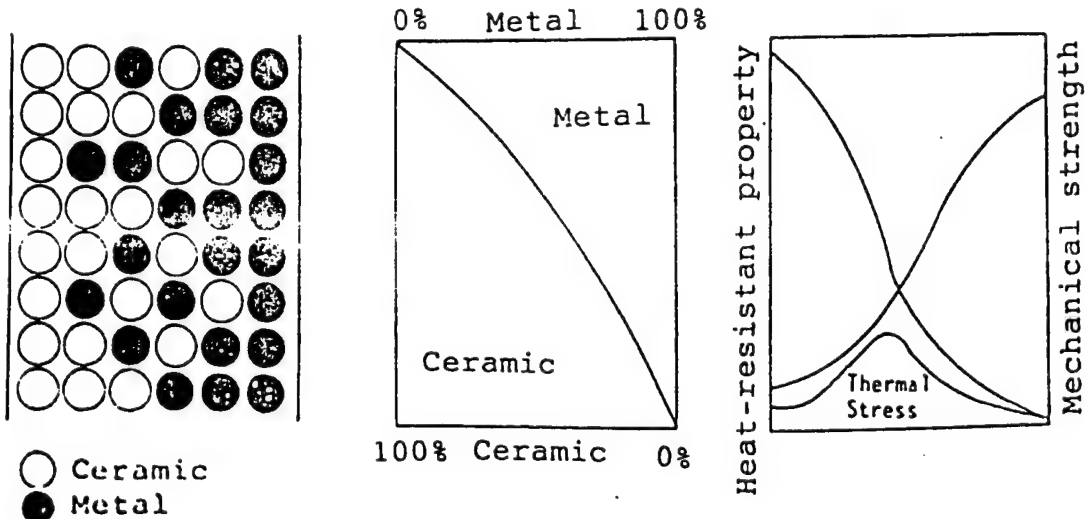


Figure 6. Basic Concept of FGMs

just recently begun, NASA claims that the specific strength of SiC/(TiAl + Nb) at high temperatures is greater than that of the super heat resistant alloys, and thus their future progress is being awaited.

It should be noted that it has been pointed out that MMCs have two problems, i.e., the behavior of the interface between two composite materials and the selection of the manufacturing technology that will be appropriate for the component in mind.

3.4.4 Functionally Gradient Materials (FGMs)

In the space plane, a cooling structure will be adopted that will use liquid hydrogen (-253°C), which will be the fuel for the plane, for those locations such as the surface of the aircraft body and the engine that will be exposed to ultra-high temperatures. For this reason, a large temperature gradient will be generated, in accordance with the heat conductivity and the dimensions (thickness) of the material, between a heated surface and a cooled surface on the opposite side. Consequently, substantial thermal stress will be generated unless the coefficient of thermal expansion of the material is sufficiently small. In order to secure heat insulation on the high temperature side while relaxing the thermal stress, development has been started, with Japan as the center, on "functionally gradient materials" (FGMs), as illustrated in Figure 6.

This material employs a ceramic on the high temperature side and a metal or the like, to provide heat conductivity and mechanical strength, on the cooled surface, and yet the goal is to synthesize materials so as to have the optimum distribution of constitution, texture and porosity between the two sides. Currently, research is being conducted for numerous material systems, such as TiC-SiC, C-SiC, ZrO₂-NiCr, TiB₂-Ni, and TiB-Cu, and the thermal barrier performance, resistance to

thermal impact, thermal fatigue characteristics, and thermal stress reduction effect, etc., of the materials are being evaluated.

3.5 Ceramics

As representative ceramics for high temperature structures, alumina (Al_2O_3), mullite ($3\text{Al}_2\text{O}_3 \cdot 2\text{SiO}_2$), and sialon ($\text{Si}_{6-z}\text{Al}_z\text{N}_{8-z}$, $z = 0$ to 4.2) can be mentioned as oxides, while SiC and Si_3N_4 , etc., represent the nonoxides.

Of the so-called fine ceramics, alumina is the most widely used material for such things as IC substrates. Research on SiC and Si_3N_4 has been full-scale since the latter half of the 1950's, but even today they have just been introduced to automotive turbochargers and the auxiliary combustion chambers of diesel engines, and their use in the future is expected.

The results of research on ceramics as ultra-high temperature materials are increasing steadily, but their full-scale introduction is still said to represent a future problem. However, their superiority over metallic materials with respect to heat resistance and mechanical strength at temperatures above 1000°C is clear, and they will be put to practical use as the development advances.

Conclusion

In this review, we defined ultra-high temperature materials as "materials that can be used in the temperature range of from 1000°C to around 2000°C," and have tried to present a brief survey of the current status of demands for and trends of the material development of these metals. Ultra-high temperature materials, which possess excellent properties such as heat resistance, thermal impact resistance, high specific strength, high specific rigidity, and oxidation resistance under the limiting environment of ultra-high temperatures that are difficult

to realize using existing materials, are expected to be developed due to the demands from a wide range of industrial fields, including the aerospace and energy technology fields. As for super heat resistant alloys, such as those based on Ni, etc., there is not much hope that their temperatures of use can be elevated in the future. Therefore, as the advanced ultra-high temperature materials that will be required by the aerospace and energy technologies in the 21st Century, intermetallic compounds and ceramics, as well as advanced composite materials, such as MMCs and C/C composites, etc., are eagerly awaited.

The research facilities that will be required for the R&D of these ultra-high temperature materials must, in many cases, be able to withstand the ultra-high temperatures themselves. Moreover, there will be many large-scale and expensive facilities involved in measurement and control technology in connection with the ultra-high temperature environment.

The "Japan Ultra-High Temperature Materials Research Center, Inc.," equipped with facilities for the manufacture of materials suitable for use under such ultra-high temperature environments and for the research and evaluation of their properties and functions, to be open to researchers within and outside of Japan, was established in 1990 in accordance with the so-called third sector mode. In conclusion, we hope that this center will serve a useful function in the effective advancement of the R&D of ultra-high temperature materials.

Role of Japan Ultra-High Temperature Materials Research Center

916C0035B Ube CHO KO-ON ZAIRYO KOKUSAI SHINPOJIUMU in Japanese 15 Mar 91 pp 14-19

[Article by Toshio Hiraki, executive vice president, Japan Ultra-High Temperature Materials Research Center/Institute: "Ultra-High Temperature Materials Development, the Role of Japan Ultra-High Temperature Materials Research Center and Future Prospects"]

[Text] [English Abstract]: A brief review of the needs of ultra-high temperature materials development and the required advanced technologies and facilities is presented together with a description of the function and facilities of the Japan Ultra-High Temperature Materials Research Center/Institute (JUTEM/JUTEMI). Some examples of corporate action to cope with ultra-high temperature materials development are discussed together with the related utilization of JUTEM/JUTEMI. Intended JUTEM/JUTEMI activities are proposed, and users' support of JUTEM/JUTEMI is requested for future evolution.

1. Introduction

According to a report prepared by MITI, it should be anticipated that the new materials market in the year 2000 will approach ¥12.6 trillion. Since it is generally said that the new products market is about 10 times

larger than the materials market, the impact of these new materials will really make us sense the arrival of a new materials era. Ultra-high temperature materials will occupy a principal section of this market in importance. In this review, a brief survey will be given of the needs for the development, technology and facilities required for the development of ultra-high temperature materials, the author's personal opinions will be expressed with regard to the generally conceivable corporate responses to these matters, and the utilization and future prospects of the Japan Ultra-High Temperature Materials Research Center, Inc., will be presented in order to solicit the cooperation and assistance of users.

2. Needs for Ultra-High Temperature Materials Development

The needs for ultra-high temperature materials development may be roughly divided into two parts. One is the need for special kinds of materials, without which products in mind cannot be realized, e.g., materials for the space plane or materials for the nuclear fusion furnace, and which may be termed absolute ultra-high temperature materials that will meet a need which will allow the cost to be disregarded to a certain extent. The other is the need for heat resistance as a means of enhancing the thermal efficiency, such as the heat resistant materials used in jet engines, high efficiency gas turbines, ceramic engines for automobiles, etc., which may be termed relative ultra-high temperature materials that should be selected on the basis of cost performance. As a need that is related to both of the above, one could mention the need for the development of heat resistant materials for use in manufacturing ultra-high temperature materials, which may also be included with the relative ultra-high temperature materials.

The technological flow is naturally directed from the former to the latter. Due to the large risk in development in the former and the societal needs in the latter, projects led by the government are proceeding for both cases. In Japan, the "Development of Advanced Materials of Ultra-High Resistance to the Environment" and the "Moonlight Project" are under way for the former and the latter, respectively.

3. Desired Ultra-High Temperature Materials, Technologies and Facilities Required for the Development

For the development of innovative new materials, not only are the technologies for the material creation required, but also needed are the analytical and evaluative technologies for the materials, as well as the facilities corresponding to each of these technologies.

The space plane is a transportation aircraft which will shuttle between the ground and a low lying orbit around the earth, and one of Japan's projects for the near future is HOPE, which is scheduled to be launched at the end of this century. This is an unmanned aircraft which will be launched by being mounted on the tip of an H-II rocket and, upon its return to the ground, will land on an

airstrip by using air resistance to decelerate itself. The guide path of the plane will be controlled in order to suppress the maximum temperature of the craft body caused by aerodynamic heating during reentry into the atmosphere to 1700°C. The temperatures at various parts of the craft body are shown in Figure 1. In HOPE, the payload for the total weight of 10 tons is said to be 1 ton, and in order to secure the payload it becomes necessary to employ structural materials of the highest efficiency for the various temperature regions. In Figure 2, the specific strength of the materials versus the temperature is shown. The material development for HOPE has been consigned by the National Space Development Agency to several companies, and the use of carbon/carbon (C/C) composite materials is being considered for structures that will exceed 1300°C (Figure 3 [not reproduced]).

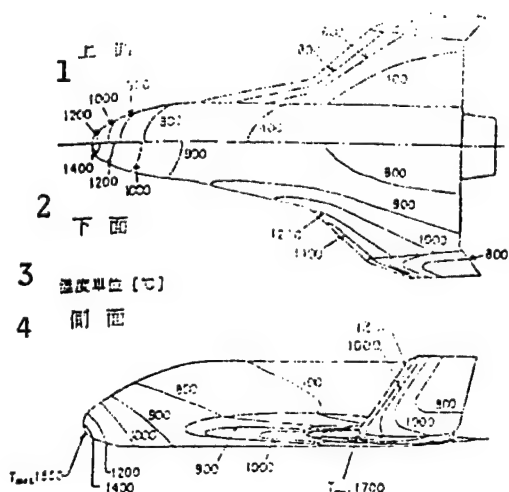


Figure 1. Surface Temperature Distribution for HOPE
Key: 1. Top surface 2. Bottom surface 3. Unit of temperature (°C) 4. Side surface

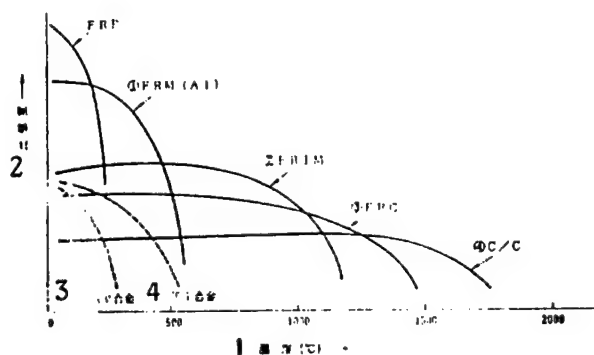
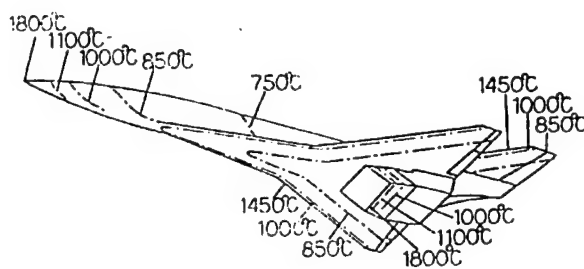


Figure 2. Specific Strength vs Temperature for Various Materials

Key: 1. Temperature (°C) 2. Specific strength 3. Ag alloy 4. Ti alloy



Distribution of Maximum Temperature in Space Plane
(Mach No=3, Altitude=20km)

Figure 4. Conceptual Shape of Space Plane and Assumed Temperature Distribution

As opposed to the HOPE, which will be launched from a rocket, the space plane will have an air breathing engine, take off horizontally from the runway, and will accelerate itself to about Mach 25 to reach a low lying orbit. In 1986, the United States aroused a sensation when President Reagan announced the National Aerospace Plane (NASP) Project, in which an experimental plane, the X-30, would be flown by the end of the 1990's. As for HOPE, whose ascending velocity in the atmosphere during the launch by a rocket does not reach too high a value, the tip of the craft body and the front edges of the wings can be made blunt. With regard to the space plane, however, the tip of the body, etc., must be sharp in order to reduce the air resistance, causing more severe aerodynamic heating conditions, and the maximum temperature can reach 2000°C. In Figure 4, the conceptual shape of the space plane and the assumed temperature distribution (for a maximum assumed temperature of 1800°C) are shown.

The development of ultra-high temperature materials resistant to 2000°C heat, which would be applicable to the space plane, is being carried out under "Research on Advanced Materials of Ultra-High Resistance to Environment" in accordance with the "Research and Development System for the Next Generation Industrial Base Technologies," with the material for the maximum temperature regions here again being the C/C composite.

It is already known that the mechanical strength of C/C composites will not deteriorate in a vacuum, even if the temperature exceeds 2000°C, and the topics for development are to further improve the strength (especially the tenacity) and to provide them with resistance to oxidation. The technologies required for these purposes include fiber matrix interface processing, coating technology (chemical vapor deposition (CVD), chemical vapor infiltration (CVI), etc.), and surface structure analysis. In addition, since infrastructure technologies, such as the methodology and device for measuring the strength, durability (resistance to oxidation), resistance of thermal impact, thermal conductivity, coefficient of thermal expansion, specific heat, etc., have not yet been

established on an international basis, these will also be included in the elements for development.

The intermetallic compounds (IMCs) and fiber reinforced intermetallics (FRIMs) that exhibit maximum specific strength in the vicinity of 1000°C in Figure 2 are also included as the developmental objects of "Research on Advanced Materials with Ultra-High Resistance to Environment." These materials are expected to be applied to a portion of the body structure or to engine parts for the space plane. However, for the purpose of exploring this possibility, the preparation of equilibrium state diagrams for the materials will be required first, with a melting technology/facility required for the IMC's and a powder manufacturing technology/facility and molding technology (such as HIP)/facility for the FRIMs.

In the development of the so-called big science, i.e., nuclear fusion, which is being carried out all over the world as an eventual energy source, there are many tasks for technological development. One of them is the development of the material for the first wall, which faces the ultra-high temperature plasma. For this material, not only is resistance to temperatures exceeding 1500°C required, but also complicated environment resistance, such as resistance to sputtering and resistance to radiation, etc., is demanded. For these materials, C/C composites have again been suggested as candidates.

The thermal efficiency of jet engines for aircraft is obtained by an enhancement in the cycle-pressure ratio and the rise in the turbine inlet temperature. Figure 5 shows the shift in the heat resistance of a super nickel alloy for a turbine material. The latest technologies include the precision casting of unidirectional crystals and single crystals by means of crystal control of superalloys and the development of oxide dispersion strengthened (ODS) alloys, both of which were taken up by the

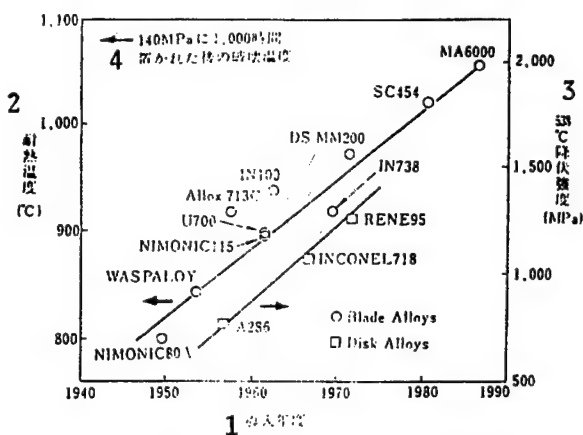


Figure 5. Changes in Heat Resistant Temperature of Turbine Materials

Key: 1. Fiscal year of introduction 2. Heat resistant temperature 3. 538°C yield strength 4. Resulting temperature under 140MPa after 1,000 hours

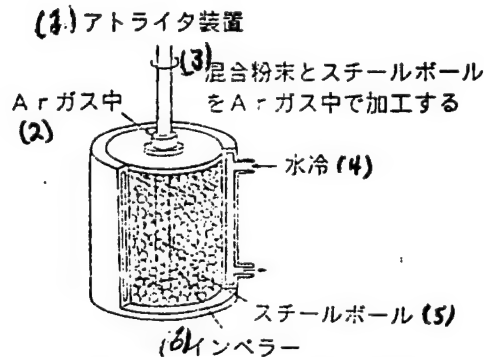


Figure 6. Mechanical Alloying

Key: 1. Attritor device 2. In Ar gas 3. Treat mixed powder and steel balls in Ar gas 4. Water cooling 5. Steel ball 6. Impeller

"Research and Development of Crystal Controlled Alloys" of the "Next Generation System" that was completed in 1989. The ODS alloys here were manufactured by mechanical alloying (Figure 6).

The blades made of these superalloys basically represent an extension of conventional metallic blades which require air film cooling (Figure 7), and relatively high tenacity and high reliability can be obtained.

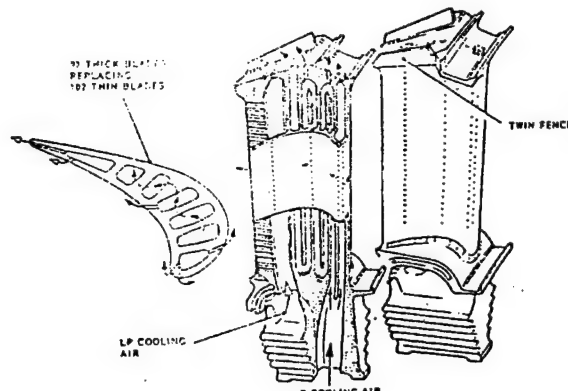


Figure 7. Air Film Cooling of Turbine Blades

Since air film cooling, which is indispensable for metallic blades, is carried out by air extraction from the engine, the thermal efficiency will be improved if this process can be eliminated. For this reason, the manufacture of combined turbines and disks is being attempted using fiber reinforced ceramics (FRC's), such as C/C or C/SiC (silicon carbide), and SiC/SiC composites which have higher tenacity than monolithic ceramics. In Figure 8 [not reproduced], an experimental model made by SEP Corp. in France is shown. The technologies required for FRC production include a packing technology, CVD or

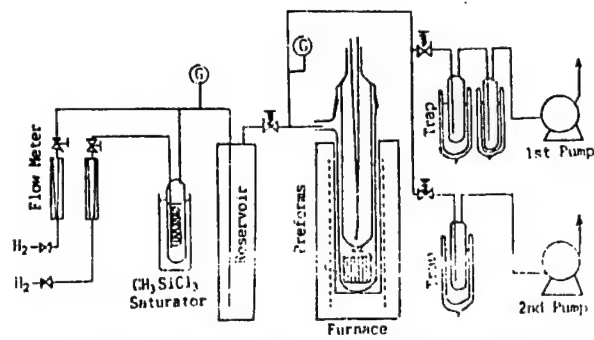


Figure 9. Conceptual Diagram of Pulsed CVI

CVI to provide resistance against oxidation, and crystal analysis/surface analysis technology. Figure 9 illustrates a pulsed CVI device.

The turbine blades of jet engines are subjected to combustion gas at ultra-high temperatures over a long period of time, as well as to a strong centrifugal force. Accordingly, it is necessary to accurately understand the creep characteristics, resistance to erosion, fatigue strength, rupture tenacity, etc., at high temperatures as the characteristics of the materials. Many elements remain to be developed with regard to these testing methods and devices.

These ultra-high temperature techniques will not contribute to an increase in the worldwide energy efficiency and the resulting reduction in CO_2 emission unless they are applied to general industrial heat engines. From this viewpoint, Japan, Europe and the United States are each developing compact ceramic gas turbines (CGTs) for industrial and automotive use. Figure 10 shows an example of a ceramic gas turbine. In Japan, an 8-year research and development project for a 300 kW CGT for cogeneration has been under way since 1988 as part of MITI's Moonlight Project, aimed at obtaining 42 percent higher thermal efficiency by elevating the turbine inlet temperature of 900°C in the conventional metallic compact gas turbine to approximately 1350°C by changing it to a ceramic one.

In all cases of Japan, Europe and the United States, the developmental goal is to come up with the technology for using a monolithic ceramic for a part. In Japan, the developmental goal is to improve the rupture tenacity of the monolithic tenacity of $7 \text{ MPa} \times \text{square root of } m$ to $15 \text{ MPa} \times \text{square root of } m$. In this case, the basis of the material technology is the power HIP method. Although the direction of development involving the employment of FRCs is toward improving the rupture tenacity, in either case the development of low cost processing technology is strongly required in order to popularize the ceramic gas turbines for general industrial use.

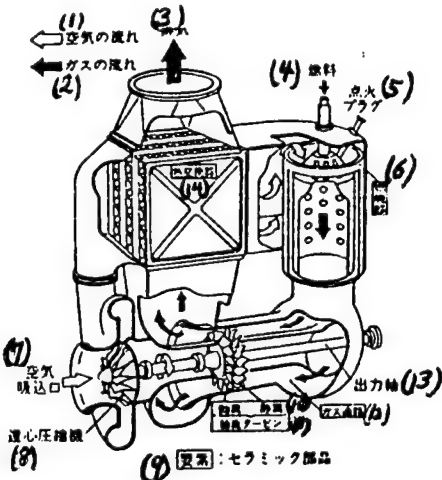


Figure 10. Uniaxial Ceramic Gas Turbine

Key:

- | | |
|---------------------|------------------------------------|
| 1. Air flow | 8. Centrifugal compressor |
| 2. Gas flow | 9. Element: ceramic part |
| 3. Exhaust | 10. Moving blade, stationary blade |
| 4. Fuel | 11. Axial flow turbine |
| 5. Ignition plug | 12. Gas passage |
| 6. Combustion unit | 13. Output shaft |
| 7. Air suction port | 14. Heat exchanger |

4. Introduction of Japan Ultra-High Temperature Materials Research Center/Institute, Inc.

The Japan Ultra-High Temperature Materials Research Center (JUTEM) is a research center intended to back up the R&D of ultra-high temperature materials that currently are having a significant impact on society, as mentioned above, and is operated under the so-called third sector mode, with one-half of the total funds invested by the New Energy and Industrial Technology Development Organization (NEDO), and the remaining shared by four local governments and 45 private companies. It was founded in March 1990, and will begin partial operation in April 1991. It has centers in Yamaguchi and Gifu prefectures, where large-scale and advanced research facilities of mainly material creation and property evaluation are located, respectively, and which have been widely opened to personnel in Japan and abroad. In addition, the Japan Ultra-High Temperature Materials Research Institute (JUTEMI), entirely funded by the private sector and attached to the center, has been set up so to handle tests and research on consignment. Figure 11 lists the facilities currently scheduled to be introduced to the center. It can be seen that facilities that are considered necessary for the creation, analysis and property evaluation of ultra-high temperature materials have been almost completely covered. They are all very advanced kinds of facilities, and the facilities themselves contain elements for development.

Figure 11. Facilities Scheduled To Be Installed at JUTEM

Facilities to be installed at the Yamaguchi Center			
Facility Number	Facility Name	Facility System	Delivery Time
MC-1	Ultra-high temperature alloy high purity and composition control fusion facility	Ultra-high temperature crystal controlled material experimental manufacturing system	March 1992
MC-2	Large volume crystal controlled alloy experimental manufacturing facility (Bridgman method)	Same	November 1991
MC-3	Large volume crystal controlled alloy experimental manufacturing facility (FZ method)	Same	November 1991
MC-5	Ultra rapid cooling metallic powder experimental manufacturing facility	Same	December 1991
MS-2	Micro-level reaction controlled ceramic alloy synthesizing facility	Ultra-high temperature structure controlled compounding system	November 1991
MS-3	Vapor phase controlled composite material experimental manufacturing facility	Same	March 1992
MP-1	Dispersed structure controlled mechanical alloying facility	Powder composition structure control system	March 1991
MP-2	High function solid phase controlled heat treatment facility (heat treatment furnace)	Same	
MP-3	High function shape controlled high temperature powder formation facility (hot press)	Same	Same
MF-1	Multipurpose ultra-high temperature and ultra-high pressure calcination facility (ultra-high temperature HIP)	Multipurpose ultra-high temperature powder formation and calcination system	November 1991
MF-2	Multipurpose ultra-high temperature and ultra-high pressure calcination facility (ultra-high temperature HIP)	Same	Same
MF-3	High function shape controlled powder formation facility (CIP)	Same	Same
ML-1	Facility for enhancing surface function - thin film (CVD, PVD)	Facilities for enhancing surface function	November 1991
ML-2	Facility for enhancing surface function - thick film (flame spraying)	Same	Same
ES-1	Mult-functional high voltage microanalysis apparatus (transmission electron microscope)	Structure analysis apparatus	November 1991
ES-2	Extreme surface structure analysis apparatus	Same	Same
ES-3	Multipurpose crystal structure analysis apparatus (X-ray diffraction apparatus)	Same	March 1991
ES-4	Internal fine structure nondestructive observing apparatus (ultrasonic microscope)	Same	March 1992
EB-1	Thermal property evaluation apparatus (thermal diffusion factor, thermal conductivity, specific heat)	Basic property evaluation apparatus	November 1991
EB-4	Thermal property evaluation apparatus (enthalpy)	Same	March 1992
EB-5	Thermal property evaluation apparatus (radiation factor)	Same	March 1992
EB-6	Thermal property evaluation apparatus (coefficient of thermal expansion)	Same	November 1991
EB-7	Mechanical property evaluation apparatus (uniaxial tensile, compression and bending testing machine)	Same	March 1991
EB-8	High temperature multi-axial evaluation apparatus with in-situ observation function	Same	March 1992
Facilities to be installed at the Gifu Center			
Facility Number	Facility Name	Facility System	Delivery Time
EU-1	Hyper-high temperature materials testing machine	Material utilization property evaluation apparatus	March 1991

Figure 11. Facilities Scheduled To Be Installed at JUTEM

Facilities to be installed at the Yamaguchi Center			
Facility Number	Facility Name	Facility System	Delivery Time
EU-2	Hyper-high temperature fatigue testing machine	Same	November 1991
EU-3	Hyper-high temperature creep testing machine	Same	March 1992
EE-1	Heat cycle/thermal impact testing machine	Resistance to environment evaluation apparatus	November 1991
EE-2	Hyper-high temperature oxidation and volatilization testing machine	Same	Same
EE-3	Erosion testing machine	Same	Same

For example, both the ultra-high temperature (3000°C) HIP apparatus (Ar or N₂ atmosphere) and the ultra-high pressure (10,000 normal atmospheres HIP apparatus (Ar or N₂ atmosphere, but is 2000 normal atmospheres for Ar + 5 percent O₂) to be delivered in November of this year demonstrate the highest performance level in the world. In addition, the hyper-high temperature material testing machine to be delivered in March of this year is capable of carrying out tests for tension, compression, bending and rupture tenacity temperatures of up to 1700°C in the atmosphere and of up to 2300°C in a vacuum/inert gas.

Moreover, EB-8, the high temperature multi-axis evaluation facility with an in-situ observation mechanism, is a highly motivated apparatus which is aimed at the in-situ observation of the rupture phenomenon under multi-axial stress at high temperatures, and its specifications are currently being adjusted.

According to the interim plan, it is believed that

- it is possible to test the static tension, compression, fatigue and creep of a plate-form biaxial test piece up to 1800°C, and
- it is possible to carry out in-situ observation of one surface of the above-mentioned test piece by utilizing a laser scanning microscope under a biaxially loaded state in a vacuum, inert gas, or atmosphere at temperatures up to 1600°C.

When completed, it will become a unique facility, the first of its kind in the world.

As for the facilities scheduled to be ordered in the future, in order to make the center a well-equipped research organization, we will determine the specifications based on the opinions solicited from workers in various fields. The fees for using these facilities will be determined based on their original costs, and they will be open to all enterprises and researchers impartially, regardless of whether they are Japanese or from overseas. Since usage by many enterprises and researchers will make the center the place to be for exchanging ideas, we are soliciting opinions regarding the effective use of these facilities from the user's point of view.

5. Corporate Action in Ultra-High Temperature Materials Development and the Role of JUTEM/JUTEMI

How should enterprises deal with the development of ultra-high temperature materials?

The enterprises involved in the ultra-high temperature material development for such a large-scale system as HOPE may be roughly divided into three groups—aircraft body assembling enterprises (integrators), component manufacturing enterprises (vendors), and material supplying enterprises (suppliers). In the development of members that make use of composite materials, such as C/Cs and FRCs, since no clear-cut distinction exists between the material production and the member manufacture, close cooperation among the above three groups is demanded. In the "Research and Development of Advanced Materials with Ultra-High Resistance to Environment" of the "Next Generation System," such a grouping has actually been introduced.

Regarding the integrators, ultra-high temperature materials represent the key technology, and the fact that they possess ultra-high temperature material development technology is one of the qualifications for their nomination as eligible contractors. Toward this end, by breaking them down so that they correspond to the requirements of the components and materials, the integrators have to be completely aware of the operating conditions of the craft body so that they can be given to the vendors and suppliers. In addition, they have to be able to determine which materials can be applied to various parts by constantly collecting information concerning the characteristics and limitations of the components and materials, and by judging the degree of maturity of the materials. In addition, they have to possess the so-called optimum design capability by means of which the capabilities of each material are designed.

For the suppliers, the possession of ultra-high temperature material technology means that not only can they secure the business of supplying materials for the project concerned, but it also makes them explore new materials as part of the repercussions of that technology. For that purpose, the suppliers have to have the ability to pursue

the material characteristics that respond to the requirements of the integrators and vendors. In order for these groups to eventually arrive at a creation technology and component formation technology for the materials to be adopted for the craft body, it will be necessary to try as many methods as possible. The installation of all these apparatuses and facilities represents a burden too heavy for the individual enterprises. This is where the role of JUTEM/JUTEMI comes into play.

For the development of an advanced material of especially high risk or a material which requires extensive exploration, it would be wise to participate in the "next generation system," but it may also be possible to form a multi-client project by gathering researchers from universities, etc. Further, it is also conceivable that the creation of materials and their evaluation be carried out, and that each individual company be allowed to independently develop the production of items that use the ultra-high temperature material obtained, as well as to develop a low cost production method for the items.

One substantial problem with ultra-high temperature material technology involves the evaluation technology. In particular, regarding composite materials, no sufficient standardization has yet been effected, even for materials at ordinary temperatures. At ultra-high temperatures, all of the methods for measuring the test piece shape, temperature, distortion, and displacement, as well as the heating method, are development elements, but their standardization is necessary in order to build a reliable data base for the materials. This goes beyond the category of R&D by the individual enterprises, and research by Japan as a whole is desirable. In "Research and Development for Advanced Materials with Ultra-High Resistance to Environment," there exists a corresponding topic, and its application to this problem is expected. If Japan actively advances research on the standardized test methods and presents the results to JIS and then to ISO, it will mean a great contribution to international cooperation. As to the established standardized test methods, it is considered that JUTEM should handle them and act as an authorized standardized testing organization, serving as the source point for information issuing while accumulating data on the materials.

6. Future Prospects of JUTEM/JUTEMI

Ultra-high temperature materials development has just entered the period of technical expansion, and the expectations and demands for more ultra-high temperature materials will apparently last for some time while, at the same time, stimulating the progress of the technology. During the upcoming year, JUTEM will put in order those facilities that are required for the above purposes so that they can be offered widely for the use of domestic and foreign workers. In order to be of constant use for advanced R&D, the facilities to be installed must be updated in accordance with the progress in the technology. Although JUTEM is basically public, it still is a joint stock corporation and reinvestment is impossible

unless the investment can be recovered. From the viewpoint of the company, we will try hard to make its operation efficient and, at the same time, we will constantly strive to improve the availability factor by improving the operating conditions, thereby making it more convenient for the users. In addition, the center can serve as a focal point for the international exchange of technologies by allowing many researchers from within Japan and abroad, as well as from various fields, to use the center's facilities. Toward that purpose, JUTEMI will actively carry out not only independent research, but also investigative work on research trends, cooperative research, international symposia, etc., that will be conducive to information exchange by means of data bases, etc.

The keywords for the 1990's include the globalization of environmental problems and the economy, as well as the accompanying international cooperation. In light of this, although the establishment of JUTEM/JUTEMI has been timed accurately, for the purpose of further development toward the 21st Century we are soliciting your demands as well as your assistance.

Advanced Materials for Aircraft Gas Turbine Engines

916C0035C Ube CHO KO-ON ZAIRYO KOKUSAI SHINPOJIUMU in Japanese 15 Mar 91 pp 21-31

[Article by Yukiya G. Nakagawa, Ishikawajima-Harima Heavy Industries Co., Ltd.]

[Text] [English Abstract]: Developments involving high performance jet engines depend on the application of advanced materials and the associated design technology. The short-term improvements of the existing materials have been gradual, but steady. The technology upgrades consists of a combination of process and composition modification in polymeric composites, titanium alloys, powder-metallurgy parts, and single crystal castings. Achieving the goals of the next-generation thrust systems requires "revolutionary" materials, such as heat-resistant polymeric composites, intermetallics and metal/ceramic matrix composites. However, it is expected to prove more difficult to establish those than it has the existing materials, i.e., the specification and control of the composition and production process, secondary processing, the design and life prediction method, and non-destructive examination methods. As an example, alloy and process developments for refractory metal intermetallics are reviewed.

1. Introduction

It is said that materials with high temperature properties that can withstand use at temperatures exceeding 1573 K are required for the thrust systems for the next-generation aircraft. These properties include tensile strength, creep strength, thermal fatigue strength and resistance to surface corrosion. In the foreign development projects set at one time (in 1985), although the

goals were to attain thermal resistance to the stoichiometric combustion temperature (≤ 2273 K) of the fuel and to reduce the specific gravity of the fuel to below 5 g/cm³, they were revised three years later. For the materials related to turbines where the Ni-based superalloys are the mainstream, a temperature increase of about 7 K/year has been achieved so far in alloy and process development. During its progress, since the Ni-based superalloy has, on several occasions, reached maturity, it is impossible for it to reveal a performance which surpasses the above results. Nonetheless, rapid progress has been made on every occasion thanks to a new discovery or invention. The experience accumulated during this period is considered to be of considerable value in the development of substitute materials for Ni-based superalloys. For example, setting the temperature at the turbine inlet at above 2273 K means changing the rate of the heat resistance temperature to about 50 K/year, which, in view of a span of several years, is unrealistic. For the Ni-based superalloys, since a gas temperature exceeding 1673 K has been achieved as a result of the advancement of the air cooling technology, the substitute material has to be of a type that can take advantage of this fact. Moreover, for Ni-based materials that contain a large amount of γ' precipitate, we experienced many accidents during the 1970's due to the lack of ductility. Because of the mutually contradicting natures of the rupture tenacity and the lightweightedness of the material, limiting the specific gravity to below 5 g/cm³ must be revised.

However, it is also clear that a remarkable performance improvement is difficult to achieve through modifications and improvements of the existing materials that have already been studied in great detail. The reason for this is that the materials and their design have matured to an extremely delicate stage and the temperature of use is approaching the melting point of the materials, so that the strength and resistance to environment represent limitations. Accordingly, a remarkable improvement in the engine performance is believed to depend on the application of innovative materials and the development of design techniques able to make full use of these materials. Examples of innovative materials include composites based on heat-resistant polymers, Ti-Al and Ni-Al intermetallics, composites of high melting point materials and intermetallics, intermetallic-based composites, ceramic-based composites, etc. While the expectations for these innovative materials are high due to their individual unique characteristics, it is anticipated that numerous hurdles must be faced before these characteristics can be put to practical use. One thing in common is that it is necessary to achieve a manufacturing process as well as a method for its management, sufficient manufacturing capability (it is desirable to have more than one manufacturer), an appropriate design and life prediction method, an inspection method and quality control technology, and cost competitiveness. For example, the data concerning the mechanical properties and rupture mechanical behavior of the innovative materials are utterly incomplete compared with

those of the existing materials. These properties are extremely different from each other, and the appearance of a rupture mode which has not yet been experienced is predicted. That these properties greatly depend on the manufacturing process is well known, and undoubtedly time and money will be required in order to introduce them to practical use. In order to achieve a timely material supply for a project such as a space plane, management must shift from competition among enterprises and nations to the development of materials under an international division of labor.

In this review, after analyzing the current status and future outlook of materials for engines, the author's group's experiences with the processing technology of high melting point metals and the intermetallics of high melting point metals will be presented. We hope this presentation will be of some use to future research in the field.

2. Engine Materials for the 1990's

As materials for new engines currently under production or that will enter production in the near future, polymer-based composites, titanium alloys, powder metallurgical titanium and superalloys, and cast superalloys, including directionally-solidified (DS) materials, etc., are being used to a large extent. These materials have been steadily modified and improved, although not rapidly, by extending their record of use. Many of these improvements combine the manufacturing process (making the process clean and automated) and the optimization of alloy composition, with the advancement of the manufacturing process and the improvement in strength of turbine moving blades being a concrete example. Figure 1 is a schematic representation of this situation for the past 40 years and a prediction for the future. Of these, the optimization of the process and composition in DS turbine blades (Figure 2 [not reproduced]) that has been advanced during the past 15 years will be presented.

The high speed solidification method is currently the main method employed for the commercial production

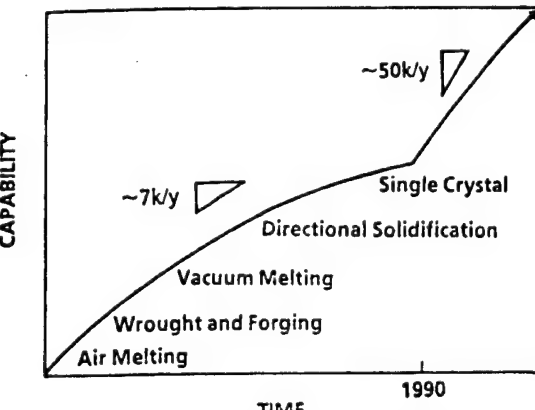


Figure 1. Developments of Ni-based Superalloys for Turbine Blades

of DS blades. A method in which a heat generating agent is employed in some cases has also been tried in Japan, but it is not suitable for the precision casting of long and complicated air-cooled blades. In a large-scale high-speed solidification furnace, use is made of a cluster die close to 400 mm², but the temperature gradient (G) that can be realized in the stationary drawing is 20-30 K/cm. In the DS of a single crystal alloy containing many high melting point alloying metals with strong segregation tendencies, a large temperature gradient is desired in order to decrease the microporosity, make the dendrite texture fine, and suppress the freckle defects. A simple method for achieving this is to reduce the diameter of the heating furnace, with PW's ACF and PR's DS furnace serving as examples of practical furnaces. The effect of a high G value is conspicuous in the high cycle fatigue (Figure 3), which is considered to be due chiefly to the first two reasons mentioned above. The second improvement tendency involving the process is the improvement of the cleanliness of castings, and for the reduction of fraction defects due to the mixing of nonmetallic enclosures such as oxides, the removal of oxide films by electron beam skull melt is adopted for ACF, while isolation from the crucible by high frequency induction melting and the void casting method has been adopted for the RR furnace. A third method is the improvement of the thermal stability (of strength, dimensions and surface reactions) of the casting mold or the core material. In particular, during the past 10 years of the present author's experience, the thickness of the casting mold has been reduced by one-half due to the effectiveness of thin dies in solidification control. A single crystal blade is cast so as to have the lengthwise direction of the blade be within several degrees of the <001> direction. When an improvement in the direction's yield and in the optimization of the characteristic in the direction perpendicular to that of DS are required in the future, it can be anticipated that it will proceed to three-dimensional direction control, and, in fact, single crystal blades are being manufactured by the seed crystal method in the RR furnace. Other recent features include automation by use of computers for the operation of the DS apparatus, control of solidification, analysis of the crystal direction,

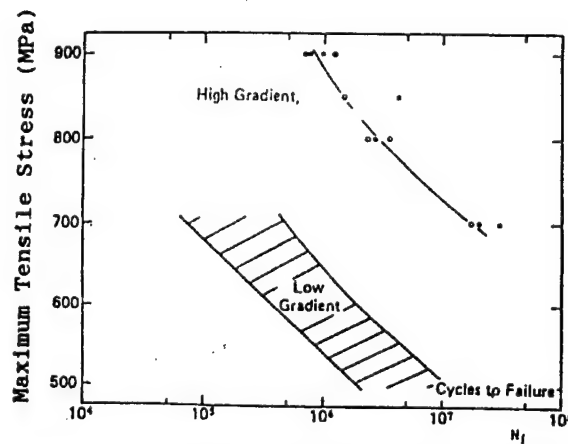


Figure 3. DS Temperature Gradient and High Cycle Fatigue Life (N_f) CMSX-2 at 1143 K

etc., for reasons of advancements in DS solidification analysis and energy conservation.

The compositions of alloys related to the DS blades are shown in Table 1. In the columnar crystal blade, although the composition is basically identical to that of the equi-axed crystal blade, there are many Hf-added Ni-based alloys that contain large quantities of γ'. The first effect of Hf is to prevent the crack that will be generated along the grain boundary of the columnar crystal of hollow thin wall parts during contraction by solidification. Hafnium is enriched between the dendrite arms by solidification segregation to form a relatively large quantity of γ/γ' eutectics, and γ' that contains Hf has substantial strength at high temperatures, while the eutectic phase in the vicinity of the grain boundary is expected to enhance the resistance to solidification cracks. The second effect of Hf is an increase in the creep strength at intermediate temperatures by the ductility in the direction perpendicular to that of DS, which is considered due to a deterrent of the crack propagation on the grain boundary by Hf-enriched γ'.

Table 1. Chemical Composition of Superalloy for Turbine Blade

Alloy	Ni	Co	Cr	Al	Ti	C	Ta	Mo	W	Nb	Zr	B	Other	Reference
MarM200	Remainder	10	9	5	2	.15	-	-	12.5	1	.05	.015		CC
MarM247L	Remainder	9.5	8	5.5	.8	.07	3	-	9.5	-	.015	.015	1.5 Hf	DS
PWA1422	Remainder	10	9	5	2	.15	-	-	12	-	.05	.015	1.5 Hf	DS
PWA1480	Remainder	5	10	5	1.5	-	12	-	4	-	-	-		SC
ReneN4	Remainder	7.5	9	3.7	4.2	-	4	1.5	6	.5	-	-	1 V	SC

CC: common cast alloy; DS: columnar crystal cast alloy; SC: single crystal cast alloy

In contrast to the columnar crystal blade, an alloy has been developed for exclusive use in the single crystal blade. The European and American strategy for the

development of the single crystal alloy is based on logic and experience, as well as on the setting of goals with specific applications. Regarding experiences and goal

setting, it is felt that there is a definite difference between domestic development and the European and American development. As to logic for the determination of composition, the first involves removing grain boundary reinforcing elements, such as C, B, Zr and Hf, all of which, except for C, are elements that lower the solidus curve temperature. Similarly, since O and N increase microporosity and induce the generation of crystals with different orientations, the trend is to lower their content to the maximum extent possible. In order to determine the remaining composition, knowledge of physical metallurgy and trial and error experiences are required. Designs are being undertaken which are well balanced in heat resistance, thermal fatigue strength, phase stability, resistance to environment, specific gravity, and strong element segregation characteristics of DS, and which have a temperature region ("window") that permits solution annealing. Following PWA1480, ReneN4, NASAIR100 (and its improvement Ally100), SRR99 and CMSX-2/3/4 form the second generation single crystal alloy group, the first three alloys of which are being tested for practical use by GE, Garrett, and PR, respectively. The CMSX system is a development by an ingot manufacturer whose application to about 19 kinds of engines, including the TM333B (France), is currently in progress.

3. Engine Materials for the 21st Century

A comparison of the relative capabilities of candidates for advanced materials for gas turbines, as viewed from a longer-term standpoint, is given in Figure 4. The figure covers a fairly wide temperature/strength range, and the selection of a material varies, depending on the purpose of use. Generally speaking, an enhancement of the heat resistant strength is achieved by sacrificing strength. From Figures 5 and 6, which show the material application to next generation engines, it can be predicted that the situation will differ, depending on the kind of engine. In high Mach number military engines (Figure 5), raising the temperature is emphasized, while in high efficiency civil engines (Figure 6), the application of polymer-based composites is extended to make the engines light in weight.

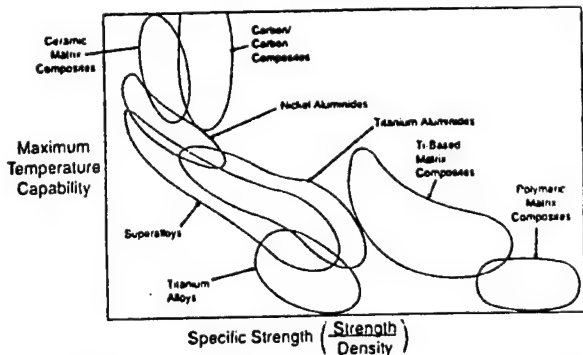


Figure 4. Relative Capabilities of Conventional and Advanced Materials (12)

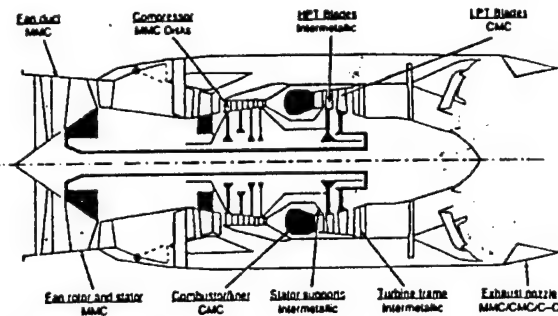


Figure 5. Advanced Materials Applications to Future Military Engines (12)

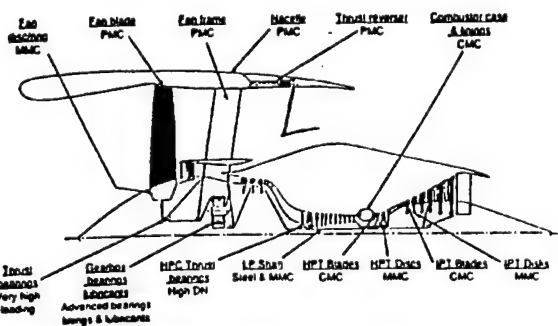


Figure 6. Advanced Materials Applications to Future Civil Engines (12)

The intermetallics have properties that are similar to those of the metallic materials currently being used. In fact, among the superalloys currently in use are materials that contain intermetallics of more than 60 percent by volume. While the Ni-Al and Ti-Al intermetallic compounds make it possible to simultaneously raise the temperature of use and reduce the weight, there are basic defects, such as the lack of ductility and rupture tenacity and difficulty in manufacture. The experimental manufacture of turbine blades and nozzle support rings, etc., employing TiAl has been attempted, with even engine demonstrations having been carried out. It is considered impossible for the temperature of use of these components to be raised to higher than 1273 K, even when the techniques of heat resistant coating are developed, so their application will naturally be limited to parts for the post-stage of compressors in low pressure turbines. On the other hand, the NiAl alloy is being used for the trial manufacture of high pressure turbine blades by precision manufacture, but the limiting temperature of use is said to be 1773 K. Efforts for alloying all of these materials to improve ductility/rupture tenacity has been continued for a fairly long time, but putting them to practical use in the future is considered to hinge upon the development and application of inspection technology and the design of low ductility materials. For parts used in high temperature regions, the use of high melting point materials or intermetallic compounds can also be considered.

A series of advanced composite materials represents an important candidate for next generation engine materials. Polymer-based composite materials have the lowest specific gravity and highest specific rigidity and specific strength (Table 2), but their application is

limited to the low temperature parts of engines, and since the temperature of carbon fiber/polyimide composite materials with high heat resistance is conjectured to be below 550 K, they are not capable of replacing inorganic materials.

Table 2. Properties of Advanced Materials (12)

a) Monolithic					
Property	Superalloys	Ti-Base Alloys	Ti ₃ Al-Base Alloys	TiAl-Base Alloys	Nickel Aluminides
Density (g/cm ³)	8.3	4.4	4.1-4.7	3.7-3.9	5.6
RT Modulus (GPa)	130-210	96-115	120-145	160-176	100-190
Yield Strength (MPa)	300-900	380-1,150	700-990	400-630	200-600
Tensile Strength (MPa)	400-1,700	480-1,200	800-1,140	450-700	400-1,400
Creep Limit (°C)	1,090	600	750	1,000	1,350
Oxidation (°C)	1,090	600	650	900-1,000	1,350
Ductility (%) at LT	3-5	10-20	2-7	1-3	1-3
Ductility (%) at HT	10-20	High	10-20	10-90L1	5-20

b) Composite					
Property	Polymer Matrix Composites	Ti-Base Matrix Composites	Ceramic Matrix Composites		
Density (g/cm ³)	1.7	4.7	3.1		
RT Modulus (GPa)	75-150	140-230	140-230		
Yield Strength (MPa)	-	-	-		
Tensile Strength (MPa)	500-1,000	1,300-1,700	100-200		
Creep Limit (°C)	-	700-900	1,650		
Oxidation (°C)	280-370	650-900	1,650		
Ductility (%) at LT	0.8-1.5	0.8	0.3		
Ductility (%) at HT	0.8-1.5	0.8	0.3		

Metal (intermetallic compound)-based composite materials are expected to exhibit a heat-resisting capability of 800-1270 K. In particular, in comparison to the parts in the above-mentioned temperature range for which Ni-based alloys are currently in widespread use, components in which Ti alloys and Ti-Al interalloy compounds are employed as the parent phase make it possible to reduce the weight by about one-half (Table 2). They are particularly effective as substitutes for parts which are subjected to high stress, and ring-structured rotors, etc., are being trial manufactured.

Although it has been predicted that ceramic-based composite materials can be used up to about 1900 K, many more unsolved problems remain with them than with the metal-based composite materials.

4. High Melting Point Intermetallic Compounds

In accordance with NASA's estimate (Figure 7) of future materials for thrust system structures, it is predicted that high melting point metals will be used for about 10 weight percent, replacing the Ni-based superalloys. Research aimed at the application of high melting point materials, centered around Nb-based alloys, to aircraft

and the space shuttle was active from the 1950's to 1960's. The current interest includes Mo-based alloys, focusing on Nb-based alloys, but the most serious problem is the resistance to oxidation. Among the recent developments in Nb-based alloys that are aimed solely at improving the resistance to oxidation is an example in which an alumina protective film has been successfully formed by the selective oxidation of Al, but the development of alloys that can withstand use for a long time at temperatures exceeding 1600 K remains a problem to be resolved in the future. On the other hand, when attention is shifted to high melting point intermetallic compounds, Nb-based compounds of the A15 structure have been studied for a long time as superconductor materials, and in particular, the formation process into plates and wires will represent a substantial reference for their development into heat resistant materials.

4.1 Conditions for Alloy Design and Problems with Process

As experienced in conjunction with the Ni-based superalloys, the development of the elements (composition) constituting the materials used and that of the process

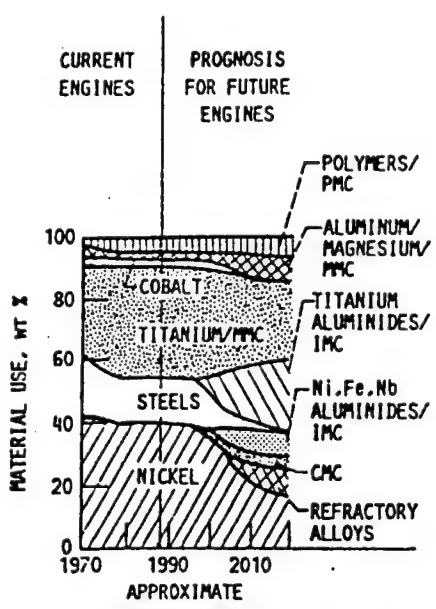


Figure 7. Estimate of Incorporation and Growth of New Engine Materials (1)

for forming them into parts are expected to be advanced side by side. It is desired that an alloy system be selected which will form the basis by compensating for the defects as a material, while, in the process, making positive use of its merits. Therefore, we will try to narrow down the object materials by roughly classifying the required characteristics into four types.

A. Creep Strength—The First Requirement for Heat Resistance

The deformation occurring during the use of many gas turbine parts is designed to fall within 1 percent, and this basis will not be changed in the future. For the γ/γ' dual phase texture of the Ni-based superalloys, this condition is conveniently satisfied. For many intermetallic compounds (Ni, Ti, Fe, Al), the 1 percent distortion at higher than 700°C occurs during the initial creep. Figure 8 shows the maximum service temperature evaluated at $10^{-9}/\text{sec}$ (1 percent distortion occurring 1,000 hours later) under 150 MPa as relative to the melting point of the material. It can be clearly seen that the creep resistance is larger for a crystal lattice with a higher atomic packing factor. In addition, regular lattices are more advantageous, and the multiphase effect is not negligible either. On the other hand, Figure 9 compares the creep rupture strength for the noted aluminide intermetallic compounds and other commercially available alloys. In contrast to the fact that the former is not particularly high relative to the existing Ni-based superalloys, even after allowing for the difference in specific gravities, it can be seen that the Nb-based alloys have a conspicuously high creep strength.

B. Thermodynamic Phase Stability in Alloy Design

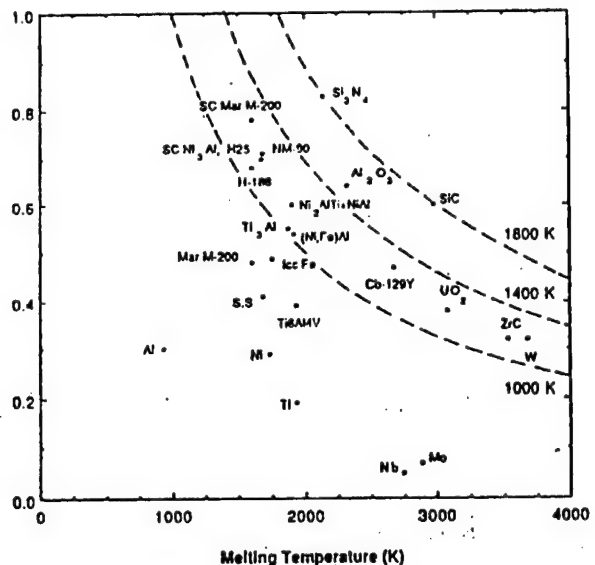


Figure 8. Service Temperature ($de/dt = 10^{-9}/s$ at 150 MPa) versus Melting Point (2)

The composition design of many of the heat resistant alloys is centered around the effort to obtain resistance to oxidation, and no exception is made for the substitute materials. Although a plan exists to gain creep strength by compounding Ti_3Al , NiAl and TiAl, all of which have excellent resistance to oxidation, this should be clearly differentiated from the γ' reinforcement of the Ni-based alloys. It is difficult to obtain thermodynamic stability through the dispersion of reinforcing phases that possess extremely different physical and chemical properties, which currently represents the mainstream approach to the problem. Although a technique is also being attempted to suppress the rate of diffusion reaction by providing a surface coating of zirconia, etc., to the reinforcing phase, it is insufficient when applied at high temperatures, which is our concern.

C. Discussion of Ductility and Rupture Tenacity

The low ductility at room temperature of intermetallic compounds is not an absolute property, but this behavior varies depending on the compound system. For example, it has been reported that the interstitial impurity elements and microcracks introduced by mechanical processing are the causes of the low ductility, but, more recently, that polycrystalline NiAl exhibits ductility at room temperature through an improvement of the process. As is seen in the effect of B in Ni₃Al, there are many unsolved points concerning ductility, so the selection of the alloy should not be made hastily because of the above report. Although some Ni-based superalloys have been put to practical use even when the ductility at room temperature is only about 2 percent, what is important is the rupture tenacity. Intermetallic compounds are effective because they enable damage tolerance design and

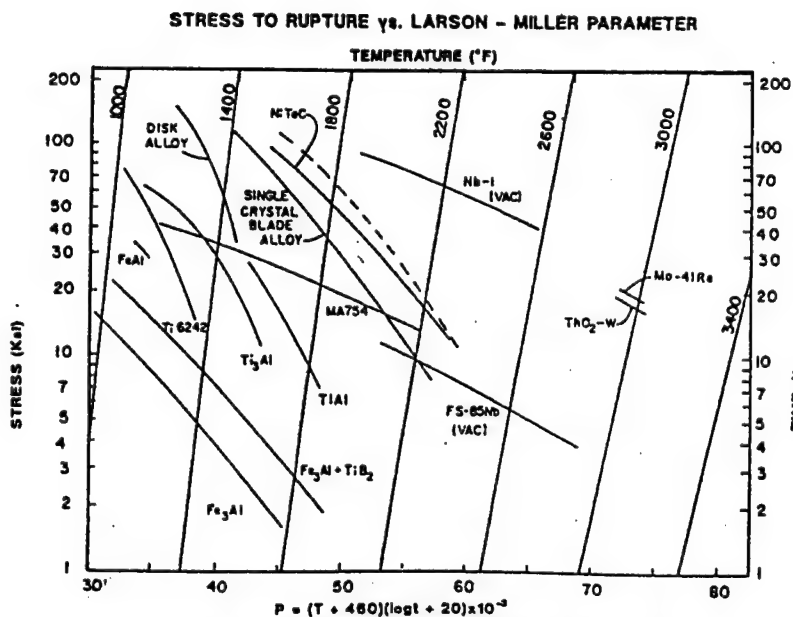


Figure 9. Creep Rupture Lines for Intermetallics (2)

excellent heat transfer, which is a characteristic of metals, to be utilized, as well as the brittle-to-tough transition temperature.

D. Discussion of Anisotropy

We have recognized the significant role of the process in ductility, but similarly to our experience with columnar crystals and single crystals of Ni-based superalloys and particle dispersed reinforced (ODS) alloy members, the anisotropy of the mechanical properties becomes more conspicuous with a greater contribution of the process. Further, in intermetallics with less symmetry, the above trend is anticipated to be accelerated since the slip system during hot working can also be constrained.

Representative examples of the metallic compounds that are promising for structural members at high temperatures are summarized in Table 3 along with the melting points and crystal structures. That the table contains many Al compounds that bring about slight nonmetallicity is due to the fact that those with slight resistance to oxidation and excellent crystal symmetry have been selected, although they are not adequate enough to be put to practical use. Among them, those that show reverse temperature dependence and those with high melting points, as shown in Figure 8, are desirable from the viewpoint of strength at high temperatures, but it is obvious that the Nb- and Mo-based high melting point materials will become the focus when the application to turbines at temperatures

exceeding 1873 K is considered. Of the high melting point alloys, since Nb alloys have low specific gravity, as well as excellent ductility and thermal conductivity, some of them are applied to the high temperature parts of turbines through coating. In order to surpass the Ni-based superalloys, it is necessary to improve the resistance to oxidation and creep strength, and research in this area has been very active recently. As for resistance to oxidation, two alloy systems are being developed. One is a group of alloys including Ti-W, Ti-Mo and Ti-V, which have resistance to oxidation two orders of magnitude greater, but do not possess sufficient strength at high temperatures to be used as the material for the turbine moving blades. The other is an alloy group which has resistance to oxidation that is three to four orders of magnitude greater, but whose ductility is extremely low, and which is obtained by alloying a large quantity of Cr/Al. Table 4 presents data on the oxidation rates of the Nb alloys at 1273 K and 1473 K. The metals Cr, Mo, Ti, V and Zr are effective for improving the resistance to oxidation, and the alloys obtained by adding Al to the binary systems of these elements are very much improved. It is anticipated that various intermetallic compounds exist among many of the alloys listed in Table 4. According to other research, it is recognized that Nb-15Fe-25NbAl₃ has a minimum oxidation corrosion rate, i.e., 0.9 mm/100 hours, with the formation of a protective film due to the presence of intermetallic compounds considered to be the reason for this.

Table 3. High Temperature Intermetallics

Compound	Melting Point (°C)	Crystal Structure
Ni ₃ Al	1385	L1 ₂
TiAl	<1500	L1 ₀
NiAl	1638	B2
TiAl ₃	1350	DO ₂₂
NbAl ₃	1750	DO ₂₂
Nb ₃ Al	1960	A15
MoSi ₂	2020	C116
Nb ₅ Si ₃	2484	D8

Table 4. Oxidation Resistant Nb Alloys (3)

Alloy Composition, Wt. Pct.	Avg. Oxidation Rate, mg/cm ² /hr.	
	1000°C	1200°C
Nb-14Al-15Co-10Fe-4Mo-1Ce	0.01	0.05
Nb-25Ni-9Fe-10Al	0.01	0.04
Nb-19Cr-15Co-10Al	0.01	0.06
Nb-15Ni-10Cr-10Al-4W-2Ce	0.02	0.05
Nb-19Al-10Fe	0.03	0.09
Nb-20Al-15Cr	0.03	-
Nb-24Fe-20Al	0.04	0.08
Nb-20Cr-15Al-2Ce	0.05	0.14
Nb-15Al-10Cr	0.05	-
Nb-26Cr-5Al-2Ni	0.05	0.16
Nb-10Cr-10Al-4W	0.05	0.17
Nb-15Mo-15Al-2Ce	0.05	0.45
Nb-20Fe-9Al	0.08	0.20
Nb-20Fe-15Al-5Mo	0.08	-
Nb-20Mo-20Al	0.08	0.62
Nb-10Ni-10Al-5Fe	0.09	0.15
Nb-10Fe-6Al-2B	0.09	0.34
Nb-15Mo-14Al-10Zr-4W-1B	0.12	0.32

For comparison, Fe-Cr-Al oxidizes at 0.05 mg/cm²/hr at 1000°C.

Oxidation rates <0.1 considered outstanding; <1.0 is very good at 1200°C.

The Nb alloys are reinforced by the employment of a solid solution of the high melting point metallic elements W, Ta and Mo (Table 5). The C-103 alloy plate is used for the combustor liner by silicate coating. Thanks to the advancement and application of the power metallurgical process, a use limit which is higher

by 533 K than that of the Ni-based superalloys is said to be made possible. In addition to reinforcing, alloys obtainable by reinforcement through the dispersion of intermetallic compounds (Nb₃Al and NbFe₂) or an oxide (TiO₂) are being studied by the strengthening of intermetallic compounds.

Table 5. Chemical Composition of Nb Alloys (9)

Alloy	Major Alloy Elements, W/O							Other
	W	Mo	Ta	Ti	Zr	Hf	V	
Cb-1	30				1			0.60 C
B-88	28					2		0.07 C
VAM-79	22					2		0.07 C

Table 5. Chemical Composition of Nb Alloys (9) (Continued)

Alloy	Major Alloy Elements, W/O							
	W	Mo	Ta	Tl	Zr	Hf	V	Other
Cb-132M	15	5	20		1.5			0.10 C
AS-30	20				1.0			0.10 C
F-48	15	5						
SU-31	17					3.5		0.10 C
WC-3009	9					3.0		0.10 C
Cb-752	10				2.5			
SCb-291	10		10					
C-129 Y	10					10		0.10 Y
B-66		5					5	
AS-55	5				1.0			0.20 Y
PWC-U					1.0			0.10 C
Cb-753					1.25		5	
C-103				1.0		10		
B-33							5	
D-14					5			
D-36					10	5		
Cb-1Zr								

4.2 Advancement of and Problems with Processes

A. Ingot Manufacturing

The ingots of high melting point alloys and intermetallic compounds are manufactured by electron beam melting, vacuum arc melting (consumable electrode system), or plasma beam melting. Since they are active metals, they react strongly with the crucible, and thus a water-cooled copper crucible or skull formation is generally used. Problems related to the manufacturing include the removal or control of impurities in the melt base material, the component adjustment of metallic (Al, etc.) elements with high vapor pressure and, especially in single bodies of intermetallic compounds, the securing of stoichiometric composition and the introduction of cracks due to contraction upon solidification. In the Nb alloys treated under a high vacuum, it is possible to reduce the concentration of impurities, including Nb oxides, by repeating the electron beam melting. It is advantageous to add high melting point alloying elements or low vapor pressure elements by electron beam melting. The adjustment of components of alloys that contain large amounts of low melting point metals or high vapor pressure metals, such as Al and Si, is frequently done during remelting in a vacuum furnace that employs consumable electrodes or during the sintering of powder materials. Note, however, that when melting in a vacuum is conducted again during the post-stage, it is necessary to carry out extra component adjustment that takes evaporation into account during the ingot manufacturing stage. During arc melting, the alloying elements are dispersed uniformly into the ingot, but the method is not as effective for controlling impurities.

B. Powder Processes

In order for a powder to be used as a powder metallurgical raw material, generally a fine texture, small powder grain size, uniform composition distribution, high cleanliness, no fluctuation in composition, etc., are required, but the process also has to be appropriate for the alloy type. In active metals such as Nb alloys, use is made of a mechanical method (grinding) or a chemical reaction. A grinding method is one which granulates a raw material ingot by impacting it mechanically with a stamp mill or ball mill, and is appropriate for relatively brittle materials, such as intermetallic compounds. However, the Nb powder obtained by the plain ball mill method contains oxygen levels exceeding 3,000 ppm and its processability is very poor. Powders are currently obtained by the hydride-dehydride process (HDHP), which utilizes a reduction reaction by hydrogen, and in this case the oxygen concentration can be suppressed to approximately 1,000 ppm.

With the HDHP method, a hydrogen compound is generated by annealing ingot pieces that have been cut into appropriate sizes in a high temperature hydrogen furnace. Since the Nb hydride is brittle, it is dispersed into irregular small pieces, smaller than 25 mm, during cooling to room temperature. The small pieces are then mechanically ground in a noble gas to give them the desired grain size distribution, and are reduced to metallic Nb by dehydration processing in a heated vacuum furnace. A typical relationship between the impurity concentration and grain diameter of HDHP-Nb powders is shown in Table 6. Since their main application so far has been to superconductive materials

and their oxygen content is relatively high, they are not suited for powder metallurgical members of structures which require better processability and higher impact value. In contrast, the impurity levels in powders manufactured by the atomizing method, employing electron beams, are shown in Table 7, and the ductility of the heat resistant Nb alloys that use the above-mentioned powders exceeds 15 percent over the entire temperature region. In the electron beam atomizing method, an ingot solution is dropped on a rotating water-cooled copper disk to atomize it, and these atomized particles are then solidified by quenching. The intermetallic compounds, carbides and nitrides are also finely and uniformly dispersed.

Table 6. Impurity Levels of HDHP Nb Powder (9)

Element ¹	Size Fraction, mesh		
	-60+200	-200+325	-325
C	100 ppm	100 ppm	100 ppm
O	800 "	1000 "	2000 "
N	100 "	150 "	150 "
H	50 "	50 "	50 "
Al	50 "	50 "	50 "
Fe	200 "	200 "	300 "
Si	100 "	100 "	100 "
Ta	2000 "	2000 "	2000 "

¹The impurities' contents listed are maximums.

Chemical analysis of hydride-dehydride niobium metal powder

Table 7. Impurity Levels of EB-Atomized Nb Powder (9)

Element	Content (ppm)
C	<50
Fe	<50
Mo	<50
Ni	<20
Ta	<2000
W	<200
Zr	<100
H	<5
N	<50
O	<100

Chemical analysis of spherical niobium metal powder.

C. Examples of Powder Metallurgy for Superconductive Materials

Superconductive materials are frequently found among the A15 structure compounds, such as Nb₃Sn and Nb₃Al. Powder metallurgical methods can roughly be divided into the method which starts with a powder alloyed in advance, and one which causes a reaction by infiltrating a liquid metal into a presintered material of Nb powder. In the former method, it is difficult to realize

a densification process which achieves the theoretical density, while in the latter it is difficult to control the stoichiometric composition.

The results of plotting the achieved density versus temperature for both sintering after CIP of a Nb₃(Al, Ge) alloy powder and densifying by hot pressing are shown in Figure 10. The CIP is carried out for 2 hours under a pressure of 42 kgf/mm², while the sintering lasted for 1 hour. For hot pressing, a jig made of graphite is used under a pressure of 0.4 kgf/mm². Plastic fluidity by hot pressing is generated at about 1623 K (0.76 times the melting point of the alloy). Complete densification is considered possible by giving HIP processing after molding. The infiltration method causes an intermetallic compound to form basically by utilizing a diffusion reaction. When Sn is infiltrated and diffused in Nb, there is the possibility of creating Nb₆Sn₅ and NbSn₂, in addition to Nb₃Sn, but these have a critical temperature of 2 K, which is not acceptable. An experimental example of forming an Nb alloy tape in which Nb₃Sn fibers are dispersed will be presented. The pre-sintered body of Nb is manufactured by sintering an HDHP powder of -270 mesh (53 µm) after cold rolling. A green tape of about 0.55 mm in thickness is made by using (5 rpm) a grooved roller of about 50 mm in diameter and by subjecting it to 3 minutes of sintering under 4 x 10⁻⁵ Torr and 1253 K. A material is obtained with a porosity of approximately 25 percent. The sintered tape is thrown into an Sn bath of 1133 K for 3 minutes, and is again subjected to a cold rolling of 75 to 85 percent. The formation of Nb₃Sn is accomplished by causing a final reaction for 3 minutes at 1223-1248 K, and fibers with cross sections of 30 µm x 50 µm are dispersed in the Nb base material. The important steps in this process are the cold rolling after Sn infiltration and the temperature selection for the accompanying Sn bath. For the formation of Nb₃Sn without subjecting the sample to rolling, prolonged heat treatment is required. For example, even after heat treatment for 16 hours at 1273 K, unreacted Sn remains and the tape is very brittle. Treatment in the Sn bath is possible at temperatures above 623 K, and reactions between Sn and the above-mentioned three kinds of intermetallic compounds become possible at this time at the respective temperatures (see Figure 11). When the strength is low, the amount of unreacted Sn is large, with the unreacted Sn becoming fluidic under rolling during the post stage and seeping out of the sample. With the infiltration at 1123 K, the major portion is formed into Nb₆Sn and is cured, thereby preventing its flowing by rolling.

In superconductive materials, it is said that the diameter of the fibers of intermetallic compounds should be less than 10 µm. The diameter of the fibers and their dispersed conditions strongly depend on the gap of the green tape. However, control of the gap is advantageous in the greens of the bulk (rod-like) material obtained by CIP. The manufacturing of Nb-Nb₃Sn wire material obtained from a 4.8 mm diameter CIP rod is shown in Figure 12. The CIP is carried out using a rubber mold

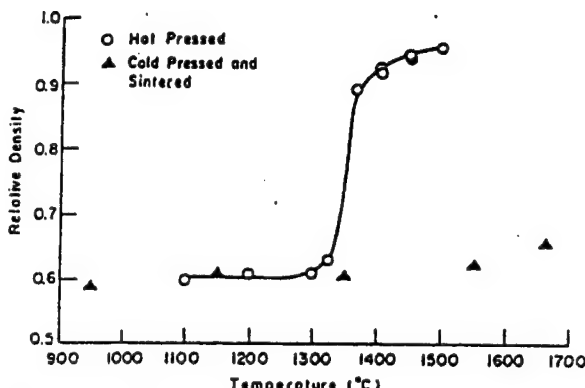


Figure 10. Relative Density of $\text{Nb}_3(\text{Al}, \text{Ge})$ Compacts for Hot Pressed and Cold Pressed + Sintered Samples As a Function of Temperature (S)

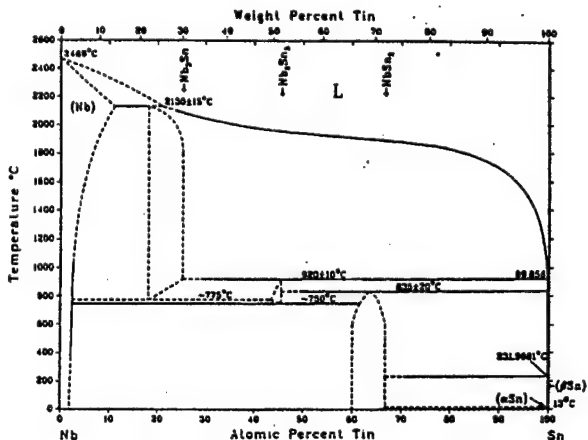


Figure 11. Nb-Sn Phase Diagram

under a pressure of approximately 20 kgf/mm^2 , and the sintering is carried out in a vacuum at 1523 K. The Sn infiltration is carried out by low temperature treatment, and the surface is cladded with Ta. By reducing the cross section by the ratio of 4000:1 using rolling and drawing, a fine wire of the composite material is obtained. The cross section of the Nb_3Sn fibers obtained becomes about 1 μm . Three important points are, first, that the control of the gap (i.e., the fiber diameter) is possible by the CIP and sintering conditions, second, that no Sn seepage occurs due to the cladding, and, third, that the workability is satisfactory since no cured layer results from the Sn bath treatment at low temperatures.

D. Quenching Effect in Nb_3Al

Research for obtaining workability by the active utilization of the quenching effect has been reported recently. The degree of solid solution in Nb shown in the state diagram is about 8 at percent around room temperature. However, when the drops of alloy solution are quenched

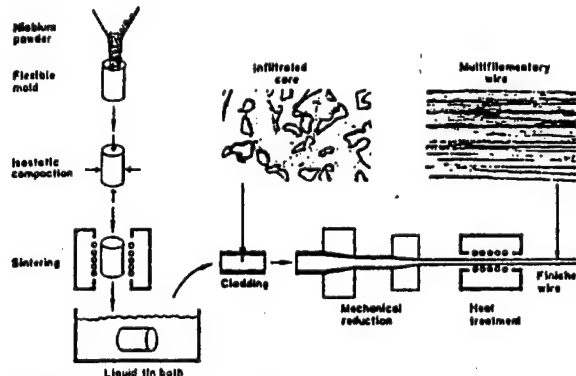


Figure 12. Infiltration Process for Production of Multi-filamentary Superconducting Wire (S)

(at 10^4 to 10^6 K/sec) by the anvil method, as shown in Figure 13, it is possible to obtain a quasi-transition solid solution of the A-2 structure (BCC) Nb up to 27 at percent. In this state the sample naturally exhibits satisfactory malleability and, when pulverized by HDHP, it becomes a promising material. The transformation of the sample to Nb_3Al after molding is possible in the 983-1133 K range.

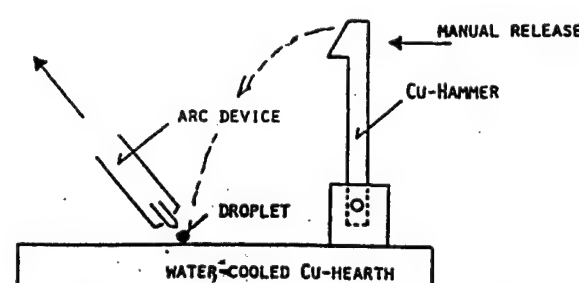


Figure 13. Hammer and Anvil Method (7)

E. Existing Processes for Nb Superalloys

The Nb alloy powder metallurgical process for high temperature structures is carried out centered around HIP processing. The example of the C-103 alloys will be presented below. A raw material powder placed in a carbon steel pipe, degassed in a vacuum, is thrown in an Ar glow box (purged Ar for 24 hours), and after densification on a vibration table, it is degassed at room temperature for 1 hour at 80 millitorr, and again at 673 K for 16 hours, then sealed. The first HIP processing is applied for 3 hours under a pressure of 10.5 kgf/mm^2 and a temperature of 1533 K. After dissolving the carbon steel vessel using an acid, the reacted layer on the material surface is removed with a mixed solution of $\text{HNO}_3\text{-HF}$, a second HIP treatment is applied at a temperature above 1873 K, then the sample is formed into a billet. Many of the Nb alloys possess excellent hot

processability, regardless of whether they are cast ingots or powder billets. However, note that, in view of the recrystallization temperature, the control of crystal grains which is analogous to that of other alloys is needed. In high temperature processing, for the purpose of preventing oxidation, billets are coated in an Al-10Cr-2Si bath, then a surface film (0.1-0.05 mm) is formed by diffusion, or a glass coating is applied as the preprocessing.

4.3 Processes for Forming Single Crystals

In the Ni-based superalloys, columnar crystals, single crystals and ODS alloys with controlled crystal orientation have been developed in order to improve the ductility or thermal fatigue life. Even for intermetallic compounds with low symmetry or high melting point materials that contain large quantities of such intermetallic compounds, it is necessary to consider uses that take advantage of the above-mentioned characteristics. For these purposes, two methods can be considered, i.e., the method in which secondary recrystallization is utilized, and that in which directional solidification (DS) is employed.

A. Method Utilizing Secondary Recrystallization

In secondary recrystallization, equi-axed crystal grain growth occurs in which a large number of nuclei of primary recrystallization are generated all over the member and are then gradually formed into coarse grains, and anomalous grain growth in which there are fewer nucleus generation sites, but a small number of specific grains grow explosively by taking in many other primary crystal grains. In order to form columnar crystals or single crystals, it is reportedly necessary to disperse an appropriate second phase in the member and to subject the member to hot processing in advance to generate the anomalous grain growth. As was also experienced during the recrystallization of particle dispersion reinforcing-type alloys of the Ni-based superalloys, the problems with the process include the disappearance of processing distortion prior to reaching the recrystallization temperature and maintaining the second dispersed phase by preventing it from becoming unstable (forming a solid solution or becoming coarse). According to the method for manufacturing Mo single crystals as set forth by the Research Institute for Metallic Material Technology, a powder metallurgical material doped with approximately 0.01 at percent of Ca or Mg (dispersed CaO or MgO) is formed by sintering, and a giant single crystal plate of $40 \times 20 \times 200 \text{ mm}^3$ is obtained by heating a sample with a large distortion (greater than 60 percent) by rolling, etc., at a temperature exceeding 2473 K (Figure 14).

B. Single Crystals by DS

The casting process for high melting point alloys hinges on the success of the future development of ceramics for casting molds and cores. In particular, the melt process is considered to be solvable by the use of electron beams and plasma beams and the formation of skull. Ti precision casting, which has already been put to practical use, will serve as a valuable reference when considering

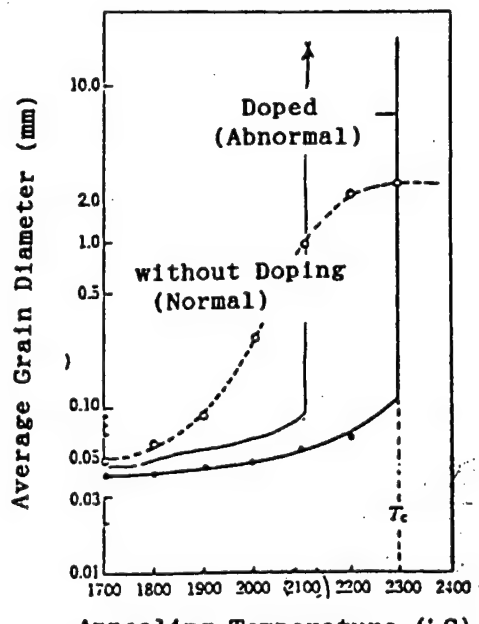


Figure 14. Abnormal Grain Growth of Mo Plate (10)

casting mold materials for general active metals. There are examples, although for a short time, of the use of Y_2O_3 slurry, BeO, BN, CaO, etc., including their experimental utilization.

Single crystal rods of high melting point metals have been manufactured by DS in the past. The Chochralski method, which is used widely for semiconductor substrate crystals, will not be appropriate for active metals unless a crucible becomes available which can withstand melt holding for a long time. Accordingly, the floating melt zone method is generally employed utilizing electron beams, high frequency waves and lamp image furnaces. Since the floating melt zone is supported by the surface tension of the molten body, the rod diameter is limited. From the relationship between the specific gravity and the surface tension, the typical diameters of the single crystal rods of Mo and W obtained by the vertical floating melt zone method are 18-20 and 10-12 mm, respectively.

Regarding intermetallic compounds, there is a report concerning the experimental manufacture of single crystals of MoSi_2 . After manufacturing a rod, 7 mm in diameter, by making a raw material containing Si 2 mol percent greater than that of stoichiometric composition, the floating melt zone DS is carried out using an image furnace with a halogen lamp, as shown in Figure 15. The growth rate is 6-10 mm/h, and the orientation can be controlled by the use of seed crystals. The MoSi_2 grown contains a slightly higher (approximately 0.9 at percent) amount of Mo than that of the chemical equivalent, and the composition in the length direction has a uniform distribution.

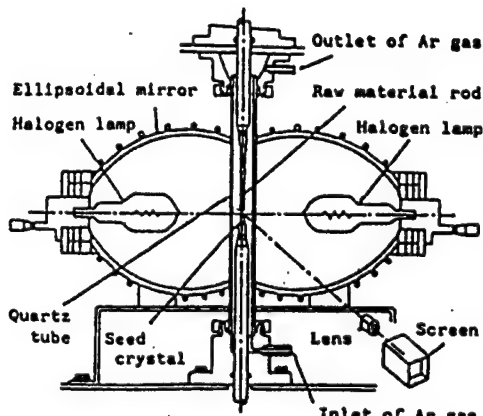


Figure 15. Lamp Image FZ Furnace (12)

5. Conclusion

The improvement in performance of future jet engines depends on the application of new materials and the development of design techniques that can take full advantage of the new materials. Regarding the relatively near future, steady advancement is anticipated by improving existing materials. Polymer-based composite materials, new titanium alloys, powder alloy metals, next generation single crystal alloys, etc., are being employed in a widespread manner, and the development of the manufacturing processes and the optimization of compositions are being advanced side by side. On the other hand, since the goals already set for the thrust systems of the 21st century far exceed the capability limits of existing materials, it will be necessary to develop innovative materials which will enable the weight to be reduced and the service temperature to be elevated to a dramatic extent. As candidates for such materials, one may mention intermetallic compounds and heat-resistant polymer-based, metal-based and ceramic-based composite materials, etc. However, before they can be put to practical use, the following has to be established:

- (1) Specification control of composition and manufacturing processes,
- (2) secondary processing (mechanical, joining and repairing),
- (3) ample supply systems,
- (4) design data base, design method, and life estimating method,
- (5) nondestructive inspection method, and
- (6) price/capability evaluation method.

In this review, we have probed the current status and problems with the processes, keeping in mind the utilization of reinforced members for heat-resistant structures of high melting point metallic alloys and intermetallic compounds. As for commercial alloys, the process has been established based on powder metallurgy and its results will serve as a valuable reference for the application and expansion to intermetallic compounds. In the production of the intermetallic compounds themselves

and the manufacturing of composite materials, the experiences gained in dealing with superconductive materials will apparently serve as an effective source of information. It is much desired that a method utilizing solidification be developed around the future secondary technologies for refractory materials. However, it seems that we cannot afford to detour this method in the practical use of materials. Although the oxidation resistant coating treatment process is an important task in connection with practical applications, we did not touch upon it since too little information is available. Considering the advancement of the process technology and the adaptability of the materials to the processes, the data concerning the texture, strength and corrosion resistance should be understood as contributing to further improvement.

References

1. Stephens, J.R., et al., "Status and Progress for Alternative Engine Materials," SUPERALLOYS, 1988 p 183.
2. Dimiduk, D.M., et al., "Directions in High Temperature Intermetallic Research," "High Temperature Ordered Intermetallic Alloys III," MRS SYMP PROC, Vol 133, 1988 p 349.
3. Loria, F.A., J OF METALS, July 1987 p 22.
4. Moriyama, et al., PROC MET SOC JPN, Vol 16 No 8, 1977 p 468.
5. Pickus, M.R., et al., "A15 Multifilamentary Superconductors by Infiltration Process," "Filamentary A15 Superconductors," Plenum, 1980, p 331.
6. Schulze, K., et al., J OF THE LESS COMMON METALS, Vol 139, 1988 p 331.
7. Himmelblau, C., et al., "Mechanical Properties of HIP Columbium C-103 Alloy," PROG IN POWDER METALLURGY, Vol 79, 1983 p 525.
8. Condliff, A.F., MPR, July/August 1987, p 539.
9. Fujii, METALS, Feb 1985 p 9.
10. Degawa, BOUNDARY, Jun 1988 p 7.
11. Tabata, et al., J MET SOC JPN, Vol 52 No 11, 1988 p 1154.
12. Johnson, A.M., et al., "Application of Advanced Materials to Aircraft Gas Turbine Engines," AIAA 90-2281, 26th Joint Propulsion Conference, July 1990.
13. Ota, et al., "Formation of Single Crystals of Ni-Based Superalloys," PROC MET SOC JPN, Vol 24 No 6, 1985 p 462.
14. Dix, D.M., et al., "Aircraft Engine Technology Gets a Second Wind," AEROSPACE AMERICA, July 1990 p 36.

Trends of Research, Development in Carbon/Carbon Composites

916C0035D Ube CHO KO-ON ZAIRYO KOKUSAI SHINPOJIUMU in Japanese 15 Mar 91 pp 45-56

[Article by Shiushichi Kimura and Eiichi Yasuda of the Faculty of Engineering, Tokyo Institute of Technology]

[Text] [English abstract]: Carbon fiber reinforced carbon matrix composites (C/C composites) have been studied since 1971, and are already being applied as airplane and space materials. They have recently attracted attention as strong candidates for the first wall material of fusion reactors.

In this paper, the fundamentals of C/C composite fabrication are mentioned, and the importance of the fiber/matrix interface is described by reporting results. The authors will refer to the importance of microstructural control, which is the major parameter of the C/C composite as a tailored material. Finally, the research and development trends in C/C composites are described, including those from the most recent international conferences held in France and Japan in 1990.

1. Introduction

The carbon/carbon composite material, also termed a C/C composite, is an all-carbon advanced composite material that employs carbon fibers for reinforcement and whose matrix also consists of carbon. Thirty years have passed since carbon fiber was developed as a reinforcing fiber, and carbon fiber is becoming a household name with regard to leisure items. In addition, nearly 20 years have passed since research on C/C composites, which has been aimed at making active use of the excellent characteristics of the carbon fiber, was started, and the material is being actively used, generally in invisible places, such as tiles for the space shuttle and brakes for the Concorde, air buses, etc. The C/C composite is lightweight, and since it has excellent high temperature strength (the strength continues to increase up to temperatures exceeding 2000°C) and a low coefficient of thermal expansion, it has good potential for being used as a high temperature structural material in addition to the aerospace materials, with its use in the experimental manufacture of gas turbines serving as an example. Further, it is becoming possible to obtain materials with the high thermal conductivity of 400 W/mK, and its use as the first wall material of the nuclear fusion furnace, which requires a low Z material, is being examined. In addition, it has already been used in transport plates, spacers, extrusion pads, etc., in the glass industry, as well as as electric furnace material for high purity materials in the semiconductor and furnace industries. However, C/C composites have problems with resistance to oxidation, as is generally the case with carbon materials. When a protective coating is applied, thermal stress is generated due to the large difference in the coefficient of thermal expansion between the coating material and the C/C composite, and, concerning this

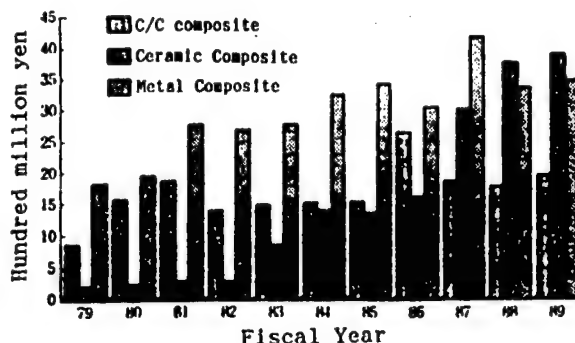


Figure 1. Changes in Research Funds for Three Different Kinds of Composites in the United States

point, a solution is being sought through the application of functionally gradient materials.

Although knowledge of the current status of research in this field in the United States is not accurate, a partial report on research funds is available.⁽¹⁾ As shown in Figure 1, the U.S. DOD-related research funds for C/C composites during the past 10 years have been stable, ranging from ¥1.5 billion to 2.5 billion. This sum is by no means large compared with the funds for other metallic or ceramic composites, but it is conspicuous as the funding for one kind of fiber and matrix material.

The C/C composite is thought of as a military material in the United States and France, and the relevant research results, etc., are available only to American citizens. Moreover, there are many cases in which the characterization of samples has not been made clear and in which tests on oxidation resistance have been carried out without having been announced, even within the United States. We understand that these circumstances are hampering the development of the C/C composite in the United States. Available pieces of information are also extremely limited, which naturally represents an impediment to us in Japan. Under these circumstances, the current status is that the published data are being supplied mainly by West Germany and Japan, and that South Korea, China and the Eastern European countries are going to be joining the group. With this background, two international conferences related to carbon were held in 1990. One was Carbone '90 Paris, held in July in Paris, France, and the other was Carbon '90 Tsukuba held in November in Tsukuba, Japan. There were 19 reports related to C/C composites at the Paris conference and 21 at the Tsukuba conference, nearly the same number. However, there were five items related to oxidation resistance at the Paris conference, while at Tsukuba, there were seven related to the nuclear fusion furnace, reflecting the interest of each country.

In this paper, we will present the latest research trends and problems related to the manufacturing processes and capabilities of the C/C composite.

2. Carbon Fiber

The present carbon fiber is a material born and grown in Japan, based on technology independently developed in Japan. The carbon fiber for which polyacrylnitrile (PAN) is employed as the raw material was reported in 1961 by Shindo of the Government Industrial Research Institute, Osaka, while "Thermoron H" and "Carboron Z" were put on the market in 1968 as high strength carbon fibers by Yamada, et al., of Tokai Carbon Co., Ltd., and Nippon Carbon Co., Ltd., respectively. Recently, strength reaching as high as 7 GPa has been achieved, and high elasticity products have attained the 600 GPa level.⁽²⁾ The technology in Japan is attracting worldwide attention, and Japan's share of the world carbon industry is 60 percent, as shown in Figure 2 which illustrates carbon fiber enterprises worldwide.⁽³⁾ Carbon fibers in which pitch was used as an inexpensive raw material were reported by S. Otani (Gumma University) in 1963. In 1976, a pitch-based carbon fiber with high strength and a highly elastic mesophase system was placed on the market by UCC of the United States. Recently, high performance products have been developed and put onto the market by oil companies and steel manufacturing companies in Japan. Although an ultra-high elasticity of 850 GPa has been reported, the product is not yet satisfactory in compressive strength and ductility, so research is being conducted in this direction. In Figure 3, the current status of the mechanical properties of carbon fibers is shown.⁽⁴⁾ In the figure, the number within parentheses indicates the ductility. The price of high performance carbon fibers is high, ranging from ¥ 5,000/kg to ¥ 100,000/kg. The key to the popularization of carbon fibers is the general purpose carbon fiber, and the properties of carbon fibers of the general purpose grade are currently being rapidly improved. However, a dilemma seems to exist in that the price of the carbon fibers is not coming down, even though the raw material depends on the inexpensive material pitch. At the recent meetings of academic societies, many CF related reports have been presented, but they will be omitted here due to lack of space.

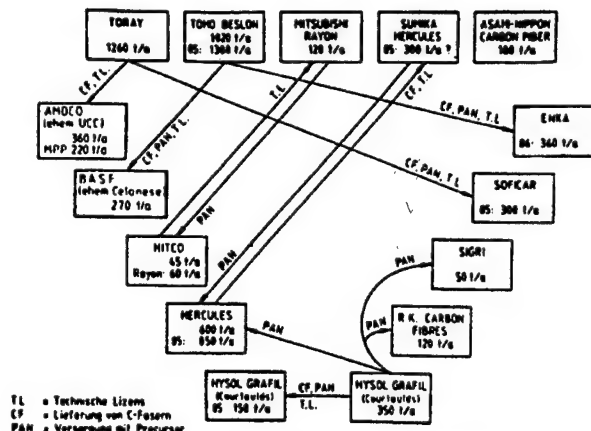


Figure 2. Major Carbon Fiber Manufacturers in the World and Their International Relationships

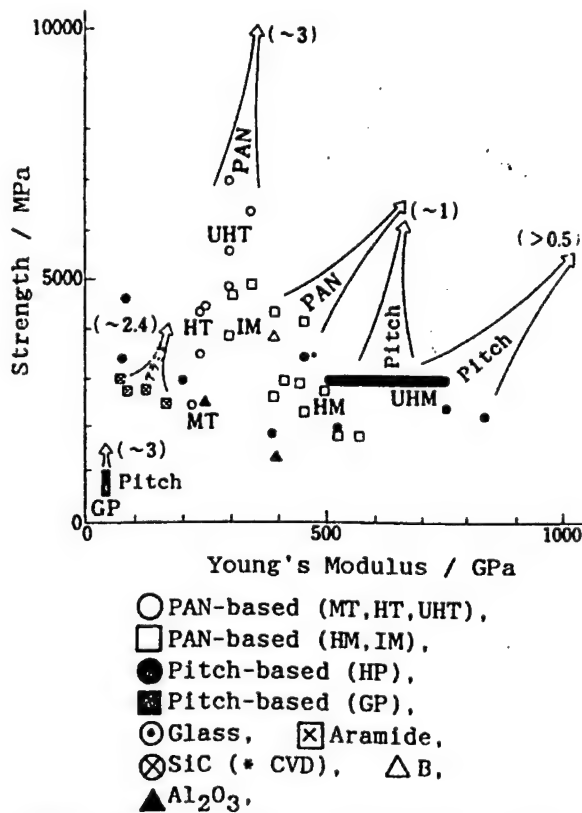


Figure 3. Trends in Mechanical Properties of Carbon Fibers

3. Compounding and Matrix Structure

The C/C composite manufacturing methods are sketched in Figure 4.⁽⁵⁾ Since these methods are not limited to single processes (arrows pointing to the right), often composite processes and the reprocessing of single processes (arrow pointing to the left) are employed. The C/C composite is a compounded body with carbon fiber having an extremely strong anisotropy, and its properties depend strongly on the manner by which the fibers are woven. As shown in Figure 5, although there are methods that use felt or chopped fibers⁽⁶⁾, two-dimensional fabrics are employed that use long fibers or three-dimensional fabrics, such as three-directional weave, four-directional weave, six-directional weave, etc. The two-dimensional weaves include the plain weave, satin weave, twilled weave, etc., but considering the fact that the linearity of the fibers is effective in enhancing the strength, five- or eight-sheet satin is frequently used. In three-dimensional weaves, since matrix precursors must be impregnated in the fabrics, it is said that the four-directional weave, which is open pore, has a high fiber content and its high rigidity is excellent. In any case, one should choose a type of weave that enables as many fibers as possible to be configured linearly in the required direction, taking the stress distribution of the member into consideration.

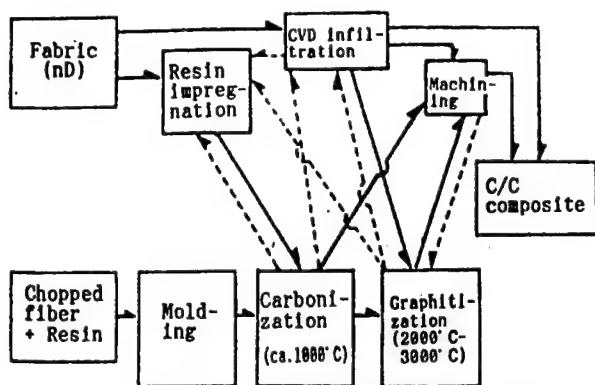


Figure 4. C/C Composite Fabrication Process

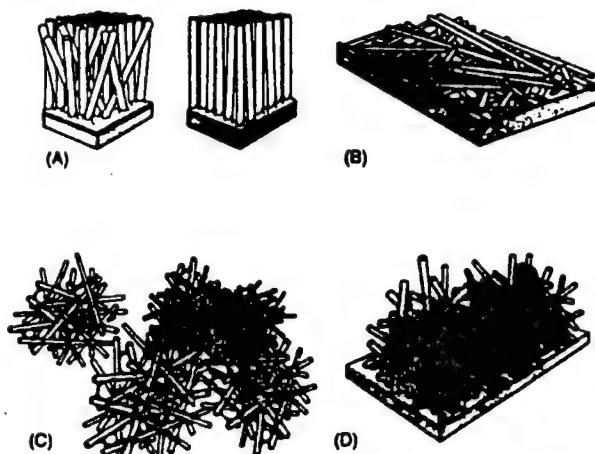
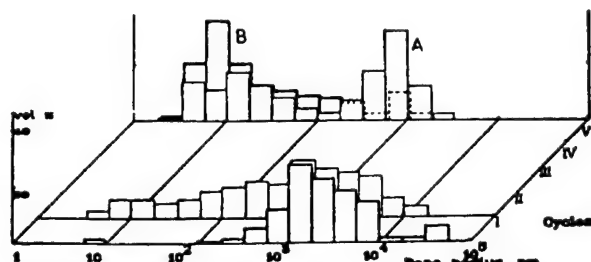


Figure 5. Models of Fiber Configurations. A: Flocking layup; B: Pulp molding; C: Isotropic casting; D: Spray layup

The C/C composite manufacturing method varies with the kind of matrix (resin charcoal, CVD charcoal, etc.), and the properties of the product differ accordingly. When a thermoplastic raw material, such as pitch, is used, the bulk density of the composite obtained by a single carbonization impregnation process is low, ranging from 1.2 to 1.3 g/cm³, since the carbon yield is 55 percent at the most. For this reason, it is necessary to repeat the carbonization impregnation several times, making it possible to raise the density to 1.7-1.9 g/cm³. One method which is drawing attention is that in which carbonization is carried out under pressure in an autoclave in order to raise the carbon yield. According to this method, the carbon yield of 43 percent (softening point of 53°C) for the carbonization under normal pressure can be elevated to, for example, higher than 80 percent by pressurized carbonization under a pressure of 10 MPa, making it possible to raise the bulk density to 1.64 g/cm³ during the initial carbonization impregnation, and to 1.87 g/cm³ for the second one.⁽⁷⁾ Chlopek, et al.⁽⁸⁾, report that by repeating five pressure carbonization cycles for

pitch, the number of large pores, ranging from several dozen micrometers to several hundred micrometers, decreases, and peaks appear at two points, i.e., below 1 μm and several hundred angstroms, while the number of pores of the micrometer order decreases markedly by graphitization, as shown in Figure 6. Soda, et al.⁽⁹⁾⁽¹⁰⁾, carried out carbonization under extremely high pressure. This process, referred to as HIP, is one in which not only can the number of impregnation cycles be decreased (density of 1.95 g/cm³ is obtained by five impregnation cycles) due to the increased yield of carbon, but also in which a phenomenon seems to be occurring that is entirely different from that seen in carbonization in the past. This is clearly observable in the texture of the product. As shown in Figure 7 [not reproduced], pitch exhibiting a certain flow structure under normal pressure or under pressurization of about 10 MPa will no longer show this flow texture under the high pressure mentioned above. It is believed that perhaps all of the gas generated by decomposition is compressed and smaller bubbles are unable to rise in the molten pitch, completely lacking in convection and with no apparent flow structure, forming closed pores. We have heard that this phenomenon was discovered in the United States, but this is the first time that concrete data has become available. The matrix of such a texture is expected to have better shear strength than that of the flow texture, but data on this point has not yet been reported.

Figure 6. Effect of Impregnation Cycles on Pore Distribution of C/C Composite Under Pressure Carbonization.
A: without graphitization; B: with graphitization

The texture of a composite material that uses a pitch charcoal as a matrix presents a flow texture. As a result of a detailed investigation of this texture in the pore or fiber periphery, it is reported that the wettability between carbon fibers and pitch is very good, as shown in Figure 8 (the contact angle is nearly zero), and an examination of disclination reveals that the Brooks-Taylor type mesophase droplet has its layer surface configured so as to encircle and be closely attached to the fiber.⁽¹¹⁾ Due to the flow of pitch between fiber bundles, in addition to the epitaxial growth of the mesophase, the matrix forms a flow structure. As can be seen from the fact that many cracks are introduced along the flow structure when a material having a flow structure is graphitized, the interlayer shear strength of the matrix is reduced. For this reason, texture control through the addition of

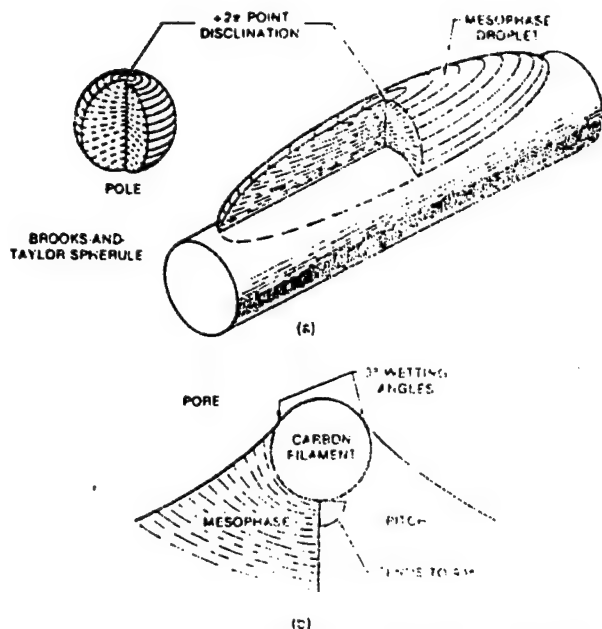


Figure 8. Wetting Behavior and Molecular Alignment for Mesophase Pitch on Carbon Fiber

graphite powder, etc., is effective⁽¹²⁾, and this technique is apparently being employed for C/C composites by some foreign manufacturers.

Since the 1971 report by Fitzer, et al., of West Germany, many research results involving the use of thermosetting resins as a matrix precursor have been reported. As matrix precursor resins, three kinds, i.e., phenol, epoxy and furan, are generally used, but polyphenylene (carbon yield of 85 percent), polyimide, and copra resins with high carbon yields are also being tried. Form shaping for this system is easier than that for the thermosetting resins and the fiber reinforced plastic (FRP) technology can be applied as it is, but sharp cracks tend to be introduced due to matrix contraction at the time of carbonization. When a thermosetting resin is employed as a precursor, the carbons in the matrix transform from brittle materials, as shown by vitreous carbon, to ductile carbons in which the surfaces of the graphite layers are developed, as shown in Figure 9 [not reproduced]. This change depends strongly on the bonding between the matrix precursor and the fibers⁽¹³⁾ (Figure 9B⁽¹⁴⁾ [not reproduced]), and requires attention when considering the mechanical strength of the sample. The authors and their colleagues have already reported in outline form that the graphitization of this matrix depends on the shear deformation of the matrix at the time of carbonization⁽¹⁵⁾, and its more detailed examination is in progress by means of laser Raman studies, etc.⁽¹⁶⁾

The chemical vapor deposition (CVD) method, in which thermally decomposed carbons are deposited directly on the fabric, is sometimes called the infiltration method in

order to differentiate it from the above-mentioned resin impregnation method. With CVD, it is possible to have a mold without deforming the shape of the fabric, less damage occurs to the fibers, and the degree of hand fouling caused by the surface of the molded products is relatively small. For these reasons, this method is indispensable for medical materials. With the CVD method, a raw material gas (methane, propane, benzene, dichloroethylene, etc.) is introduced into a heated fabric at high temperatures (800-2,000°C), allowed to decompose on the inner surface of the fabric to deposit carbon, and is being actively studied in the nuclear fusion furnace field which requires high thermal conductivity.

It has been recognized by many researchers that various physical properties are intimately related to the fine structures, and since the control of these structures is important for the design of C/C composites, fine structure control is being emphasized among the workers.⁽¹⁷⁾ It is believed that with the promotion of the systematic study of fine structures and of various physical properties, it will become possible to obtain composite materials as tailored materials.

4. Surface Treatment and Mechanical Characteristics of Carbon Fibers

Since carbon fibers are widely used for FRP's, a sizing reagent is attached to them to provide surface treatments suitable for FRP's and to facilitate their handling. The sizing reagent acts in a direction which obstructs the bonding of carbon fibers with the matrix, and can become a cause of nonuniformity due to the frequent concentration on the outer surface of the fiber bundle. For these reasons, carbon fibers are often used after the sizing reagent has been removed.

In general, the end portions of the carbon network surface are oxidized to produce oxygen-containing groups, such as carboxyl, carbonyl and hydroxyl groups, etc., and these products are involved in the bonding of carbon fibers with the matrix. In FRP's, the interlayer shear strength and the bending strength are increased with the increase in the amount of oxygen on the surface. In brittle matrix C/C composites, the interlayer shear strength exhibits the same tendency as the FRP's, but the bending strength tends to be in the opposite direction. The authors and their collaborators have reported that the bending strength is increased when use is made of CF's that have not been given surface treatments.⁽¹³⁾ The tendency is in the opposite direction based on the difference in the amount of rupture stress and the brittleness between the matrix and the carbon fiber. As shown in Figure 10, in carbonized products, the strength is extremely low when the carbon fiber is given a surface treatment. On the other hand, in graphitized products, the strength is high when the carbon fiber is subjected to a surface treatment.

This experimental finding can be interpreted as follows. It is believed that the surface functional groups of the carbon fibers are bonded with the matrix resin, and that

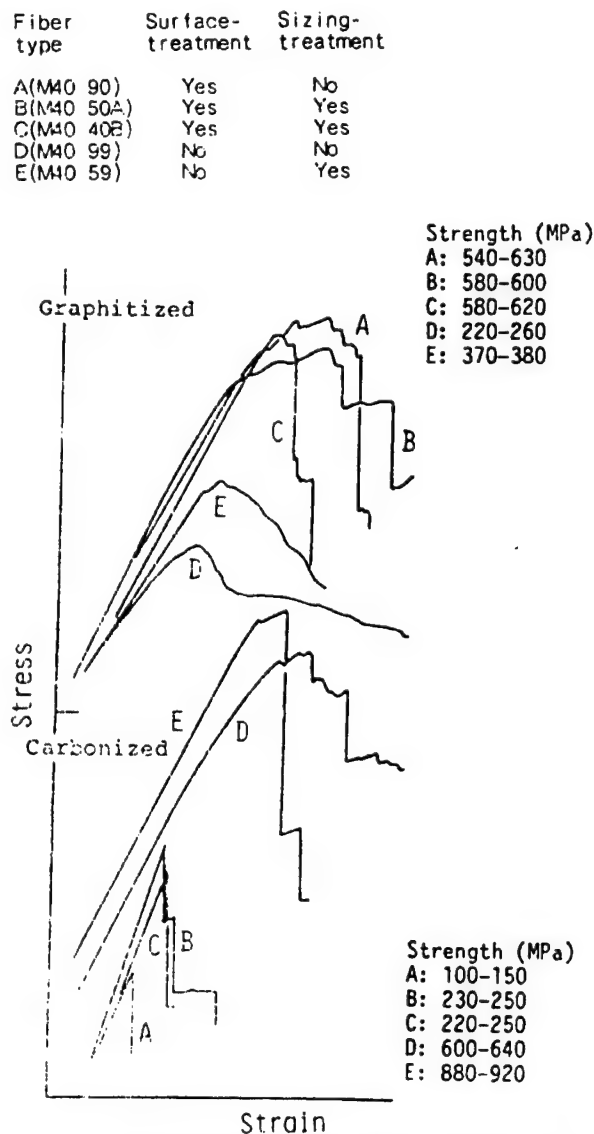


Figure 10. Change in Bending Strength of Resin Derived Char Matrix Composite Following Different Surface Treatments of the Fiber

this bonding remains effective even during carbonization and determines the strength of the bonding of the carbon fibers with the matrix. In other words, when the matrix consists of brittle carbon, such as in the case of carbonized products, the rupture stress of the matrix is comparable to or less than that of the carbon fiber, and cracks generate from the matrix. As shown in Figure 11, which contains the results of analysis by finite elements of the stress field at the tip of a crack of a brittle material⁽¹⁸⁾, the stress at the tip of the crack perpendicular to the crack is extremely high. In contrast, the tensile stress in the propagation direction of the crack becomes maximum at a spot slightly in front of and away from the crack. That is, a peeling occurs at the fiber/matrix

interface before the crack reaches it, making it possible to avoid an extreme concentration of stress on the fiber. If the bonding between the matrix and CF is strong, the crack will give a concentration of stress to the CF without changing its direction of propagation, readily cutting the CF. As a result, it is not possible to effectively utilize the strength of the carbon, and the strength of the composite is lowered. In order to avoid this, a method can be considered in which the bonding between the fiber and matrix is weakened to an appropriate degree. By so doing, it becomes possible to cause interface peeling in front of a crack, enabling the fiber strength to be used in an effective manner as a result of fiber drawing.

In contrast, when the matrix demonstrates plasticity, as in graphitized products, the stress concentration on the fiber at the tip of the crack will not take place, enabling the force to be distributed uniformly over the entire fiber. As a result, it can be considered possible to obtain higher strength for higher bonding at the interface. In this case, since shearing rupture can take place readily when the bonding between the fiber and matrix is weak, it is necessary to strengthen the bonding. It is also believed that the surface coarsens with high temperature treatment, and that the mechanical bonding dominates the strength. However, this point has not yet been clarified.

Graphite is a material with extremely strong anisotropy, and carbon fibers have particularly strong anisotropy as well. Therefore, it can be easily understood that C/C composites utilizing carbon fibers also have strong anisotropy. However, data concerning this point is extremely scarce, with one report appearing in the proceedings of an international conference in the United States and one reported by us.⁽¹⁹⁾ An example is shown in Figure 12. As the inclination from the fiber axis increases, it proceeds from the tensile rupture of the fiber, through the shear rupture, to the tensile rupture of the matrix. However, the strength drops rapidly from a certain small angle down.

The measurements of the shear strength of C/C composites are generally made by the short beam method, the contraction of a notched sample in accordance with ASTM's D2344-84, tensile tests, etc. Recently, however, a report has been made available in which samples of three-dimensional weaves and samples of extremely high shear strength were measured by similar methods. At the same time, reports are being seen in which the shear strength calculations are based only on the rupture load, without paying attention to the mode of rupture or the distribution of stress (multiaxial stress). We would like to comment that such an approach is an extremely dangerous one.⁽²⁰⁾

The strength of C/C composites increases, as is well known, by about 5-20 percent with a rise in temperature to nearly 2200°C, similarly to other carbon materials. In contrast, what would happen if these materials were used in space, with hyper low temperatures? According to a

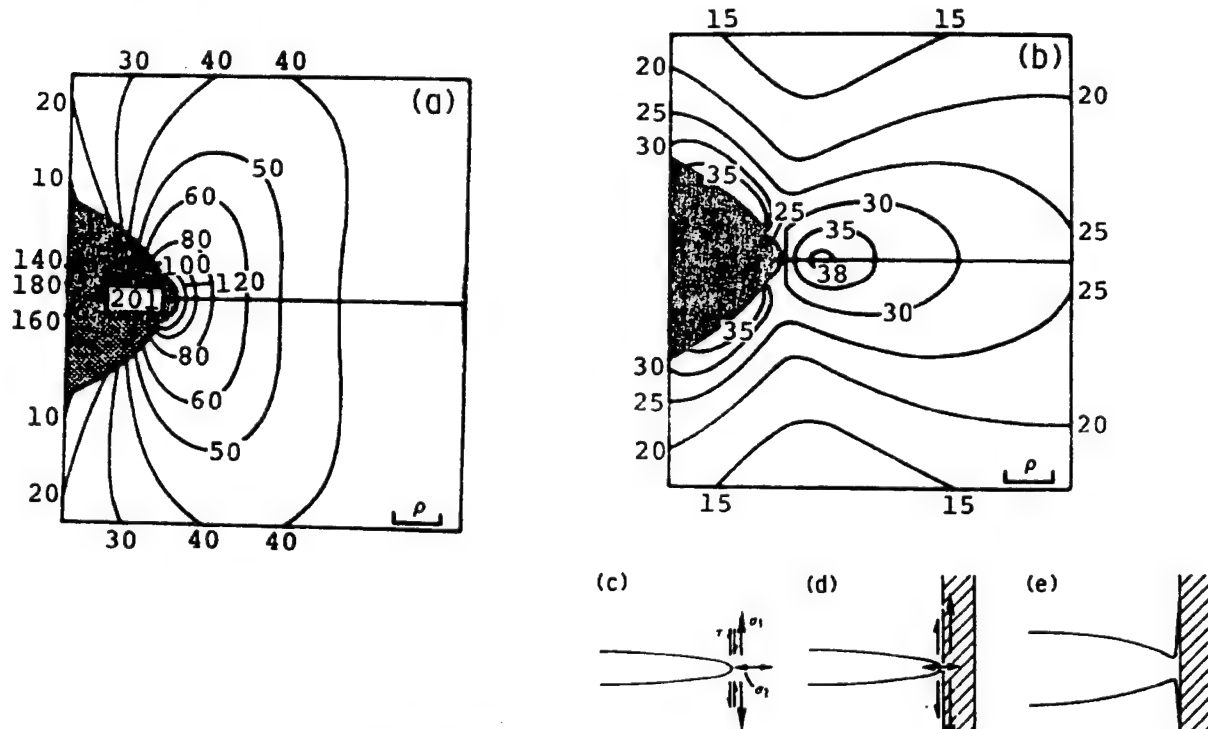


Figure 11. Stress Distribution Around Crack Tip. A: σ_1 in (c), B: σ_2 in (c), D: crack tip at the fiber, E: crack opening at the fiber/matrix interface

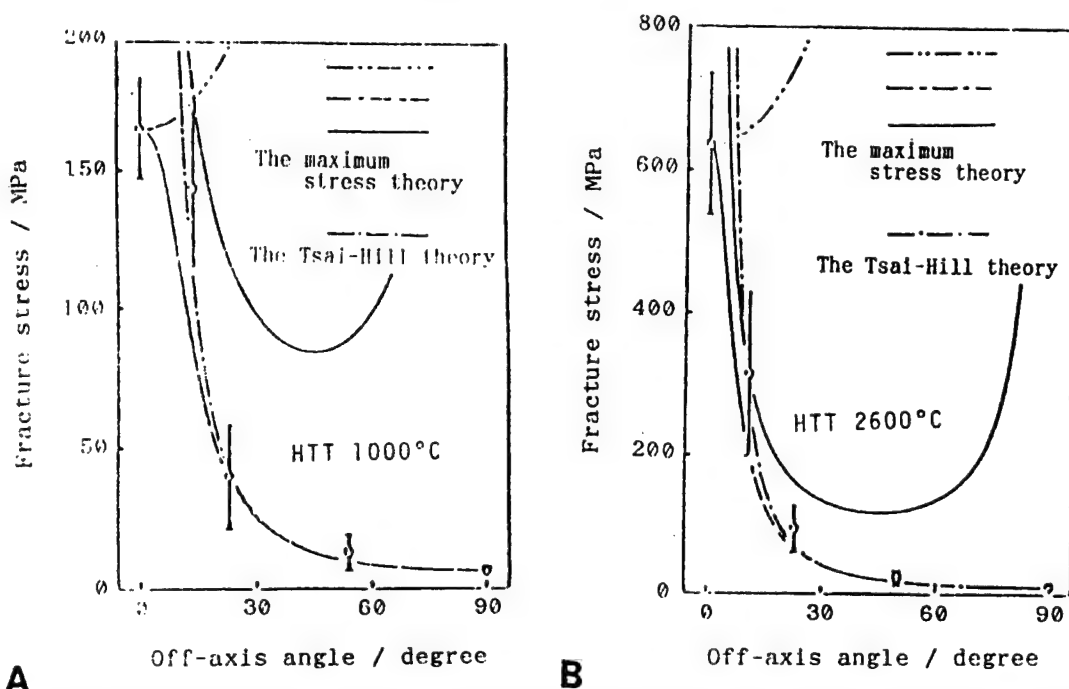


Figure 12. Change of Strength with Different Off-Axes for Resin Derived Char Matrix Composite. A: Carbonized, B: Graphitized

recent report⁽²¹⁾, the strength of two-dimensional and three-dimensional C/C composites at liquid nitrogen temperature (-195°C) is increased by about 20 percent over that at room temperature. Although the reason for this is not clear, it may be related to the influence of the water in the atmosphere on the strength.⁽²²⁾

5. Graphitization and Thermal Properties of Matrix

Next to the mechanical properties, important characteristics of the C/C composites are the thermal conductivity and thermal expansion. The thermal conductivity at 100 K of thermally decomposed graphites with extremely high orientability has the extremely high value of 5000 W/mK for the direction of the layer surface, while it is 40 W/mK perpendicular to the layer surface, which is smaller by more than two orders of magnitude than that for the layer surface direction. The thermal conductivity for the direction of the layer surface and that perpendicular to it shows a maximum value at these temperatures, then falls off with an increase in temperature. At any rate, it has a high value of 1500 W/mK around room temperature.⁽²³⁾ The increase at low temperatures is due to the increase in the capacity of specific heat, while the decrease at high temperatures is due to the scattering of the lattice vibration of the phonons. The thermal conductivity of the graphite materials depends on the degree of graphitization and the orientability. For C/C composites, it is also strongly dependent on the degree of graphitization of the matrix. In Figure 13, which gives the case of uniaxially oriented C/C composites in which furan is employed as the raw material for the matrix, it is seen that the thermal conductivity is raised more than 20 times as the heat treatment temperature is increased.⁽²⁴⁾ The thermal conductivity of graphite is represented as the product of the capacity of specific heat, the velocity of the phonon and its mean free path. The capacity of

specific heat is less easily affected by the heat treatment temperature. The velocity of the phonon is related to its modulus of elasticity, which undergoes changes of several times but not by an order of magnitude. Considering the above factors, it can be said that the changes in thermal conductivity correspond to the development of the surface of the graphite layer or, in other words, on the development of the size La of the crystallite in the a-axis direction. That is, if a material with high thermal conductivity is desired, it is effective to increase the size La of the crystallites by improving the orientability and increasing the degree of graphitization by subjecting it to heat treatment at high temperatures. Although a high thermal conductivity of 400 W/mK, which is comparable to that of copper, is required for the first wall of the most recent nuclear fusion furnace, the C/C composites seem to have already met that goal.

The coefficient of thermal expansion is an important property when a material is used at high temperatures, and many reports have been found on this subject. The coefficient of thermal expansion for the direction of the layer surface of graphite with high orientability is extremely low, exhibiting negative expansion up to 400°C, and is about $4 \times 10^{-6}/^{\circ}\text{C}$ at the most, even at temperatures exceeding 400°C. Perpendicular to the layer surface it is under Van der Waal's coupling and its coefficient of thermal expansion has the large value of $27 \times 10^{-6}/^{\circ}\text{C}$. The coefficient of thermal expansion in the direction of the fiber axis of C/C composites is mainly dominated by the coefficient of thermal expansion of fibers with high moduli of elasticity. Figure 14 shows the coefficient of thermal expansion in the fiber axis direction of representative carbon fibers.⁽²⁵⁾ The coefficient of thermal expansion in the direction perpendicular to the fiber axis is strongly affected by the matrix

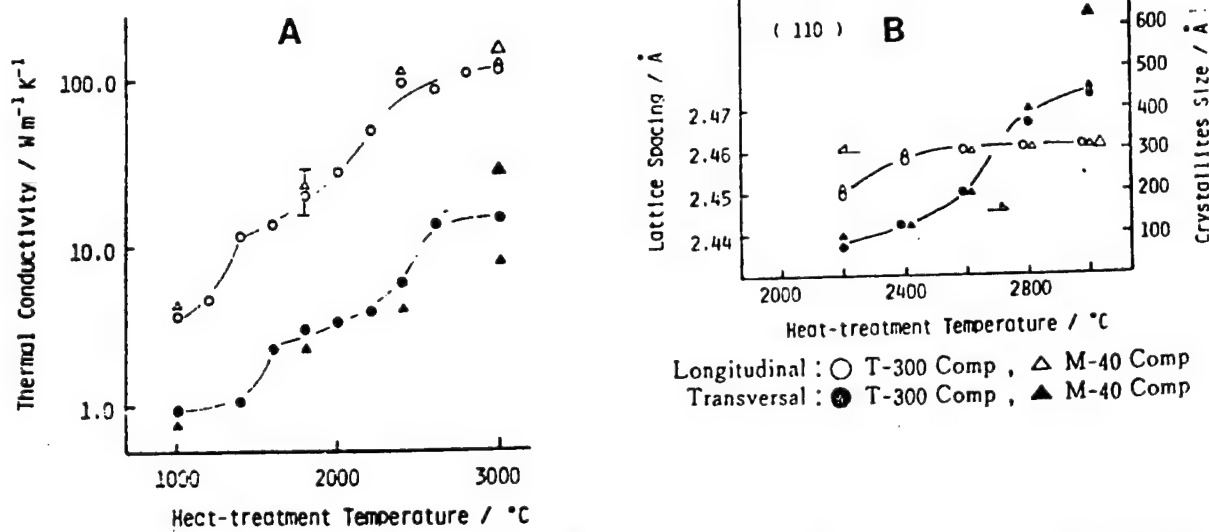


Figure 13. Changes in Thermal Conductivity with Different Heat Treatment Temperatures (A), and Crystallite Size of (110) Plane (B) in Resin Derived Char Matrix Composite

employed. As in the above, the coefficient of thermal expansion of the C/C composite depends on the degree of graphitization and the texture (orientability, etc.) of the matrix and exhibits considerable anisotropy. When a material is coated in order to increase the resistance to oxidation, a subject covered in the next section, the anisotropy mentioned above becomes a matter of concern in that peeling or cracks arise during the cooling process due to discrepancies in the coefficients of thermal expansion.

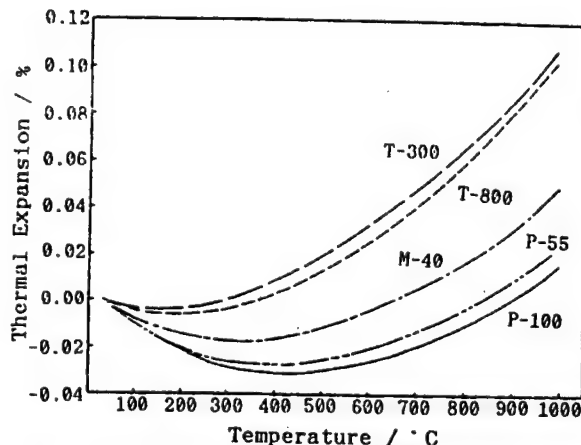


Figure 14. Thermal Expansion of Different Carbon Fibers

6. Prevention of Oxidation

The latest topic regarding C/C composites is the prevention of oxidation. Before proceeding to oxidation prevention, however, a discussion of the problem involving the oxidation of C/C composites is in order. The oxidation of carbon materials has frequently been observed to propagate with a defect serving as the starting point, although it is also strongly affected by a metal (alkali metal, alkaline earth metal, iron group metal, etc.) having a catalytic action that is contained in the raw material (Figure 15 [not reproduced]). Namely, oxidation occurs at the boundaries of the fibers and the matrix, where it is anticipated to have a residual stress, as well as at the boundaries of the domains.⁽²⁶⁾ In addition, the rate of oxidation of a thermosetting resin char matrix becomes slower with an increase in the heat treatment temperature, i.e., with the progress of graphitization. However, in either case the rate of oxidation is higher than that for high density graphite materials in general. The oxidation occurs mainly at the surface, and continues to the outer surface. H. Marsh and his research group manufactured a C/C composite by making a matrix precursor using a resin mixed with pitch in order to control the outer surface area of the sample, and by carbonizing it under pressure. They examined the oxidation characteristics of the product, and reported that the surface area was small for systems with much pitch that had well-developed anisotropic structures and had larger reaction activation energy, lowering the rate of oxidation

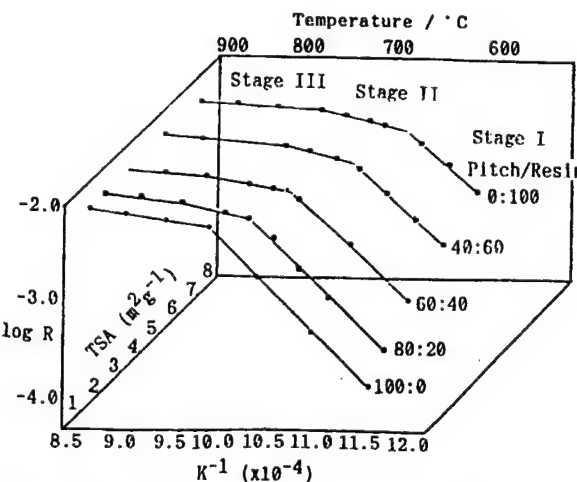


Figure 16. Variation of Kinetic Parameters of Oxidation with Total Surface Area Controlled by Pitch/Resin Ratio

in the reaction region, and, as a result, the transition temperature from the reaction rate determination to the diffusion rate determination increased (Figure 16⁽²⁷⁾).

As can also be seen from these results, the key points for enhancing the resistance to oxidation include reducing the defects which are potential starting points for oxidation, reducing the surface area and reducing the amount of impurities.

The prevention of carbon material oxidation is performed by coating the material in general with glass or by coating it with the vitrified film obtained by the preferential oxidation of an oxidation preventive reagent to retard the oxygen diffusion. As the oxidation preventive reagent, use is made of a boron-based material for use at temperatures below 1200°C, and an SiC-based material for use at temperatures below 1500°C. In the SiC coating, the vapor pressure of the ternary system SiC-SiO₂-C in the vicinity of 1500°C is one normal atmosphere, as shown in Figure 17⁽²⁸⁾, but it is also usable at 1700°C since the reaction rate is low. In the field of refractory materials for steel making, carbon, metal and oxide are used under an oxidizing atmosphere. The application of this technology to oxidation prevention in C/C composites is also being studied.^{(29),(30)}

For use in an environment of repeated heating and cooling, it is important to bring the coefficients of thermal expansion of the oxidation preventive material and the C/C composite close to each other. As methods for resolving this problem, an attempt has been made to sandwich TiC, which is easier to oxidize, with SiC as the coating material and a C/C composite base material, and to bury the cracks generated in SiC with TiO₂ as an oxide⁽³¹⁾, as well as an attempt to apply functionally gradient materials, namely SiC, which continuously

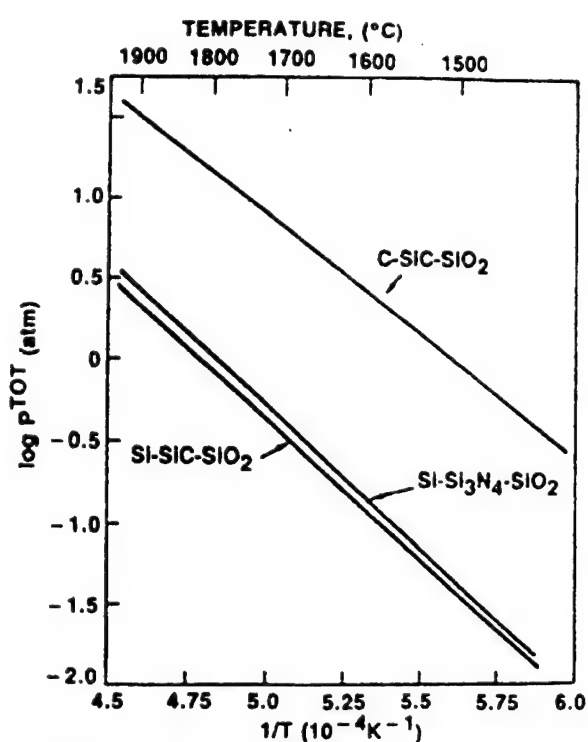


Figure 17. Total Vapor Pressure in C/SiC/SiO₂ and Si/SiC/SiO₂ Systems

change the coefficient of thermal expansion by giving a gradient of concentration to the material.⁽³²⁾

Moreover, for boron/silica/SiC system glass, use is made of a glass frit whose coefficient of thermal expansion can

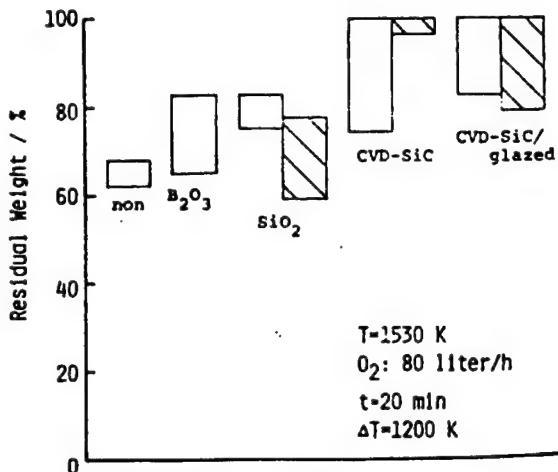


Figure 18. Residual Weight of C/C Composite Coated with Multilayer of SiC and Glass (oxidized in pure oxygen at 1260°C)

be controlled by regulating its composition.⁽³³⁾ A proposal was made recently to apply a compound film obtained by mixing a small amount of SiC in a material, coating it with SiC by CVD, then coating it further with glass. As shown in Figure 18, it has been reported that even under the severe conditions of being placed in pure oxygen at 1200°C, excellent capabilities are demonstrated.⁽³⁴⁾

As an oxidation preventive reagent at temperatures exceeding 1700°C, no promising material has yet been found, while of the metallic carbide and oxygen or carbon system members, no material has been found which is stable at temperatures exceeding 2000°C. The possibility of using Ir metal has been reported⁽²⁸⁾, but information regarding its reaction with oxide or other compounds is scarce.

7. Application to Nuclear Fusion Furnace, etc.

The first wall of the nuclear fusion furnace is exposed to an ultra-high temperature plasma. Because of this, the wall material evaporates, lowering the temperature of the plasma. From the fact that the drop in temperature is smaller for a material with a smaller atomic number, and that the drop in the surface temperature due to wall cooling is greater for a material with larger thermal conductivity, C/C composites are considered to represent the most promising candidates. As was mentioned earlier, seven papers related to the nuclear fusion furnace were presented at the international conference on carbon held in Japan late in 1990. Some of them will be introduced below.

When weight reduction is generated as a result of the irradiation of C/C composites with high electron beam, hydrogen beam, etc., energy, although the weight decrease increases with an increase in the absorbed energy and the irradiation power, as shown in Figure 19, this tendency is considerably less for C/C composites with high thermal conductivity. Evaporation due to irradiation with high energy beams takes place all over the sample surface, but it is reported that irradiation with excessively high energy, i.e., above 1200 MW/m², causes a disturbance on the surface due to reverse evaporation.⁽³⁵⁾

A plan for applying C/C composites to the divertor part of the improved JT-60U for the Tokamak-type nuclear fusion experimental furnace has been under way, and the characteristics of seven kinds of materials to be used have been presented. The characteristics measured include thermal conductivity, tensile strength and the degassing rate. Samples with thermal conductivity in the range of 60-427 W/mK were selected, but since all of them had high anisotropy, it is said that the investigation of those with high resistance to thermal shock will be emphasized.

Not many reports on neutron irradiation data are available. Y. Tanabe, et al.,⁽³⁶⁾ carried out the irradiation of $4.5-6 \times 10^{24} \text{ n/m}^2$ ($E > 1 \text{ MeV}$) at 240 and 640°C. For the irradiation at 240°C, the rupture stress, bending

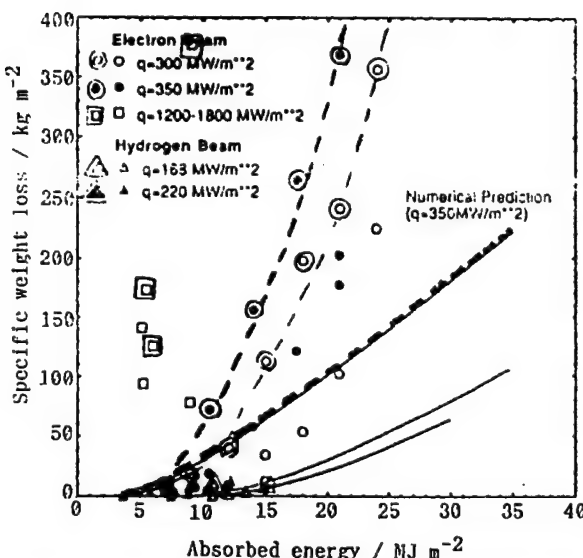


Figure 19. Specific Weight Loss of C/C Composites as a Function of Absorbed Energy from Electron Beam

strength and breaking energy were all high. It was reported that these events can be explained in terms of P. Walker, Jr. and group's theory⁽³⁷⁾ that the disturbance of crystallites becomes large, and neutrons that enter the space between the layers reduce the number of voids, making the shear strength high. Sato, et al.⁽³⁸⁾ examined the changes in various kinds of physical properties by irradiating three kinds of C/C composites with $1-2 \times 10^{25} \text{ n/m}^2$ at 650-1000°C. It was reported that the porosity was decreased by 4-5 percent, Young's modulus (30-40 percent), strength (20 percent) and fracture toughness (20 percent) increased by the numbers indicated in parentheses, and that the thermal conductivity decreased by 20-50 percent. These changes were reportedly roughly the same as those of high density, fine particle and isotropic carbon materials, but the drop in resistance to thermal shock fracture is greater than that of the carbon material. This fact should perhaps be noted in designs involving these C/C composites.

In addition, there are reports^{(39),(40)} regarding the boronized graphite developed to improve the tritium absorption, chemical sputtering, sublimation due to irradiation, etc., which have represented problems when graphite material has been applied to the first wall of the nuclear fusion furnace, which state that these graphites also demonstrate excellent resistance to oxidation and to erosion by heavy hydrogens.

For the past 15 years, C/C composites have actually been used for aircraft brakes. However, reports on the frictional abrasion of C/C composites are extremely scarce. On this subject, a partial report was presented by the authors and their collaborators at the international conference on carbon held at Toyohashi in 1982. However, perhaps due to the strong dependence of friction and

abrasion on the moisture content of the surface, it can hardly be said that their essential aspects are clearly understood. At the recent conference at Tsukuba, a report was also given on the friction and abrasion of C/C composites. Narita, et al.⁽⁴¹⁾ demonstrated that there was a certain relationship, as shown in Figure 20, between the product of the rotational speed V of the sliding plate and the holding pressure P, and the friction coefficient μ at that speed. The product $P \cdot V \cdot \mu$ represents the rate of heat generation, i.e., the heat flow flux. This may also be regarded as the quantity of heat that the brake plate can dissipate to the outside of the system.

When C/C composites are applied to the nose cone, etc., of a flying body in space, the shock characteristic is an important property to take into consideration. At the international conference at Tsukuba, Ogawa, et al.⁽⁴²⁾ reported that the shock resistance is strongly dependent on the manner in which the fibers are woven, and that materials with excellent shock resistance seem to be the two-dimensional materials with good interlayer peeling, although the experimental conditions were such that the velocity used was less than that of space dust.

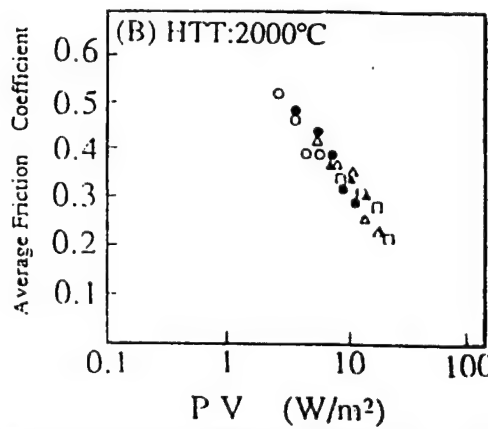
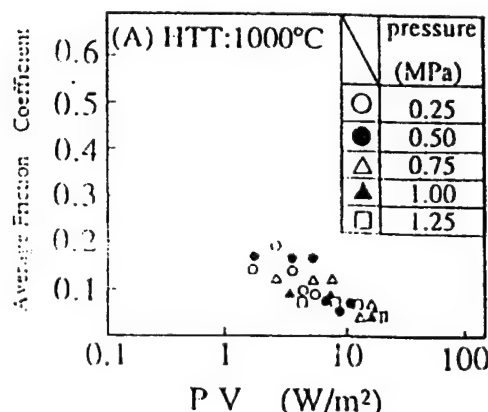


Figure 20. Friction Coefficient of Resin Char Matrix C/C Composite as a Function of Absorbed Energy by Braking

8. Conclusion

Although research on C/C composites was initiated around 1970, the reports available regarding the results are far from what one may term sufficient. This is due to the fact that some have been military-related and, as shown in the literature⁽⁵⁾, the development in the United States has been very fast-paced, as can be surmised from the joint seminars sponsored by NASA, etc. In contrast, reports on C/C composites from Japan are not very many, and neither has the pace of the research been very fast. The reasons for this seem to lie in the lack of qualified researchers and in the fact that there has been no demand for these materials in Japan, where there has been hardly any space industry to talk about. In addition to the high price of carbon fibers, the high cost of electric power and the time required for carbonization and graphitization may also be said to represent factors regarding the advancement of the research. However, MITI's project on next-generation ultra-high resistance to the environment and the HOP project have been promoted recently as national projects. Moreover, in the special research on energy conducted by the Ministry of Education and the Japan Atomic Energy Research Institute's JT-60U project, C/C composites are being investigated as the most promising candidates for use in the first wall of the nuclear fusion furnace. Furthermore, it is recognized that C/C composites have been drawing attention, as can be seen in the research on C/C composites conducted by the New Carbon Forum, which is comprised of carbon related enterprises, etc. Under these circumstances, it is needless to say that active research and development is necessary for the future advancement of C/C composites. Among the evaluations of recent C/C composites, there are some in which the natures of the materials have not yet been made known. In order to fully understand the C/C composites combining a matrix that employs a carbon material with an extremely strong anisotropy and carbon fibers with strong anisotropy, both crystallographically and morphologically, and to obtain them as tailored materials, it is absolutely necessary to discuss these materials in terms of their relationship to fine structures. Nonetheless, the authors are confident that the further advancement of C/C composites will occur.

References

1. Persh, J., CERAMIC BULLETIN, Vol 68, 1989 pp 1174-1176.
2. Otani, S., et al., "Carbon Fibers," Kindai Henshu Sha, 1983.
3. Fitzer, E., CARBON, Vol 27, 1989.
4. Okada, K., "Carbon Fibers and Composite Materials," Kyoritsu Shuppan, 1988.
5. Yasuda, et al., CARBON, No 115, 1983 pp 196-208.
6. Buckley, J.D., AM CERAM SOC BULL, Vol 67, 1988 pp 364-368.
7. Fitzer, E., Terwiesch, B., CARBON, Vol 11, 1973 pp 570-574.
8. Chlopek, J., et al., Ext abst., Carbone '90 Paris, 1990, pp 508-509.
9. Soda, Y., et al., Ext. abst., Carbon '90 Tsukuba, 1990, pp 430-433.
10. Fujioka, J., et al., Proc. 1st Japan Int. SAMPE, 1989, pp 1160-1165.
11. White, J., Sheaffer, P., CARBON, Vol 27, 1989 pp 697-707.
12. Yasuda, E., et al., CARBON, Vol 26, 1988 pp 255-257.
13. Manocha, L., et al., CARBON, Vol 26, 1988 pp 333-337.
14. Manocha, L.M., Ext. abst., Carbon '90 Tsukuba, 1990, pp 422-424.
15. Yasuda, E., et al., CARBON, No 128, 1987 pp 7-11.
16. Ragan, S., et al., Ext abst., Carbone '90 Paris, 1990, pp 506-507.
17. Weiss, R., Ext abst., Carbon '90 Tsukuba, 1990, pp 10-14.
18. Cook, J., Gordon, J., PROC R SOC LONDON A, Vol 282, 1967 pp 508-520.
19. Yasuda, E., et al., COMPO SCI & TECH, Vol 41, 1991, at press.
20. Peres, P., Silverstrini, P., Ext. abst., Carbone '90 Paris, 1990, pp 474-476.
21. Zhao, J., et al., Ext. abst., Carbone '90 Paris, 1990, pp 482-484.
22. Maruyama, T., et al., Ext. abst., Carbon '90 Tsukuba, 1990, pp 256-258.
23. Touloukian, Y., et al., "Thermal Conductivity," "TPM Vol 2," IFI/Plenum, 1970 p 41.
24. Kimura, et al., J OF CERAMIC ASSOC JAPAN, Vol 93, 1985 pp 89-95.
25. Tanaka, et al., CARBON, No 132, 1988 pp 2-5.
26. Yasuda, E., et al., TRANS JAP SOC COMPO MATER, Vol 6, 1980 pp 14-23.
27. Dillon, F., et al., Ext. abst., Carbone '90 Paris, 1990, pp 514-515.
28. Strife, J.S., Sheehan, J.E., CERAM SOC BULL, Vol 67, 1988 pp 369-374.
29. Yamaguchi, "Handy Thermodynamics," Jpn Assoc of Refractory Tech., 1990.

30. Brant, P., et al., Ext. abst., Carbone '90 Paris, 1990, pp 502-504.
31. Kawai, et al., "Digests of Papers, Annual Meeting of Jpn Ceramic Assoc, 1989," 1989, p 395.
32. Uemura, et al., "Digests of Papers, Annual Meeting of 16th Carbon Materials," 1989, pp 86-87.
33. Tanabe, et al., CARBON, No 131, 1987 pp 181-186.
34. Huettner, W., et al., Ext. abst. 19th Biennial Conf. on Carbon, Penn State Univ, 1989.
35. Araki, M., et al., Ext. abst., Carbon '90 Tsukuba, 1990, pp 210-213.
36. Tanabe, Y., et al., Ext abst., Carbon '90 Tsukuba, 1990, pp 166-169.
37. Walker, P.L. Jr., et al., CARBON, Vol 14, 1976 p 326.
38. Sato, S., et al., Ext. abst., Carbon '90 Tsukuba, 1990, pp 214-217.
39. Hirooka, Y., et al., Ext. abst., Carbon '90 Tsukuba, 1990, pp 890-893.
40. Sogabe, T., et al., Ext. abst., Carbon '90 Tsukuba, 1990, pp 886-889.
41. Narita, N., et al., Ext. abst., Carbon '90 Tsukuba, 1990, pp 386-389.
42. Ogawa, A., et al., Ext. abst., Carbon '90 Tsukuba, 1990, pp 470-473.

Future of Thermal Plasma Processing Discussed

916C0035E Ube CHO KO-ON ZAIRYO KOKUSAI
SHINPOJIUMU in Japanese 16 Mar 91 pp 58-65

[Article by Toyonobu Yoshida, Faculty of Engineering,
Tokyo University]

[Text] [English Abstract]: The purpose of this review is to identify the areas in thermal plasma processing in which scientific and/or engineering advances are highly expected in the near future, and specifically in terms of ceramics technology. To this end, "state-of-the-art" and "research needs" associated with the area are discussed extensively. In particular, we characterize three types of injection plasma processing (IPP) and review the problems relating to IPP. In order to demonstrate the feasibility and prominent features of IPP, special attention is paid to radio-frequency (rf) and hybrid plasma processing, which is discussed in conjunction with our recent research concerning ceramic coating. "High-rate deposition of SiC by thermal plasma CVD," "In-situ deposition of YBCO by thermal plasma flash evaporation," and "RF and hybrid plasma spraying of ceramics" are proposed as three distinctive candidates for the development of IPP in the field of ceramics technology in the near future.

1. Introduction

Plasma is the fourth state, following the solid, liquid and gaseous states, and is the generic term for ionized gases consisting of charged particles of electrons and ions and neutral particles of atoms and molecules that satisfy the condition of electrical neutrality, and covers a wide range of states from the perfectly ionized plasma utilized in the nuclear fusion furnace to a weakly ionized plasma, such as glow discharge. However, the plasma region that can be utilized for processing is not as wide and can generally be classified as thermal plasmas, which are statistically and mechanically close to the thermal equilibrium state, and low pressure plasmas that are in the nonequilibrium state. The author and his collaborators have been engaged in research aimed at obtaining new processing methods under diversified plasma environments, extending from thermal plasma to low pressure plasma, under the title of "plasma material engineering." In this paper, we will mainly discuss "ceramic coating by thermal plasma processing," whose advancement in the near future is definitely expected in connection with ultra-high temperature materials.

The application of thermal plasma to ceramic coating was put to practical use in the field of thermal spraying in the 1960's. However, numerous unsolved problems remain concerning the bonding property and compactness, and it is just at the stage at which the basic research, such as the modeling and diagnosis of the system as a whole, is being initiated. On the other hand, a representative example of the application of thermal plasma to CVD is the synthesis of high purity quartz, research on which was begun in the early 1970's. As for coating, which does not require the liquid phase intermediary, it is at the stage at which its potential has just been discovered. When classifying plasma processing, this field belongs to in-flight or injection plasma processing, and its roots can be found in processes that use chemical combustion flames, e.g., an oxyhydrogen flame. In the belief that the advancement of IPP in many fields will contribute to the expansion of the thermal plasma application field, we have developed various kinds of plasma torches for IPP and, during the past several years, have mainly studied applications primarily for the ceramic coating field.

In Figure 1, IPP-related topics which have been or are being prepared for research by the author's group are summarized. The basis is heat and mass transfer, thermodynamics, and magnetohydrodynamics, and torch and reaction design based on them are the central problems, while partial research involving the spectroscopic diagnosis of the reaction processes is being initiated. As for applications, the development of characteristic processes that contain (1) rapid heating, (2) rapid deposition, and/or (3) rapid quenching as necessary conditions are aimed at. Ceramic coating covers (1) and (2) above.

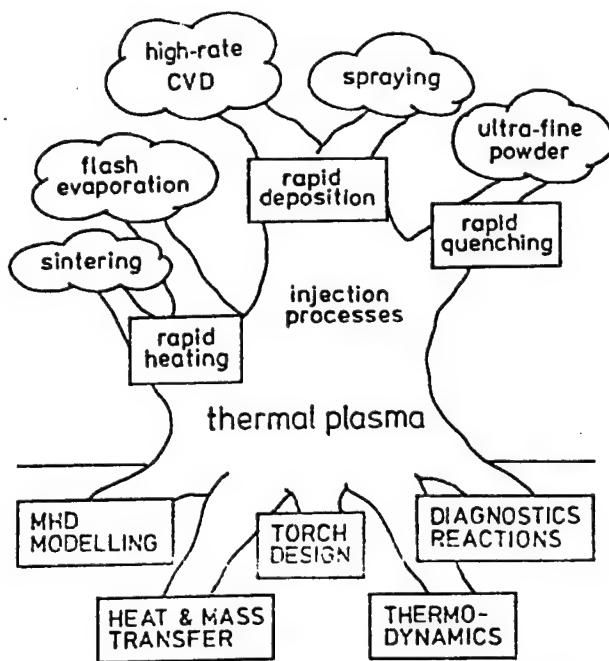


Figure 1. Promising Fields for Thermal Plasma Processing

2. Characteristics and Systems of IPP

Figure 2 shows a conceptual diagram of IPP. As can be seen in the figure, IPP consists of four zones, i.e., (1) reaction material injection zone, (2) heating and dissociation zone, (3) flame tail part reaction zone and (4) deposition zone. In zone (1), the key is the uniformity with which the reaction substances can be injected into the high temperature portion of the plasma. However, many unsolved problems remain for the future due to the fact that the sharp temperature gradient generated in the plasma boundary and the high viscosity of the plasma obstruct the injection of materials into the plasma, and that the required conditions for material injection and plasma generation are mutually exclusive, etc. In zone (2), it is necessary to achieve heating and dissociation that are well controlled, uniform and effective, requiring highly accurate control of the plasma parameters. The problems with zones (1) and (2), such as whether it is possible to inject materials in the direction of the plasma axis, are closely related to the torch structure, and hence it may even be said that, in a sense, the success of IPP is more than 90 percent dependent on the torch design. In addition, in zone (3) the problems to be investigated include the precise control of the temperature and velocity of the gas, concentration of reactive gas species, etc., in correspondence with the coating material, while in zone (4) the control of the substrate temperature that determines the film characteristics and of the plasma-surface interaction is particularly important.

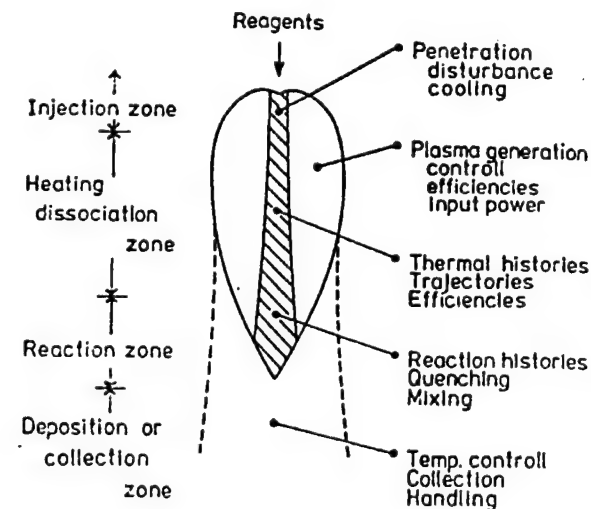


Figure 2. Conceptual Drawing of IPP

The three IPP categories are schematized in Figure 3. The thermal plasma CVD in (a) is characterized by the injection of gaseous reactive substances. This method differs from the ordinary CVD method in that the injected material is completely dissociated until it is brought to the element state, so that it may be thought of as a modification of the ordinary CVD method. The thermal plasma flash evaporation method in (b) is characterized by the injection and evaporation of solid particles. In this method, the most important factor is the capability for the perfect evaporation of solid particles, and it is required that powder of smaller than $30 \mu\text{m}$ be injected, even with the use of a high power plasma. This method is closer to PVD in that a multi-component high-temperature vapor with controlled composition can be readily obtained and that the handling of the byproducts can be ignored. In the plasma spraying method in (c), it is necessary to satisfy the condition that the diameter of the injected particles be large enough to inhibit their evaporation, but small enough to be allowed to achieve a completely melted state. The droplets are deformed by the collision with the base material and are solidified. Revision of the process as a whole and the scientific treatment is expected since it has become known in recent years that the structure of the sprayed film is essentially more dependent on the temperature of the liquid drops than on the velocity at the time of collision.

Our guiding principles concerning the applications of IPP to coating fields are shown in Figure 4. Our research has been conducted in the direction shown by the guide lines that, as indicated by the arrows in the figure, the role of IPP in the coating fields should satisfy either the condition of improving the deposition rate by several orders of magnitude or elevating the value of the coating in mind by several steps, or accomplishing both of the above, from the viewpoint that it is usual for the functional value of the coating to require a process with a

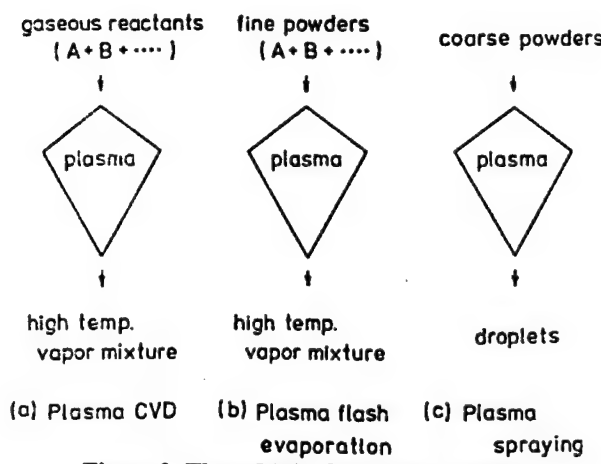


Figure 3. Three Main Categories of IPP

minimum deposition rate that matches its economical side, or, conversely, it is usual for a process that has a certain deposition rate to be applied to a coating that has a functional value that matches the deposition rate.

3. Development of Torches for IPP

Since the generation of a stationary thermal plasma flow generally must occur in an open system, the plasma flow is ordinarily blown out of a generation device termed a torch. Representative examples include dc plasma torches and high frequency plasma torches. When these are seen from the viewpoint of plasma generation for processing, problems are encountered in independently controlling not only the thermodynamic and transportation variables, but also the mechanical variables accompanying them, as well as due to the fact that the variable range is strongly dependent on the generation method and is extremely narrow.

Because of this, if one expects to apply IPP to a large number of fields, the first requirement is to develop a torch that can stably generate a low-flow-speed plasma of

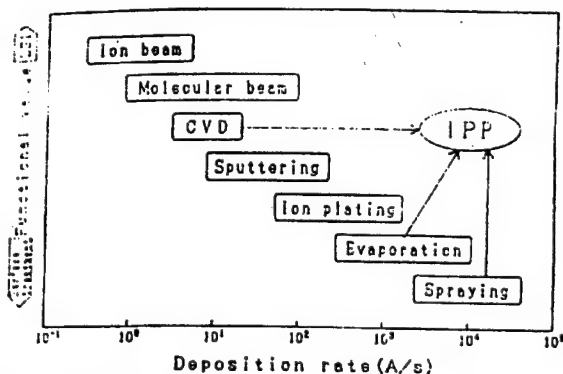


Figure 4. Guiding Principles of Our Research Involving the Development of IPP in Coating Fields

relatively high volume, even with the injection of reactive materials. In this respect, the priority of the high frequency (RF) or hybrid plasma torch over the dc plasma torch is definite. Figure 5 shows the simulation results of the velocity and temperature distribution within both the rf and hybrid plasmas of Ar. The computation conditions include a coil current of 100 A at 4 MHz, a sheath gas flow rate of 40 l/min, a rotational speed of 10 m/s, a carrier gas flow rate equivalent to a dc gas flow rate of 5 l/min, and an output at the arc jet outlet of 0.6 kW. Concerning the temperature distribution, in the rf plasma, the cooling effect in the upper part of the plasma due to the jetting of the carrier gas is conspicuous, and in the injection of a large quantity of raw material, a sharp reduction in heating efficiency is anticipated due to the penetration of a low temperature partial plasma. In the hybrid plasma, the central portion is also maintained at high temperatures since it is blown out of the arc jet, making the heating efficiency superior to that of the rf plasma. On the other hand, regarding the velocity distribution, a vortex flow due to magnetic pressure in the upper portion of the rf plasma coil is characteristic. Because of this, a portion of the injected

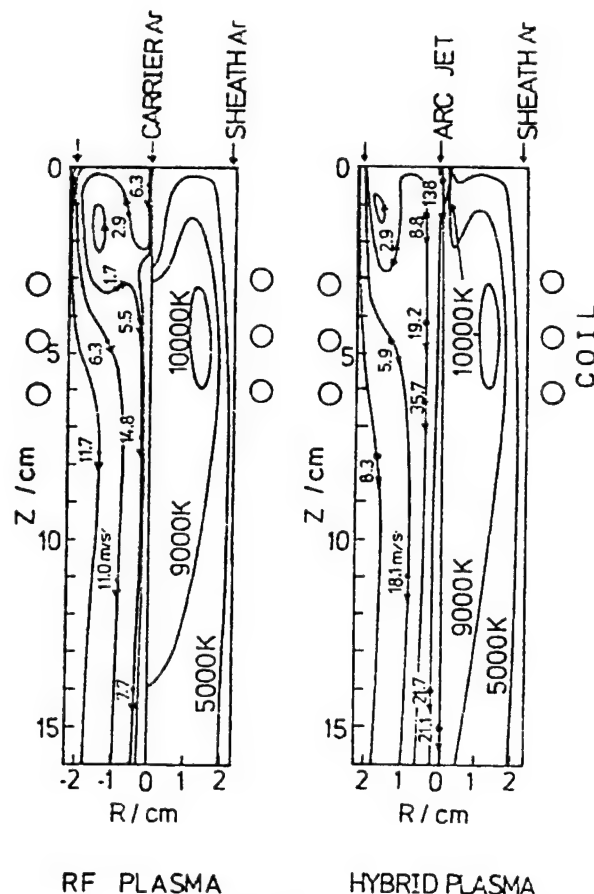


Figure 5. Stream-Line Patterns and Temperature Distributions for RF and Hybrid Plasmas

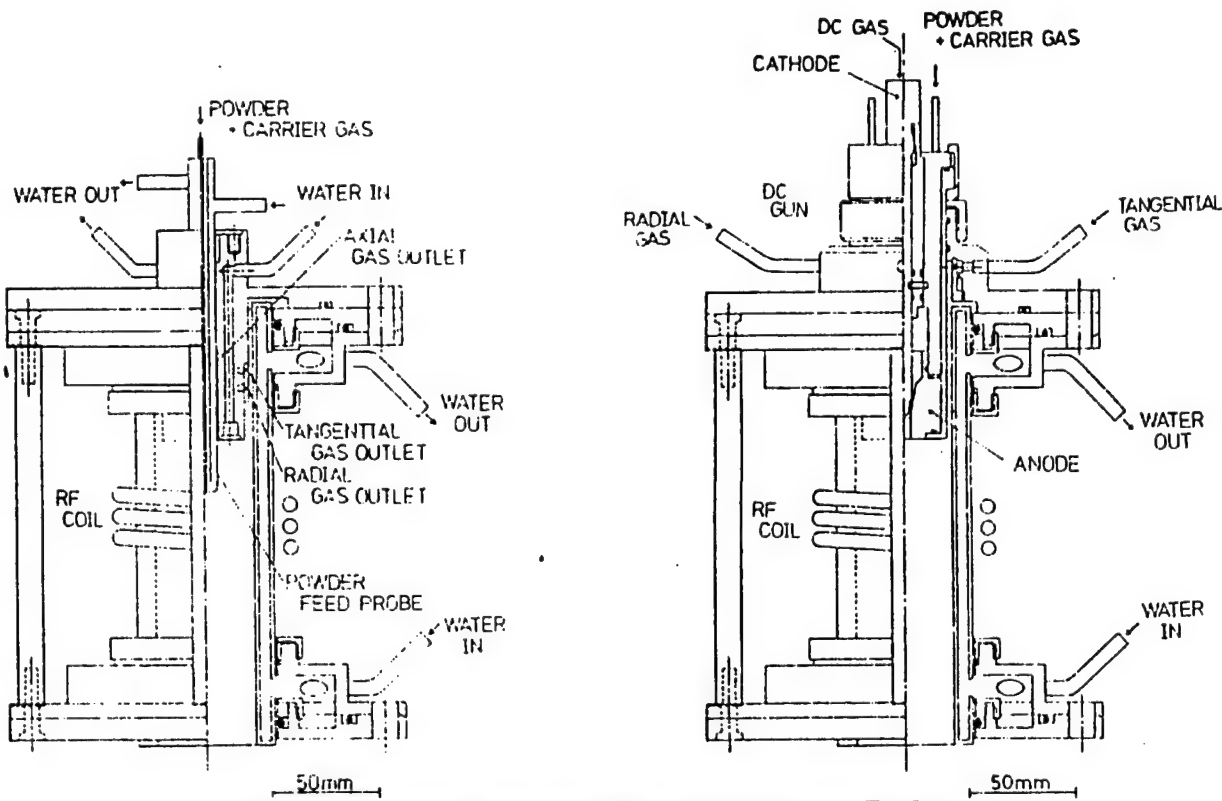


Figure 6. Schematic Diagrams of RF and Hybrid Plasma Torches

material is carried away by this counterflow to pass the periphery of the plasma, resulting in the nonuniformity of the heated reaction history. Therefore, a careful examination of the flow rate and the jetting position of the carrier gas is required. In contrast, in the hybrid plasma, a uniform heated reaction history is expected with the injection of the reacting material in the arc jet portion. However, the velocity at the hybrid plasma outlet is about three times higher than that of the rf plasma, and the reaction times are expected to be 3-5 ms and about 10 ms, respectively.

Figure 6 is a schematic diagram of the rf and hybrid plasma torches being used in our laboratory which were designed and experimentally manufactured based on the above-mentioned results.

4. Examples of Recent Research

4.1 Thermal Plasma Fast CVD^{2,3}

The beginning of the development of the present process is the synthesis of nonoxide ceramic fine particles^{4,5} and research on their plasma sintering.⁶ The surface of a fine particle of several dozen nanometers is very active, in spite of the particle being a ceramic, and oxidation proceeds readily in the air, making it mandatory to handle it in a glove box. As a result of examining plasma sintering in order to extract the intrinsic properties of the

fine particles, it was determined that the sintering proceeded readily for metals and ionically-bonded materials, but that densification was not achieved, although grain growth was observable, for covalently bonded materials such as SiC. Interestingly enough, however, for SiC fine particles of about 30 nm, island-like sintering was observed for the surface layer of about 1 μm over a region of several dozen micrometers, as shown in Figure 7 [not reproduced]. From these findings we concluded that during this stage we should develop a technique for directly sintering the synthesized fine particles without removing them from the plasma. In other words, a process is being developed which combines the fine particle synthesizing process and plasma-surface interaction, and its conceptual diagram is shown in Figure 8. When a base material is placed in the nucleation zone, the cluster produced, several nanometers in size, will be deposited on the base by thermal diffusion due to the steep heat gradient, and a dense coating layer will be formed due to the plasma sintering action. In the particle growth zone, since particles greater than 10 nm will be deposited and the characteristic time for sintering will be greater than that for clusters, the deposition of a fine particle film will be observed due to the lowering of the sintering action and the lowering of the thermal diffusion effect.

In accordance with the above-mentioned hypothesis, we tried to deposit SiC by reacting SiCl_4 and CH_4 ,

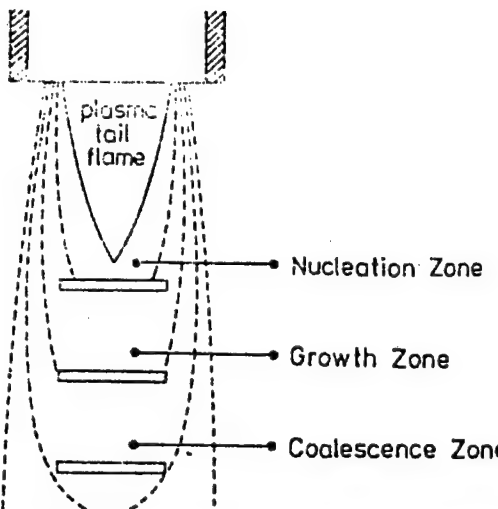


Figure 8. Conceptual Drawing of High Rate Deposition Processes

employing a 25 kW-level hybrid plasma. The deposition of a dense SiC film was observed within the zone of the broken line in Figure 9. In the figure, L denotes the distance from the nozzle, and the fact that the deposition of a dense film occurs for small values of L is considered to be due to the inability of sintering action to follow because of the flux that varies with L in the form of a cosine. In addition, the deposition rate for the SiCl_4 flow rate at $L = 70 \text{ mm}$ is shown in Figure 10. Up to a flow rate of approximately 1.8 g/min, the deposition rate increases rapidly, but this rate decreases sharply with further increases in the quantity of SiCl_4 . This decrease corresponds to the fine particle formation condition, which supports the qualitative plausibility of the scheme shown in Figure 8. Figure 11 [not reproduced] shows the cross section of the coating layer obtained. The figure on the left shows the ruptured state, while the figure on the right shows an SEM image after polishing. It can be seen from these figures that defect-free β -SiC is deposited at about $10 \mu\text{m}/\text{min}$. The density is 3.2 g/cm^3 , and H_v exhibits a value greater than 3000 kg/mm^2 . For details, the reader is referred to the reference.²

4.2 Thermal Plasma Flash Evaporation Method⁷⁻⁹

Since the discovery of high temperature oxide superconductors, various methods of synthesis have been examined. However, the majority of the methods for depositing films from the vapor phase are two-stage processes that require heat treatment in an oxygen atmosphere after synthesis. Moreover, the deposition rate is about $1 \mu\text{m}/\text{h}$ at the most, and when considering applications to various fields in the future, it is urgent that a high speed deposition method be established. The author and his colleagues have attempted to overcome the above-mentioned two points by means of a reactive plasma flash evaporation method that employs high frequency

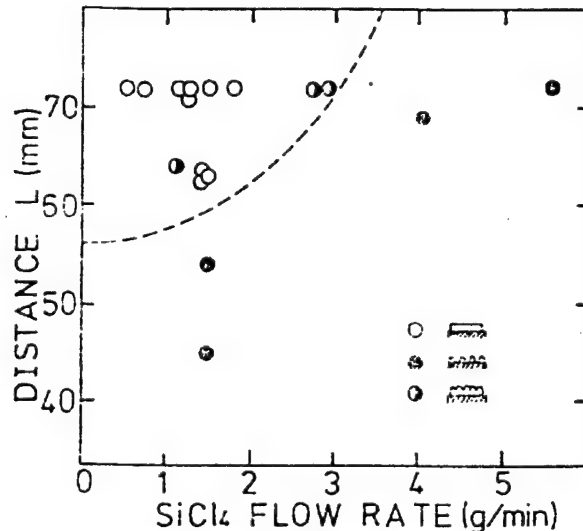


Figure 9. Effects of SiCl_4 Flow Rate and L on the Appearance of Deposits.²

plasma and have discovered the possibility of synthesizing films with high J_c values, which will be presented briefly in the following.

The reactive plasma flash evaporation method is, as mentioned above, a method in which solid particles are injected into a plasma, obtaining a high temperature vapor by completely evaporating the particles, and in which chemical reactions are introduced during the condensation process. The key to this process with respect to the synthesis of high temperature oxide superconductors is a method for generating a normal pressure oxygen plasma with high power, and of the generation

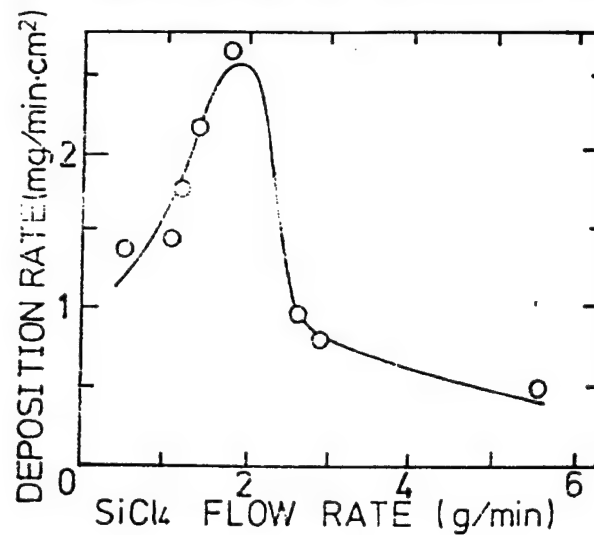


Figure 10. Deposition Rate as a Function of SiCl_4 Flow Rate²

methods, the one most appropriate is the electrodeless discharge-type high frequency plasma torch method. If the particles are smaller than 25 μm , the injected particles are completely evaporated up to the rate of approximately 1 g/min in a plasma flame of above the 30 kW class. Therefore, for YBCO, it is usable whether it is a simple mixture of various kinds of oxides or a powder blended by the coprecipitation method as long as the composition ratios of Y:Ba:Cu are 1:2:3. As for the deposition part, a substrate such as MgO is positioned at the flame tail portion to obtain a substrate temperature of around 700°C. In this way, a dense film that exhibits superconductivity in the as-grown state can be deposited at the rate of about 10 $\mu\text{m}/\text{min}$ (Figure 12 [not reproduced]). This value is 100-1,000 times faster than that of the sputtering method, and oxygen atoms caused by a frozen boundary layer on the surface of the deposited film seem to have the potential to play an important role in the deposition mechanism.

Recently, in order to examine the enhancement of J_c , a film exhibiting the characteristics shown in Figure 13 was obtained with excellent reproducibility by using a reduced pressure plasma of about 200 Torr, controlling the temperature with high precision, and choosing the powder injection rate of approximately 10-20 mg/min. Specifically, a film deposited on an SrTiO₃ substrate had a J_c value of 300,000 A/cm², confirming the effectiveness of this process. For details, the reader is referred to the literature^{8,9}, but it should be mentioned that this is an economically attractive process which employs a high frequency plasma of about 100 kW to completely evaporate the injected powder at the rate of about 20 g/min.

4.3 RF and Hybrid Plasma Spraying Method^{10,11}

The motivation behind the development of this spraying method is the widespread use of the dc reduced pressure spraying method which has been increasingly popular during the past several years. The reduced pressure spraying method was developed to remedy the defect of the ordinary atmospheric pressure dc spraying method which, especially in ceramic synthesis, has been able to

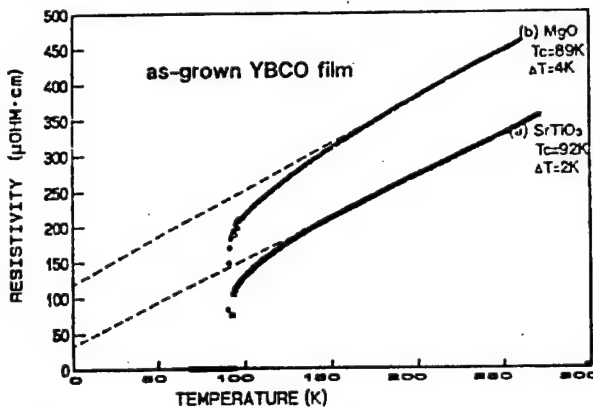


Figure 13. Temperature Dependence of Electrical Resistance for As-Grown YBCO Film

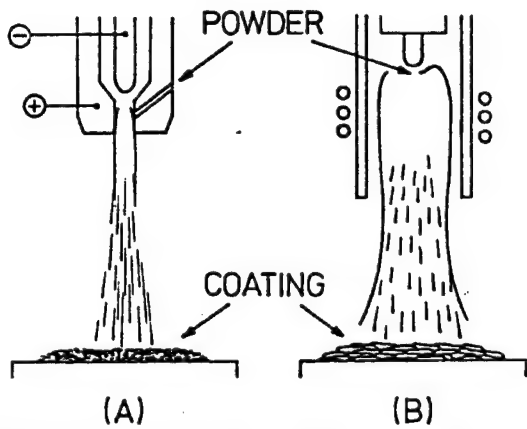
form only porous films. It was the intention of the method to extend the plasma zone by jetting a plasma into a pressure reduced space and to form a film with fewer pores by spraying the particles onto a substrate at an ultra-high speed by means of a gas flow speed of 2,000-3,000 m/s. However, because of operating under reduced pressure, the transfer of momentum and heat has been reduced to about 20 percent that under atmospheric pressure. Because of this, the limitations on the particle size necessarily become severe, and it has gradually been made clear that the spraying of ceramics is particularly difficult. In fact, according to the measurements made recently, it has been revealed that the particle speed is only 200-300 m/s at the most. An enhancement of several steps in the compactness of the sprayed film, in spite of the above, is considered to be due to the uniform heating of particles as a result of the expansion of the plasma zone and the plasma-surface interaction on the surface of the sprayed film. Considering the above, the rf plasma spraying method under atmospheric pressure is regarded as being superior, in several respects, to the reduced pressure dc spraying method.

Figure 14 shows conceptual diagrams for dc plasma spraying (DCPS) and rf plasma spraying (RFPS). The essential differences between the two reside in the difference in flow speeds and the temperature distribution of the plasmas, and the difference in the feeding methods of the particles, and can be reduced to the difference in trajectories and thermal histories of the sprayed particles. Since it is clear that the nonuniformity in the history of the sprayed particles for RFPS is smaller than that for DCPS, a reduction in the porosity of RFPS can be expected. However, since the particle speed is 20 m/s at the most for RFPS and about 70 m/s for hybrid plasma spraying (HYPS), and since the residence time of the particles in the plasma is 5-10 ms, which is longer than that for DCPS, it is necessary to use particles with large diameters, i.e., 70-100 μm , in order to avoid particle evaporation. From what has been said above, RFPS and HYPS can be characterized as uniformly-heated low-speed spraying methods for large-diameter particles.

Figure 15 shows an example of results of the deformation behavior of sprayed particles calculated by the SMAC method, confirming the difference between DCPS and RFPS. These calculations are based on the assumption that Al₂O₃ collides with the substrate at the initial speed V_0 and is deformed at the melting point (2327 K), with 30 μm ($V_0 = 100 \text{ m/s}$) and 100 μm ($V_0 = 30 \text{ m/s}$) conceived for DCPS and RFPS, respectively. There is not much difference in the deformation patterns, but the time required for deformation differs by about one order of magnitude. That is, the thermal flux from the deformed particles of droplets to the substrate or the sprayed layer is increased by about one order of magnitude over that for DCPS, and an enhancement of the bonding properties can be expected. In addition, from the series of calculations above, it has been determined that the degree of deformation (D/d) can be approximated by the following expression:

$$D/d = 0.83(\rho d V_0 / \mu)^{0.21}$$

In the above equation, D is the diameter of the flattened particle, d is the diameter of the sprayed droplet, ρ is the



DC Plasma Spraying RF Plasma Spraying

Figure 14. Schematic Illustration of (A) DC Plasma Spraying and (B) RF Plasma Spraying

density and μ is the viscosity of the droplet which, in general, can be represented by $\mu = \mu_0 \exp(3.8T_b/T)$. According to the above equation, a speed elevation of approximately five times is required for a 40 percent increase in the degree of deformation exclusively by means of a change in the spraying speed. In contrast, the same change in the deformation degree can be achieved by a simple 30-percent elevation of the particle temperature. In addition, when V_o is small, as in RFPS, a degree of deformation equivalent to that of DCPS can be obtained by increasing the particle diameter and raising the temperature by several hundred degrees. (Example: A degree of deformation of about 3 can be obtained for the collision of an Al_2O_3 particle of 30 μm - 2700 K at the speed of 100 m/s and that of a particle of 100 μm - 3000 K at 20 m/s.) From the above, it can be seen that the influence of the droplet temperature on deformation is much more conspicuous than the influence of the speed, so it can be concluded that the low speed property of RFPS can be overcome by the proper choice of the droplet temperature at the time of collision.

Figure 16 shows the experimental results of the influence of the grain size on the degree of deformation of RFPS. For the grain size range of 60-80 μm , the peak of the degree of deformation is in the region $D/d < 1$, and as the diameter decreases with the progress of evaporation, many particles have already solidified by the time they reach the substrate. For a grain size of 105-125 μm , D/d is almost equal to 1, which means that for RFPS of a 50 kw level, the grain size is too large to achieve sufficient melting. On the other hand, for a grain size of 80-100 μm , the peak is when D/d is approximately 2.5-3, and this is the most appropriate size for RFPS. The spraying of such large particles has not been reported in the past, but several interesting results have been obtained so far. Figure 17 [not reproduced] is an SEM image of a cross section of an Al_2O_3 sprayed layer which shows that a very compact sprayed film is being obtained. Even more

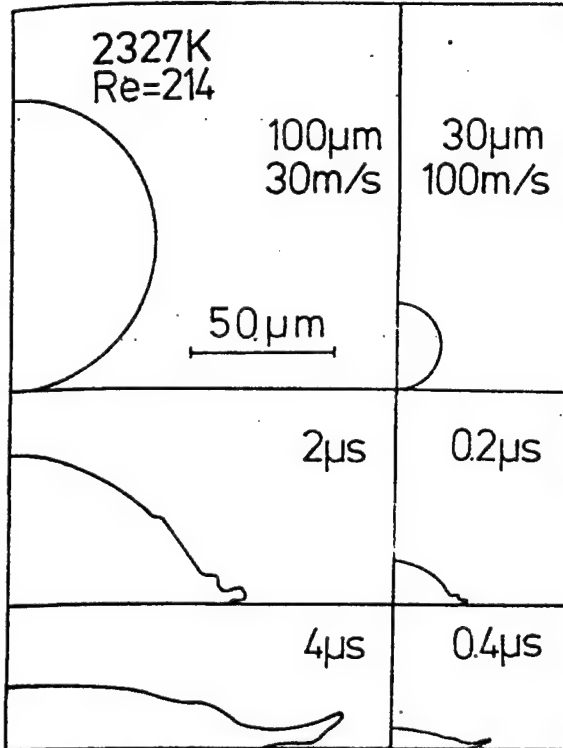


Figure 15. The Deformation Process of a Droplet on a Substrate with a Constant Temperature—2327 K (melting temperature of Al_2O_3) during the deformation of RFPS (left) and DCPS (right)

interesting is the fact that the film consists of the α single phase, which is considered to be due to a cooling speed of approximately 10^4°C/s . Further, as shown in Figure 18, it has become clear that a sprayed film with a relative density of 98 percent is obtained for ZrO_2 by HYPS. The features of the rf and hybrid plasma spraying seem to enable spraying to be applied to highly functional coating. At present, we are examining the possibility of applying the method to a high temperature solid fuel cell (SOFC) through manufacturing process.

5. Conclusion

In this paper we surveyed the problems with and potential for IPP while presenting research performed in our laboratory. Although portions seeking our own advantages may be found, we solicit the reader's criticism after he has examined the references given in conjunction with the applications. The history of this field is short and there is a tendency to seek superficial "material manufacturing." In fact, papers entitled "...by high frequency plasma" or "...by hybrid plasma" show how strongly dependent this field is on the apparatus, and the reverse side of the coin is revealing the nonmaturity of the field as a "science." The biggest reason for this is that the control regions of the physical variables are almost

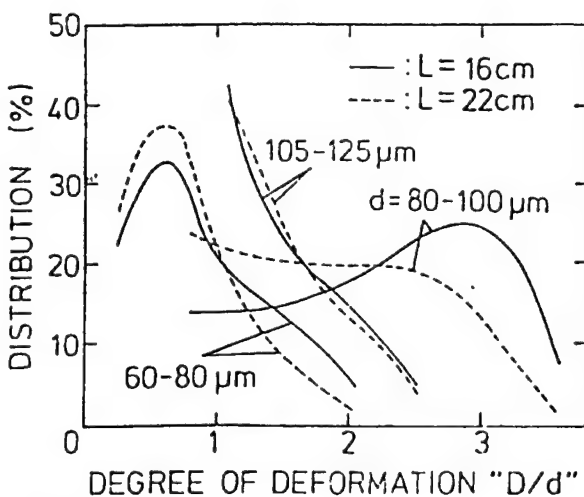


Figure 16. Effect of Al_2O_3 Powder Sizes (d) on Deformation Parameter (D/d) With Distance (L)¹¹

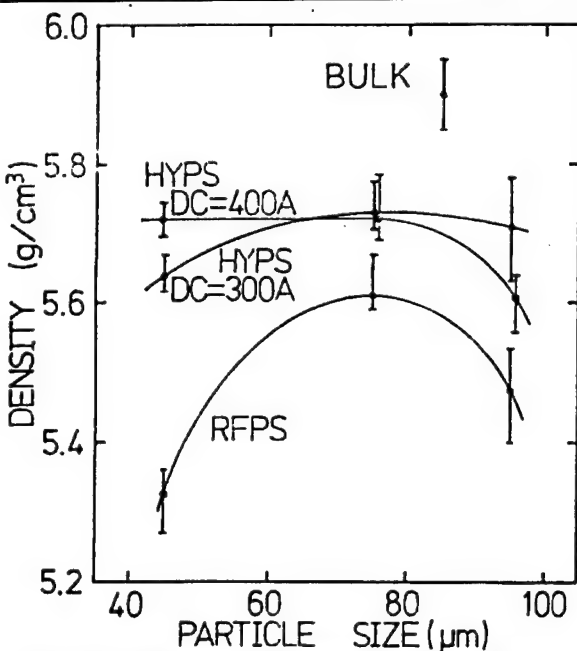


Figure 18. Effect of YSZ Powder Size (d) on Coating Density for RFPS and HYPS

uniquely determined by the apparatus employed, or in a sense, the success of research is determined by how appropriate the process or object is to the apparatus. For these reasons, for both research level and application-oriented cases, what is most desired is the development of an apparatus which will enable a wider range of variables to be controlled. Finally, we would like to inform the reader that one enterprise in Japan is testing IPP employing an rf plasma of an input level of 400 kW, which can serve as an example indicating the direction of the future development of this method.

References

- Yoshida, T., MATER TRANS JIM, Vol 31, 1990 p 1.
- Murakami, H., et al., ADVANCED CERAM MATER, Vol 3, 1988 p 423.
- Murakami, et al., J CERAM ASSOC JPN, Vol 97, 1989 p 49.
- Eguchi, et al., J METAL SOC JPN, Vol 53, 1989 p 1236.
- Lee, H.J., et al., J AM CERAM SOC, Vol 73, 1990 p 3356.
- Ban, et al., J CERAM ASSOC JPN, vol 96, 1988 p 317.
- Terashima, K., et al., APPL PHYS LETT, vol 52, 1988 p 1274.
- Terashima, K., et al., to be published in IEEE TRANS ON PLASMA SCI, Vol 18, 1990.
- Terashima, K., et al., to be submitted.
- Takeuchi, et al., J METAL SOC JPN, Vol 52, 1988 p 711.
- Okada, T., et al., J AM CERAM SOC, Vol 72, 1989 p 2111.

Nanocomposite Technology of Structural Ceramics 916C0035F Ube CHO KO-ON ZAIRYO KOKUSAI SHINPOJIUMU in Japanese 16 Mar 91 pp 67-72

[Article by Koichi Niihara, professor, Institute of Scientific and Industrial Research, Osaka University]

[Text] [English Abstract]: Structural ceramic composites can be divided into three categories: microcomposites, nanocomposites and nanocomposites combined with microcomposites. In microcomposites, the second-phase micrometer-size dispersions, such as particulates, platelets, whiskers and fibers, are dispersed at the grain boundaries of the matrix, while in nanocomposites the second-phase nanometer-size particulates, whiskers and structural defects, such as dislocations, twins and stacking faults, are incorporated within the matrix grains or at the grain boundaries. The main reasons for using microcomposites are to improve the fracture toughness and then fracture strength. On the other hand, nanocomposites, such as $\text{Al}_2\text{O}_3/\text{SiC}$ and $\text{Al}_2\text{O}_3/\text{Si}_3\text{N}_4$, $\text{Al}_2\text{O}_3/\text{TiC}$, MgO/SiC , mullite/SiC, $\text{Si}_3\text{N}_4/\text{SiC}$ and $\text{B}_4\text{C}/\text{SiC}$, $\text{B}_4\text{C}/\text{TiB}_2$, in which the second-phase particulates are dispersed within Al_2O_3 , MgO , mullite, Si_3N_4 and B_4C matrix grains, have recently been developed in our laboratory. These nanocomposites were fabricated by normal powder metallurgical techniques. The fracture toughness and strength have been improved by approximately two to four times by dispersing the nano-size second-phase particles into the matrix grains. The remarkable improvement in hardness and strength can even be observed at high temperatures.

Furthermore, machinability and superplasticity similar to those of metals have also been found for SiC and Si_3Ni_4 -based nanocomposites. In this paper, the recent results for the nanocomposites developed in our laboratory will be reported in detail, and the potential for combining nanocomposites with microcomposites in order to develop ceramics that will be strong and tough, even at high temperatures, will also be discussed. Special emphasis will be placed on understanding the effects that the nanostructure design has on the mechanical properties.

1. Introduction

Improving the characteristics of ceramic structural materials has been accomplished by refining the manufacturing processes and controlling the fine structures, such as the dimensions and shape of the crystal particles, pores and grain boundaries. However, there are already limits to the functions and capabilities that are achievable by such techniques, and new material designs that differ from the conventional ones are required in order to pursue materials that will be demanded in the 21st century.

The author and his colleagues have engaged in this research by classifying ceramics into monolithic materials and composite materials, and further classifying

composite materials into microcomposites, nanocomposites and hybrid materials combining the two, aiming at introducing new material designs into the ceramic region. As a result, we have found that various kinds of mechanical properties of ceramics can be improved drastically by nanocomposite technology. These findings will be outlined in the following.

2. Microcomposite Materials

Microcomposite materials are conventional composite materials which are formed by compounding particles, whiskers or long fibers of the micron level, aimed mainly at improving the brittleness or, in other words, toughening ceramics.¹ There are various toughening mechanisms on this extended line, such as multi-toughening, in which one can make stress phase modifying toughening by means of ZrO_2 , crack deflection by whiskers, and toughening by whisker withdrawal, work simultaneously and effectively without any obstruction.² Research on toughening by means of microcomposite technology has shifted from particle dispersion to whisker reinforcement, with recent interest focusing on the long fiber reinforcing method which enables the highest degree of toughening to be achieved, and which is being studied vigorously throughout the world.³ As a result, very tough long fiber reinforced composite ceramics have been developed that have toughness of 20-30 MPam^{1/2}, comparable to that of cast iron, as shown in Table 1.

Table 1. Long Fiber Reinforced Ceramics

Composite	K_{1c} (MPam ^{1/2})	Fracture Strength (MPa)		
		RT	1000°C	1200°C
LAS/SiC Fiber	1.2-24	850	820	
SiC/SiC Fiber	3.5-33	300	400	280
SiC/C Fiber	3.5-36	500	700	700
$\text{Si}_3\text{N}_4/\text{C}$ Fiber	4.6-29	481		443

3. Nanocomposite Materials

On the other hand, nanocomposites can be roughly classified into intragrain nanocomposites, which compound the crystal grains themselves by dispersing particles or whiskers (or structural defects) on the nanometer order within crystal grains, which are considered to be the smallest constituent units of ceramics, and grain boundary nanocomposites in which particles of nanometric dimensions are dispersed in the grain boundary.

In the nanocomposites in which nanometric particles are dispersed within grains, first, the local residual stresses that are generated within or surrounding the dispersed particles due to differences in the coefficients of thermal expansion and the moduli of elasticity between the matrix and the dispersed phase are used effectively. For example, when the dispersed phase remains harder under higher temperatures than the matrix phase does, dislocations are generated by the local stresses and sub-grain boundaries are formed by pinning the dislocations with the hard nanometric dispersed particles and assembling them, thereby redividing the inside of the

grains. In this way, the number of fracture sources is markedly reduced, enhancing the strength. In addition, it is possible to use this local residual stress to alter the fracture mode and cause intergranular fractures at high temperatures. If this is done, effective crack deflection becomes possible by means of nanometric particles that exist within the grains, improving the toughness by about 1.5 times. At the same time, it becomes possible to reduce the undesirable influence on the high temperature strength of the grain boundaries where impurities have been generated during sintering. Moreover, if the difference between the coefficients of thermal expansion of the matrix phase and the dispersed phase is chosen skillfully, it becomes possible to cause the very small cracks that are generated during crack development (in fracture) to occur only within the crystal grains of the matrix and, by so doing, improve the toughness by about twice. It also becomes possible to pin down the movement of the dislocations generated within the matrix during its use at high temperatures with the hard dispersed particles, thereby enabling the high temperature hardness, strength, creep, fatigue, etc., of the ceramics to be improved sharply. Still further, since the crystal grains

are redivided into nanometric particles and sub-grain boundaries, the decrease and fluctuation in strength can be minimized, even if abnormal grown particles exist, hence making it possible to markedly enhance the reliability of the ceramics.

Grain boundary nanocomposites are materials in which particles of nanometric dimensions are compounded in the grain boundaries and, by so doing, it is intended that the structure or chemical bonding of the grain boundaries be controlled and that the ceramics be endowed with new functions.

3.1 Oxide Nanocomposite Materials

Oxide nanocomposites being manufactured by ordinary sintering technology, such as hot pressing and normal pressure sintering, include $\text{Al}_2\text{O}_3/\text{SiC}$, $\text{Al}_2\text{O}_3/\text{Si}_3\text{N}_4$, MgO/SiC , mullite/SiC, etc.⁴⁻⁷ The important conditions for manufacturing nanocomposites by sintering may be summarized as follows: (1) Fine powder with grains smaller than 0.1–0.2 μm is selected as the starting raw material. (2) Two kinds of powder are dispersed uniformly. (3) Sintering conditions which permit grain growth for the matrix but not grain growth for the dispersed phase are selected.

Photo 1 [not reproduced] shows a transmission electron micrograph of the $\text{Al}_2\text{O}_3/5$ vol percent SiC nanocomposite. It can be observed that the nanometric SiC particles, indicated by arrows, are dispersed within an Al_2O_3 crystal grain of 2–3 μm . In this composite system, by dispersing 5 vol percent of SiC particles within the Al_2O_3 crystal grains, the fracture strength can be improved immediately by three times, from about 350 MPa to about 1,000 MPa, and can be drastically improved further to above 1,500 MPa by annealing the sample for a short time, as shown in Figure 1. Moreover, as is clear from Table 2, marked improvement of the fracture strength can be seen, i.e., from about 350 MPa to 850 MPa for the $\text{Al}_2\text{O}_3/\text{Si}_3\text{N}_4$ nanocomposite and from about 350 MPa to about 700 MPa for the MgO/SiC nanocomposite. The fracture toughness is improved by about 1.5 times for the $\text{Al}_2\text{O}_3/\text{SiC}$ and $\text{Al}_2\text{O}_3/\text{Si}_3\text{N}_4$ systems, and by about four times for the MgO/SiC system.

Table 2. Improvement of Mechanical Properties for Some Ceramic Nanocomposites

Composite	Toughness (MPam ^{1/2})	Strength (MPa)	Maximum Use Temperature* (°C)
$\text{Al}_2\text{O}_3/\text{SiC}$	3.5–4.8	350–1520	800–1200
$\text{Al}_2\text{O}_3/\text{Si}_3\text{N}_4$	3.5–4.7	350–850	800–1300
MgO/SiC	1.2–4.5	340–700	600–1400
$\text{Si}_3\text{N}_4/\text{SiC}$	4.5–7.5	850–1550	1200–1400

* Maximum use temperature under high loads

Figure 2 shows the temperature dependence of the fracture strength of oxide nanocomposites. It can be seen

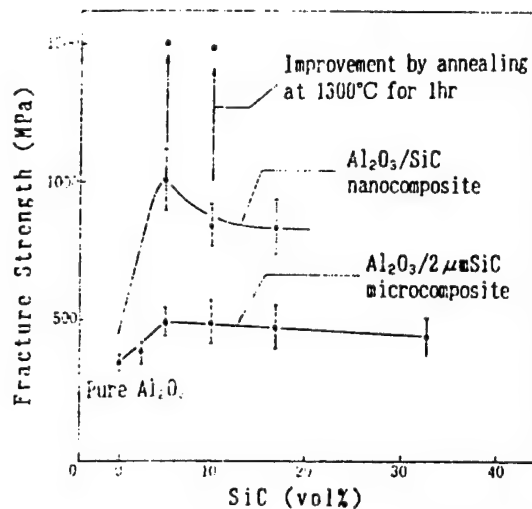


Figure 1. Improvement in Fracture Strength of $\text{Al}_2\text{O}_3/\text{SiC}$ Nanocomposites

that an astonishing improvement in the high temperature strength has been made possible by nanocomposite technology. Also, as shown in Table 2, the maximum usable temperature (considered to be the transition temperature from brittleness fracture to ductility fracture) under high loads has been improved by about 400°C in the Al_2O_3 system composites and by about 700°C in the MgO system composite. In addition, in the $\text{Al}_2\text{O}_3/\text{Si}_3\text{N}_4$ nanocomposite, the thermal shock fracture resistance for quenching in water has been improved by up to about 200°C, having a value of 400°C, which is comparable to that of the SiC material, recognized as a material with strong resistance to thermal shock. Judging from the data on the hardness creep (time change of hardness load at high temperatures), it is believed that the creep at high temperatures has also been sharply improved by converting the materials to nanocomposites.

In general, oxide ceramics, as represented by Al_2O_3 and MgO , possess not only excellent properties for use in high temperature structures, but also permit easy sintering and excellent cost performance. However, in contrast to the nonoxide ceramics, as represented by Si_3N_4 and SiC, they have such problems as (1) low fracture strength and toughness, (2) generate strength deterioration when approaching high temperatures from relatively low temperatures, (3) inferior creep characteristics at high temperatures, and (4) a large coefficient of thermal expansion, which leads to weakness against strong thermal shock. These are the reasons for many workers having attempted to overcome these problems through reinforcement by particle or whisker dispersion. However, no one has successfully improved these problems in one blow. On the other hand, as was mentioned earlier, the above-mentioned problems with oxide ceramics can be overcome in a single action by applying nanocomposite processing. Therefore, it is expected to

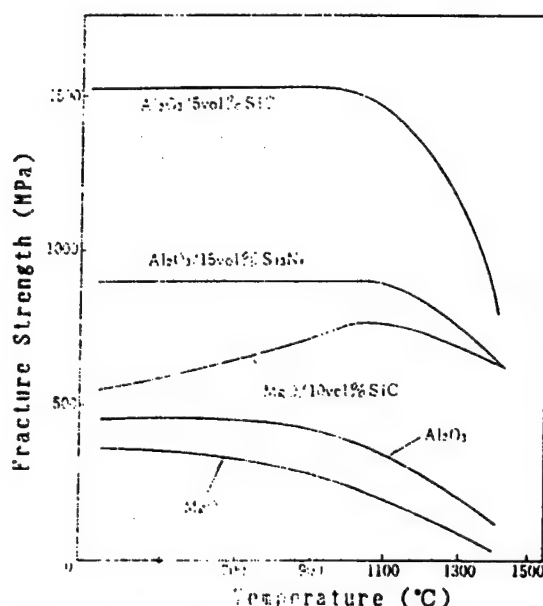


Figure 2. High Temperature Strength of Al_2O_3 - and MgO -Based Nanocomposites

be possible in the future to put oxide ceramics to practical use in place of nonoxide ceramics as materials for high temperature structures for use at temperatures approaching 1200°C by promoting nanocomposite processing in a more efficient manner.

3.2 Nonoxide Nanocomposites

Nonoxide intragrain nanocomposites that have been developed include α - Si_3N_4 /granular TiN,⁸ β - Si_3N_4 /whisker TiN,⁸ SiC/stacked defect,⁹ Si_3N_4 /SiC,¹⁰⁻¹² etc. Of these, the nanocomposites α - Si_3N_4 /granular TiN, β - Si_3N_4 /whisker TiN and SiC/stacked defect were developed by the CVD [chemical vapor deposition] method, and as for the SiC/stacked defect nanocomposite, it is recognized that the fracture toughness can be improved by nearly twice if crack deflection can be caused by the stacked defects. However, in the Si_3N_4 /TiN nanocomposite, no improvement in fracture toughness or strength has ever been observed, perhaps due to the combination of materials.

On the other hand, the Si_3N_4 /SiC nanocomposite, in which nanometric SiC powder is dispersed within the crystal grains or at the crystal grain boundaries, can be manufactured by using an amorphous Si-C-N composite precursor powder, synthesized by the CVD method of the $[\text{Si}(\text{CH})_3]_2\text{NH}-\text{NH}_3-\text{N}_2$ system, as the starting powder and sintering it by adding Al_2O_3 and Y_2O_3 , or with Y_2O_3 alone used as the sintering assistant. Photo 2 [not reproduced] shows a high resolution transmission electron micrograph of one of the SiC particles dispersed within an Si_3N_4 crystal grain. The particle diameter of the SiC dispersed inside the Si_3N_4 grain is less than 0.1 μm , and no impurities have been observed on the

interface. The SiC particles dispersed at the grain boundary of Si_3N_4 have particle diameters nearly equal to those of the SiC particles dispersed inside the grain.

The dimensions and shape of the Si_3N_4 grain are strongly influenced by the dispersion of the nanometric SiC particles and also depend sharply on the sintering process. However, for a quantity of SiC of less than about 25 vol percent, the growth of uniform rodlike Si_3N_4 grains is promoted, increasing the fracture toughness from 4.5 to about 7.5 $\text{Pam}^{1/2}$ and the strength from 850 to 1550 MPa. As the quantity of SiC is increased further, the growth of the rodlike Si_3N_4 grains is obstructed and the fracture toughness is somewhat reduced, while, on the other hand, since the Si_3N_4 grains are becoming finer, the number of fracture sources is decreased and the strength is maintained at a high level.

It is well known that the fracture strength of the Si_3N_4 ceramic deteriorates at temperatures above 1200°C due to the softening of the low melting point impurity phase formed on the grain boundary caused by SiO_2 that exists in the sintering assistant and on the surface of Si_3N_4 grains. However, in the Si_3N_4 /SiC nanocomposites, similar to the case of Si_3N_4 and SiC particles dispersed within the grain shown in Photo 2 [not reproduced], impurity phases do not exist on the Si_3N_4 interface or on the SiC particles dispersed at the grain boundaries. Therefore, the grain boundaries are reinforced and a strength exceeding 1000 MPa is maintained at temperatures of 1400°C, as shown in Figure 3.

It should be noted that when a very fine texture nanocomposite is manufactured to intentionally leave about 35 percent of α - Si_3N_4 through the adjustment of the sintering conditions, which differs from the nanocomposites consisting of β - Si_3N_4 and β -SiC and the grain boundaries described that are sintered at 1750-1800°C aimed at high strength at high temperatures, it is possible to give an ultraplastic deformability as shown in Photo 3 [not reproduced].

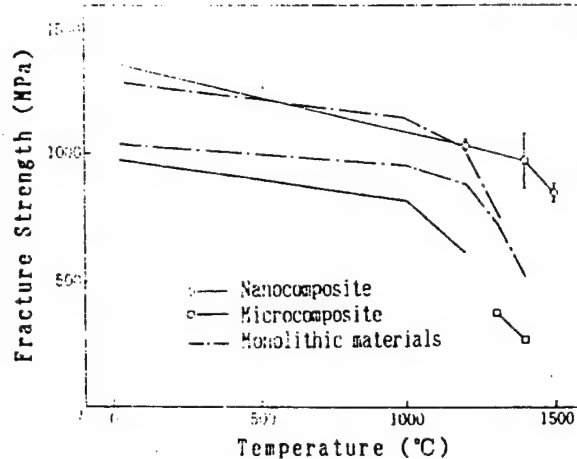


Figure 3. High Temperature Strength of Si_3N_4 /32 vol percent SiC Nanocomposite

Moreover, by adding polysilastystrene organic compound precursor, which turns into SiC upon heating, to the SiC powder, and sintering the compound at 1600-1900°C, it is possible to manufacture a grain boundary nanocomposite with amorphous SiC particles of nanometric dimensions at the SiC grain boundaries.¹⁴ Recently it has been discovered that this nanocomposite exhibits a free-cutting property that makes its machinability similar to that of metals, while nearly maintaining the properties of SiC and exhibiting high strength, i.e., about 450 MPa, even at 1500°C. That the SiC/amorphous SiC grain boundary nanocomposite exhibits free-cutting similar to that of metals is considered to be due to the open pores of nanometric size and to the nanometric particles that exist at the grain boundaries of SiC.

3.3 Roles of Nanometric Dispersed Particles

When one considers the correlation between the micro- and nano-structures of the nanocomposites and their mechanical properties, the roles of the nanocomposites apparently differ for the oxide and nonoxide systems.

The roles of the nanometric particles in such nanocomposites as the Al₂O₃/SiC, Al₂O₃/Si₃N₄ and MgO/SiC systems, in which the matrix material has a larger coefficient of thermal expansion than the dispersed phase and the dispersed phase maintains hardness at higher temperatures than does the matrix phase, may be considered to be as follows:

- (1) Rendering the texture fine, suppressing abnormal grain growth and controlling grain shape: Improves the strength and its fluctuation.
- (2) Deflection of crack tips by the particles dispersed within the crystal grains and formation of microcracks within the grains: Improves the fracture toughness by 1.5 to 4 times.
- (3) Formation of sub-grain boundary by local stress generated within the grains: Controls the formation of coarse grains, suppresses the degradation and fluctuation of strength due to nonuniformity of the texture, improves the strength by reducing the number of destructive sources and improves the strength at high temperatures.
- (4) Guidance of ingrain fracture by the local stresses generated around the particles dispersed within the grains: Attains efficient toughening deflecting the tips of the cracks effected by the nanometric particles dispersed within the grains, and suppresses the delayed fractures at high temperatures due to impurities at the grain boundaries (i.e., improves high temperature strength).
- (5) Pinning of dislocation at high temperatures by hard paraticles dispersed within the grains: Brings about improvements in high temperature hardness, high temperature strength, fatigue, creep resistance and brittleness/ductility transition temperature (highest serviceable temperature under high load).

(6) Control of Young's modulus, coefficient of thermal expansion and thermal conductivity: Improves resistance to thermal shock, linked with improvement in strength and tenacity.

The rodlike grains observed during the liquid phase sintering of Si₃N₄ are said to be formed when α-Si₃N₄ is dissolved in the melt phase generated in the grain boundaries at high temperatures due to the sintering assistant and is reprecipitated as β-Si₃N₄. Accordingly, that the nanocomposite can be formed when Si-C-N composite powder is used as the starting material is considered to be due to the fact that the SiC particles generated at high temperatures from the Si-C-N powder are dispersed into the liquid phase without being dissolved, playing the role of growth nuclei when the rodlike β-Si₃N₄ precipitates uniformly from the liquid phase, and the SiC particles are incorporated into the Si₃N₄ grains in the above-mentioned process. As the quantity of SiC is increased, the growth of the rodlike Si₃N₄ grains is halted and the overall structure becomes fine. This is due to the fact that the number of SiC particles acting as growth nuclei becomes excessive. Therefore, the roles of the nanometric dispersed phase may be considered to be the following:

- (1) The SiC particles dispersed within the grains act as growth nuclei at the time of precipitation of the rodlike β-Si₃N₄ from the melt phase at the grain boundaries, bringing about an improvement in such mechanical properties as fracture tenacity, strength, etc.
- (2) The dispersed SiC particles control the structure at the grain boundaries, serve to realize a strong interface up to high temperatures, and contribute strongly to improving the high temperature strength.
- (3) In addition, the dispersed SiC particles bring about Si₃N₄ grains that are fine in size and, depending on the conditions, contribute to ultraplastic deformability.

4. Future Image of Ceramic Structured Materials

Research on ceramic nanocomposites has just recently been initiated and many points must still be cleared up. Specifically, many unsolved problems remain such as whether the residual stresses inside and outside the nanometric particles dispersed within the grain are really on the levels evaluated by calculations, when and how the sub-grain boundaries are formed, whether the crack deflection by the nanometric particles and the multi-toughening due to microcracks are really being realized, what roles will be played by nanometric particles whose coefficients of thermal expansion are opposite those of the composite systems discussed above, etc. Nonetheless, regarding the systems for which data has been given above, it has been made clear that the nanocomposite formation drastically improves the mechanical characteristics of the ceramics.

Ceramic materials of the future are expected to be used in the forms of monolithic materials, microcomposites and nanocomposites. However, judging from the roles of

the micro- and nanocomposites described in this article, it is anticipated that the ceramics that remain tough up to high temperatures, aimed at being able to withstand the most severe conditions, will be realized as combinations of microcomposites and nanocomposites. The fracture toughness and strength of the Al_2O_3 /5 vol percent SiC nanocomposite formed by dispersing ZrO_2 (containing $2\text{Y}_2\text{O}_3$) in the Al_2O_3 /5 vol percent SiC nanocomposite can be improved by about 30 percent and 70 percent, respectively, by a stress-induced phase-modifying toughening mechanism.¹⁵ These experimental results actually demonstrate that a hybrid composite of micro- and nanocomposites is realizable.

Accordingly, the author and his colleagues believe that combinations or microcomposites and nanocomposites are possible, that the structural materials with the highest strength, highest toughness and highest performance can be developed in that field, and that, in the future, in addition to the ZrO_2 -reinforced nanocomposites, whisker-reinforced nanocomposites and long fiber reinforced nanocomposites will become important.

References

1. Becher, P.E., Wei, G.C., J AMER CERAM SOC, Vol 67 No 12, 1984 pp C267-269.
2. Niihara, K., et al., NEW CERAMICS, Vol 2 No 5, 1989 pp 78-83.
3. Niihara, K., KOGYO ZAIRYO, Vol 1 No 17, 1989.
4. Niihara, K., Nakahira, A., PROC OF MRS INT MEETING OF ADVANCED MATERIALS, Vol 5, 1989 pp 129-134.
5. Niihara, K., et al., HUNTAI OYABI HUNMATU YAKIN, Vol 36, 1989 pp 239-242.
6. Niihara, K., et al., PROC OF 1ST INT SAMPE SYMP, 1989 pp 1120-1125.
7. Niihara, K., NIKKEI MEKANIKARU, Vol 6-25, 1990 pp 129-238.
8. Hiraga, K., et al., J AMER CERAM SOC, Vol 66, 1983 pp 539-542.
9. Niihara, K., HYOMEN, Vol 27 No 1, 1989.
10. Niihara, K., Nakahira, A., PROC OF MRS INT MEETING OF ADVANCED MATERIALS, Vol 5, 1989 pp 107-112.
11. Niihara, K., et al., J MATER SCI LETT, Vol 10, 1991 pp 112-114.
12. Niihara, K., et al., J MATER SCI LETT, Vol 9, 1990 pp 598-599.
13. Wakai, S., et al., NATURE, Vol 344 No 3, 1990 pp 421-423.
14. Niihara, K., et al., "Proc of 3rd Int Symp on Ultrastructure Processing of Advanced Ceramics," John Wiley, 1988, pp 547-556.
15. Niihara, K., et al., HUNTAI OYABI HUNMATU YAKIN, Vol 36, 1989 pp 746-751.

Functionally Gradient Materials as Nanocomposites

916C0035G Ube CHO KO-ON ZAIRYO KOKUSAI SHINPOJIMU in Japanese 16 Mar 91 pp 86-91

[Article by Toshio Hirai, professor, Institute for Materials Research, Tohoku University]

[Text] [English Abstract]: A composite is composed of a matrix and a dispersion. Studies are under way to develop "nanocomposites" which have much smaller dispersions, i.e., on the nanometric order. Here, the dispersion is a solid material. In recent years, much research has focused on the development of new composites, termed "fine composites," prepared by in-situ CVD. In these composites, dispersion is no longer a solid material, but rather an element. "Fine composites" are composed of materials (matrix) and elements (dispersion). Elements include pores, defects, crystal structure, crystal orientation, dispersion conditions and other factors involved in the "dispersion phase." In past studies of composites, a uniform distribution of the dispersion within the matrix was considered essential. By gradually changing the concentration of the dispersion or the type or kind of dispersion within the matrix, new composites, called functionally gradient materials (composites), can be obtained. The preparation and properties of CVD-SiC/C functionally gradient composites are introduced.

1. Introduction

In recent years, materials have often been used under severe environments, and hence the development of materials possessing various kinds of properties, specifically, new composite materials, is expected.

Although attention is being paid to fiber reinforced composites, represented by FRP's and C-C composites, as practical materials, considering the next generation composites, ideas for designing new composites are needed that are free from the conventional concepts.

The author is proposing nanocomposites which contain an ultrafine dispersed phase, fine composites which contain elements as the dispersed phase, and functionally gradient composites in which the distribution of the dispersed phase continuously changes rather than remaining uniform.

In this paper, these composites will be discussed briefly.

2. Manufacturing Methods of Composite Materials

Although various methods are employed for the manufacture of composites, they may roughly be classified into phase connection methods and phase separation (in-situ) methods.

In ceramics, the former is the mixed sintering method. On the other hand, the latter is a composition method utilizing the inhomogenization of homogeneous raw materials (gaseous, molten, liquid or solid) and is also called the in-situ composition method.¹

Examples of in-situ methods are shown in Table 1.

Table 1. In-Situ Composition Methods for Preparation of Nanocomposites, Fine Composites and Functionally Gradient Composites

Raw Materials	Methods
Gas	Chemical vapor deposition
	Physical vapor deposition
Liquid	Sol/Gel
	Co-precipitation
	Hydrothermal
Molten	Precipitation
	Eutectic reaction
Solid	Partial crystallization
	Grain-boundary reaction
	Thermal decomposition

3. In-Situ Composition by CVD Method

Ceramic composites are normally manufactured by the solidification of raw material powder by baking. Since nonoxide ceramics are difficult to sinter, as opposed to the situation for oxide ceramics which is somewhat different, a sintering assistant is often added in order to accelerate the sintering. In addition, because they are necessarily subjected to the complex processes of preparation, mixing, molding, calcining, sintering, etc., it is not easy to control the properties of ceramic sintered composites.

In contrast, in the chemical vapor deposition (CVD) method, solidification is achieved by giving various amounts of energy to the raw material gas, causing the gas to be dissociated and to engage in chemical reactions. By this process, a film or sheet can be obtained with extremely high density without the use of a sintering assistant. Moreover, in-situ composition can be achieved readily by letting the raw material gas be of multiple components.

A handy laboratory-scale CVD apparatus is shown in Figure 1.

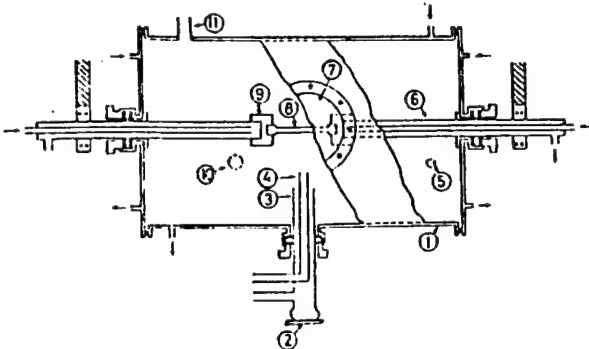


Figure 1. CVD Chamber for Fabricating In-Situ Ceramic Composites

Key: 1. Water-cooled vacuum chamber 2. Quartz glass window 3. Gas inlet 4. Gas inlet 5. Pressure gauge 6. Water-cooled copper electrode 7. Quartz glass window 8. Graphite heater (substrate) 9. Graphite socket 10. Gas outlet 11. Gas outlet

4. CVD Nanocomposites

Professor Roy of Pennsylvania State University synthesized composite ceramics with a dispersed phase of from several to several dozen nanometers by using the solution-sol/gel method, and gave the generic name of nanocomposite to this kind of material.

By the simultaneous vapor phase dissociation of many kinds of raw material gases, it is possible to manufacture a sheetlike or filmlike in-situ ceramic composite. The size of the dispersed phase for this kind of composite is on the order of nanometers, and new properties have been revealed that cannot be explained by the ordinary composition rules.

The nanocomposite structures of the nanocomposites obtained by the CVD method take on various forms, as shown in Figure 2.³ These nanocomposite structures can be controlled by the CVD conditions and the kind of raw material gas system. Figure 2 shows examples of some of these.

5. CVD Fine Composites

The conventional composition method has been to mix or combine a material for the base phase and a material for the dispersed phase. However, with recent advancements in material synthesis techniques, it has become possible to synthesize better controlled and fine composites. Under these circumstances, a new proposal has been made by the author and his colleagues to design composites by combining a material and element, forgoing the conventional concept for composites, i.e., material and material, aimed at the development of new materials. It is a method in which many of the elements summarized in Table 2 can be employed not only as the solid phase, but also as the dispersed phase.

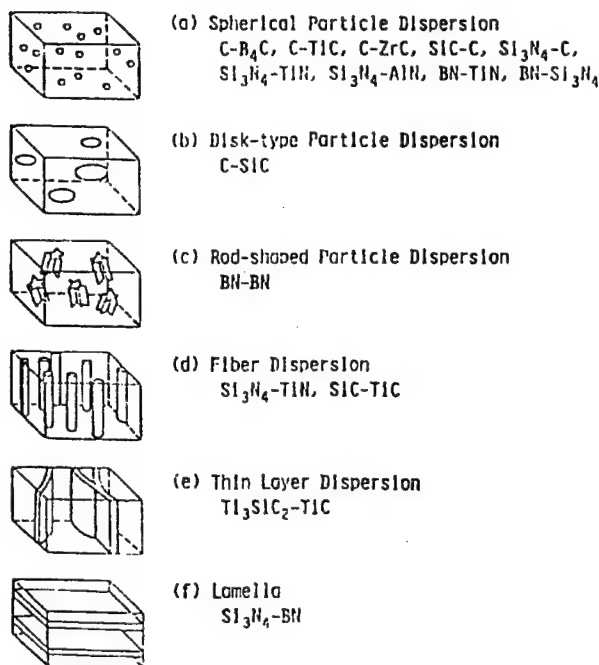


Figure 2. Nano-structures of CVD Composites

Table 2. Elements To Be Considered in Synthesis of CVD Fine Composites

Elements	Examples
Morphology of dispersion	Sphere, rod, fiber, flake, lamella
Type of dispersion	Solid, vapor (void, pore), liquid
Structural combination	Crystalline, turbostratic, amorphous
Boundary	Matching, reaction
Dispersion state	Uniformity, continuity

For example, we take up as objects of composition combinations other than those of materials, such as the dispersion of lattice mismatch, lattice defects or ultrafine voids in the base phase, or varying the crystal structure or crystal orientation even when the dispersed phase and the base phase have equal chemical composition and are of the same material.

Many stacked defects are contained in the crystal grains of CVD SiC. By means of these stacked defects, the direction of crack propagation can be changed and the value of the fracture toughness can be increased. In this case, the stacked defects are regarded as the dispersed phase.

In CVD BN-BN fine composites, the base phase is a disturbed layer structure, while the dispersed phase is a crystalline (hexagonal) BN. It is thought that the layer

peeling property, which is a defect of BN, can be improved by controlling the shape and the dispersed quantity of crystalline BN.

In applying superconductive oxide films to the energy field, it is indispensable that a high J_c (critical current density) be demonstrated, even for high magnetic fields. For that purpose, it is reportedly necessary to introduce a kind of "element" that will be effective in pinning down the vortex line.

In synthesizing YBCO system superconductive oxide film by CVD, the author and his colleagues tried to form a fine composite and a nanocomposite by considering an a-axis crystal orientation as the "element" and a Cu-rich disk-like ultrafine deposit as the nanometric dispersed phase. As a result, a superconductive film has been developed which exhibits a J_c of about 2 million A/cm² under the absence of a magnetic field at 77 K, and which still exhibits J_c of about 60,000 A/cm² at 27 tesla.⁵ The nanocomposite structures of the superconductive oxide films are (b), (d) and (e) in Figure 2. The dispersed phase is a Cu-rich ultrafine dispersed phase for Figure 2 (b), CuO for Figure 2 (d), and an a-axis oriented crystal grain for Figure 2 (e).

6. New Material Development by Inhomogenization: Functionally Gradient Materials

In ordinary composites it is common to disperse the dispersed phase homogeneously in a base phase. However, an attempt has been made to give a new property by inhomogeneously dispersing (sometimes continuously in ultrafine portions) a dispersed phase (material or element) in a base phase.

In an Si₃N₄-C fine composite with amorphous C, several hundred nanometers in diameter, in amorphous CVD Si₃N₄, the C particles form a three-dimensional network, and the thermal conductivity can be increased by 10 orders of magnitude, even with the addition of only 0.2 wt percent of C.⁶

Recently, functionally gradient composites, which exhibit local changes in properties and have been given diversified functions which differ from one point to another in the same kind of material, by continuously varying the concentration, kind and structure of the dispersed phase from one surface toward the other surface, or by locally varying these factors, have been attracting worldwide attention as new materials.⁷

In recent years, the development of ultra-high temperature heat shielding materials for perfectly reusable space planes has been awaited. In this case, one surface of the material is exposed to an oxidizing atmosphere at high temperatures (2000 K), while the other surface is cooled to 1000 K. Therefore, a temperature decrease of 1000 K is generated inside the material. Existing materials cannot withstand such an extreme environment. Neither can laminations of different materials withstand the thermal stress generated within the material.

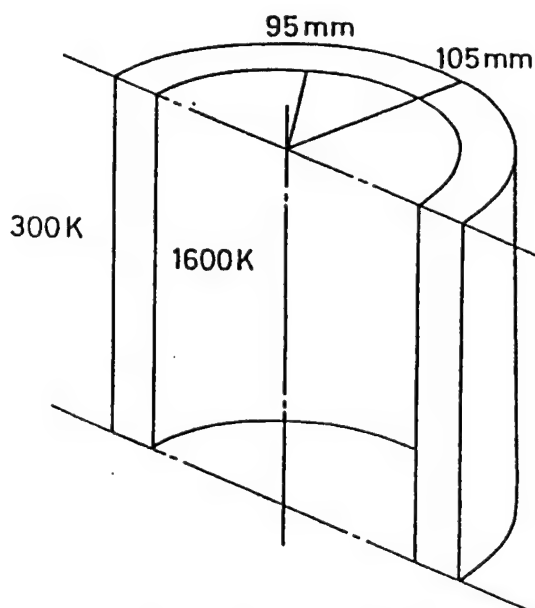


Figure 3. Cylinder Model for Calculation of Thermal Stress in SiC/C Functionally Gradient Composite (inside: SiC, outside: C)

Beginning in summer 1984, five researchers (including the author) from the National Aerospace Laboratories, Government Industrial Research Institute, Tohoku and Tohoku University gathered at the author's laboratory. As a result of heated discussion, they determined it will be effective to design materials of gradient composition in order to relax thermal stress, and proposed "functionally gradient materials" based on the new concepts.⁸

"Functionally gradient materials" were adopted as a large-scale project by the Science and Technology Agency in 1987. A research group was then started, with enterprises related to heavy industries serving as the center, which has been engaged in active research. The first international conference was held last October (1990) at Sendai and attracted the interest of researchers worldwide.⁹ The term "functionally gradient material" is currently included in various dictionaries, as well as being recognized by society in general.

7. CVD SiC/C Functionally Gradient Composites

In developing ultra-high temperature heat stress relaxation-type heat shielding materials, various materials have been examined. This has resulted in a combination of silicon carbide (SiC), which has excellent oxidation resistance at high temperatures and excellent high temperature strength, and graphite (C), which has satisfactory compatibility with C-C composite, the structural base material, a low Young's modulus and high thermal conductivity. This is the SiC/C functionally gradient material, with SiC on one surface of the material and C on the other surface, and in the interior of which the composition continuously changes from SiC to C.

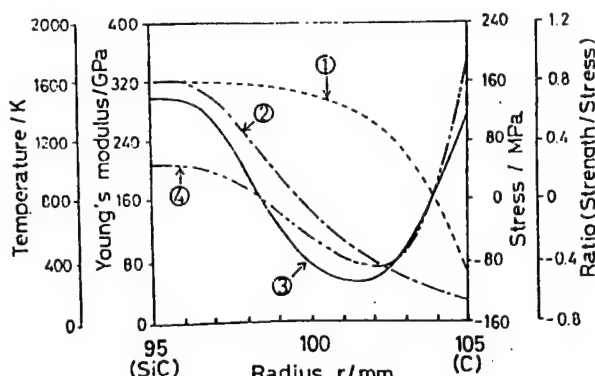


Figure 4. Calculated Distributions of Temperature (1), Young's Modulus (2), Stress (3) and Strength/Stress Ratio (4) in SiC/C Functionally Gradient Composite

In order to predict the optimum distribution of graded composition, thus minimizing the thermal stress, the inside of an almost infinitely long cylinder, having an inner radius of 95 mm and thickness of 10 mm and with only one of its ends constrained, is set at a temperature of 1600 K and the outside at 300 K so as to generate a temperature gradient of 1300 K, as shown in Figure 3, and the stress conditions for the case of vanishing stress in the axial direction have been determined. It is assumed that it is an SiC/C functionally gradient film in which the region from the inner surface to a depth of 1 mm is a monolithic SiC, in the region from 1 mm to 10 mm deep the composition (and various properties) is functionally gradient from SiC to C, and that the composition distribution in the axial direction is uniform.¹⁰

The internal stress under various graded compositions and temperature gradient conditions has been determined. In Figure 4, the distributions of stress, temperature and Young's modulus are shown for the case when the ratio of the strength to the internal stress is less than unity. Then, the compositional distribution for the same case is shown in Figure 5.

In the SiC/C functionally gradient film, the thermal stress can be reduced to one-sixth that of SiC monolithic SiC by grading the composition, as can be seen in Figure 4.

The functionally gradient material with the gradient composition shown in Figure 5 can be synthesized by CVD as follows.

The raw material gas system is $\text{SiCl}_4 + \text{C}_3\text{H}_8 + \text{H}_2$, and the temperature of synthesis is 1773 K. The ratio $[\text{Si}] / ([\text{Si}] + [\text{C}])$ in the material gas changes stepwise under the conditions shown in Table 3 by making the flow rate of C_3H_8 constant and adjusting the flow rate of H_2 , which is the carrier gas of SiCl_4 . With this method, it is possible to synthesize an SiC/C functionally gradient film on a

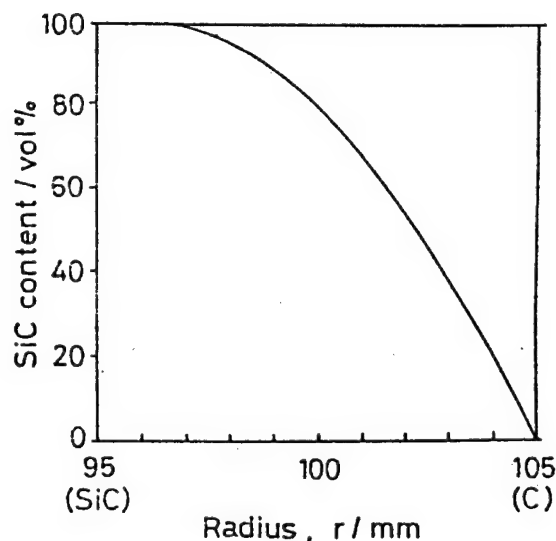


Figure 5. Suitable Compositional Distribution in SiC/C Functionally Gradient Composite As Predicted by Calculation

graphite substrate, where the composition changes continuously from SiC to C. The thickness of the film obtained in 100 minutes of synthesis is approximately 1 mm.

Table 3. CVD Conditions for Preparation of SiC/C Functionally Gradient Composite Using $\text{SiCl}_4 + \text{C}_3\text{H}_8 + \text{H}_2$ System

Deposition Temperature, K	1773		
Total Gas Pressure, kPa	6.7		
Si/(Si+C) in Input Gas	0.66	0.62	0.58
	0.52	0.23	0
Deposition time, min	10	15	15
	10	20	30

An SEM photograph of a cross section of the functionally gradient film is shown in Figure 6 [not reproduced]. A dense SiC phase with a thickness of 150 μm is formed on the graphite substrate, and an SiC/C functionally gradient film, 800 μm thick, which contains voids is formed on top of it. In this region, the ratio of SiC to C varies continuously, and a 50 μm thick C phase is formed on top. The region with a dispersed phase of 10-90 mol percent contains pores about 10 μm in diameter. An especially large number of pores is observed in the portion where the dispersed phase is 40-60 mol percent. The reason for the inclusion of the micropores is believed to be that the dissociation process during the vapor phase is influenced by the change in the mixing ratio of the gas containing Si and that containing C and, as a result, a change in the growth process of SiC and C is produced. The pores begin to be included with the

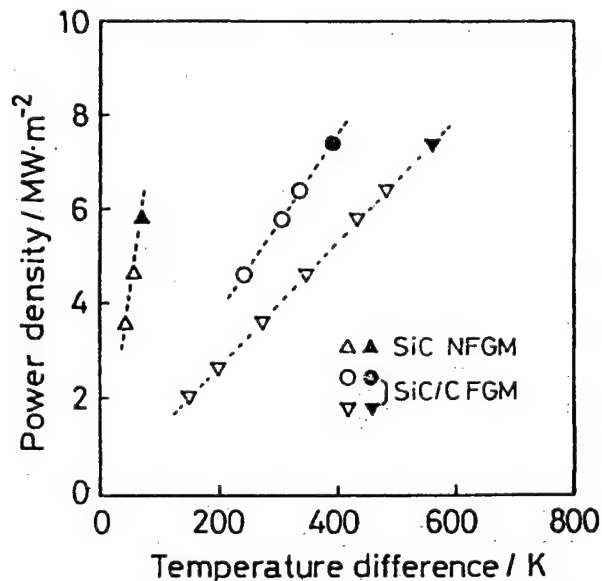


Figure 7. Relationship Between Laser Power Density and Calculated Temperature Difference Under Thermal Shock Resistance Test (open mark: no cracking; closed mark: cracking)

start of growth of the SiC crystal in the direction perpendicular to the deposition surface. The existence of the pores has a favorable influence on the relaxation of thermal stress.

In the region where a trace of SiC has been dispersed in the matrix, the size of SiC is several dozen angstroms, and it is platelike, as shown in Figure 2 (b). The direction of growth of the SiC crystals varies depending on the amount of C. From these observations, it can be concluded that the SiC/C functionally gradient film is a nanocomposite as well as a fine composite.

The thermal shock resistance of the SiC/C functionally gradient film has been examined.¹¹ The results are shown in Figure 7. Using a 5 kW CO_2 laser heated thermal shock testing apparatus (Mitsubishi, ML50C), it is compared with the monolithic CVD SiC. In Figure 7, the relationship between the laser power density and the calculated temperature difference within the film is shown.

In contrast to the 5.8 MW/m^2 laser power density at which cracks are generated (indicated in figure by filled-in shapes) in monolithic SiC, it was found that this value reaches 7.4 MW/m^2 for the SiC/C functionally gradient film. In addition, with an increase in thickness of SiC/C from 0.8 to 1.8 mm, the temperature difference in the film increases from 390 to 560 K. As in the above, since the SiC/C functionally gradient film exhibits excellent

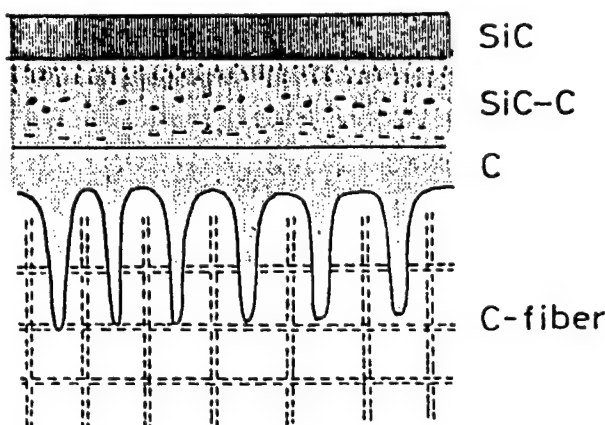


Figure 8. Schematic Diagram of Cross-Sectional View of C-C Composite Coated with SiC/C Functionally Gradient Composite

resistance to thermal shock, it is expected to be used as a thermal stress relaxation type heat shielding material.

An SiC coating has been experimented with in order to give oxidation resistance to the C-C composite, but cracks tend to be generated in the SiC film due to the large difference between the coefficients of thermal expansion of the C-C composite and the CVD SiC. For this reason, application is expected of an SiC/C functionally gradient film in which the composition will be graded from CVD-produced C, with a coefficient of thermal expansion close to that of the C-C composite, to CVD-produced SiC that has oxidation resistance. Figure 8 shows a schematic view of an SiC/C functionally gradient film formed on a C-C composite.

8. Conclusion

In this article, it is shown that the development of new materials is possible by the ultrafine control of the structure, i.e., the forming of a nanocomposite, and by the compounding of elements, i.e., the forming of fine composites.

Today's industrial materials have been produced as a result of homogenization, and are homogeneous materials that have the same properties for all portions of the materials. However, countless things around us found in nature may be termed inhomogeneous materials.

The fibrous tissues in bamboo and wood, the laminated structure of a shell and the inorganic and organic structures of bones change continuously. These are precisely functionally gradient materials. Our effort to develop new materials by the nonuniform dispersion (giving functional gradient properties) of nanocomposites and fine composites involves learning about structures from the materials found in nature.

In this article, we picked up CVD SiC as a functionally gradient material and described it in detail.

As mentioned earlier, research on functionally gradient materials was initiated by focusing on the development of thermal stress relaxation type structural materials which would functional mechanically at high temperatures, with the development of materials for space planes in mind. Proposers of functionally gradient materials, including the author, have been thinking from the beginning that the true stage for these materials includes the fields of energy, electronics, optics, biology, etc. The future development of functionally gradient materials is wholeheartedly expected.

References

1. Hirai, T., "Emergent Process Methods for High Technology Ceramics," "Materials Science Research Series," Vol 17, ed. by R.F. Davis, et al., Plenum, NY, 1984, p 329.
2. Roy, R., MATER SCI RES, Vol 21, 1986 p 25.
3. Hirai, T., Goto, T., "Tailoring Multiphase and Composite Ceramics," ed. by R.E. Tressler, et al., Plenum, NY, 1986, p 165.
4. Hirai, T., et al., J METAL SOC JPN, Vol 28, 1989 p 960.
5. Watanabe, K., et al., APPL PHYS LETT, Vol 54, 1989 p 575.
6. Goto, T., Hirai, T., J MATER SCI, Vol 18, 1983 p 383.
7. Hirai, T., et al., J COMPOS SOC JPN, Vol 13, 1987 p 257; Hirai, T., Sasaki, M., JSME INTERNATIONAL JOURNAL, in press.
8. NEW CERAMICS, No 5, 1989 p 33.
9. "Proc 1st International Symposium on Functionally Gradient Materials," 8-9 October 1990, Sendai, ed. by M. Yamanouchi, et al., FGM Forum, 1990.
10. Sasaki, M., et al., J CERAM ASSOC JPN, Vol 97, 1989 p 539.
11. Hirai, T., et al., POWDER AND POWD METALL, Vol 37, 1990 p 966.

Analysis of Deformation, Strength of Engineering Ceramics at Elevated Temperatures, Its Further Development

916C0035H Ube CHO KO-ON ZAIRYO KOKUSAI SHINPOJIUMU in Japanese 16 Mar 91 pp 103-113

[Article by Kenji Hatanaka, professor, Faculty of Engineering, Yamaguchi University]

[Text] [English Abstract]: A test system equipped with a laser beam-type displacement measuring system has been developed to precisely evaluate the strength of ceramics at elevated temperatures. Tensile and four-point bending tests were performed on silicon-nitride

ceramics at elevated temperatures from 800°C to 1400°C. The linear relationship held between the load, P, and the displacement, δ , at test temperatures below 1200°C. However, the P vs. δ plot deviated from the linear relationship at test temperatures above 1200°C, suggesting the occurrence of inelastic deformation.

The nominal stress-strain relationship is derived from the P- δ relationship measured for the tensile test specimen with four projections. Moreover, the stress-strain relationship has been corrected so that the P- δ curve calculated using the elastic-plastic finite element method agreed with the measured P- δ curve. The corrected stress-strain response seems to give the intrinsic one of silicon-nitride ceramics at elevated temperatures.

The fracture toughness obtained from the Knoop-indented specimen is discussed in comparison with that from the Chevron Notch-type specimen at elevated temperatures.

1. Introduction

Engineering ceramics that excel in heat-, corrosion- and abrasion-resistance have been expanding their range of applications as mechanical structural members in recent years. However, while the practical use of ceramics is being advanced, data on fundamental mechanical properties, such as Young's modulus, Poisson's ratio, yielding stress and nonelastic deformation characteristics, of these materials are currently extremely limited.

In order to develop new ceramics that possess excellent mechanical properties at high temperatures, it is necessary to accurately evaluate the material's mechanical characteristics at high temperatures and form a closed loop connecting the creation and evaluation processes of the ceramics by feeding the results of the evaluation to the creation stage of the ceramic.

In order to define the mechanical characteristics of ceramics at high temperatures and to clarify the microscopic structural and mechanical mechanisms governing the mechanical characteristics, it is necessary to establish accurate mechanical test methods for the materials. At that time, the measurement of the displacement generated in ceramics under temperatures exceeding 1000°C represents a problem.¹

In our laboratory, we have developed a test system which makes it possible to accurately evaluate the mechanical properties of engineering ceramics under temperatures of 1000-1500°C.²⁻⁵ This system is constructed by a noncontact displacement measuring system that uses laser beams, a bisected cylindrical high temperature electric furnace employing the Quantal Super 33 as the heater and a temperature controller, and a closed loop electrohydraulic material testing machine as the loading device. Using this testing system, bending and tensile tests of silicon nitride ceramics at temperatures above 1000°C have been carried out. We have made an effort to clarify the deformation characteristics of these materials

under ultrahigh temperatures through accurate measurements of the bending and tensile displacement. In particular, the stress-strain response of the ceramics to the tensile test provides the most fundamental mechanical characteristics for when these materials are applied to mechanical parts. Only after the tensile stress-strain response of ceramics at ultrahigh temperatures has been clarified will it become possible to carry out the strength design of these materials at high temperatures. In this article, the nonelastic deformation behavior at high temperatures and the basic concepts for the nonelastic design of silicon nitride ceramics will also be touched upon.

2. Outline of Testing Apparatus²⁻⁵

Figures 1(a) and 1(b) are schematic diagrams in which portions with specimens for the bending and tensile tests are loaded on a four-point bending jig and a tensile loading jig, respectively, and a laser-type extensometer is applied to each jig. In Figure 1(a), since the central part of the specimen is deflected with an increase in the load, the sectional area through which a laser beam can pass is decreased. On the other hand, in Figure 1(b), since the distance between the upper and lower projected parts provided on the specimen is increased with an increase in the tensile load, the sectional area through which the laser beam can pass is increased. The laser beam receiver continuously catches the decrease and increase in the light quantity of the passing laser beam accompanying the bending and tensile displacements, and converts the results to displacements. This is the principle of the displacement measuring method employing laser beams.

Under a high temperature environment, the mechanical characteristics of the materials in general are strongly influenced by the rate of displacement. In this test system, a system has been adopted in which the displacement rate of the actuator of an electrohydraulic fatigue testing machine is controlled by a personal computer. Technical investigation is currently under way so as to make possible, in the near future, the control of the displacement rate between the projected parts on the specimen shown in Figure 1 (b). The exterior of the laser beam type extensometer configured for an electrohydraulic material testing machine loaded with a heating furnace is shown in Figure 2 [not reproduced]. It should be added that windows are provided on the heating furnace to pass the laser beams.

3. Calibration of Extensometer Using Laser Beams

Prior to conducting high temperature tests, the accuracy of the laser beam type extensometer was calibrated at room temperature.

3.1 Calibration of Bending Load^{2,3}

During a four-point bending test at room temperature, the surface strain, ϵ , at the central part of the specimen as determined by a strain gauge, and the deflection, δ_1 , at the central part of the specimen are measured simultaneously. The surface strain measured by the strain gauge

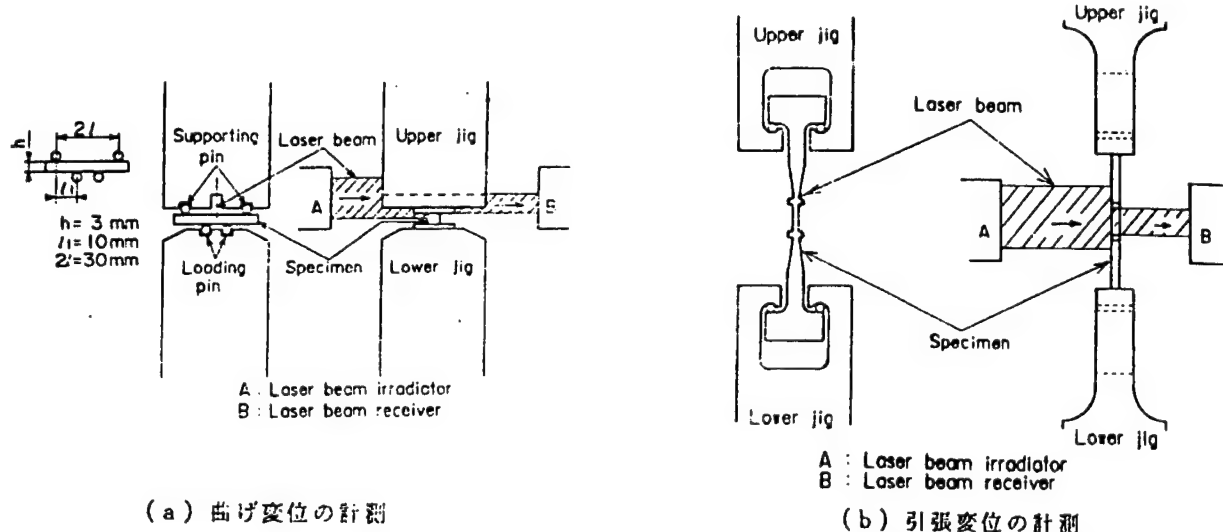


Figure 1. Principle of Displacement Measurement Device Employing Laser Beams. (a) Measurement of Bending Displacement; (b) Measurement of Tensile Displacement

is converted to the deflection, δ_2 , at the central part of the specimen by the following equation:

$$\epsilon = (3 \times \delta_2 \times h) / (3l^2 - l_1^2), \quad (1)$$

where h is the height of the specimen with a rectangular cross section, and which has been set at 3 mm. In addition, l_1 and $2l$ are the distances between a loading point and a supporting point, and between the loading points, and have been selected as 10 mm and 30 mm, respectively. These are indicated in Figure 1(a). The results of the plot between the values of δ_1 and δ_2 are shown in Figure 3. This diagram shows that a displacement of 20-200 μm generated in the ceramics can be detected with sufficiently high accuracy (within 2 percent of the measurement range) with this extensometer.

3.2 Calibration by Tensile Test^{4,5}

In order to measure the tensile displacement of the laser extensometer, it is necessary to use a specimen with projected parts, as shown in Figure 4. The shape and dimensions of the specimen are shown in Figure 4. The strain derived from the elongation between the projected parts on the specimen is under the influence of the stress concentration at the roots of the projected parts, and it is expected to differ from the stress detected at the central part of the specimen. Therefore, the influence of the stress concentration at the roots of the projected parts on the strain at the central part of the specimen has been investigated by the elastic finite element method.

A tensile test was carried out at room temperature by using a specimen which has a strain gauge attached to the central part of the specimen. Concurrently with the strain measurement for that part, the elongation between the projected parts of the specimen was obtained by a

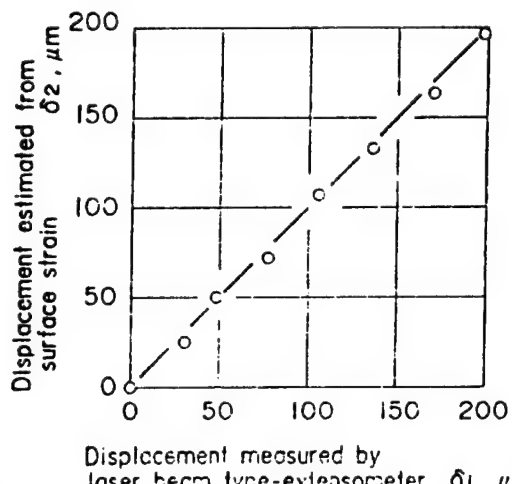


Figure 3. Results of Calibration at Room Temperature by Four-Point Bending Test of Laser Extensometer

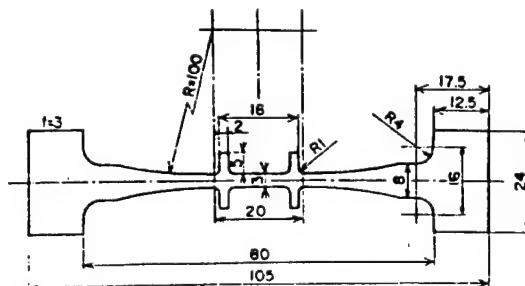


Figure 4. Shape and Dimensions of Tensile Specimen with Projected Parts

laser extensometer. The stress-strain relationship obtained by the strain gauge, the stress-strain relationship obtained by dividing the elongation between the projected parts calculated by the finite element method based on the stress-strain relationship measured by the strain gauge by the original distance between the projected parts, and the stress-strain relationship calculated by dividing the elongation between the projected parts detected directly by the laser extensometer by the distance between the projected parts before the loading are shown in Figure 5. From the figure it can be seen that this extensometer can detect the strain of 100-500 μe generated in the ceramic with an error rate that is within 2 percent that of the results obtained by finite element analysis. Moreover, the strain calculated from the elongation between the projected parts on the specimen by the use of the finite element method can be seen to be about 10 percent larger than the strain detected by attaching the strain gauge directly to the surface of the central part of the specimen. In this way, by combining the displacement measurement using a tensile test piece with projected parts and the stress-strain analysis by the finite element method, it is expected to be possible to determine a stress-strain response which is accurate under high temperatures as well as, needless to say, at room temperature.

4. Nonelastic Deformation Behavior of Silicon Nitride Ceramics at High Temperatures

4.1 Bending Displacement^{2,3}

Figures 6(a), 6(b) and 6(c) show the relationship between the load P obtained by the four-point bending test at high temperatures of silicon nitride shown in Figure 1(a), and the deflection δ_1 at the central part of the specimen measured by the laser extensometer. Figures 6(a), 6(b) and 6(c) represent the $P-\delta_1$ relationship for specimens with pre-introduced cracks formed by pressing the indentor of the Knoop hardness meter with load $P = 294$ and 490 N, and a smooth specimen, respectively. From these figures it can be seen that in both the Knoop indented specimens and the smooth specimen a linear relationship exists between P and δ_1 in the test temperature range below 1200°C . However, at higher test temperatures, there is no linear relationship between the two quantities, and the $P-\delta_1$ line curves convexly upward. The degree of curvature becomes more conspicuous with an increase in the test temperature. Moreover, as can naturally be expected, the deflection at the time of the eventual fracture of the silicon nitride ceramic is larger for smooth specimens than for crack-pre-introduced specimens. It can be understood that this laser extensometer satisfactorily catches the deformation situation of ceramics under such high temperatures. From these observations, it can be seen that although silicon nitride ceramics generate macroscopically only elastic deformations in the test temperature range up to 1200°C under a bending load, they generate nonelastic deformations at temperatures exceeding 1200°C .

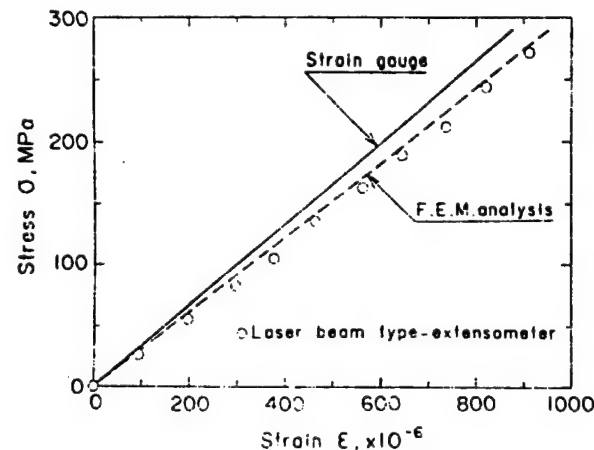


Figure 5. Comparison at Room Temperature Between Analysis Results and Test Results Regarding Stress-Strain Relationship of Specimen and Projected Parts. The measurement results obtained by the laser extensometer and those by finite element analysis represent the mean strain between the projected parts, while the measurement results obtained by the strain gauge represent the strain at the central part between the projected parts.

It should be added that the dimensions of the cracks pre-introduced to the specimens by the Knoop indentor with load P of 294 and 490 N are, respectively, surface lengths $2c$ approximately equal to 710 and 1010 μm , and depths a approximately equal to 310 and 470 μm .

4.2 Tensile Displacement⁶

Tensile tests of the silicon nitride ceramics at room temperature and high temperatures by the technique shown in Figure 1(b) have been carried out. Here, the control of the rate of tensile displacement is controlled by regulating the displacement rate of the actuator of a closed-loop-type electrohydraulic material testing machine with a personal computer. The displacement rate of the actuator is set at 0.06 mm/min.

Stress analysis employing the elastic finite element method was conducted for a quarter of the specimen shown in Figure 4. Figure 7(a) shows the plot, relative to the longitudinal direction, of the dimensionless value obtained by dividing the maximum principal stress on the side face of the specimen calculated by this method by the maximum principal stress on the side face at the central part of the specimen. From the figure it can be seen that the stress at the roots of the projected parts of the specimen is about 1.4 times larger than that at the parallel portion. Figure 7(b) is the distribution of stresses for the same specimen obtained by applying the elastic and plastic analysis under test conditions of temperature = 1300°C and displacement rate = 0.06 mm/min. From the figure it can be seen that the stress concentration at the roots of the projected parts under high temperatures

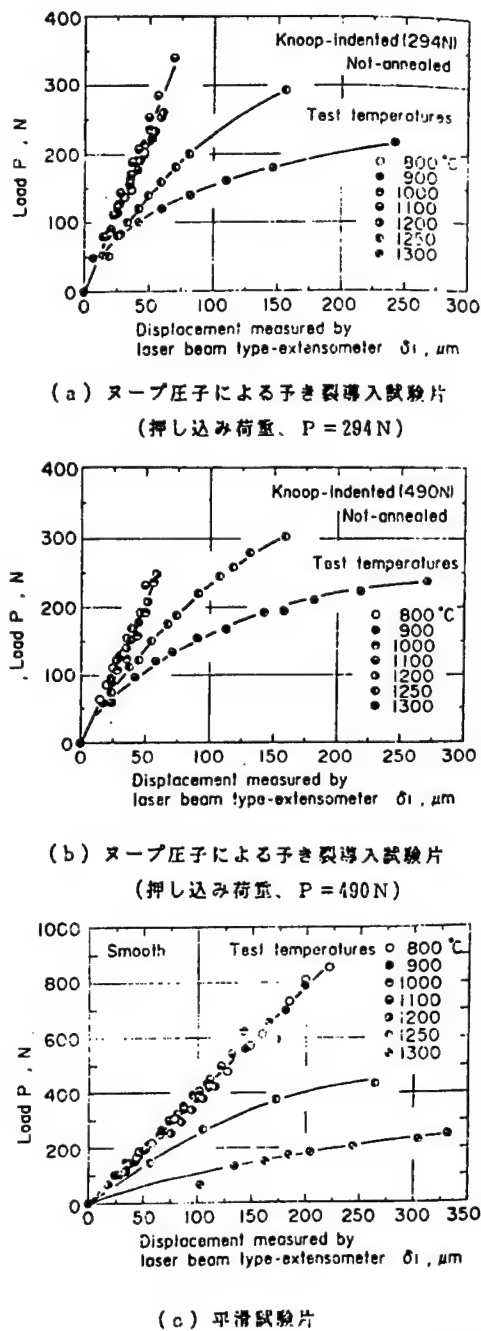


Figure 6. Relationship Between Load and Deflection at Central Part of Specimen in Bending Test

Key: (a) Specimen with pre-introduced crack by Knoop indentator (indentation load $P = 294\text{ N}$) (b) Specimen with pre-introduced crack by Knoop indentator (indentation load $P = 490\text{ N}$) (c) Smooth specimen

is sharply reduced compared to the case at room temperature due to the nonelastic deformation generated at the roots of the projected parts.

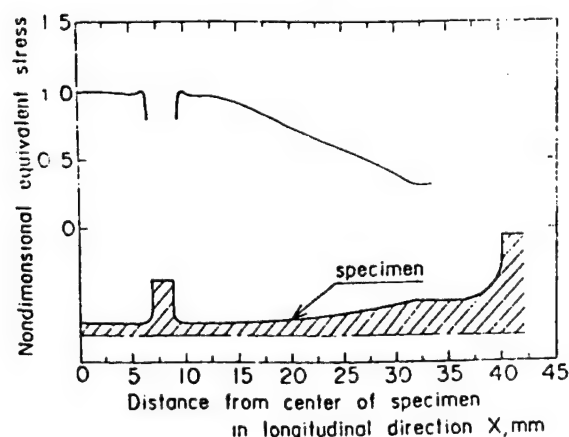
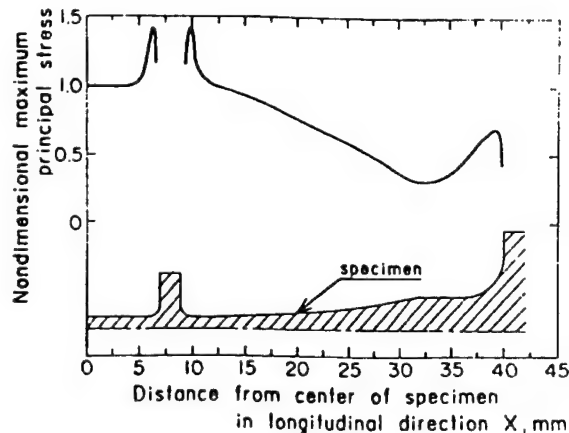
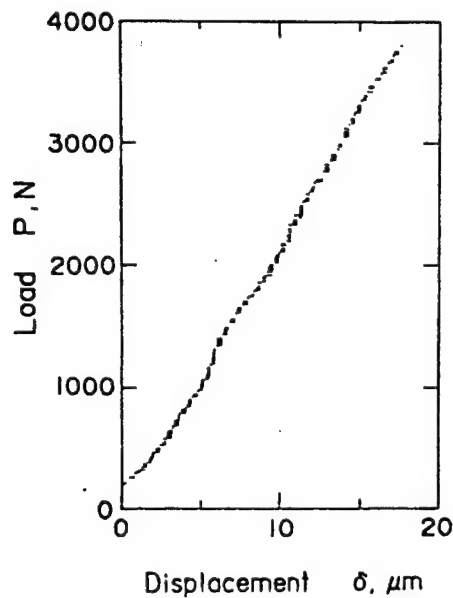


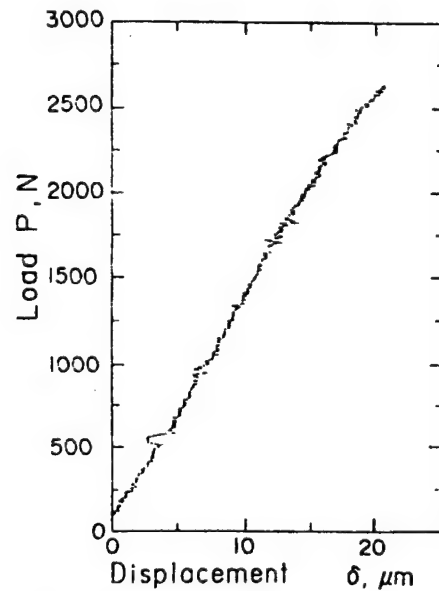
Figure 7. Plot of Stress Ratio in Axial Direction on Side Face of Specimen Against Distance from Specimen Center

Key: (a) Distribution of main stress calculated by elastic finite element method at room temperature (b) Distribution of stresses calculated by elastic and plastic finite element methods under temperature = 1300°C and displacement rate = 0.06 mm/min

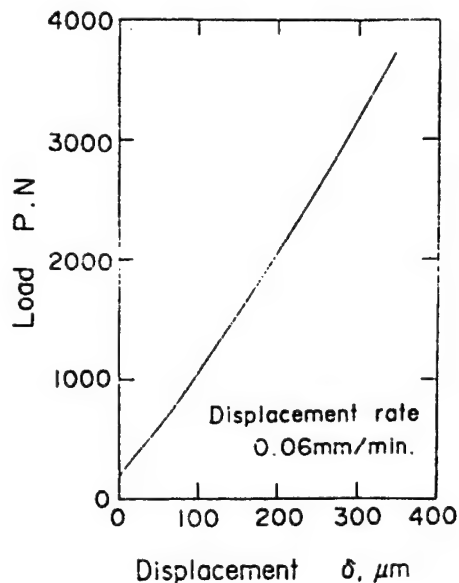
The load (P)-displacement (δ) relationships measured at the test temperatures of room temperature, 1200°C , 1300°C and 1400°C by controlling the displacement rate of the actuator at 0.06 mm/min are shown in Figure 8-11, respectively. In all of the figures, (a) and (b) represent the relationship between the load and the displacement between the projected parts of the specimen measured by the laser extensometer, and that between the load and displacement of the actuator,



(a) 荷重を試験片の二つの突起部間の変位に
対してプロットした結果



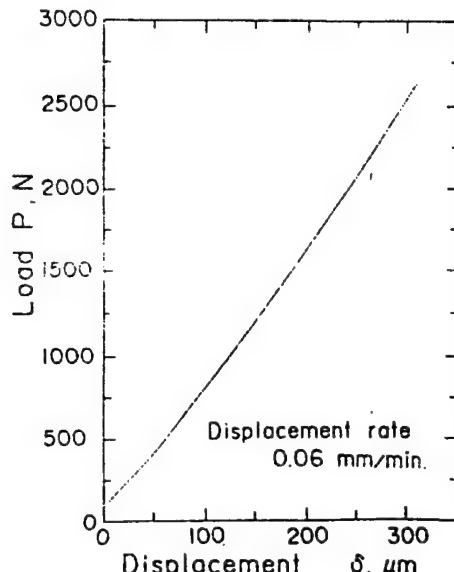
(a) 荷重を試験片の突起部間の変位に対して
プロットした結果



(b) 荷重を試験機のアクチュエーターの
変位に対してプロットした結果

Figure 8. Load-Displacement Curve at Room
Temperature

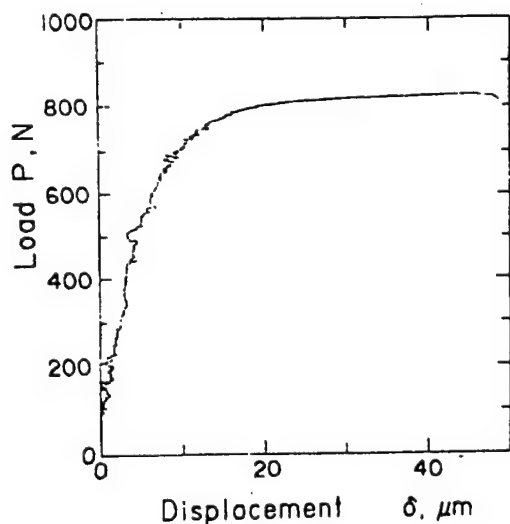
Key: (a) Plot for load versus displacement between two projected parts (b) Plot for load versus displacement of actuator of testing machine



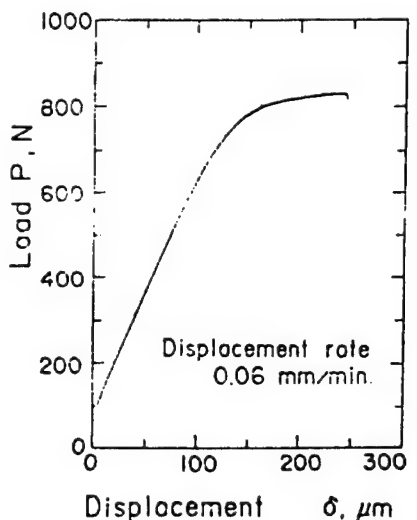
(b) 荷重を試験機のアクチュエーターの変位に
対してプロットした結果

Figure 9. Load-Displacement Curve at $T = 1200^\circ\text{C}$

Key: (a) Plot for load versus displacement between two projected parts (b) Plot for load versus displacement of actuator of testing machine



(a) 荷重を試験片の二つの突起部間の変位に
対してプロットした結果

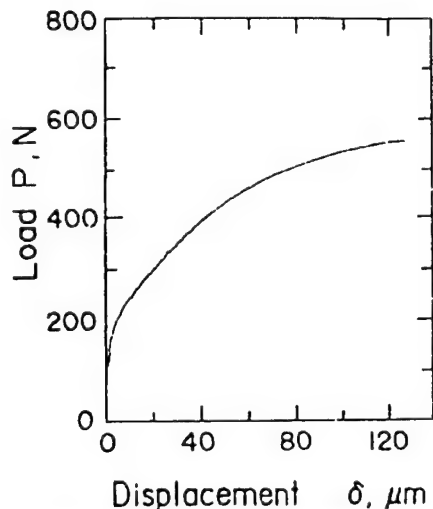


(b) 荷重を試験機のアクチュエータの変位に
対してプロットした結果

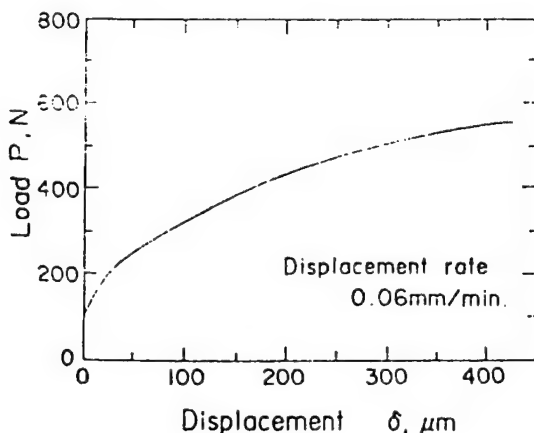
Figure 10. Load-Displacement Curve at T = 1300°C

Key: (a) Plot for load versus displacement between two projected parts (b) Plot for load versus displacement of actuator of testing machine

respectively. At room temperature and 1200°C, the load-displacement relationship for both (a) and (b) is nearly



(a) 荷重を試験片の二つの突起部間の
変位に対してプロットした結果



(b) 荷重を試験機のアクチュエータの
変位に対してプロットした結果

Figure 11. Load-Displacement Curve at T = 1400°C

Key: (a) Plot for load versus displacement between two projected parts (b) Plot for load versus displacement of actuator of testing machine

linear, indicating that the specimen is undergoing an elastic deformation. In contrast, at 1300 and 1400°C, the curves for the P- δ relationship are convex upward, and it should be noted that these specimens are clearly undergoing nonelastic deformations.

A comparison of the P- δ relationship (a) obtained by means of the extensometer and the P- δ relationship (b) obtained by the displacement of the actuator reveals

nearly similar behavior exhibited qualitatively for all test temperatures. This can be considered to serve as evidence for the measurement of high temperature deformation by the laser extensometer having been performed accurately. As can be observed from the measurement results obtained by the laser extensometer at room temperature and at 1200°C, the resolution is about 0.5 μm. As can be seen from the P-δ relationship (Figure 8(a)) at room temperature, minute displacements on the order of 20 μm generated in ceramics can be measured with high accuracy, at a resolution of about 0.5 μm, by this extensometer. Moreover, as is clear from Figures 9(a) to 11(a), this extensometer can accurately measure high temperature tensile displacement on the order of 20-120 μm generated in ceramics at high temperatures of 1200-1400°C.

In the P-δ relationship obtained by the four-point bending test shown in Figure 6, silicon nitride ceramics displayed a linear response for test temperatures below 1200°C, and a nonlinear response for test temperatures above that temperature. Such load-displacement responses nearly coincide with the load-displacement under tensile load shown in Figures 8-11.

The relationship for the nominal stress-nominal strain obtained by the P-δ relationship from the tensile test is shown in Figure 12. Here, the nominal stress σ is obtained by dividing the load P by the initial sectional area at the parallel portion of the specimen, and the nominal strain ϵ is obtained by dividing the elongation between the two projected parts of the specimen by the initial separation between the projected parts before the loading. Accordingly, in evaluating σ and ϵ , the influence of the stress concentration generated at the roots of the projected parts is not taken into account. Naturally, the test temperature dependence of the σ - ϵ relationship becomes the same as the test temperature dependence of the P-δ relationship mentioned above. The bending in the σ - ϵ relationship generated at test temperatures above 1200°C is considered to be caused by the flow of glass layers in the crystal grains of silicon nitride whose viscosity is lowered at high temperatures, or the generation or combination of cavities at the triple point of the grain boundaries, etc.

The fracture strain at room temperature is about 1300×10^{-6} . This value tends to increase slightly at 1200°C. However, in the temperature range above 1300°C, non-elastic deformation occurs and the fracture stress increases rapidly with the rise in the test temperature, reaching about seven times that found at room temperature at 1400°C. It can be seen that this laser extensometer correctly measures the deformation situation of ceramics at high temperatures.

4.3 Correction to Stress-Strain Response at High Temperatures by Elastic and Plastic Calculations

The nominal stress-nominal strain relationship shown in Figure 12 has been determined without taking into

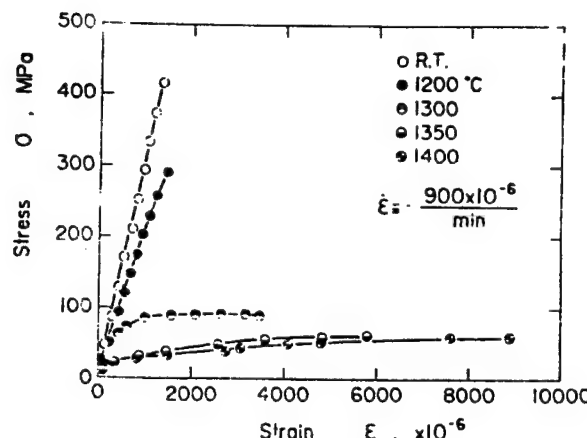


Figure 12. Nominal Strain-Nominal Stress Response for Silicon Nitride Ceramics Obtained for Various Test Temperatures

consideration the influence of the projected parts provided on the specimen. In other words, the above results are not considered to represent the exact stress-strain response of the material. Therefore, in order to correct this situation, the relationship between the load generated in the specimen and the displacement between the projected parts has been calculated by carrying out elastic and plastic finite element analysis for the specimen shown in Figure 4, based on the nominal stress-nominal strain relationship.

Figure 13 compares the P-δ relationship obtained under test conditions of a 1300°C temperature and 0.06 mm/min displacement rate with that calculated from elastic and plastic finite element analysis. According to the figure, it can be seen that this P-δ relationship has a displacement difference of approximately 10-15 percent for a given load. For this reason, the stress-strain relationship to be introduced to the finite element analysis has been corrected so as to make the P-δ relationship obtained by finite element analysis coincident with that obtained by the experiment. This was accomplished by correcting the stress in the nominal stress-nominal strain relationship by making the rate the same as that of the displacement difference between the P-δ relationship obtained by the experiment and that obtained by the analysis.

Figure 14 compares the load-displacement relationship calculated by the elastic and plastic finite element method using the corrected stress-strain relationship as the material constitution formula with that obtained by the experiment. From the figure it can be seen that the two load-displacement relationships show good agreement. From these results, it can be seen that it is possible to correct the stress-strain relationship by the above-mentioned technique without repeating the calculation, thus determining the correct stress-strain response for the material.

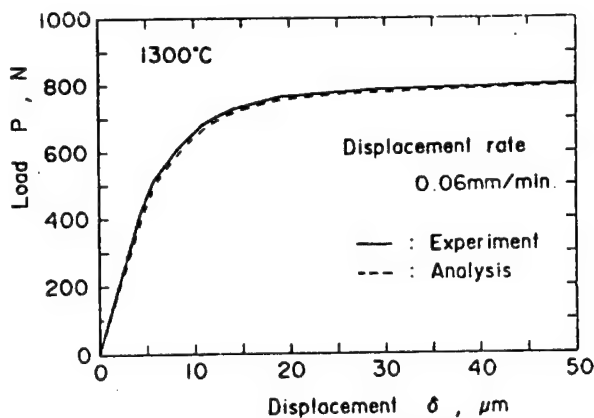


Figure 13. Comparison Between Load-Displacement Curve Calculated by Elastic and Plastic Finite Element Method Using Nominal Strain-Nominal Stress Relationship. The test conditions are temperature = 1300°C and displacement rate = 0.06 mm/min.

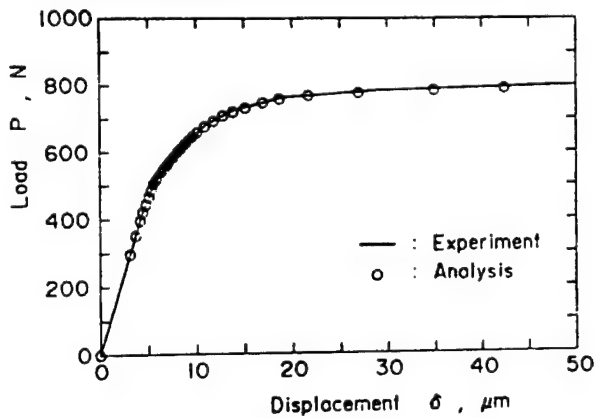


Figure 14. Comparison Between Load-Displacement Curve Derived from Elastic and Plastic Finite Element Method to Which Corrected Strain-Stress Relationship Has Been Introduced and Experimental Results. The experimental conditions are temperature of 1300°C and displacement rate of 0.06 mm/min.

The results of the deformation analysis of the tensile specimen with projected parts shown in Figure 4 by the elastic and plastic finite element method by means of the corrected stress-strain relationship is shown in Figure 15. In the figure, part (a) shows the division of the deformation region into seven parts in the corrected stress-strain relationship. Then, (b) and (c) show the progressive conditions of deformation in the quarter portion between the two projected parts, that includes the parallel portion of the specimen generated as a result of loading, in relation to (a). Specifically, these diagrams show the corresponding stress-strain curve shown in (a) under two kinds of loads. From the figure it can be seen that the nonelastic deformation in the portion between

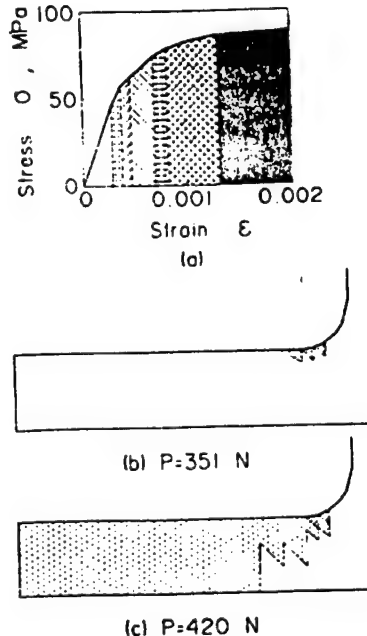


Figure 15. Results of Calculation by Elastic and Plastic Finite Element Method of the Development Process of the Nonelastic Deformation Region Accompanying the Loading of a Specimen with Projected Parts. The experimental conditions are a temperature of 1300°C and displacement rate of 0.06 mm/min.

the projected parts of the specimen advances in the order of (1) the root sections between the projected parts and (2) the parallel section of the specimen. From these findings it can be seen that the nonelastic deformation in the root sections of the projected parts will not enlarge too much under the constraints of the elastic deformation region remaining in the central region of the specimen, but that the nonelastic deformation will advance in the parallel section of the specimen instead. This seems to be the reason for a strain difference of only about 10-15 percent being generated between the $P-\delta$ relationship calculated from the nominal stress-nominal strain curve and that obtained from the experiment, as shown in Figure 13.

5. Fracture Strength Characteristics²⁻⁵

5.1 Flexural Strength^{2,3}

Figure 16 plots the flexural strengths σ_{bf} of Knoop-indented specimens and a smooth specimen against test temperature T. From the figure it can be seen that the flexural strength of the smooth specimen remains approximately equal to that measured at room temperature up to a test temperature of 900°C, while it decreases at higher temperatures. The rate of decrease is larger at temperatures exceeding 1200°C than at 900-1200°C.

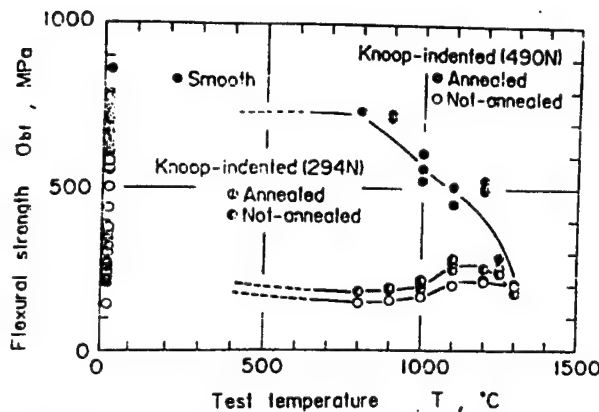


Figure 16. Test Temperature Dependence of Flexural Strength

On the other hand, the test results for the specimens with pre-introduced cracks under Knoop loads of $P = 294$ and 490 N reveal the following fact. Namely, although the flexural strength is approximately constant for tests when the temperature ranges from room temperature to 900°C , it reaches a maximum in the neighborhood of 1000 - 1200°C . Furthermore, in the test temperature region of 1250 - 1300°C , the flexural strength of the indented specimens becomes approximately equal to that of the smooth specimen.

In Figure 16, the flexural strength at room temperature is compared for a Knoop-indented specimen subjected to annealing at 1000°C for one hour and one which was not annealed. At room temperature, for specimens that had been Knoop-indented with loads of 294 and 490 N, the annealed specimen demonstrates higher flexural strength than the unannealed specimen. This is thought to be due to the releasing, by annealing, of the tensile stress remaining in the vicinity of the tip of the pre-introduced crack.

The fact that σ_{bf} exhibits a maximum value in the σ_{bf} - T relationship for the indented specimens is thought to be due to the slowing down or coagulation of the tip of the crack in the temperature range of 1100 - 1200°C , in addition to the release of the residual tensile stress in the vicinity of the crack tip in the 1000 - 1200°C range. Moreover, the fact that the indented specimens demonstrate approximately equal flexural strength to that of the smooth specimen in the 1250 - 1300°C range is also considered to be due to a further promotion of coagulation at the tip of the pre-introduced crack in that temperature range.

5.2 Tensile Strength^{4,5}

5.2.1 Specimen for Tensile Strength Measurement

The shape and dimensions of the specimen used for investigating tensile strength are shown in Figure 17. This shape was determined following stress analysis by the finite element method by considering such factors as the

ease with which the specimen could be mounted on the jig and fractures caused at the gauge section of the specimen. In addition, a smooth notch, $150\ \mu\text{m}$ deep, is provided on both side faces at the central part of the specimen in order to prevent it from rupturing at the roots of the tapers. The coefficient of concentration of the notch's elastic stress is 1.05. Elastic stress analysis was carried out by the finite element method and, in Figure 18, the dimensionless value obtained by dividing the maximum principal stress on the side face of the specimen by the maximum principal stress on the side face at the central part of the specimen is plotted against the distance from the center of the specimen in the longitudinal direction. In addition, a specimen with a semi-elliptical Knoop-indented surface crack formed by a load of $P = 490$ N, given at the central part of the specimen shown in Figure 17, has also been manufactured.

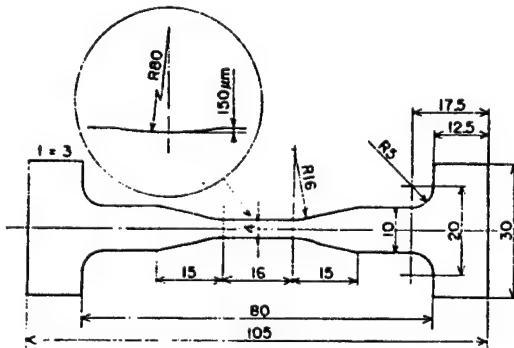


Figure 17. Shape and Dimensions of Specimen for Tensile Strength Measurement

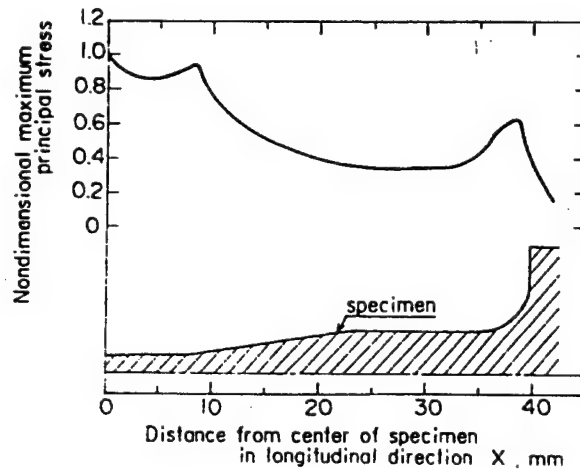


Figure 18. Stress Distribution on Side Face of Specimen for Tensile Strength Measurement Calculated by Finite Element Method

5.2.2 Tensile Strength

In Figure 19, the tensile strengths for a smooth specimen and a Knoop-indented specimen are plotted as functions of the test temperature. The curve for the four-point bending strength test temperature is also included in the figure. It should be mentioned that the shape coefficient of 1.05 at the central portion of the specimen mentioned above is taken into account in the tensile strength. The flexural strengths are all maximum stresses on the specimen surface at the time of fracture as obtained by elasticity calculation, and the effect of the inelastic deformation is not taken into account in calculating the fracture stress at high temperatures. From the above it can be understood that, for the smooth specimen at temperatures ranging from room temperature to 1000°C, the fracture stress as determined by the tensile test is about 70-85 percent that obtained by the bending test. The difference between the fracture stress determined by the four-point bending test and that by the tensile test barely changes with the rise in the test temperature. Further, the fracture stresses determined by the bending and tensile tests are decreased somewhat at 800°C from the values obtained at room temperature, but values are constant, without change, up to 900°C. However, the fracture stress decreases sharply at temperatures exceeding 900°C. Namely, the rate of the decrease increases markedly in the temperature range above 1200°C for the bending test, and above 1000°C for the tensile test. Moreover, the behavior of the fracture stress test temperature curve for a Knoop-indented specimen nearly agrees with that mentioned in conjunction with Figure 16. It should be mentioned here that the fracture strength shown in Figures 16 and 19 were obtained using silicon nitride ceramics created by means of different processes.

6. Fracture Toughness^{4,5}

In order to obtain fracture toughness values, a specimen with a chevron notch, introduced for the bending test, as shown in Figure 20, has been manufactured in addition to the Knoop-indented tensile and bending specimens.

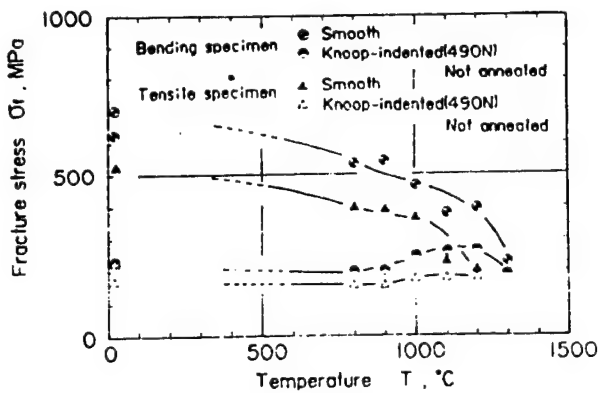


Figure 19. Test Temperature Dependence of Tensile and Four-Point Bending Strength

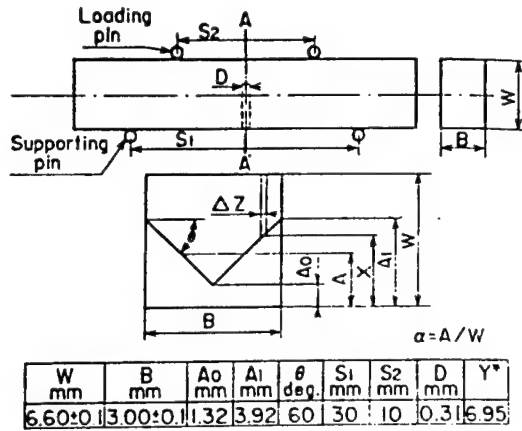


Figure 20. Various Data Concerning Chevron Notched Specimen. Here, Y^* is the shape correction parameter included in the formula for calculating the fracture toughness based on Bluhm's slice model.^{8,9}

Figure 21 shows the fracture toughness K_{IC} obtained by the bending test for a Knoop-induced specimen and a chevron notched specimen, and by the tensile test for the Knoop-indented specimen. From the figure it can be seen that, for both Knoop-indented specimens, the fracture toughness test temperature diagram exhibits approximately the same tendency as does the fracture strength test temperature diagram.

The fracture toughness values obtained by the Knoop-indented specimens are comparable for both the bending and tensile specimens in the test temperature range of from room temperature to 800°C, but the fracture toughness of the bending specimen becomes larger than that of the tensile specimen when the test temperature exceeds 800°C. The reason for this change is now yet clear.

The strength at high temperatures seems to be conspicuously influenced by the rate of strain, and it can be considered that the difference in the rates of strain in the

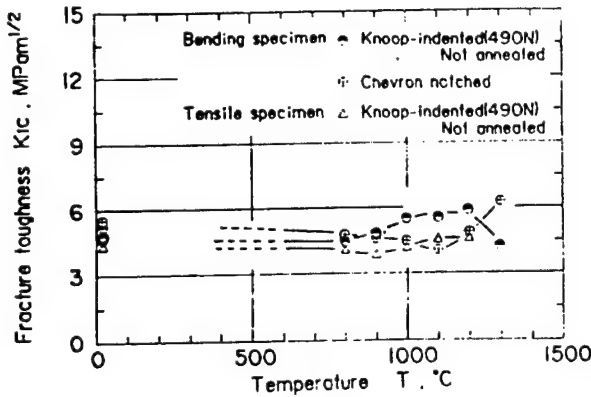


Figure 21. Test Temperature Dependence of Fracture Toughness

tensile and bending tests also influences the fracture toughness at high temperatures. Regarding such an influence of the rate of strain, it seems to be necessary to measure the displacement generated in the tensile specimen at high temperatures, and to discuss it further by clarifying the dependence of the stress-strain response on the rate of strain.

It should be noted that the fracture toughness for a chevron-notched specimen exhibits a minimum value around 1100°C. This contrasts with the results for the Knoop-indented specimen which exhibited a maximum value in this temperature region. It is thought that K_{IC} increased apparently due to the coagulation at the tip of the pre-introduced crack in this temperature region, as was mentioned earlier. Moreover, the increase in the K_{IC} of a chevron-notched specimen at temperatures exceeding 1100°C is considered to be due to the effect of inelastic deformation.

7. Future Prospects and Summary

At so-called ultrahigh temperatures, i.e., those which exceed 1000°C, even the fundamental mechanical properties, such as the moduli of rigidity and of direct elasticity, Poisson's ratio, yield stress and the stress-strain response in the inelastic region, have not been made clear. This is because no techniques have yet been established to correctly evaluate these properties.

In this article, the stress-strain response, fracture strength, fracture toughness, etc., of silicon nitride ceramics at high temperatures have been described, focusing on the results of research obtained in our laboratory. In particular, it has been shown that the inelastic stress-strain response of this material at high temperatures can be determined by using a noncontact displacement meter employing laser beams. This can be realized by the finite element method, combining displacement measurement and numerical calculations.

Needless to say, one aspect of indispensable research involves applying this material as a component to a machine that is operated at ultrahigh temperatures in order to accurately grasp the fundamental mechanical characteristics of ceramics at ultrahigh temperatures. If this becomes possible, then it will also become possible to design high temperature strength machine parts with generally complex shapes. In our laboratory, stress-strain analysis under high temperatures for specimens of shapes such as the one shown in Figure 22 has been carried out based on the knowledge obtained so far. Such research is considered to have important significance as a process on the application of this material to high temperature equipment parts.

Whether or not a newly-developed material will have excellent properties as a structural member can be judged only after an accurate evaluation of the mechanical characteristics of the material. Going one step further, it is important to pursue the microstructural and micromechanical factors that govern the excellence of the mechanical characteristics. The development of

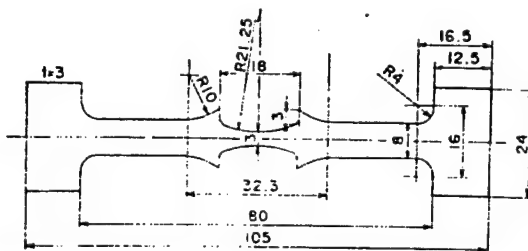


Figure 22. Specimen with Complex Shape Employed in Performing Elastic and Plastic Finite Element Analysis

newer materials with better mechanical characteristics should be tried based on the knowledge obtained by such research. The Japan Ultra-High Temperature Materials Research Center, Inc., is expected to be capable of fully satisfying these requirements regarding the development of new materials.

References

1. Hirano, K., PROC OF 5TH JAPAN-U.S. CONFERENCE ON COMPOSITE MATERIALS, 1991, to be published.
2. Hatanaka, K., et al., PAPERS OF JPN SOC OF MECHAN ENGINEERS, Vol 55 No 512, 1980 p 773.
3. Hatanaka, K., et al., JSME INTERNATIONAL JOURNAL, Ser I, Vol 33 No 4, 1990 p 542.
4. Hatanaka, K., et al., PAPERS OF JPN SOC MECHAN ENGINEERS, Vol 56 No 524, 1990 p 997.
5. Hatanaka, K., et al., JSME INTERNATIONAL JOURNAL, Ser I, Vol 34 No 2, 1991, to be published.
6. Hatanaka, K., et al., "Abstracts of Papers for Strength of Materials Sympos. on Fracture and New Technologies, Jpn Soc Mechan Engineers, August 1990, p 173.
7. Hatanaka, K., et al., to be presented at 68th Plenary Session of Jpn Soc. Mech. Engineers, March 1991, Tokyo.
8. Bluhm, J.I. Jr., ENG FRACT MECH, Vol 7, 1975 p 539.
9. Munz, D., et al., J AM CERAM SOC, Vol 63, 1980 p 300.

The Activities of Japan Ultra-High Temperature Materials Research Center (JUTEM) and Japan Ultra-High Temperature Materials Research Institute (JUTEMI)

916C00351 Ube CHO KO-ON ZAIRYO KOKUSAI SHINPOJIUMU in Japanese 15 Mar 91 pp 115-118

[Article by Koh Miyamura of JUTEM and Toshio Yarii of JUTEMI]

[Text] English abstract: Japan Ultra-high Temperature Materials Research Center (JUTEM) and Ultra-high

Temperature Materials Research Institute (JUTEMI) was established on the 1st of March in 1990 in Ube city and Tajimi city. JUTEM is one of the five semi-public corporations which are financially supported by the Ministry of International Trade and Industry, local governments and private companies. These corporations are aiming to help the promotion of R&D of advanced technology by installing the latest apparatus, which private companies can not afford, and renting these apparatus to the public. One of the JUTEM's objects is to install the apparatus for the trial production and evaluation of materials to be used at ultra-high temperature of about 2000 deg. C.

JUTEMI, supported financially by private companies, performs commissioned evaluation and testing, research works and various information exchange activities etc.

JUTEM is now under construction, and will start some of its business activity from April of 1991 and full activity from April of 1992.

1. Introduction

Japan Ultra-High Temperature Materials Research Center (JUTEM) and Institute (JUTEMI) was established on 1 March 1991 with the cooperation and support from the Ministry of International Trade and Industry, New Energy Development Organization (NEDO), local economic federations, Yamaguchi and Gifu prefectural governments, Ube and Tajimi city governments, not to mention innumerable private corporations in the Chubu and Chugoku areas.

Corporations and research centers were finding it more and more difficult to individually own the equipment and facilities necessary to carry out advanced research. As a result, the Ion Technical Center (Ion Kougaku Senta), the Technical Research Center for Mining Engineering Using Marine Life (Koukougyou Kaiyou Seibutsu Riyou Gijutsu Kenkyu Senta), and the Subterranean Gravity Experimental Center (Chika Mujyuryoku Jikken Senta) were established during the third phase of construction in 1988 with financial assistance from NEDO and several other organizations. These centers will function as the basic research facilities for the National Government and NEDO and will be leased out to private organizations to complement their research facilities. In 1990, the Ultra-High Temperature Materials Research Center (JUTEM) was added to the Laser Engineering Center.

JUTEMI was then established to help manage the activities of JUTEM as well as perform its own research to facilitate information exchanges.

The activities of JUTEM and JUTEMI are outlined in Table 1.

Table 1. Outline of JUTEM and JUTEMI

Name	Japan Ultra-High Temperature Materials Research Center (JUTEM)	Japan Ultra-High Temperature Materials Research Institute (JUTEMI)
Location		
1) Head Office	Ube City, Yamaguchi Pref.	Ube City, Yamaguchi Pref.
2) Works	Yamaguchi Center, Ube City Gifu Center, Tajimi City, Gifu Prefecture	Yamaguchi Instit., Ube City Gifu Institute, Tajimi City, Gifu Prefecture
Establishment	1 March 1990	1 March 1990
Capital	¥ 2,250 million	¥ 1,500 million
Initial Investment	¥ 4,500 million: Yamaguchi Center 3,400; Gifu Center 1,100	

2. Activities

1) Japan Ultra-High Temperature Materials Research Center (JUTEM)

- a) Leasing of large-scale and advanced research equipment and facilities to public-type private organizations or universities.
- b) Long-term leasing of research laboratories to the public to enable joint research between private organizations and universities.
- c) Provide guidance and support regarding usage of facilities.

2) Japan Ultra-High Temperature Materials Research Institute (JUTEMI)

- a) Perform analytical tests for industrial, academic and government sectors.
- b) Constantly perform basic research on materials production and evaluation techniques in order to maintain the state-of-art techniques and reliability. Also conduct joint national projects between industrial, academic and government sectors on themes for the 21st century. Also provide support to domestic and international researchers on international themes.
- c) Provide information and facilitate research exchanges through organization of both domestic and international talks, symposiums and seminars. Conduct joint surveys on research trends and through the above-mentioned exchanges, create a database on the experts involved in each industrial, academic and government sector.
- d) Provide workshops and technical training to engineers and technicians from private organizations.

The above-mentioned activities are outlined in Figure 1.

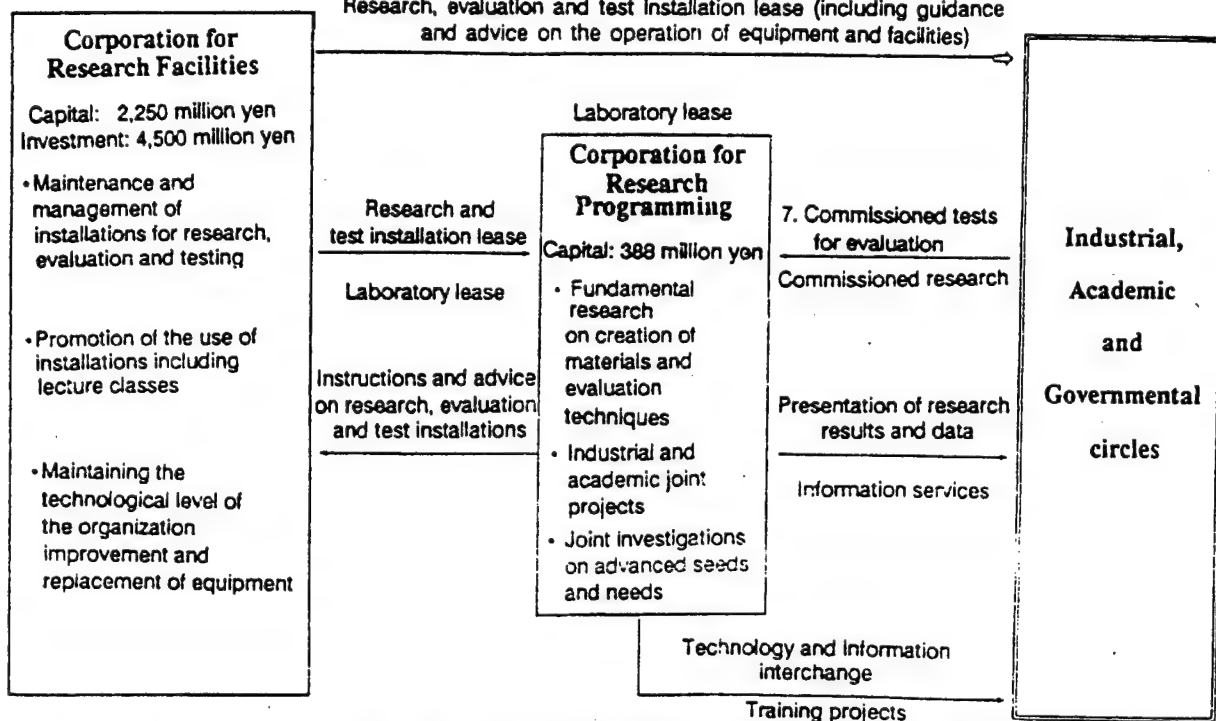


Figure 1. Relationship Between the Corporation for Research Facilities and the Corporation for Research Programming

3. Construction Schedule and Facilities Available 1) Construction Schedule

Table 2 shows the construction schedule and the dates when the facilities will be ready for use at the Yamaguchi and Gifu Centers.

The Yamaguchi Center is scheduled to be completed by March 1991. Five facilities will start operation from April 1991 and by January 1992, another 13 and by

April of the same year, another six facilities for materials test-production and characteristics evaluation will be ready.

The Gifu Center is expected to be ready by February 1991 and by April the same year, one facility will be available for use. From January 1992, five facilities and from April of the same year, another facility for the evaluation of characteristics of materials will be ready for use.

Table 2. Construction Schedule

	1990	1991	1992
Yamaguchi Center	design and construction		
1) Building		5 Apparatus → start for Use	13Ap.
2) Apparatus			6 Apparatus → start for Use
Gifu Center	design and construction		
1) Building		1 Apparatus → start for Use	5Ap.
2) Apparatus			1 Apparatus → start for Use

2) Types of Facilities Available

Under the guidance of the Ministry of International Trade and Industry and the Agency of Industrial Science and Technology, the Council for Ultra-High Temperature Materials Technology (Secretariat: Association for Research on Development of Next Generation Metals and

Complex Materials) and the Council for JUTEM (Secretariat: Japan Association for the Promotion of Industrial Technology) was established to look into the types of research facilities to be installed in the Yamaguchi and Gifu Centers. The councils gave full consideration to opinions from both public and private bodies including academic institutions before coming up with the facilities listed in Table 3.

Table 3. Outline of Apparatus

Center	Classification	Apparatus	Main application
Yamaguchi Research Center	Production of high quality metal materials	Plasma-arc melting furnace	Metal, inter-metallic compounds melting
		Bridgeman and floating zone furnaces	Single crystals, directional solidification
		Rapid quenching apparatus	Metal powders making
	Production of high quality composites	Equipment for ceramic synthesis	Nano-meter leveled ceramic particles
		Equipment for composite synthesis by CVI	Composite materials
	Control of structure and composition	Mechanical alloying equipment (*)	Oxide dispersion strengthened materials, IMC
		Heat treatment furnace (*)	High grade crystal controlled materials
		Hot press (*)	Hot pressing, sintered materials
	Sintering and forming	Ultra-high temp. and pressure HIP	Hot iso-static pressing of materials, HIP
		Cold iso-static press; CIP	Powder forming
Gifu Research Center	Surface improvement	CVD, PVD, Plasma arc spray coating	Formation of coating layers
		High voltage trans. electron microscope	Analysis of crystal structure
		Electron probe micro-analyzer	Micro-analysis
	Structure analyzer	X-ray diffractometer (*)	In situ analysis of crystal structure by X-ray
		Ultra-sonic microscope	Internal structure observation
		Mechanical (*), thermal testing apparatus	Mechanical, thermal properties measurements
	Evaluation of properties	Multi-axial mechanical testing apparatus	Multi-axial mechanical tests in situ observation
		Ultra-high temp. mechanical test machine (*)	Evaluation of mechanical properties
		Ultra-high temp. fatigue testing machine	Evaluation of fatigue properties
		Ultra-high temp. creep testing machine	Evaluation of creep properties
		Thermal shock testing machine	Evaluation of dynamic environmental properties
	Evaluation of application properties	Ultra-high temp. oxidation, evaporation	Evaluation of chemical environmental properties
		Erosion testing machining	Evaluation of erosion properties

Apparatus marked by (*) can be used as of April 1991.

4. Other Activities

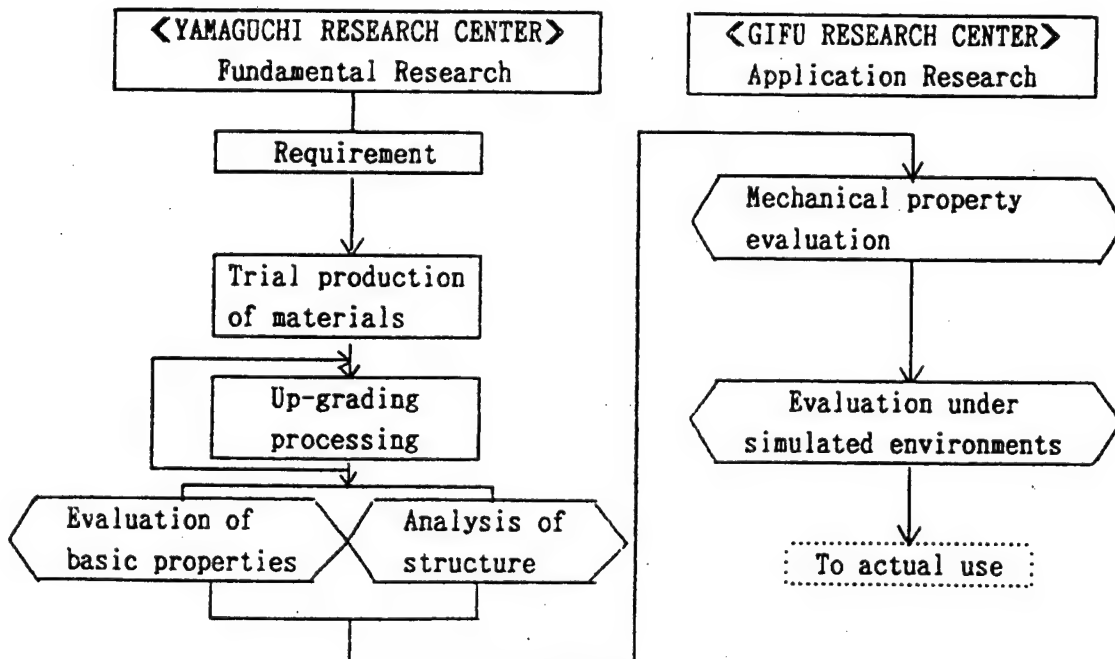
1) Surveys on Effective Applications of JUTEM

The results of "A Field Study on Evaluation Tests on Characteristics of Ultra-High Temperature Materials" conducted by the Japan Federation of Machinery Industry (Nihon Kikai Kogyo Rengokai) and funded by the Japan Association for the Promotion of Industrial Technology is reflected in the structure and use of

JUTEM's Basic Characteristics Evaluation Facilities or Environmental Control Evaluation Facilities.

2) Survey on International Centers Involved in Ultra-High Temperature Materials Research

This survey, which was originally commissioned to the Chugoku Research Center (Chugoku Chiho Sogo Kenkyu Senta) was conducted by JUTEM and funded as part of the activities for fiscal year 1989 by the Center for Promotion of Industrial Activities in the Chugoku Area



(Chugoku Chiiki Sangyo Kasseika Senta). This research included interviews with and questionnaire surveys on both domestic and international research bodies, researchers, organizations and public service corporations involved in research on ultra-high temperature materials and other related works. Based on this, a database was created to promote information and experts exchanges.

3) Organization of Seminars, Symposia, etc.

Last May, a seminar on "Current Situation and Future Possibilities on Inter-Metallic Compounds" was jointly held with the Metallic Materials Research and Development Center (Kinzokukei Zairyou Kenkyukaihatsu Senta) while in October, the Ultra-High Temperature Materials Symposium III was organized.

5. Conclusion

Both JUTEM and JUTEMI are still at their infant stages. They will begin partial operation during fiscal year 1991 and will be fully operational by fiscal year 1992.

Your guidance and unending patronage and support, in addition to those who have funded this project, will be the vital factor in achieving JUTEM's and JUTEMI's motto of "Challenging the Extreme" in the field of ultra-high temperature materials.

Development of a New Nickel-Base Single Crystal Superalloy by an Alloy Designing Method

916C0035J Ube CHO KO-ON ZAIRYO KOKUSAI SHINPOJIUMU in Japanese 15 Mar 91 pp 119-122
[Article by Takehiro Ohno, Rikizo Watanabe, and Koji Sato of Hitachi Metals, Ltd.]

[Text] English abstract: A new single crystal superalloy for single crystal turbine blades having much higher

temperature capability than conventional alloys was developed by applying an alloy-designing method to Ni-Cr-Al-W-Ta-Mo alloys. The alloy design was carried out as follows: 1) new structural parameters suitable for single crystal alloys were determined, 2) distributions of structural parameters were calculated, and 3) limitations of structural parameters were clarified based on experimental results. Consequently, optimum compositions were found by including high Mo concentration. The developed alloy, SC-83K, has a chemical composition located in the center of the optimum region and contains small amounts of Hf and Co. It has much higher creep-rupture strength than conventional alloys as well as good micro-structural stability and oxidation resistance.

Key words: superalloy, creep rupture, single crystal, nickel-base alloy, oxidation resistance

1. Introduction

Turbine blades with higher temperature capabilities is an essential factor in improving the performance of gas turbines. Creep rupture is believed to be the main factor determining the temperature capability of turbine blades. Figure 1 shows the types of alloys and their processing methods. Those shown in Figure 1 are all γ' precipitated strengthened super heat-resistant nickel based alloys. These alloys with Ni_3Al as the main component have superior creep strength at high temperatures through γ' phase precipitation. Turbine blades were originally wrought and then conventionally casted, next columnar grained and then made into single crystals. Single crystal alloys do not require alloy elements to reduce the melting points of C, B and Zr which are grain boundary strengthening elements. As such, the melting

and solidification temperatures can be increased to enable strengthened yet fine precipitation of the γ' phase.

2. Design of Single Crystal Superalloy

Alloys with super high temperature capabilities have complex alloy systems which include innumerable elements. In the past, the development of such alloys was done through trial and error and required much experience. The recent trend, however, is the use of scientific analysis to work out the optimum composition to enable more effective and reliable alloys to be developed. The strength of conventionally casted or columnar grained alloys is usually more complex since the factors involved in strengths of grain boundary or eutectic γ' phase also come into play. Since single crystal alloys can be assumed to be γ - γ' 2 phase system, such alloys can be relatively easily and accurately designed.

Let us describe the alloy designing method we developed for making single crystal superalloys. Ni-Cr-Al-W-Ta-Mo was used. Conventional single crystal superalloys are mainly strengthened by large amounts of W and Ta. This results in problems like deposition of W's primary solid solution (α -W) and the reduction in temperature difference (heat window) between the initial fusion temperature and the solid solution temperature of eutectic γ' . Another problem when only W and Ta is used is the stability of the alloy structure. Mo is now attracting a lot of attention as a solution to these problems and as a means of improving rupture strength. Mo was thought to be less effective toward creep rupture when compared to W, but now Mo is considered a prime candidate for stabilizing the alloy structure and through a reduction of the mismatch between lattice constants of alloys in the γ phase and γ' phase, to help strengthen the creep rupture strength. Some stronger alloys with Re impurities have

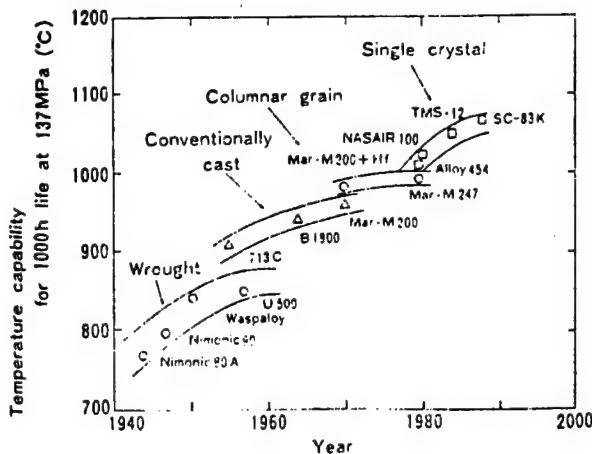


Figure 1. Trends in the Alloy and Processing Development of Superalloys for Turbine Blade Application

recently been developed. We refrained from using Re in our method because it is a very expensive element.

Next, a 1080°C treatment temperature was selected from a practical point of view since this is the actual temperature experienced by a real surface coated blade.

The flow chart in Figure 2 shows the basic superalloy designing method.

(a) The γ and γ' phase structure and alloy structure were determined by the method developed by Harada et al. In this method, the equilibrium γ structure was calculated by the Jyukaiki method after the γ' phase structure was determined. The alloy structure was determined from the composition of both phases (in this case, $\gamma' = 65$ percent). When determining the γ' phase structure, the solubility of each type of element in the γ' phase was determined from the Solubility Index (S.I.) while the amount of Al in the γ' phase was calculated from the γ' surface equation. From Wallace's Phacomp, $N_v^c - N_v$ was calculated to determine the phase deposition of harmful σ phases in the case of γ phase structure.

(b) The optimum composition of γ and γ' phases were assumed according to the method developed by Watanabe et al. where the lattice constants of the γ and γ' phases were employed as parameters. The increased solubility of the whole alloy was represented by the simple average of γ phase lattice constant (a_{γ}) and γ' phase lattice constant ($a_{\gamma'}$). Also, γ and γ' phase lattice constant mismatch (δa) were used as parameters to optimize the grain structure.

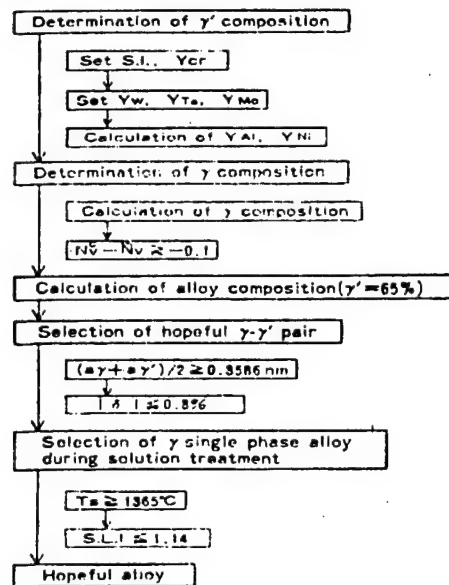


Figure 2. Flow Chart of Alloy Design for Ni-Cr-Al-W-Ta-Mo Series

(c) Parameters for single phased γ' were fixed to prevent reduction in the strength of single crystal alloys due to residual crystallization of eutectic γ' and the precipitation of α -W. First, the alloy's solidus (T_s)^{x 3} parameter was estimated to determine whether the temperature during solution treatment was sufficiently high or not. Then, the solubility limit index (S.L.I.) parameter was defined to determine if the constituents of the alloy overshot their solubility limit in γ' .

The change in the structure of the alloy was determined from the ratio of the structural factor parameters W, Ta and Mo in γ' phase and is expressed in the triangular contours in Figure 3. In the figures, S W, S Ta and S Mo represent the concentrations of W, Ta and Mo in γ' divided by the solubility limit of each element in γ' . The concentration of Cr in γ' was assumed to be 3 at.% while $S_W + S_{Ta} + S_{Mo} = 1$ (when it does not become 1, the ratio between S W, S Ta and S Mo was taken).

Several types of selected alloys based on these results are shown on the triangular coordinates in Figure 4. The alloys selected are mainly those whose $(\delta\gamma + \delta\gamma')/2$ values are large such that they have sufficiently strong solubilities. Figure 4 also shows actual structural observations. It is evident from this figure that the superalloy with Mo impurity shows structural stability. The γ' particles of alloys in the vicinity of No. 53 and 58 are cubic in shape. These alloys also have strong creep rupture strength.

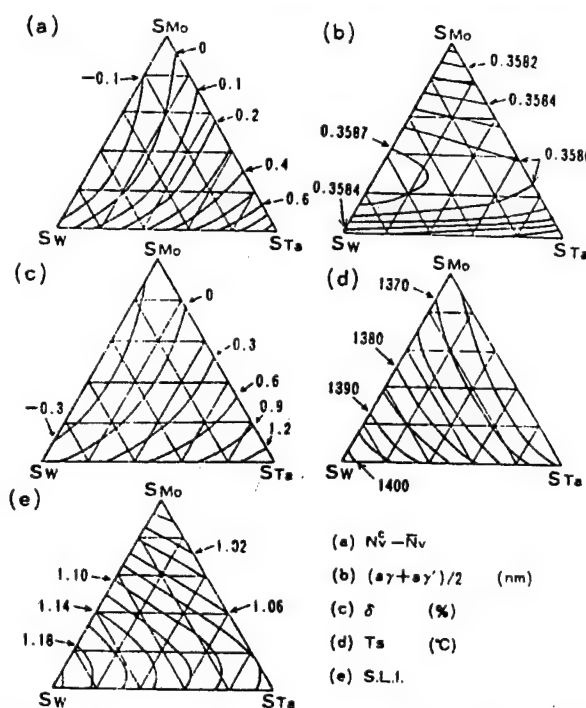


Figure 3. Structural Factor Parameter Contours in S W, S Ta and S Mo Triangular Coordinates (S.I. = 1.3, Y Cr = 3, γ = 65 percent)

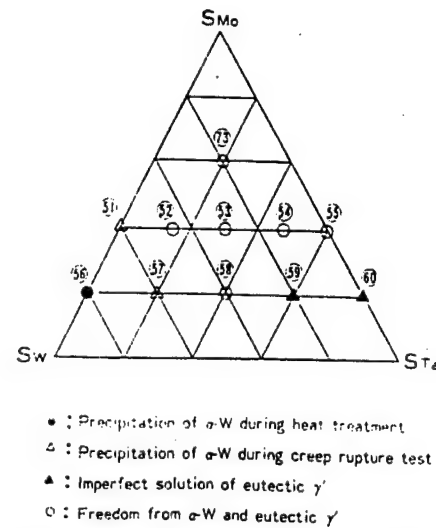


Figure 4. Locations of Designed Single Crystal Superalloys in S W, S Ta and S Mo Triangular Coordinates and Their Microstructural Characteristics

The limit of each parameter is then defined after due consideration to experimental results and those structural regions deemed hopeful are shown in the shaded region in Figure 5. It is evident from this figure that the position of conventional alloys are different from that determined by our method. Two alloys, SC-53A and SC-83 whose S.L.I. is higher than that of SC-53, were selected for analysis. It was proved that both alloys have significantly stronger creep rupture strength.

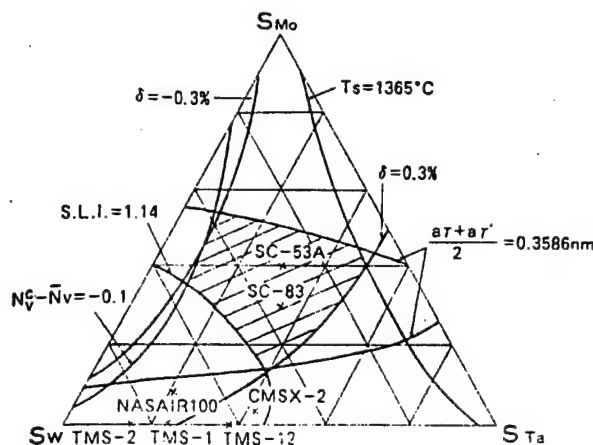


Figure 5. Hopeful S W, S Ta and S Mo Region (shaded area) and the Location of Two Selected Alloys (SC-53A and SC-83), Conventional Alloys (NASAIR100 and CMSX-2) and the Alloys Developed by NRIM (TMS alloys)

Next, oxidation resistivity of the superalloys was considered. The final alloy developed was termed SC-83K and was made with SC-83 as the foundation alloy and small amounts of Co and Hf as impurities.

3. Characteristics of SC-83K

The chemical composition of SC-83K is shown in Table 1.

Table 1. Chemical Composition of SC-83K (wt%)

Cr	Al	W	Ta	Mo	Hf	Co	Ni
6.4	5.1	7.3	7.3	4.3	0.1	1.0	Bal

The creep rupture strength of this newly developed superalloy is shown in Figure 6. Although SC-83K does not include the extremely expensive Re element, it has a significantly high creep rupture strength especially at high temperatures as a result of the proper amount of W, Mo or Ta added as impurities. Figure 7 (a) shows SEM micrographs of heat treated SC-83K while (b) shows the alloy after creep at 1040°C and 137 MPa. SC-83K's high creep rupture strength is believed to be due to the deposition of heat treated cubic γ' particles and the resulting regular raft structure formed during creep. Next, the tensile characteristics of SC-83K are shown in Figure 8 while Figure 9 shows the oxidation resistance. The oxidation resistance of SC-83K is very much higher than conventional single crystal alloys. Further, SC-83K does not precipitate any harmful phases and is structurally stable. The wide heat treatment window of about 30°C (1300-1330°C) enables easy heat treatment. The physical characteristics of SC-83K are summarized in Table 2.

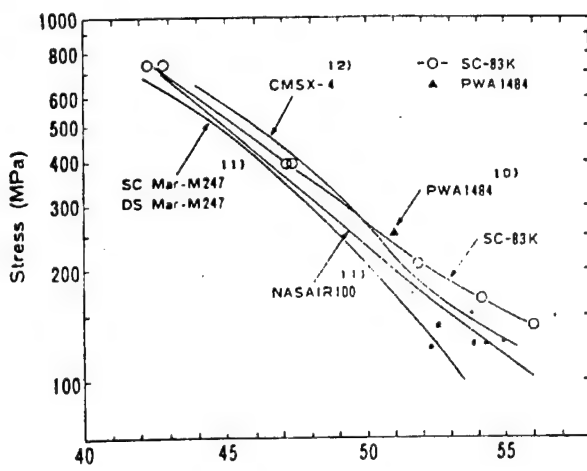
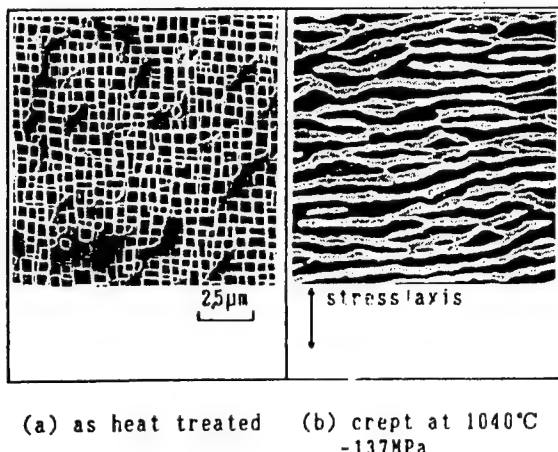


Fig. 6 Larson-Miller parameter curves of single crystal and columnar-grained superalloys



(a) as heat treated (b) crept at 1040°C - 137 MPa

Fig. 7 SEM micrographs of SC-83K

Table 2. Physical Properties of SC-83K

1. Density: 8.86 g/cm³

2. Melting range: 1362-1400°C

Solidification range: 1392-1343°C

3. Specific heat

Temp. (°C)	20	100	200	300	400	500	600	700	800	900	1000	1100
cal/g x °C	0.091	0.088	0.096	0.095	0.097	0.098	0.099	0.101	0.110	0.117	0.123	0.137
J/kg x K	381	388	402	398	406	410	414	423	460	490	515	573

4. Thermal conductivity

Temp. (°C)	20	100	200	300	400	500	600	700	800	900	1000	1100
------------	----	-----	-----	-----	-----	-----	-----	-----	-----	-----	------	------

Table 2. Physical Properties of SC-83K (Continued)

cal/cm x sec.°C	0.018	0.019	0.023	0.024	0.027	0.030	0.032	0.036	0.041	0.044	0.048	0.055
W/m x K	7.5	8.0	9.5	10.1	11.3	12.3	13.4	14.9	17.0	18.3	19.9	22.9

5. Mean coefficient of thermal expansion (30°C to Temp.)

Temp. (°C)	100	200	300	400	500	600	700	800	900	1000	
X10 ⁻⁸ /°C	11.1	11.4	11.8	12.1	12.5	12.7	13.2	13.6	14.2	14.9	

6. Dynamic modulus of elasticity (001 direction)

Temp. (°C)	20	700	800	900	1000						
GPa	130	110	100	90	80						

*2: $\delta = 2(\alpha\gamma' - \alpha\gamma)/(\alpha\gamma' + \alpha\gamma)$

*3: $T_s = 1453 - \sum (1453 - T_{Ei}) A_i / A_{SLi}$

T_{Ei} is the eutectic temperature (°C) of Ni-i bielement, while A_i is the concentration (at.%) of element i in the alloy. A_{SLi} shows the solubility limit (at.%) of element i in single Ni.

*4: S.L.I. = $\sum (A_i / A_{SLi})$

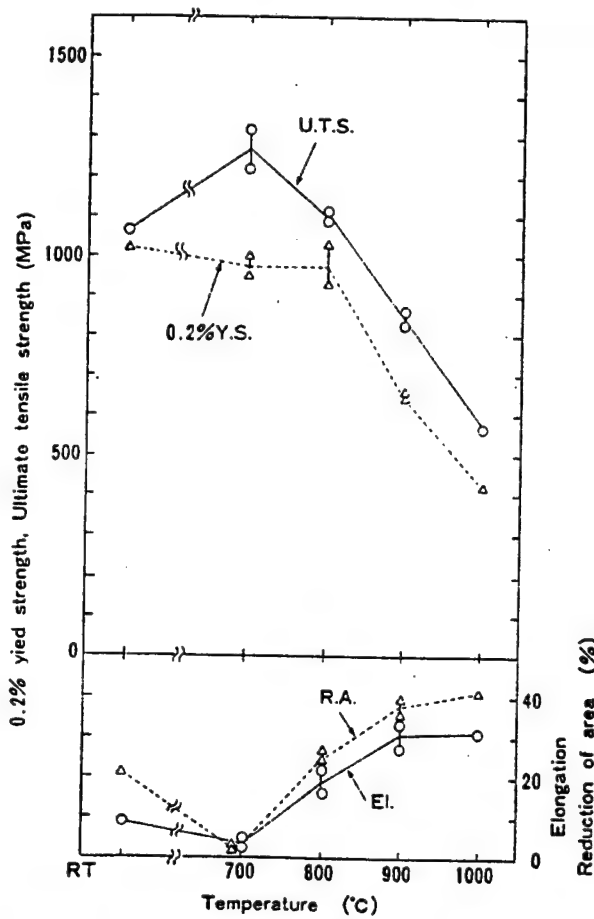


Figure 8. Tensile Properties of SC-83K at Various Temperatures

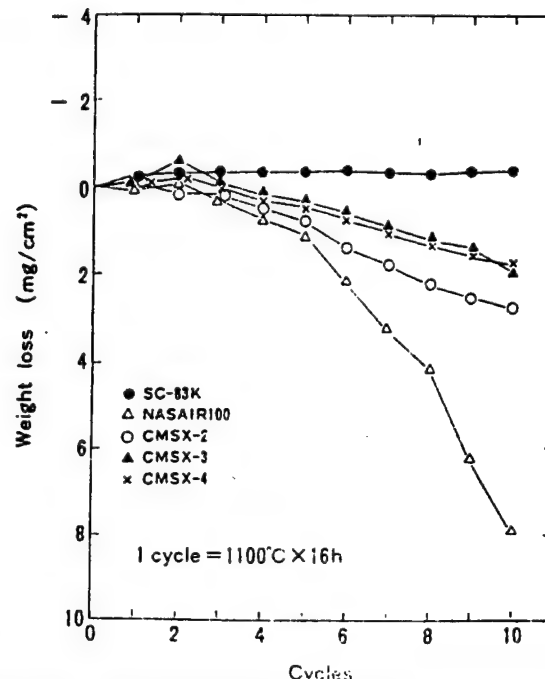


Figure 9. Oxidation Resistance of Single Crystal Super-alloys

*1: S.I. = Y_i / Y_{Li} . Y_i represents the concentration (at.%) of element i in γ' . Y_{Li} is the solubility limit (at.%) of element i in simple γ' (Ni_3Al).

Hydrogen Embrittlement of Ni-Base Superalloys

916C0035K Ube CHO KO-ON ZAIRYO KOKUSAI SHINPOJIMU in Japanese 15 Mar 91 p 123

[English abstract of article by Seiji Fukuyama and Kiyoshi Yokogawa of the Government Industrial Research Institute, Chugoku, Yoshio Yamada of the National Space Development Agency of Japan, and Tadashi Iida of Ishikawajima-Harima Heavy Industries Co., Ltd.]

[Text] Tensile properties of Inconel 718 of Ni-base superalloy being used for liquid hydrogen fueled rocket engine materials were investigated in high pressure hydrogen of 19.7 MPa at room temperature up to 773 K. Tensile behaviors of the typical steels were also investigated in the same conditions in comparison with those of the Ni-base superalloys. The results obtained are as follows:

(1) Ni-Base Superalloy

Elongation, reduction of area and ultimate tensile strength of the material in hydrogen were smaller than those in argon at room temperature up to 773 K. Hydrogen environment embrittlement (HEE) decreased slightly with increasing the temperature, however HEE still occurred severely at 773 K. The crack initiation occurred at carbides and then the crack propagated along the interface between δ phase and γ matrix in hydrogen.

(2) Steels

HEE of the steels depended on the microstructure, and decreased with increasing the temperature, i.e., hydrogen showed marked effects on the tensile properties of 18Ni-Maraging steel and Fe-30%Cr alloy even above 673 K, but no effects on those of type 304 stainless steel above 373 K.

Key Words: Hydrogen Embrittlement, Hydrogen Environment Embrittlement, Ni-Base Alloy, Superalloy, Inconel 718, MarM247LCDS, Type 304 Stainless Steel, AISI 4340 Steel, 18Ni-Maraging Steel, Fe-30%Cr Alloy, Tensile Property, Room Temperature, High Temperature.

Development of W/Cu Composite With Gradient Structure

916C0035L Ube CHO KO-ON ZAIRYO KOKUSAI SHINPOJIMU in Japanese 15 Mar 91 pp 127-130

[Article by Yoshiyasu Itoh, Masashi Takahashi, and Hideo Kashiwaya; paper received on 8 February 1991]

[Text] English abstract: Sintering and infiltration technique to fabricate functionally gradient materials is newly developed. This technique consists of two steps and is suitable for fabricating tungsten/copper (W/Cu) gradient material. The first step is to fabricate a sintered W with gradient pores, and the second step is to infiltrate a molten Cu into the gradient pores. This technique can be generally applied to several material combinations,

which are chemically unreacted and have different melting points. The W/Cu gradient material prepared by the sintering and infiltration technique is excellent for reducing thermal stresses at elevated temperature and enhancing the properties as a beam target. It is also confirmed that the properties can be improved by HIP treatments. In this study, the equivalent thermal conductivities of the W/Cu gradient material are measured in comparison with the W to Cu laminates prepared by brazing. And, the reduction behavior of the thermal stresses is confirmed by heat cycle testing.

Key Words: Sintering and infiltration technique, Functionally gradient materials, W/Cu gradient material, Thermal conductivity, Heat cycle testing.

1. Introduction

The increasingly popular functionally gradient material is made by combining, at a gradient, materials with different properties. In this manner, innumerable functions that originally did not exist in each simple material component can be effectively added to the new material. The super high temperature resistant metal/ceramic gradient material is one of the functionally gradient materials that was considered. The ceramic handles the heat resistance problems while the cooling characteristics and the mechanical strength is found in the metal. By applying a gradient to the intermediate region, the new material can be made such that the thermal stress is relaxed. The relaxed thermal stress tendency due to the functionally gradient structure is determined by the Finite Factors Method whose effectiveness has been proved.

On the other hand, recent energy machines tend to be highly effective and have large capacities. These machines will be used under more and more severe conditions like high temperatures or a corrosive environment. It is not an exaggeration to say that breakthroughs in material surfaces will be the key to the development of new machines. Here we will report on the development of a relaxed thermally stressed W/Cu functionally gradient material for use in nuclear fusion reactors and accelerators where the heat panel will be made of tungsten (W) which has a high heat resistance while the opposite surface is made of copper (Cu) which has superior thermal conductivity characteristics. These two materials are structurally combined at a gradient.

2. Development of W/Cu Functionally Gradient Material

Many processes have been proposed for fabricating functionally gradient materials. We have successfully fabricated a W/Cu functionally gradient material using our independently developed Sintering and Infiltration Method. This material combines W with high heat resistance and Cu with its superior thermal conductivity in a functional gradient structure. This structure relaxes the thermal stress resulting from the differences in their coefficients of linear expansion. Figure 2 shows the general outline of the sintering and infiltration method.

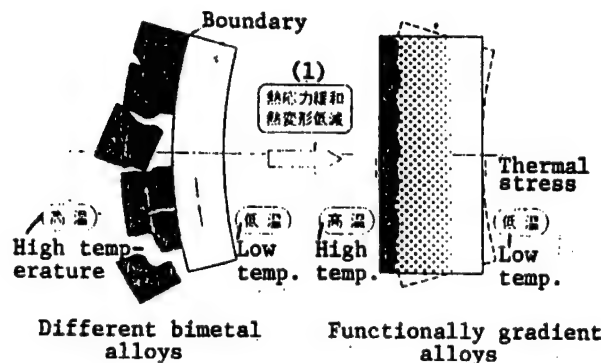


Figure 1. Relaxation of Thermal Stress for Functionally Gradient Material

Key:—1. Thermal stress relaxation, Thermal transformation reduced

The process can be roughly classified into two parts. The first is where the layers of W powder of different particle sizes are compressed into shape and then sintered to create the W skeleton whose porosity is graded while the second part is the HIP infiltration of Cu into the pores of the W skeleton. Before Cu infiltration, the W skeleton is capsule-free HIP treated to improve its characteristics. As is evident from the different melting points of W and Cu, the sintering temperatures are also different and as such, a functionally gradient material cannot be fabricated by simply mixing the powders, layering and then sintering it. The sintering and infiltration method is for fabricating a functionally gradient material. The main characteristic of this method is that both W and Cu are structured like a network. In other words, W and Cu do not exist as independent particles because of the infiltration method of fabrication. Consequently, the laminated surfaces of the functionally gradient material will be more difficult to peel while thermal conductivity from W to Cu is significantly improved.

Table 1. Physical Properties of W and Cu

	W	Cu
Melting point (°C)	3380	1083
Specific heat (cal/g x deg)	0.032	0.092
Density (g/cm³)	19.3	8.9
Thermal conductivity (cal/cm x deg)	0.39	0.94
Coefficient of thermal expansion (x E 6)	4.5	17.1
Others	Does not form solid solution with Cu	Does not form solid solution with W

Next, we will describe each step of the process in detail.

Figure 3 shows an example of the relationship between the shrinkage and relative density of W powders of different particle sizes which are structurally compressed and then sintered. As is clear from the graph, the relative

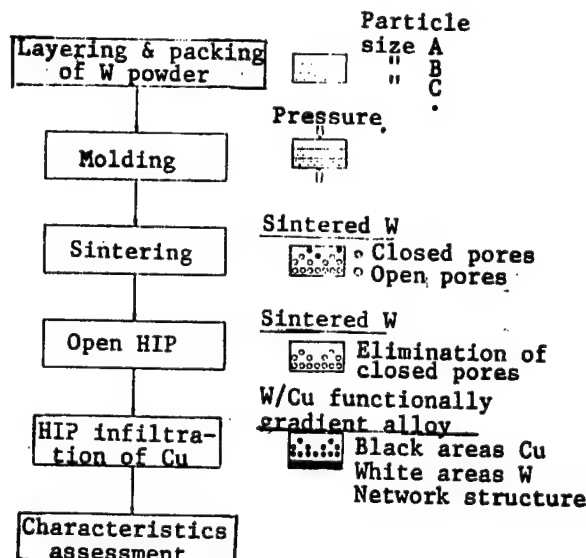


Figure 2. Preparation Process of W/Cu Gradient Material by Sintering and Infiltration Technique

density can be altered by 60-95 percent depending on the size of the W particle. In other words, the porosity of the W powders can be controlled by the size of the particles. However, sintering shrinkage, as is evident from the graph, also changes with the particle size of the W powders as well as the sintering conditions. As a result, control of the sintering shrinkage would be a vital factor in the fabrication of distortion-free, crack-free and superior functionally gradient materials. Figure 4 is a summary of the relative densities when sintered W with various initial densities are capsule-free HIP treated. As is clear from the figure, in the case when the initial density is higher than 90 percent, the relative density can be made almost 100 percent by capsule-free HIP treatment. When the outermost surface of W that is sintered according to the method shown in Figure 2 has a relative density of higher than 90 percent, it is made finer after capsule-free HIP treatment. This is effective for strengthening the outermost surface of W and improving the thermal conductivity. At the same time, this helps to prevent the Cu inside the functionally gradient material from melting and dispersing through evaporation while it is being heated. The effects of capsule-free HIP treatment on sintered W with initial relative densities of 76.6 percent is shown in Figure 5. The porosity of sintered W is separated by the Archimedes and the Mercuric Pressure Insertion methods into open and closed pores. It was found that sintered W with an initial relative density of 76.6 percent has 18.3 percent open pores and 5.1 percent closed pores. The open pores are necessary for the infiltration of Cu while the closed ones are undesirable since they reduce the strength and thermal conductivity of the material. As is evident from the figure, capsule-free HIP treatment eliminates the open pores while retaining the closed ones. [as published] This is

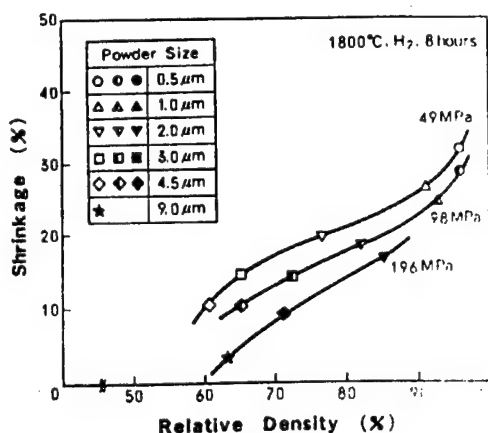


Fig.3 Relationship between shrinkage and relative density.

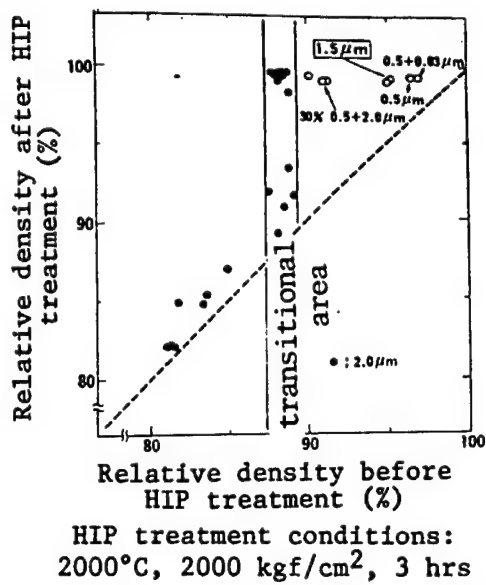


Fig.4 Effect of initial density on sintered W by HIP treatment.

because during HIP treatment, the closed pores are crushed by the external pressure while in the case of open pores, an internal pressure equivalent to the exerted external pressure in the capsule-free condition prevent them from being crushed. In this manner, a sintered W with a 100 percent relative density in the outermost surface layer and an increasing open porosity in the direction of the back surface can be fabricated. Further, as is also shown in Figure 2, infiltration of Cu into sintered W is due to the external pressure during HIP treatment. In the beginning, Cu infiltration was performed under normal temperature in a hydrogen environment. Both W and Cu leak well and have been confirmed to infiltrate well even under normal pressure

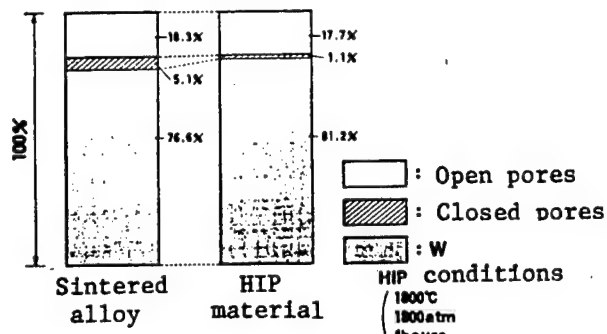


Fig.5 Effect of capsule free HIP treatment on sintered W.

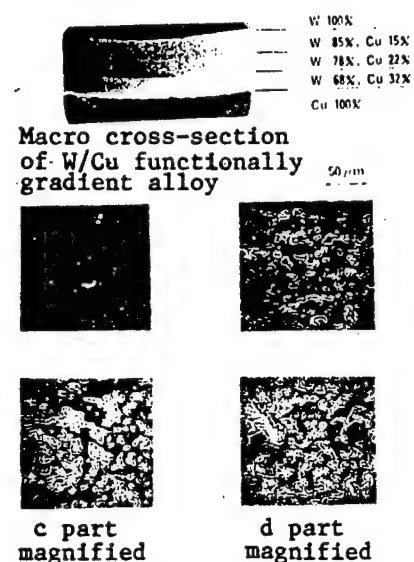


Fig.6 Macro structure and micro structure of W/Cu gradient material.

but blowholes have sometimes been observed when the resulting gas during infiltration was not removed. As such, Cu infiltration by HIP was used.

3. Assessment of Heat Conductivity Characteristics and Thermal Stress Relaxation Characteristics

Of the characteristics of the fabricated W/Cu functionally graded material, thermal conductivity which is necessary for beam targeting has been experimentally observed. The laser flash method usually used for measuring the thermal properties (thermal conductivity, specific heats) of substances cannot be directly applied in this case because of the material's complex macro structure. We measured the equivalent thermal conductivity of W/Cu functionally graded material by the steady state method. Figure 7 shows the thermal conductivities in W/Cu gradient material and for comparison, W to Cu

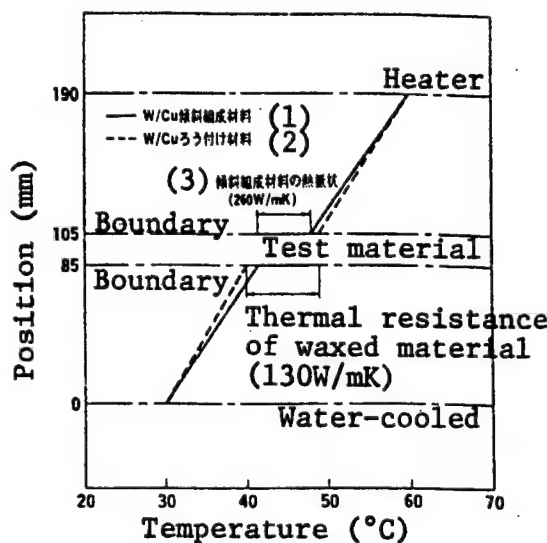
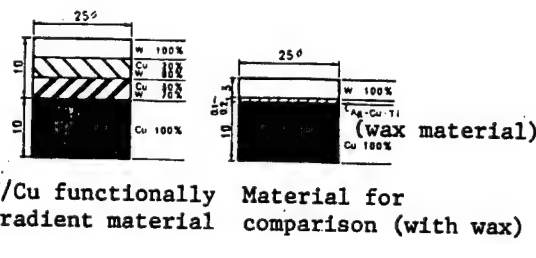


Figure 7. Thermal Conductivities Measured by Steady State Method in W/Cu Gradient Material in Comparison With W to Cu Laminate

Key:—1. W/Cu functionally gradient alloy—2. W/Cu waxed alloy—3. Thermal resistance of functionally gradient alloy (260W/mK)

laminates which are waxed together. The wax is made of Ag-Cu-Ti. In the steady state method experiment, the specimen is sandwiched by Cu which is heated to 30°C and 60°C respectively. The temperature distribution in the intermediate regions are measured by a thermocouple. As shown in the figure, the thermal conductivity of the gradient material is about two times better than that material with wax.

Next, the results of a heat cycle test for defining the thermal stress relaxation characteristics are shown in



Tempera-	Max. temp.	800°C
ture	Min. temp.	300°C
	Temp. maintained for	30 min.
Environ-	Gas	Ar
ment	Pressure	760 Torr
No. of times repeated		10 times

Figure 8. Specimens and Testing Condition Used for Heat Cycle Test

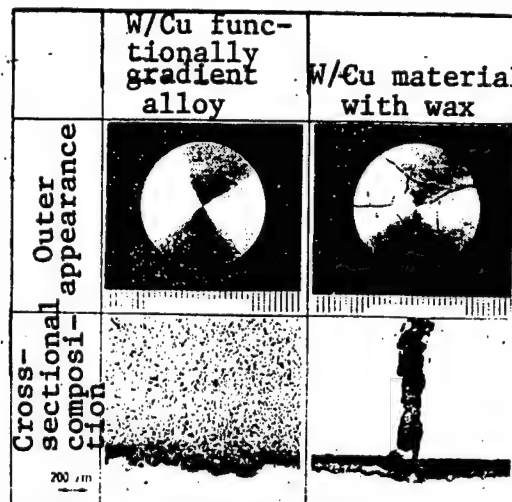


Figure 9. Appearances of Tungsten Surface and Cross Section After Heat Cycle Test

Figure 8 where W/Cu gradient material and, for comparison, W/Cu waxed material are used. During the test, the specimen was uniformly heated in an Ar gas environment in an electric furnace. The heat cycle of maintaining a maximum temperature of 800°C for 30 minutes, and heating and cooling at a speed of 30°C/min at the minimum temperature of 300°C is repeated 10 times and the rupture conditions of the specimen were observed. Figure 9 shows the experimental results. The surface conditions and the cross-section of W after the heat cycle is shown. After 10 repetitions of the heat cycle, W/Cu wax material had numerous cracks in W and peeling was observed in the combined boundary but, W/Cu gradient material showed no traces of damage.

4. Conclusion

This article describes the sintering and infiltration fabrication method developed for W/Cu functionally gradient materials. This process enables two substances whose sintering temperatures are completely different like W and Cu to be fabricated into a functionally gradient material. This material has been proved to have superior thermal conductivities and thermal stress relaxation characteristics. The capsule-free HIP treatment was found to be effective in eliminating closed pores from the W skeleton and improving Cu infiltration. We fabricated large-scale W/Cu gradient materials in the range of 80 X 80 X 30 mm in size. These fabricated materials were also used in beam target tests. Future tasks will include clarification of thermal impact resistance characteristics of the material with an incident beam. The lifespan of the material during constant or repeated irradiation must also be investigated. A reliable material for practical use is our future target.

Amorphous FeSi₂ Alloys as a New Thermoelectric Material Developed by Plasma Ion Processing

916C0035M Ube CHO KO-ON ZAIRYO KOKUSAI SHINPOJIUMU in Japanese 15 Mar 91 p 131

[English abstract of article by Kakuei Matsubara, Norimichi Minerura, Toshikatsu Miki, Kouichi Kawamura, Keigo Nagao, and Tsuyoshi Koyanagi]

[Text] Studies of iron-disilicides (FeSi₂) with an amorphous structure have been made to develop highly efficient materials usable in future thermoelectric energy conversion (TEC) system. We employed plasma-ion processing techniques including the ionized-cluster beam (ICB), ion-assisted deposition and plasma modification methods.

Major results obtained are as follows: (1) Amorphous films of FeSi₂, prepared by ion-assisted deposition, exhibit a high thermoelectric power (Seebeck coefficient) S similar to 6 mV/deg (p-type) and electrical conductivities σ from 1 to 10² Ω⁻¹cm⁻¹, indicating a breakthrough in thermoelectric conversion efficiency; (2) Films prepared by coevaporation of Fe and SiO have a granular structure, and exhibit the values of S (p-type) similar to 8 mV/deg and σ similar to 10⁻³ Ω⁻¹cm⁻¹ at temperatures up to 800K; (3) The figure of merit of FeSi₂ ceramics, composed of fine particles (0.2-2 μm in size) modified in O₂-plasma, is about ten times larger than that of unmodified ones.

Key words: Amorphous, Iron-disilicide, Thermoelectric Material, Plasma Processing, Ion Beam Technology

Effects of Microstructure on Mechanical Properties and Fracture of γ-Base Titanium Aluminides

916C0035N Ube CHO KO-ON ZAIRYO KOKUSAI SHINPOJIUMU in Japanese 15 Mar 91 pp 137-140

[Article by S. Tsuyama, S. Mitao, and K. Minakawa (NKK)]

[Text] English abstract: The effect of microstructure on mechanical properties and fracture of γ base titanium aluminides were investigated. As-cast binary titanium aluminides containing different levels of aluminum ranging from 44 to 51 at.% were prepared for fracture toughness tests and creep rupture tests. The test results indicated that the bulk strength determined by hardness measurements increases with decreasing aluminum content. However, the highest fracture toughness and creep resistance were obtained in the Ti-48%Al alloy which consisted of α₂/γ lamellae with serrated grain boundaries. The factors and mechanisms responsible for the fracture process of γ base titanium aluminides are discussed in relation to microstructure.

Key Words: TiAl, Titanium aluminide, intermetallic compound, Fracture toughness, Creep strength, Microstructure, α₂/γ lamellae, Grain boundary morphology, Dynamic recrystallization

1. Introduction

Titanium aluminide is lightweight (specific gravity 3.8), can be used in high temperatures of around 1100 K and is resistant toward oxidation. As a result, its possible application as a material for fabricating heat resistant parts in jet planes or automobiles is attracting a lot of attention. However, improvements in its low ductility and malleability at room to moderately high temperatures will become a major problem to tackle in the future. The result of adding constituent elements into the alloy does not necessarily give favorable results like in the deterioration of the aforementioned high temperature characteristics. The possibilities of improving fracture toughness at room temperature and creep rupture at high temperatures of various As-casted bi-element systems whose microstructures were altered depending on the amount of Al included, were investigated.

2. Experimental Method

Different levels of aluminum (44-51at%) were dissolved in binary titanium aluminide solvent consisting of granulated aluminum (99.9 percent) and sponge titanium (99.7 percent) with the help of an argon arc. The solution is then solidified in a water-cooled mold. From this As-casted button ingot (20*40*120 mm), a 6 mmφ specimen for tensile creep tests and a 12.7 mm thick compact type piece was extracted for fracture toughness tests. The microstructure and its hardness were observed for temperatures ranging from room temperature to 1073 K. The creep rupture at 1073 K x 196 MPa and 1223 K x 59 MPa as well as the fracture toughness of ASTM E399 at room temperature was also estimated. SEM pictures of the cross-section and rupture plane were also taken in order to determine the factors governing rupture. For comparison, rupture tests were also performed on 50 percent aluminum materials isothermally forged at 1273 K and annealed at 1373 K.

3. Results and Observations

Photo 1 shows a typical microstructure. The isothermally forged and annealed binary Ti-50%Al has the recrystallized γ lamellae structure. On the other hand, although as-cast 50%Al material has the same structure, two phases exist in the form of insular lamellae γ dispersed within the α₂/γ lamellae. When the aluminum content was reduced to 40 percent, the γ lamellae disappeared and the curved grain boundary is made up of only α₂/γ lamellae. When the content is further reduced to 44 percent, the whole material becomes lamellae-structured with a straight grain boundary. In conclusion, the structure of TiAl can be severely altered depending on the amount of aluminum content and the processing.

Figure 1 shows the change in hardness of the material when the aluminum content is changed. The hardness of the material steadily increases when the aluminum content is reduced irrespective of whether it is at room temperature or at high temperatures. Compared to this, Figure 2 shows that the fracture toughness of 48%Al material at room temperature is equivalent to 30



Photo 1. Microstructures of Binary TiAl Alloys in the As-Cast and the Isothermally Forged and Annealed Conditions

MPam $1/2$, a high value similar to that exhibited by strong aluminum alloys. This value drops by about 50 percent when at the 50%Al forged material. In the case of forged materials with the same structure, the value drops further to 10 MPam $1/2$. On the other hand, when the aluminum content is low as in 44%Al, the malleability drops again. However, this value is high when compared with that of 50%Al material as shown by the low 20 percent drop in malleability. In Figure 3, the peak in the creep rupture life graph shifts slightly to the side with low aluminum content when the temperature rises. The highest peak is at 48%Al. Both the fracture toughness and creep strength depending on the Al content, shows a different manner of change as compared with hardness or in other words, the bulk strength. This proves that they strongly affect the microstructure.

First in the fracture toughness test, the development and progress of cracks are observed to clarify their relationship with the microstructure. Photo 2 shows the fracture plane of an isothermally forged and annealed alloy as seen from a slanted position. A very flat precrack can be seen and as is evident from the fracture plane, the γ lamellae itself is basically very weak. Photo 3 shows the fracture plane of as-cast material and a schematic model of the crack paths created from observations made on the crack generation and the cross-section structure of the neighboring areas. In the case of 50%Al material, a crack generates in the equi-axial γ that is insularly dispersed, thereby reducing its malleability. However, the columnar crack planes in the lamellae will be arrested by the aforementioned cracks and as such the γ lamellae will have higher malleability than the forged and annealed material. On the other hand, grain boundary rupture and peeling in the 44%Al material is one of the reasons for the drop in the toughness of the boundary.

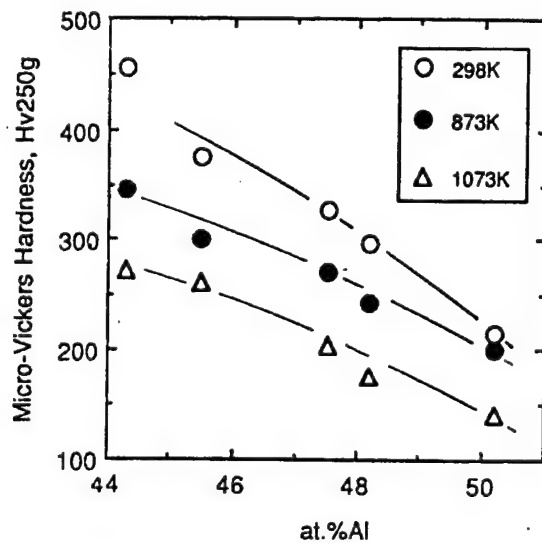


Fig. 1 - Effect of aluminum content on hardness at low to high temperatures.

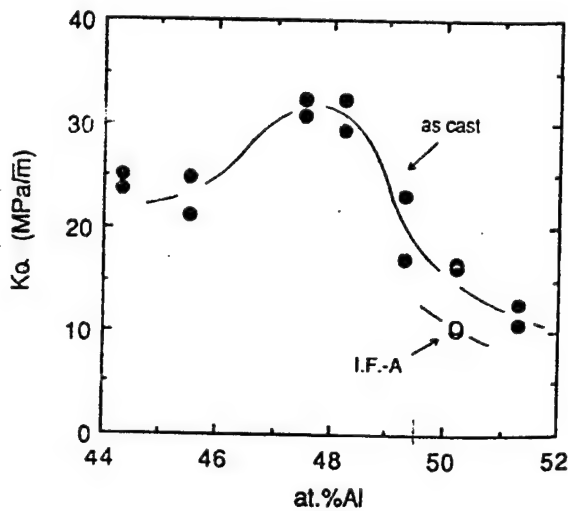


Fig. 2 - Effect of aluminum content on fracture toughness at room temperature.

Since the fractured plane is extremely uneven when compared to the cracks, it is clear that the 44%Al material presents a higher resistance to the progress of cracks. Despite the fact that 48%Al material with the highest fracture toughness value is similarly lamellae-structured all over like 44%Al, the fracture plane morphology is completely different. The whole surface is covered with the columnar cracks similarly observed in parts of as-casted 50%Al material. This columnar fracture plane is believed to be created when the cracks in γ nears the α_2 layer and the peeling off of the α_2/γ boundary plane. The cross-section showed innumerable micro-cracks along the lamellae around the cracks that were predicted to result due to fatigue. At the same time,

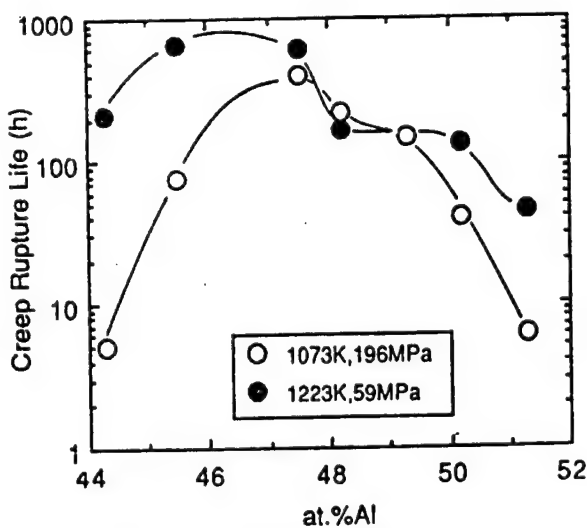


Figure 3. Effect of Aluminum Content on Creep Rupture Life

branching as a result of the micro-cracks combining with each other at the origin was also confirmed. In other words, the high fracture toughness of 48%Al material was not due to the flexibility of the matrix itself but rather due to the micro-crack toughening resulting from the peeling off of the α_2/γ boundary reported in ceramics. Similar to 44%Al, 48%Al too did not show grain boundary rupture because of the curved grain boundary, in short because of the differing lamellae transformation process and transformation temperatures.

Next, the relationship between creep rupture and the microstructure was investigated. Photo 4 shows the structure around the ruptured plane of the specimen. At 1073 K, in the case of 44%Al, micro-cracks along α_2/γ boundary and typical wedge-shaped cracks along the grain boundary were observed. In the case of 48%Al, the

lamellae structure becomes slightly wavy due to changes within the grain. Micro-axial grains along the grain boundary were generated. In the case when the aluminum content is increased to 50%Al, overall structural transformations result. At 1223 K and in the case of 44%Al, cracks can be observed along the grain boundary, a phenomenon similar to that at 1073 K. The cracks are slightly sharper and micro-axial grains are generated along the grain boundary. In the cases of 48% and 50%Al, significant structural transformations can be observed together with major creep ruptures and the whole area around the rupture becomes covered with micro-axial grains. Voids indicate (the parts of the material) pulled in the direction of the tensile axis. The equi-axial grains observed here were concluded, from separate high temperature transformation basic tests, to be dynamically recrystallized grains. In other words, at high temperature and high aluminum content, transformation in the form of dynamic recrystallization occurs easily in order to reduce the bulk strength of the material. Elongation due to overall softening progresses and constrictions which finally result in cracks are generated. The higher the aluminum content in TiAl, the softer the whole constriction (due to dynamic recrystallization) area becomes, thereby reducing the creep strength. On the other hand, in spite of the high bulk strength and low aluminum content, the creep strength drops. This was attributed to the effects of the grain boundary morphology. Similar to 48%Al, the stress on the grain boundary cannot be concentrated when the grain boundary is curved. At the same time, grain boundary slip is suppressed and even when the cracks travel along the boundary, the paths become longer and the stress-expansion coefficient drops because of the curvature of the cracks. All these reasons are believed to help increase the creep strength. But such effects will not occur in the case of 44%Al whose boundary is straight. Only those areas around the boundary will transform since the internal grain strength is very strong. Wedge-shaped cracks will reduce the creep strength. The above relationship between microstructural transformations and creep strength as well as the rupture morphology is shown in Figure 4.



Photo. 2 - Fracture appearance of the isothermally forged and annealed Ti-50at%Al alloy.

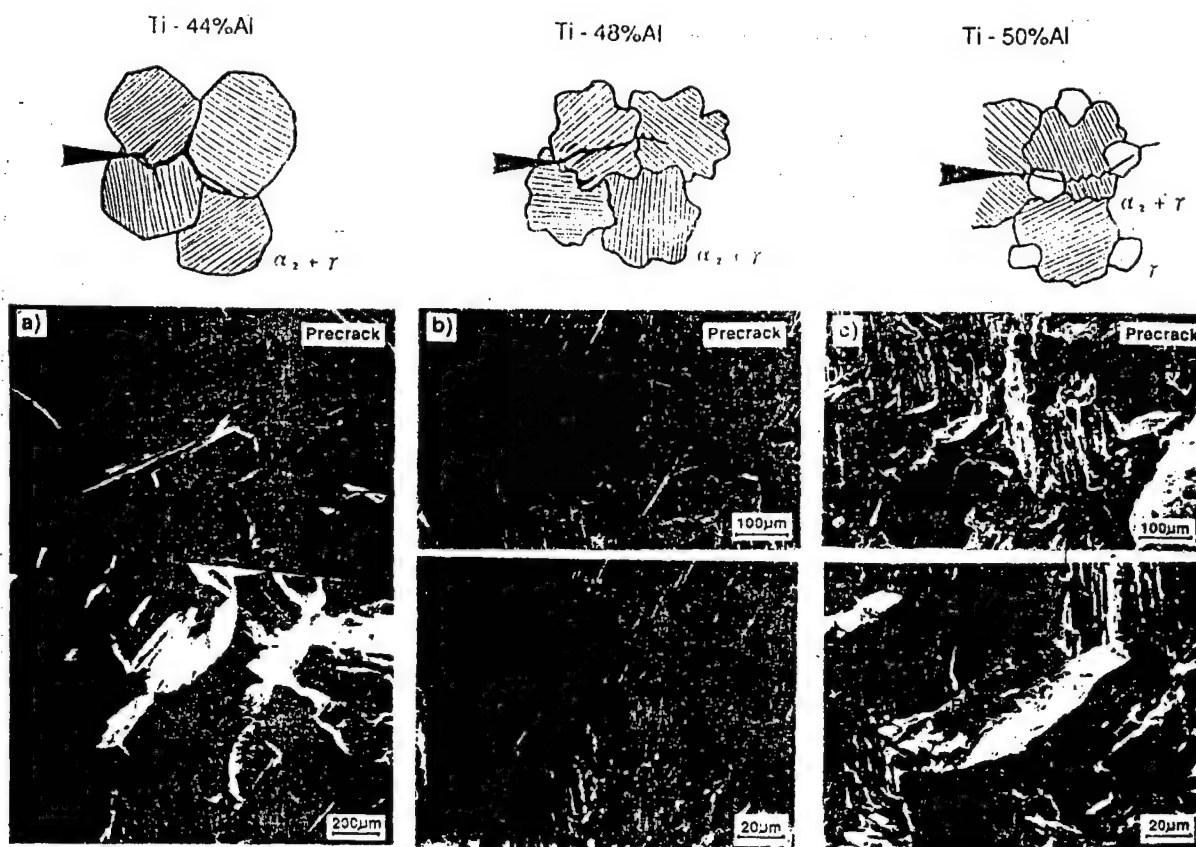


Photo. 3 - Fracture appearances and schematic crack paths of the as-cast alloys.

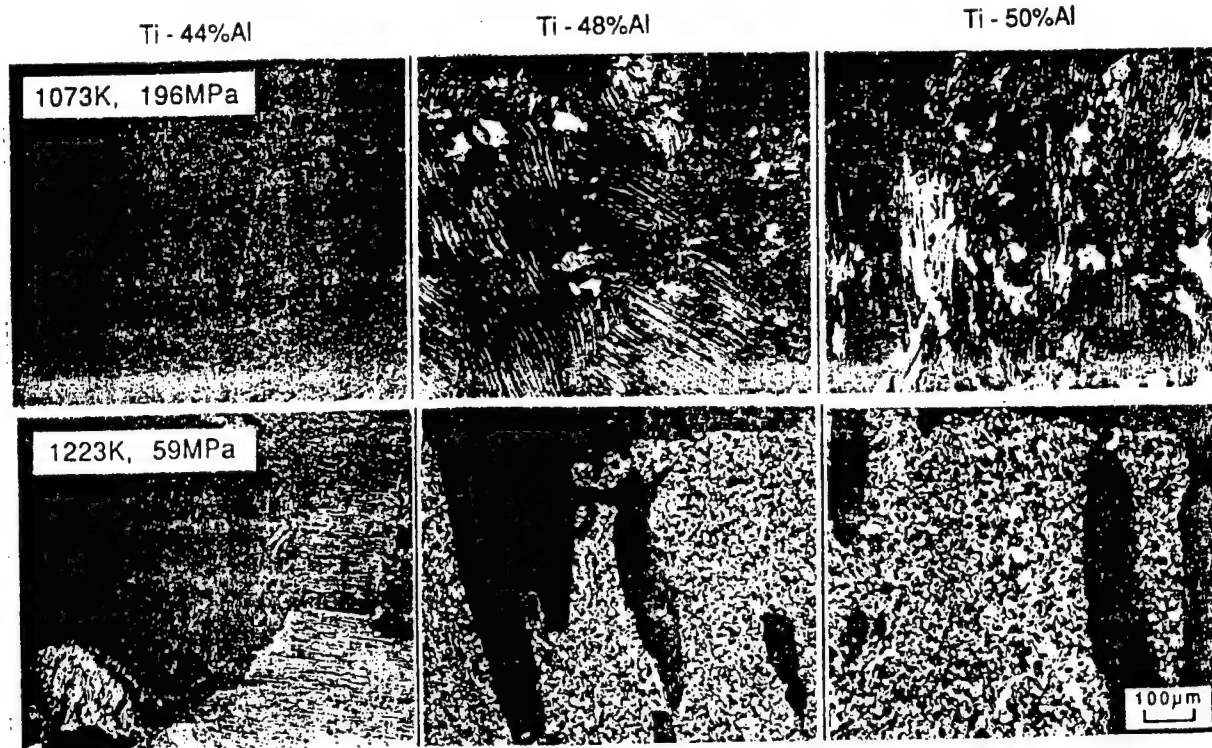


Photo 4. Microstructure and Crack/Void Appearance Near Creep Ruptured Surface

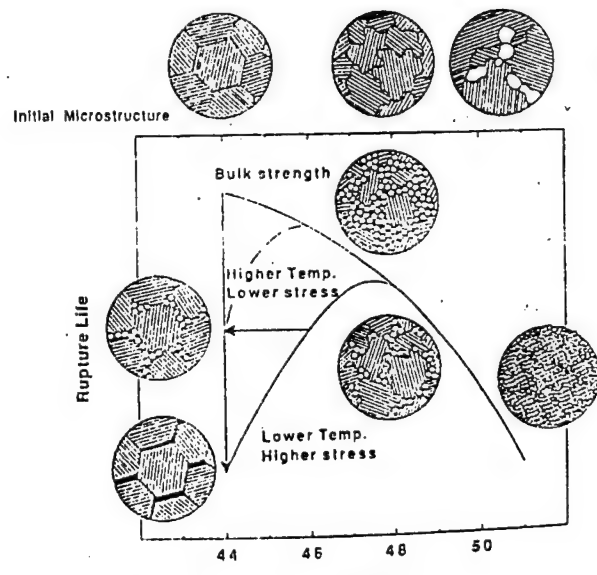


Figure 4. Schematic Drawing of Creep Rupture Property

4. Conclusion

(1) The microstructure of binary as-cast TiAl shows significant transformations depending on the aluminum content. The fracture toughness and creep strength also

changes with the microstructure change. The maximum values are in the case of 48%atAl. The whole structure of this material is lamellae with a curved grain boundary morphology.

(2) The γ phase is weak and easily ruptured by cracks. But when it is lamellae structured, the fracture toughness value can be increased through micro-crack toughening by peeling at the α_2/γ boundary plane. In this case, if the grain boundary is straight, the grain boundary will rupture and the toughness value will drop. Consequently, curving of the boundary is an important point.

(3) Since the bulk strength in materials with high aluminum content, dynamic recrystallization occurs and overall softening of the material will finally lead to cracking. On the other hand, a material with low aluminum content will result in grain boundary rupture because of stress concentration at the straight boundary. Consequently, similar to low temperature toughness, grain boundary morphology plays a very important role even in high temperature creep.

Phase Structure and Properties of Nb-Al-X Intermetallics by Rapid Solidification or Sintering
916C00350 Ube CHO KO-ON ZAIRYO KOKUSAI SHINPOJIUMU in Japanese 15 Mar 91 pp 141-144

[Article by Tetsuo Fujiwara, Ken Yasuda, and Hideya Kodama (Hitachi Research Laboratory, Hitachi Ltd., 3-1-1 Saiwaicho Hitachi-shi, 317 Japan)]

[Text] English abstract: Sintered or rapidly solidified Nb-Al and Nb-Al-X (X is Cr, Ti or Zr) ternary alloys with compositions around A15(Nb₃Al) structure, the candidate intermetallic as an advanced high temperature material, have been prepared and examined. The effects of alloying with ternary elements on the Nb₃Al phase relationship and on the lattice size of A15 structure are investigated. Although rapidly solidified ribbons with an A15 single phase are not formed, alloying with Cr or Ti in sintered alloys extends the region of the A15 single phase. Alloying with ternary elements gives rise to a change of A15 crystal size in sintered or rapidly solidified alloys.

1. Introduction

Since intermetallic Nb₃Al has a high melting point and is strong even at temperatures above 1300°C, it has been attracting a lot of attention as a replacement for Ni-base superalloys for use as ultra-high temperature material.

This alloy, however, becomes extremely brittle below 800°C and weak toward oxidation. These are the main obstacles to be overcome before it becomes practical. The main reason for this lies with the complex crystal structure of A15. If the crystal structure can be either rendered unstable or transformed into another by addition of a third element, the brittleness problem can be solved to a certain extent. But, high melting point, complex solid solution reaction and the almost 2000°C difference between the melting points of Nb and Al makes it extremely difficult to develop a structurally suppressed uniform yet simple Nb₃Al phase by normal solidifying processes. These difficulties during specimen fabrication have resulted in phase and crystal structure transformations due to addition of a third element, a process believed to be effective for improving the brittleness of the material, have not been exhaustively investigated.

The granular sintering process without the accompanying solid solution reaction and the rapid solidification process were considered for fabricating single phase Nb₃Al. The purpose of our research is to fabricate specimens of Nb-Al binary and Nb-Al-X ternary alloys, investigate the phase structure, properties and lattice constants, determine the conditions necessary for obtaining single phase Nb₃Al and to determine the effects of the A15 crystal structure on the third element.

Elements with the bcc structure for filling the Nb sites and an atomic radius larger than Nb for de-stabilization of A15 crystal structure were selected for use as the third element.

2. Experimental Method

The specimen was made up of a mixture of Nb, Al and a granulated third element. This mixture was thermally pressed after self-reaction and sintering. This sintered material was further treated for 10 hours at 1700°C in almost pure argon gas to improve dispersion and packing. This heat treated specimen was measured for its density, lattice constant while the structure and phase were observed. The cross-section of the specimen was

polished by Emery paper and wrapping tape until it shone like a mirror. After that, it was deoxygenated, and then etched by a mixed solution of HF:HNO₃:H₂O = 1:4:15 under a scanning electron microscope (SEM). X-ray diffraction was used for determining the phase and the lattice constant. The measuring conditions are 40 kV tube voltage, 150 mA tube current, 4 deg/min scan speed with Cu target.

The rapidly solidified ribbon used the pre-thermally treated sintered material as base alloy and was fabricated by the arc melt spinning process. The base alloy was about 5 g, and after replacing it in a 10⁻⁶ vacuum, it was dissolved by an argon plasma arc. The revolution of the rapidly cooled Cu roll was 15.7 mm/min.

The chemical composition of the ribbon fabricated was analyzed by ICP while the structure and phase identification as well as the lattice constant measurement were performed in the manner described above. The composition of each phase was analyzed by EDX (EMAX).

3. Results

(1) Composition and Phase Structure of Sintered Nb-Al-X

Table 1 shows the density and packing percentage of Nb-25at.%Al before and after annealing. The packing becomes about 99.5 percent after annealing. Figure 1 shows the cross-section of Nb-25at.%Al sintered alloy after annealing. The holes in the figure are believed to be those parts removed during polishing as considered from the density factor. The crystal grain was about 30-50 μm in size. The formed phases of each test material were investigated by X-ray diffraction. Figure 2 shows the relationship between the formed phases in (a)Nb-Al-Cr, (b)Nb-Al-Ti and (c)Nb-Al-Zr respectively, and their compositions after annealing. The chemical composition of each test alloy was that before annealing while the shaded part of each circle represents the existence ratio of each phase. Only bcc(Nb), A15(Nb₃Al), σ(Nb₂Al) phases are confirmed. When Cr and Ti were added into the A15 single phase area, the phase expanded. In particular, the A15 phase of that test alloy with Nb-20at.%Al-10at.%Ti composition is single phased despite the addition of even 10at.% of the third element.

Table 1. Density of Sintered Nb₃Al Intermetallics (Nb-25at.%Al)

	Pre-anneal	Annealed	Ideal density D _I
Density D (g/cm ³)	7.19	7.25	7.28
D/D _I (%)	99.0	99.5	—

Figure 3 shows the lattice constants of A15 phase created in each type of test alloy. The lattice constant of A15 phase in Nb-Al-Cr tends to be smaller than that of binary Nb-Al alloy while that of Nb-Al-Ti and Nb-Al-Zr tend to be larger. Table 2 shows the atomic radius (minimum distance between 2 atoms/2) of Nb, Cr, Ti and Zr crystal. In the case when Cr whose atomic radius is less than Nb, is employed as the impurity, the lattice constant becomes smaller while in the case of Ti or Zr whose atomic radii

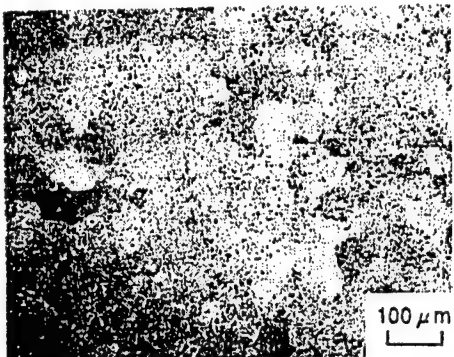


Figure 1. SEM Observation of a Nb-25at.%Al Sintered Alloy

are larger than Nb, the constant becomes larger. This is because the third element (its atomic radius) contributes to changes in the size of the crystal in A15 phase. We have found that, within the scope of our work, no new phases were formed besides the A15 phase when a third element was included in the alloy. The crystal size change and improvements on the characteristics of the alloy like its mechanical properties, can be made through de-stabilization of the crystal structure. At present, the compression strength of Nb-Al-X sintered alloys are being statistically investigated.

Table 2. Crystal Type and Atomic Radius of Ternary Elements

Element	Crystal type	Atomic radius (Angstrom)
Nb	bcc	1.43
Cr	bcc	1.25
Ti	hcp bcc	1.47
Zr	hcp bcc	1.62

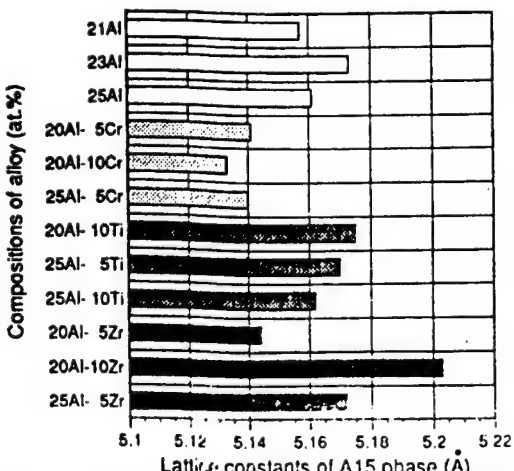


Figure 3. Lattice Constants of A15 Phase in the Sintered Nb-Al-X Alloys Where X is Cr, Ti, Zr

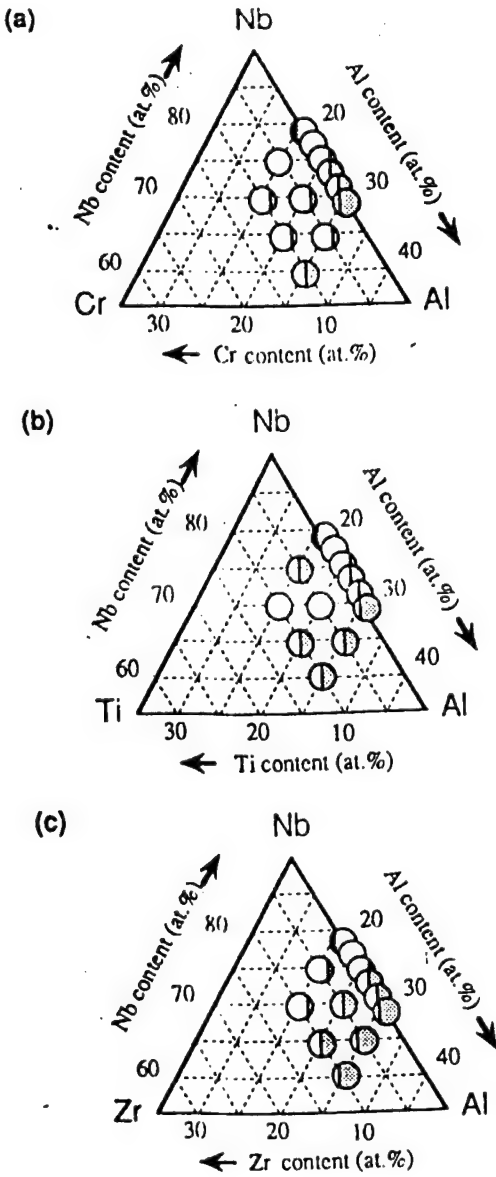


Figure 2. The Relationship Between Formed Phases in the Sintered Alloys and Their Compositions. (a)Nb-Al-Cr, (b)Nb-Al-Ti, (c)Nb-Al-Zr

(2) Composition and Phase Structure of Rapidly Solidified Nb-Al

Figure 4 shows the outer appearance of more than 1,000 mm long Nb-Al ribbons (Nb-25.2at.%Al) rapidly cooled by conventional methods.

In Figure 5, the state diagram of binary Nb-Al alloy and the phases formed in rapidly cooled Nb-14-34.4at.%Al ribbons investigated in this study, are shown. Both Nb-Al binary alloys did not have the single phase found

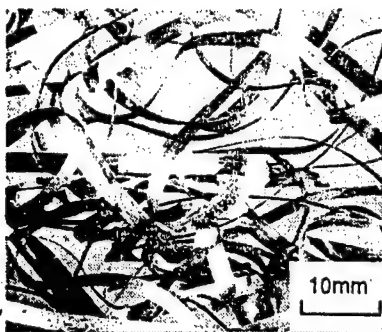


Figure 4. Rapidly Solidified Tri-Niobium Aluminide Alloy Ribbons Produced at the Wheel Speed of 15.7 m/s (Nb-25.2at.%Al)

in Nb_3Al . Figure 6 shows the composition of the deeply etched cross-section of Nb-25.2at.%Al ribbons and as is evident from this photo, an innumerable number of "block" structures were formed near the free surface region. These structures were also found in the depressions near the roll surfaces which are not in direct contact with the roll. This "block" structure, after analysis, was found to be a phase within the ribbon that was extremely poor in Al. This tendency was also observed in ribbons with different compositions. For example, "block" structures were observed in the bcc(Nb) phase of Nb-25.2at.%Al and in A15(Nb_3Al) phase of Nb-30.9at.%Al. According to the phase diagram of binary Nb-Al alloy, the initial precipitation during crystallization within the range of Nb-0.57.8at.%Al is a poor Al phase. As a result, the "block" structure is explained as the initial crystal dendrite formed in areas whose solidifying speed is slightly slower than that in other areas. From the above, it can be said that the fabrication of Nb_3Al single phase alloy is difficult, even in the case of rapid solidification process, because of the complexities in the reactions in solid solutions.

(3) Composition and Phase Structure of Rapidly Solidified Nb-Al-X

To investigate the effects of the composition of the third element on the alloy, Cr, Ti and Zr are added into the Nb-Al-X ribbons fabricated. The phases formed in each type of ribbon were analyzed by X-ray diffraction and EDX. The bcc, A15 and σ phases within the ribbons were classified according to their composition obtained from the results shown in Figure 6. In other words, when bcc, A15 and σ phases exist within the ribbon, "block" structures would be formed as the initial crystal dendrite, in the bcc phase which has the lowest Al content. The Al-rich σ phase would precipitate in the A15 phase. With

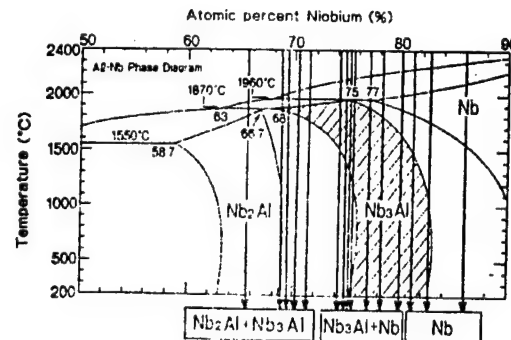


Fig.5 Aluminum-niobium phase diagram and formed phases of rapidly solidified Nb-14~34.4at.%Al ribbons in this study

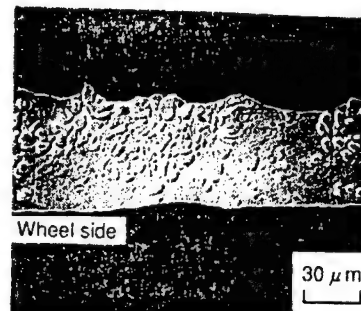


Fig.6 Deep etched cross-section photograph of Nb-25.2at.%Al ribbon

the exception of a few small precipitations, the phase compositions in the ribbon can be analyzed by EDX.

The relationship between formed phases within the ribbon and ribbon composition obtained by ICP analysis is shown in Nb-Al-X ternary alloy phase diagrams depicted in Figure 7 (a), (b) and (c). Table 3 shows the EDX analyzed results on the chemical composition of the formed phases within the ribbon. A different Zr-rich phase was formed in each of the bcc, A15 and σ phase in a few of the Nb-Al-Zr ribbons. We are still in the midst of doing detailed analysis on this. We have found that no changes occurred in A15 and σ phases when a third element was added. No other phase was formed. Figure 8 shows the lattice constants of A15 phase in each type of ribbon. A similar tendency can be observed in the lattice constants of sintered alloys summarized in Table 3. In other words, the lattice constant of the test material with Cr (atomic radius smaller than Nb) added, is smaller than that of binary Nb-Al alloy. On the other hand, when Ti or Zr whose atomic radii are larger than Nb are used, the A15 lattice constant becomes bigger than the binary alloy.

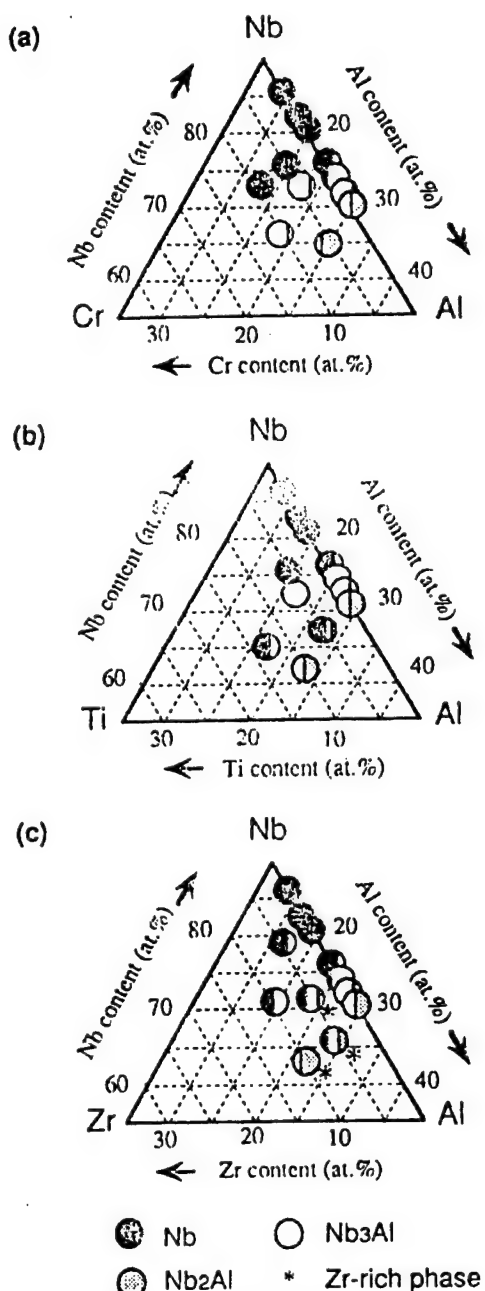


Figure 7. The Relationship Between Formed Phases in the Ribbons and Compositions of Ribbons. (a)Nb-Al-Cr, (b)Nb-Al-Ti, (c)Nb-Al-Zr

Table 3. EDX Analysis Results of Chemical Compositions for Formed Phases in Typical Ribbons

Compositions of ribbon (at%)	bcc(Nb) (at%)	A15 (Nb ₃ Al) (at%)	Sigma (Nb ₂ Al) (at%)	Others
22.4Al-4.5Cr	17.9Al-2.8Cr	22.7Al-4.9Cr	Impossible*	-
23.7Al-9.9Cr	-	21.6Al-9.7Cr	Impossible*	-
22.6Al-5.7Ti	-	22.3Al-5.5Ti	-	-
28.1Al-4.5Ti	20.2Al-4.1Ti	27.8Al-5.1Ti	Impossible*	-
24.1Al-4.8Zr	17.1Al	23.6Al-1.9Zr	25.0Al-7.4Zr	17.8Al-35.6Zr
29.4Al-4.5Zr	19.3Al	26.9Al-2.0Zr	27.7Al-3.2Zr	21.7Al-21.6Zr
27.2Al-9.0Zr	-	Impossible*	24.7Al-6.2Zr	4.8Al-58.2Zr

*Impossible to analyze due to an extremely small size.

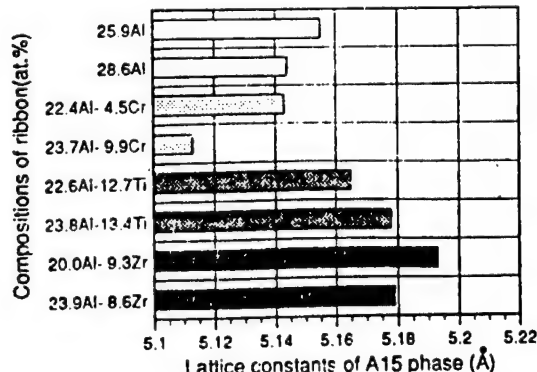


Figure 8. Lattice Constants of A15 Phase in Typical Nb-Al-X Ribbons Where X is Cr, Ti and Zr

4. Summary

- 1) In self-reaction sintering, heat press and annealing processes, A15 single phase composition was obtained from Nb-23.7%Al composition. Also, through the addition of Cr and Ti, the A15 single phase region could be expanded.
- 2) In the rapid solidifying process, Nb₃Al single phase composition was difficult to obtain because of the complexity of the reactions in solid solutions.
- 3) Within the scope of our work, we have found that the crystal structure of A15 phase did not change even when a third element was added. No new phase was formed.
- 4) The lattice constant of A15 phase changes in correlation with the atomic radius of the added element Cr, Ti or Zr when compared to that of Nb.

An Advanced Technique of X-Ray Diffractometry for in Situ Observation at High Temperatures—Application for Intermetallic Compounds

916C0035P Ube CHO KO-ON ZAIRYO KOKUSAI SHINPOJIUMU in English 15 Mar 91 pp 145-150

[Article by Masao Kimura, Keizo Hashimoto, and Hirofumi Morikawa (R&D Laboratories-I, Nippon Steel Corporation, Ida 1618, Nakahara-ku, Kawasaki 211, Japan)]

[Text] Abstract: A new type of x-ray diffractometry system has been designed for the determination of a phase diagram at high temperatures. The system is composed of an improved x-ray diffractometry and a newly-designed chamber. In the chamber, the specimen is heated to 2000°C under a controlled atmosphere of high vacuum or in various kinds of gas. The combination of angle-dispersive and energy-dispersive x-ray diffraction allows accurate and rapid measurements resulting in an improved *in situ* technique of structural analysis. By using this system, phase stability at a high temperature can be investigated by *in situ* observation. We are planning to employ this system in Ti-Al and Nb-Al systems.

1. Introduction

Phase equilibrium is one of the most fundamental aspects in understanding materials; it is especially important in the case where properties of a material are sensitive to the state of phases. There are many kinds of techniques in phase equilibria determination applicable to diverse purposes. We have designed a new type of x-ray diffractometry system for determination of phase equilibria at high temperatures, and are planning to use it for the study of high-temperature intermetallics such as titanium aluminides and niobium aluminides.

Intermetallics are a class of materials which can be viewed as occupying an intermediate position between metallic alloys and ceramics. One of the characteristics of intermetallics is the long-range ordering, which leads to unique properties; many intermetallics exhibit a very high yield stress even at a high temperature. The strong bonding and complex arrangements of atoms mean a high elastic modulus and good creep resistance. Unfortunately, these features also lead to a major challenge: limited ductility. Properties of intermetallics are strongly sensitive to their crystallographic structures and microstructures. Therefore a study of phase relation is necessary to improve the properties of intermetallics.

2. Determination of Phase Stability and Applications for Intermetallics

Many kinds of methods have been developed and used for phase equilibria determination. The most widely used among these is the quenching method which is a kind of *static method*; the sample is held constant until equilibrium is attained and quenched to room temperature for observation. This method is easy but its success

depends on the preservation of the phase assemblage present at equilibrium on cooling to room temperature.

The *dynamic method* is often used for determination of the limits of phase stability; in this method, the change on properties is observed continuously according to the change of such physical parameters as temperature and pressure. The thermal method of analysis, such as differential thermal analysis (DTA), is one of the techniques widely used. There are methods of wide variation according to the properties of measurement: electric conductivity, vapor pressure, length, weight, and so on. These types of *dynamic method* are more precise for determination of the boundaries between phases and free of the danger of a change in phase assemblage occurring during quenching.

The *in situ methods* are the most powerful techniques for direct observation of the specimen at equilibrium; high-temperature x-ray diffraction is a typical technique among these. High-temperature x-ray diffraction is capable of determining the crystallographic structures of the phases at equilibria and their fractions, which gives us direct information on phase equilibria. Capability to be measured in various types of atmosphere is another large advantage of x-ray diffraction. However, in this method, there are difficulties in maintaining a rather large area of the sample in a uniform condition during measurement, and a more complicated apparatus is required.

Suitable methods of phase equilibria determination depend on the material system in which you are interested. Our main interest is intermetallics which can be applied at high temperatures. As for phase equilibria of intermetallics, there are many studies of diagrams^{1,2} and structure³ mainly for binary systems. However, information on ternary systems is only available for some limited systems. Moreover, our interests not only exist in a theoretical case of phase equilibrium but also in real cases; properties are sometimes affected by the change of phase equilibria caused by many factors: addition of other elements, impurities, thermal history, processing, and so on. Therefore, precise *in situ* observation of specimens in our field of interests is necessary for the study of intermetallics. For this reason, we have designed an improved system for the determination of phase equilibria at high temperatures based on the *in situ* method: a new type of x-ray diffractometry system.

The *in situ* method by x-ray diffractometry has the following advantages: we can carry out a precise *in situ* observation of a bulk specimen at equilibrium and obtain quantity information on the structure. We can measure x-ray diffraction in various atmospheres as well as in a vacuum, and this measurement is non-destructive. However, complex apparatus is necessary for this method and the procedure of measurement is rather complicated. There sometimes remain ambiguities in the determination of phase boundaries.

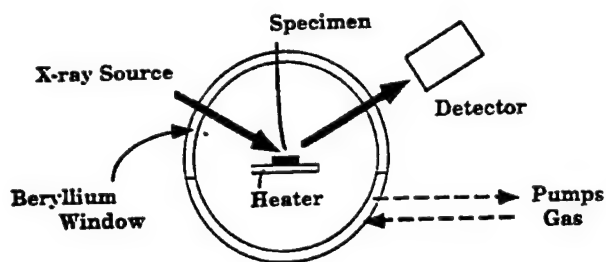


Figure 1. A Schematic Diagram of the Apparatus

3. A Newly-Designed System of X-Ray Diffractometry for *In Situ* Measurements

The new system is composed of an improved x-ray diffractometry and a newly-designed chamber. In the chamber, the specimen is heated up to 2000°C under a controlled atmosphere of high vacuum or various kinds of gas. The combination of angle-dispersive x-ray diffraction (ADXRD) and energy-dispersive x-ray diffraction (EDXRD) allows both accurate and rapid measurements, resulting in an improved *in situ* technique of structural analysis. Figure 1 shows a schematic diagram of the apparatus. The temperature of the specimen is controlled by a heater located where the specimen is mounted. The atmosphere in the chamber is controlled by pumps and systems for the introduction of gases. The chamber is equipped with a beryllium window to permit the penetration of incident and reflected x-ray beams.

Intermetallics, in which we are interested, are active at high temperature and impurities, especially oxygen, have a large influence on phase stabilities. Therefore, a high

vacuum is a necessary condition in the chamber; the chamber is designed using metal packing (ICF flange) to achieve a high vacuum. The chamber can be evacuated by a combination of pumps to attain a high vacuum and various kinds of gas can be substituted, such as He, He + H₂, N₂, and others.

The specimen is attached to a main heater made of tungsten sheet. A subheater with a parallel alignment of tungsten wires is located just above the specimen. The specimen is heated by controlling the electric current through the main and subheaters. The temperature of the specimen is measured up to 2000°C by a thermocouple attached to the main heater. The temperature is also measured by pyrometer through a glass window on the chamber. Figure 2 shows the principle of x-ray diffraction by ADXRD and EDXRD. The conditions of the diffracted x-ray beam are given by the equation $n\lambda = 2d \sin\theta$ (the Bragg equation), where n is an integer, the "order of the reflection", λ is the wavelength of the x-rays, d the interplanar spacing between successive atomic planes in the crystal, θ the angle between the atomic plane and both the incident and reflected beams. In the case of ADXRD measurements, the wavelength is fixed at λ_0 (the characteristic x-ray is used) and the detector is scanned around the 2θ axis; the diffraction intensities are measured as a function of the angle 2θ . Contrary to this, in EDXRD, the reflected angle is fixed at θ_0 and the diffracted x-rays are recorded by the energy-dispersive detector (the continuous x-ray is used).

Measurements by ADXRD (*Accurate Mode*) have a higher resolution than those of EDXRD (*Rapid Mode*), which is caused by the difference in the angle resolution of the goniometer and the energy resolution of the detector. However, measurements by ADXRD take a

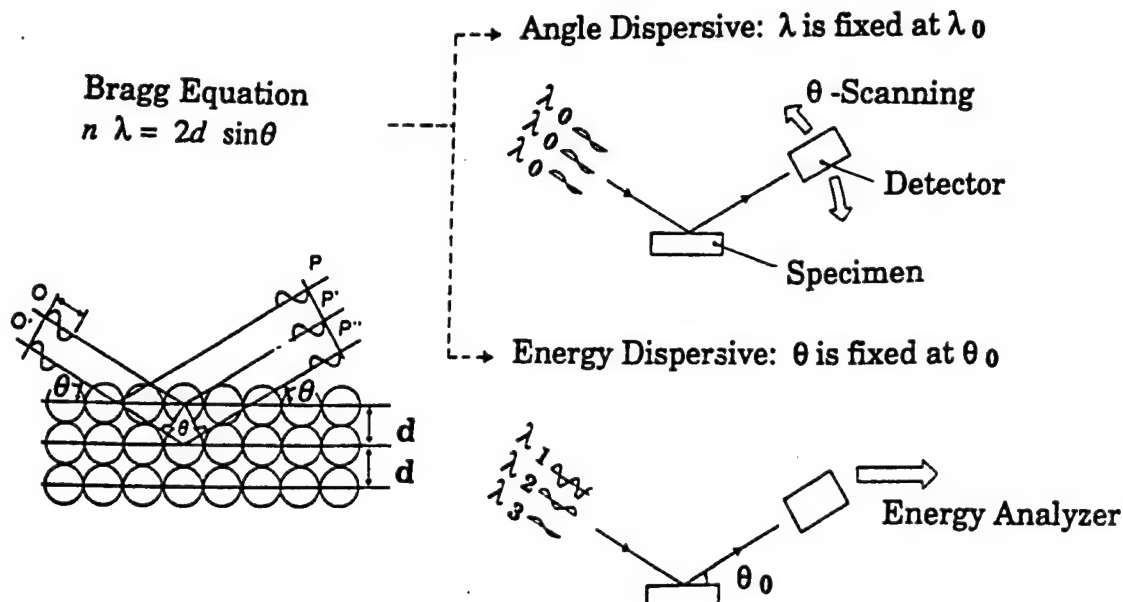


Figure 2. The Principle of X-Ray Diffraction

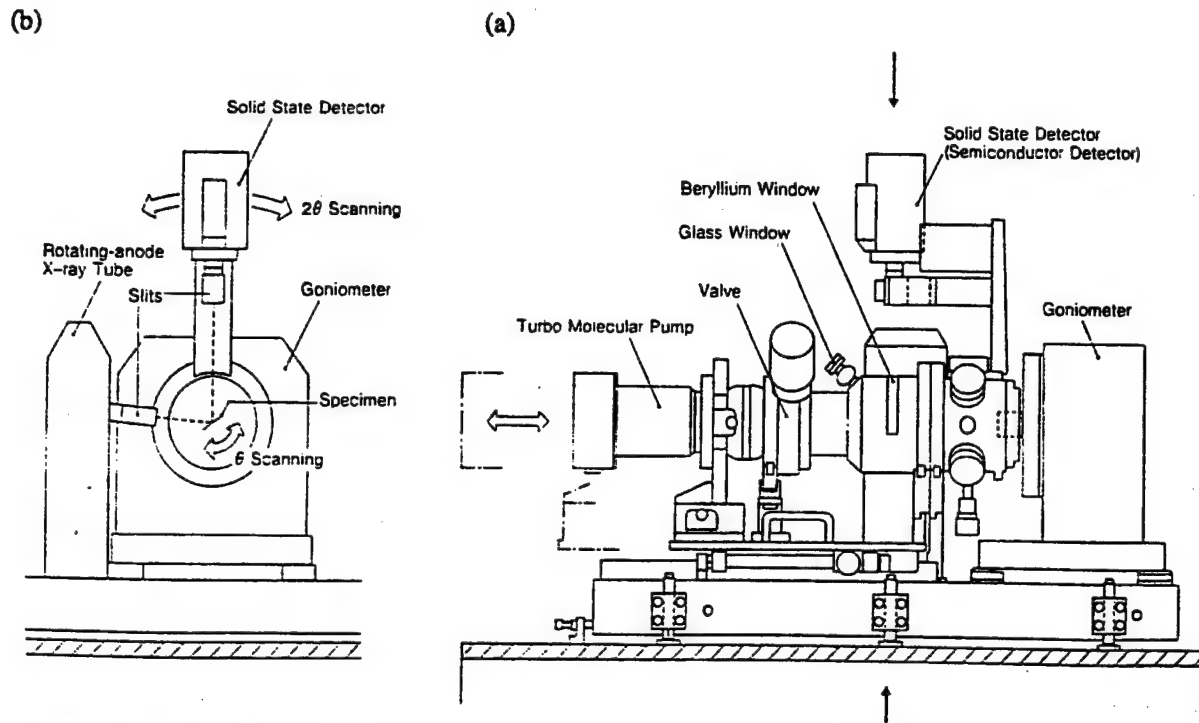


Figure 3. A Sketch of the Apparatus; (a) is a side view, and (b) is a cross-section in the pass of x-ray beams, as indicated by arrows in (a).

longer time, more than half an hour, and there is the possibility of a change occurring in the state of the specimen during the measurements. Compared with this, measurements by EDXRD only take less than ten minutes and there is no difference which is time dependent among the peaks. Therefore, a combination of ADXRD and EDXRD is one of the most powerful methods for *in situ* observation of the specimen.

Figure 3 shows a sketch of the apparatus: (a) is a side view and (b) is a cross section in the pass of x-ray beams, as indicated by arrows in Figure 3 (a). Figure 4 shows pictures: (a) the whole system of x-ray diffractometry, controller, and computer, (b) the newly-designed chamber. The goniometer can rotate the 2θ and θ axis independently. The chamber, containing the specimen on the heater, is fixed on the θ axis, and a turbo molecular pump is connected to the chamber through a valve. The connected complex of chamber, valve, and pump is maintained to be adjusted on the axis by specially-designed supporters. The detector is fixed on the 2θ arm and is rotated around the 2θ circle. Details of the apparatus are listed in the following table.

Table. Technical Data of the System

X-ray source	Rotating-anode x-ray tube (Mo, Cu,..)
	Maximum power: 60 kV, 300 mA

	Focus: Line
Detector	Peltier-cooling type of Si(Li) SSD
Goniometer	$2\theta/\theta$, 2θ , and θ -scanning
Atmosphere	Vacuum (10^{-8} Torr), He, He + H ₂ , N ₂
Temperature	R.T. similar to 2000°C
Thermometer	Thermocouple, Pyrometer

The geometry of x-ray diffraction is designed so the specimen can be kept horizontal during measurements; there may occur the need for measurement by powder specimens because of the difficulties in forming. A rotating-anode target is used as the x-ray source because of its high power. The kind of x-ray source is chosen according to wave length and strength of continuous x-ray; copper is for ADXRD for its wave length ($\lambda = 1.5418$ Angstroms) and molybdenum ($\lambda = 0.7107$ Angstroms) for EDXRD for its high continuous x-ray.

4. Example of Results

Figure 5 shows the x-ray diffraction pattern of a silicon powder obtained by ADXRD and EDXRD measurements at room temperature; in this figure the horizontal axis of EDXRD data is converted from the energy of photons to the Bragg angle which is calculated using a wavelength of copper. Sharper peaks of ADXRD data show a higher resolution of ADXRD measurements.

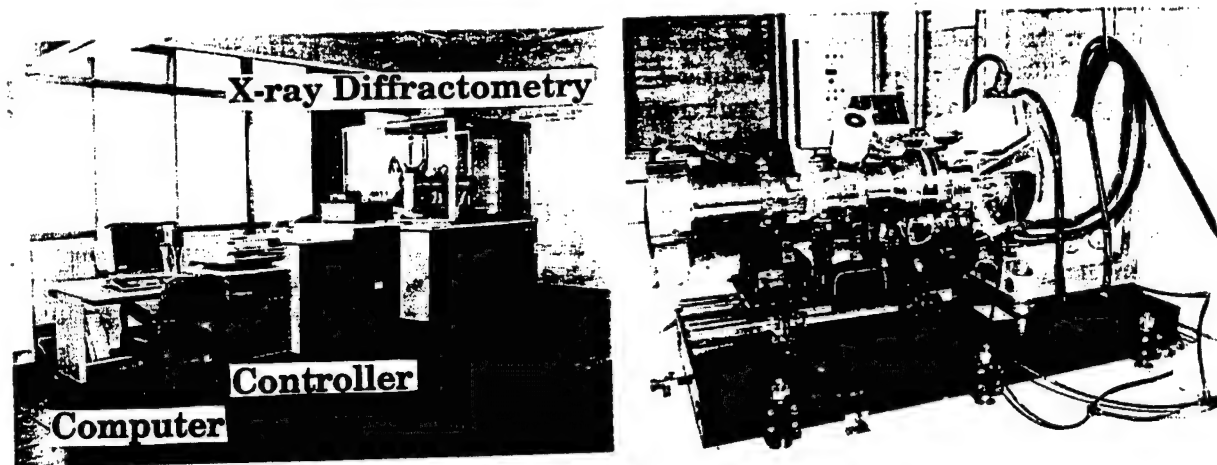


Figure 4. Pictures of the Apparatus; (a) the whole system, (b) the newly-designed chamber.

However, the measuring time of ADXRD is twenty times as long as that of EDXRD. Peaks other than silicon are those of the heater.

Figure 6 shows the diffraction patterns of EDXRD measurements of Ti-50at%Al in various temperatures, which are obtained using a prototype of the apparatus. Peaks indicated by open and closed circles represent $\text{TiAl}(\gamma)$ and Ti_3Al (α) phases respectively. These results are plotted in the phase diagram depicted by C. McCullough et al.⁴; open and half-closed circles represent γ -region and $\gamma + \alpha$ coexisting region respectively, and both results agree with each other. By measuring the specimen of different compositions in the similar way, we can obtain information on a phase diagram.

5. Conclusion

A new type of x-ray diffractometry system has been designed for the determination of a phase diagram at high temperatures. The main features of this system are its unique x-ray geometry and a newly-designed chamber. This improved *in situ* technique is intended to be applied for intermetallics: Nb-Al and Ti-Al systems.

Acknowledgements

This work has been carried out as a national project, "High-performance Materials for Severe Environments," which is supported by NEDO (New Energy and Industrial Technology Development Organization). The

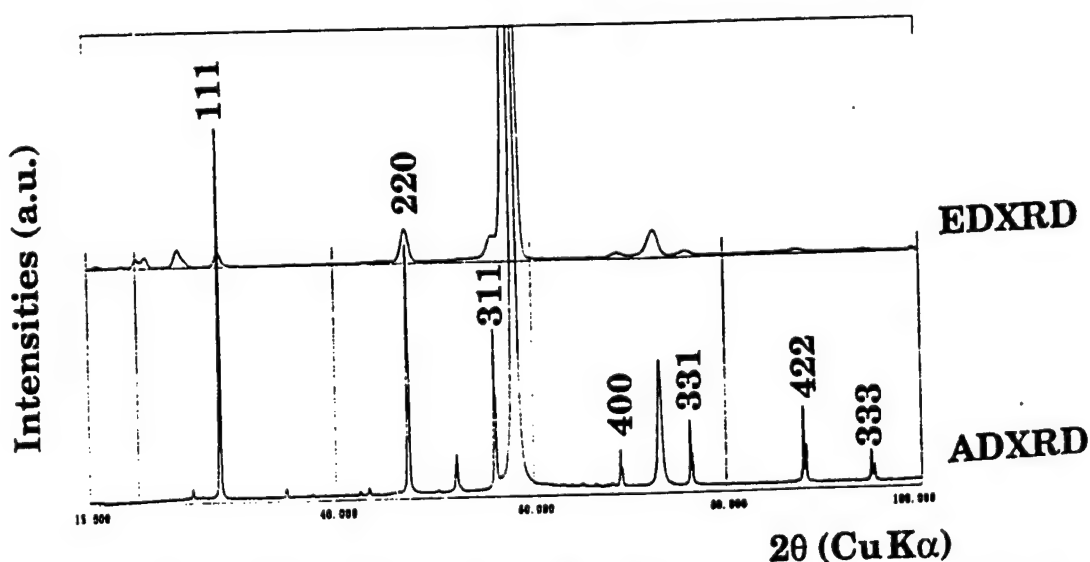


Figure 5. The X-Ray Diffraction Patterns of Silicon; measurements by ADXRD (below) and EDXRD (above)

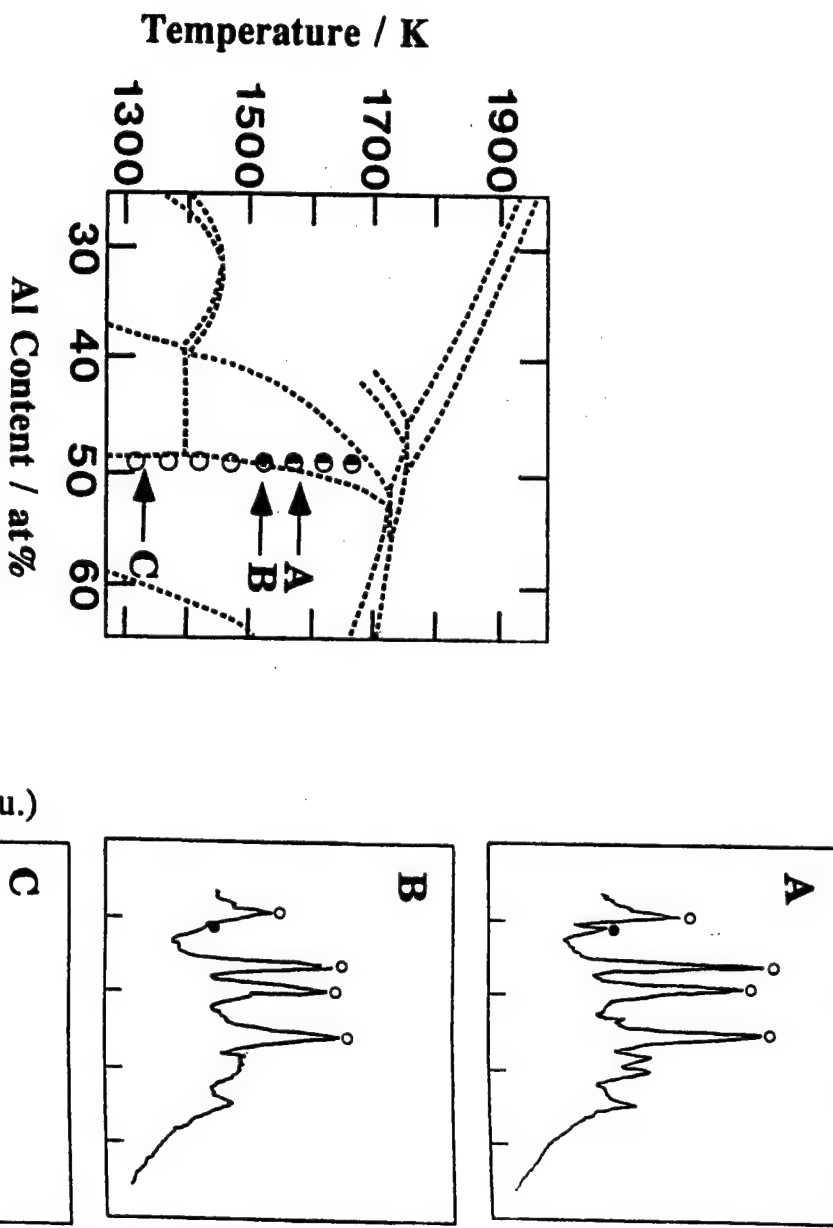


Figure 6. The X-Ray Diffraction Patterns of Ti-50at%Al and a Proposed Phase Diagram of Ti-Al System

authors would like to thank Rigaku Company, the manufacturer of the apparatus. Our discussion with the staff of Rigaku Company was of great help to us in designing the system.

References

1. M. Hansen and K. Anderko, "Constitution of Binary Alloys," 2nd Ed., McGraw Hill, (1958).
2. T. B. Massalski, ed., "Binary Alloy Phase Diagrams," Vol. 1 and 2, American Society for Metals, (1986).
3. W. B. Pearson, The Crystal Chemistry and Physics of Metals and Alloys, New York Wiley-Interscience, (1972).
4. C. McCullough, J. J. Valencia, C. G. Levi and R. Methrabian, Acta metall. 37, 1321 (1989).

Thermal Plasma Processing of High Temperature Materials in a Low Pressure Plasma Jet

916C0035Q Ube CHO KO-ON ZAIRYO KOKUSAI SHINPOJIUMU in Japanese 15 Mar 91 pp 151-154

[Article by Satoshi Sakiyama, Tetsuya Hirabaru, Tohru Sunami, and Osamu Fukumasa]

[Text] English abstract: A reactor consisting of a forced constricted type DC plasma jet generator and a feeding has been developed. In order to demonstrate the application feasibility of this reactor to low pressure plasma processing, including the control of low pressure plasma jets, production of ultrafine particles of refractory materials (Al_2O_3 , ZrC , TiC) and synthesis of diamond are studied.

According to SEM photographs, many ultrafine particles whose diameters are less than $0.1 \mu\text{m}$ are prepared. With increasing the feeding length, deposition of ultrafine particles increases.

When hydrogen and methane gas mixture is injected into the plasma flow through the feeding, diamonds are successfully synthesized on Mo substrate both at 100 and 760 Torr.

Key Words: Thermal Plasma Processing, Plasma Jet, Feedring, Ultrafine Particles, Synthesis of Diamond, Refractory Materials

1. Introduction

The highly active plasma property at high temperatures has suddenly found wide applications in plasma processing for material fabrication and material surface treatments. In fact, some applications have already become practical. The plasma applied in plasma processing can be roughly classified into low temperature plasma for use under low pressure and hot plasma for use under high pressure. Low temperature plasma allows uniform processing over a wide surface area but has the disadvantage of low treating capability. On the other hand, hot plasma has a high reactive power for treating materials but it is not easy to handle in bulk.

The plasma jet is hot plasma that can be easily obtained by forced constriction of an arc discharge in a gas flow enclosed within a vessel. This is becoming a prime candidate in high speed membrane fabrication, high temperature chemical reactions and treatment of materials with high melting points. A processing device employing forced constricted plasma jet generator was developed and tests were made on the production of ultrafine particles with high melting points and spray-coating. The purpose of our study is the use of the plasma jet in processing during decompression such that the high reactive speed of hot plasma is maintained while low temperature plasma can be handled in large volumes and at the same time, enables its uniform reactive property to be used. The production of ultrafine particles of materials with high melting points and the synthesis of diamonds by using the processing device developed enable the properties of the plasma during decompression to be investigated and at the same time, discover its possible applications.

2. Experimental Device and Method

2.1 Processing Device

The experimental device is shown in Figure 1. It is made of a forced constricted plasma jet generator, feeding (hereafter abbreviated as FR) and a pressure device.

The rod cathode of the forced constricted plasma jet generator is made of tungsten with 2 percent torium (diameter $5 \text{ mm}\varnothing$) while the nozzle anode is made of copper (internal diameter $5 \text{ mm}\varnothing$). An insulated copper constrictor nozzle (internal diameter $5 \text{ mm}\varnothing$) is placed between the anode and the cathode to force constrict the arc. The structure of the vessel allows strong constriction. For this reason, the jet generated was stable and high-powered under different driving conditions.

The material to be processed was introduced into the plasma flow via the FR whose internal diameter is equal to that of the anode. The FR is insulated from the anode and since it is at the downstream, it prevents the material which is to be processed from affecting the electrical arc discharge. The FR also helps enclose the plasma jet

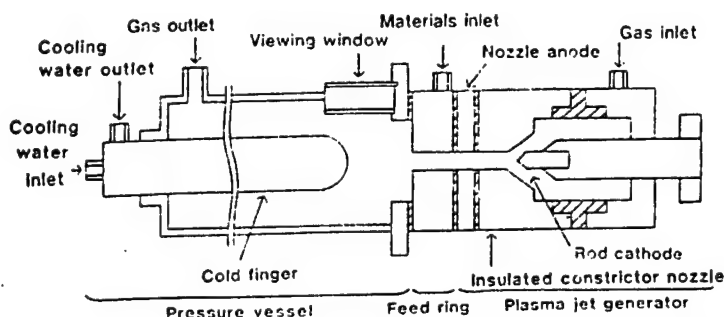


Figure 1. Schematic Diagram of the Plasma Jet Reactor System, Where the Forced Constricted Type Plasma Jet Generator Is Equipped

within the nozzle and thereby promote heating of the material through maintenance of the relatively high temperature of the plasma flow.

The pressure vessel (70 mm ϕ x 480 mm) is connected to the downstream part of FR. The pressure within the vessel is controlled by two vacuum pumps (100 l/min) and a needle valve. An observation window (35 mm x 120 mm) is included in the vessel to allow observation of the jet during the process.

2.2 Experimental Method and Conditions

Production of ultrafine particles of materials with high melting points and the synthesis of diamond were studied.

Al_2O_3 , TiC and ZrC (melting points are 2313, 3413 K respectively) with an average particle size of 20 μm were used. Every minute 0.5 g, 6 l of these materials were mixed with the feed gas (Ar) and introduced into the plasma flow within the FR. The fine particles produced inside the plasma jet are caught by the 20 mm ϕ diameter cylindrical copper cold finger (the tip is shaped like a hemisphere, hereafter termed CF) situated along the axis of the pressure vessel. The introduction and removal of the material was 2 minutes and the particles produced when the distance between FR exit and CF tip was changed from 20-200 mm, were collected. Four different axial lengths of 9.5, 15.5, 21.5 and 27.5 mm (hereafter termed FR1, FR2, FR3 and FR4 respectively) were employed to investigate the effects of FR (copper, internal diameter 5 mm ϕ) on the heating of the test material. This structure is depicted in Figure 2.

A mixture of hydrogen and methane gas was used to synthesize diamond. The mixture was introduced into the plasma flow after 10 minutes via FR. A Mo substrate (12 mm ϕ) was attached to a substrate holder affixed along the axis of the pressure vessel with a silver paste. The substrate's temperature was measured by a pyrometer.

The morphology of the particles or the membrane produced are investigated with the help of SEM while the composition is determined by X-ray diffraction. The temperature of the plasma jet was determined by spectroscopy (dual beam strength ratio method).

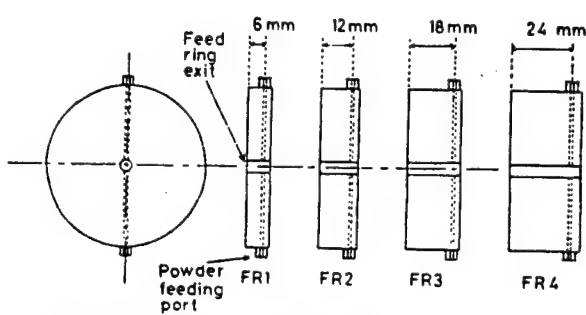


Figure 2. Feedings With Different Axial Lengths

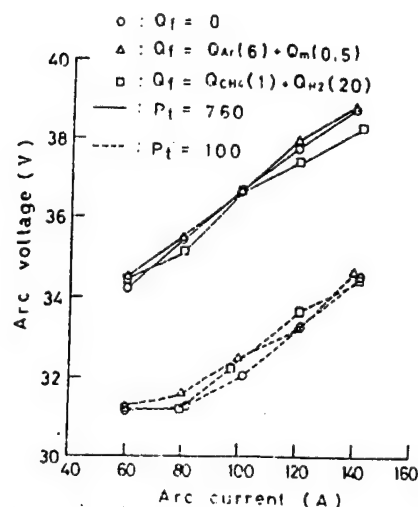


Figure 3. Arc Voltage vs. Arc Current

The experiments were conducted under 760 and 100 Torr (P_t) in the pressure vessel, the argon gas flow as 20 l/min, while the thermal output of the jet was 2.9-3.0 kW.

3. Experimental Results

3.1 Basic Properties of Plasma Jet Generator

The relationship between the arc voltage and current of the forced constricted plasma jet is shown in Figure 3. The graphs show an upward trend under both high and low pressures. This is because the constant arc length during an increasing current strength prevents arc column expansion and an increase in electric conductivity. The arc voltage change when the material to be processed was introduced was within 5 percent. The introduction of powdered materials or reactive gas has little effects on the arc characteristics regardless of the pressure vessel.

Next, the relationship between the thermal output of the jet and the arc current is shown in Figure 4. The jet thermal output was calculated by subtracting the total heat loss in the cathode of the generator, the spreadout section of the insulator and the anode, from the total input electric power which is equal to the product of the arc current and the voltage. This value represents the heat energy in the plasma flow when the material to be processed is introduced into the area below the anodic nozzle exit. The jet thermal output increases along almost a straight line with current increase. A decrease in the pressure in the pressure vessel reduces the jet thermal output by about 15 percent but still, a range of 1.1-3.1 kW is maintained. Thermal output change with material introduction is within a meager 5 percent.

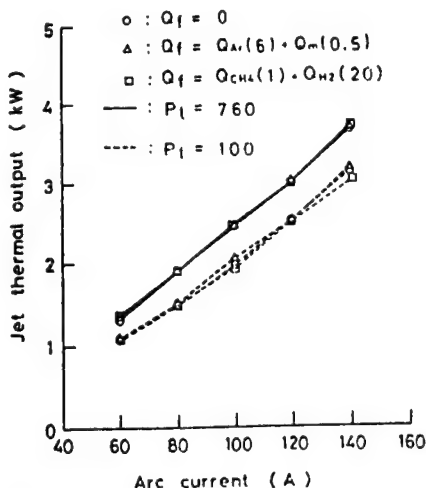


Figure 4. Jet Thermal Output vs. Arc Current

The temperature of the plasma jet is, for example when $P_t = 760$ Torr and at 4 mm below FR along the axis, 6775 K. This temperature is high when compared with the melting point of the material to be processed.

The basic characteristics of the generator are not affected by the introduction of reactive gas or powdered materials. A stable high temperature plasma jet can be maintained regardless of the pressure in the pressure vessel.

3.2 Production of Ultrafine Particles of Materials With High Melting Points

Figures 5, 6 and 7 show SEM photographs of pre- and post-plasma treated fine particles. Under both high and low pressures, masses of ultrafine particles of less than 0.1 μm can be observed. The radius distribution of pre-treated particles is 10-53 μm with a high melting point of 2313-3843 K. When this is properly introduced into the high temperature region of the plasma, it will melt and evaporate. Consequently, this device can be applied in the production of ultrafine particles.

We have previously considered the theory behind the particle heating process in a plasma flow using the Single Particle Model. The result of that consideration was that the amount of heat transmitted from the plasma flow to the particle material introduced drops with the pressure, meaning that the particles become difficult to heat. At the same time, heat transfer can be controlled by the FR length.

Next, the effects of FR length on the production of ultrafine particles was investigated. Figure 8 shows the distance of FR exit from the particle collection point (1) and the density of those particles collected which are less than 0.1 μm in size. The material processed was Al_2O_3 while the density of the particles was that number of particles per unit area ($0.1 \times 0.1 \text{ mm}^2$) on the SEM photographs. The density of ultrafine particles collected in the cases of FR2, FR3 and FR4 are high, their density

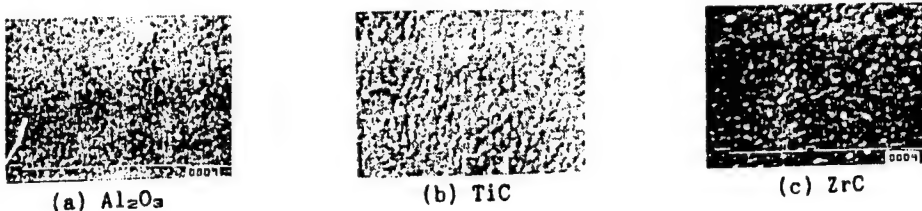
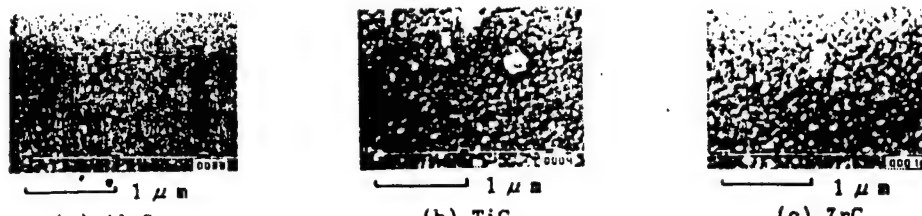
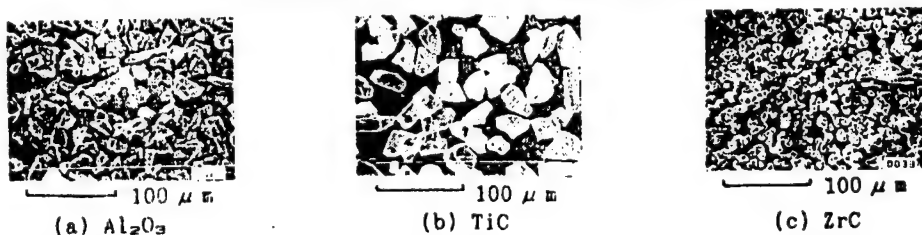
Fig.5 SEM Photographs of prepared fine particles at $P_t = 760$ Torr.Fig.6 SEM Photographs of prepared fine particles at $P_t = 100$ Torr.

Fig.7 SEM Photographs of raw powder materials.

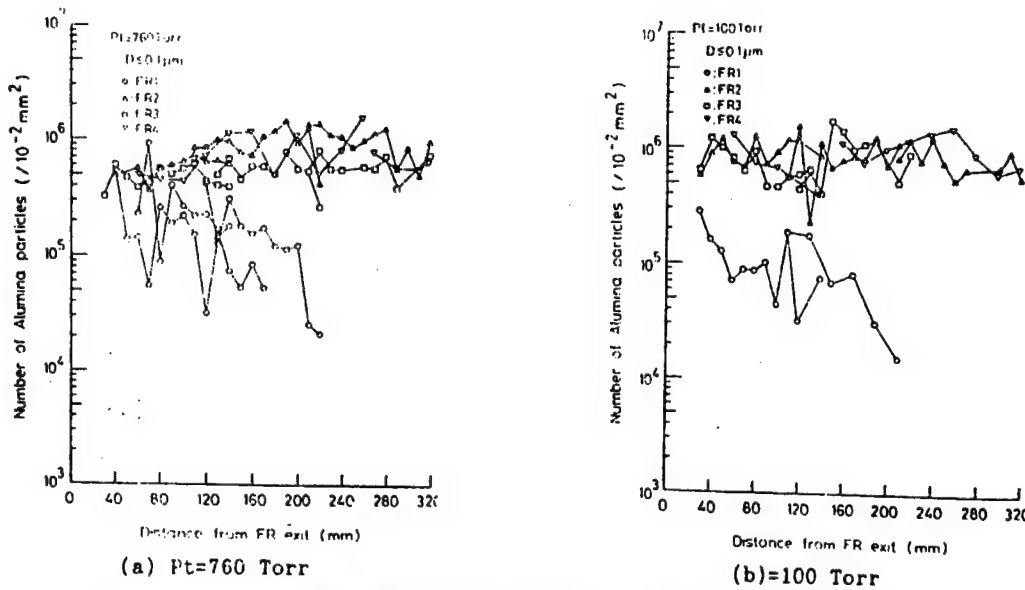


Figure 8. Collected Number of Al_2O_3 Particles vs. Distance From Feeding Exit

difference is especially high when $Pt = 100$ Torr. As an example, when $l = 80$ mm and $Pt = 760$ Torr, particle density of FR4 = 5×10^5 (about twice that of FR1) while when $Pt = 100$ Torr, the particle density jumps by about 10 times to about 7×10^5 . From this, we can say that by increasing the FR length, about the same amount of ultrafine particles produced under high pressure, can be collected even at low pressures. This tendency was also confirmed for particles of sizes ranging from $0.1\text{-}5 \mu\text{m}$.

An increase in the particle density was confirmed for collected particles of all sizes (under $5 \mu\text{m}$) and the longer the length of FR, the finer the particles produced. From the fact that particle density increases at a faster rate when $Pt = 100$ Torr with an increase in FR, we have proved that the particles can be effectively heated by increasing FR length even when the pressure in the device is reduced.

3.3 Diamond Synthesis

A gas mixture of hydrogen and methane was introduced via FR and a SEM photograph of the particles precipitated on the substrate is shown in Figure 9. Under high pressure, multi-faceted particles like that in (a) were observed. When an Al_2O_3 substrate with average particle size of $20 \mu\text{m}$ and polished for about 20 minutes was employed, a membrane of about $20 \mu\text{m}$ in thickness was formed as in (b). The resulting membrane on a polished substrate was because of the increased probability for the growth of particle nucleus on the substrate. The formed particles then combine during their growth to form a membrane. Figure 10 shows the X-ray diffraction of the multi-faceted particles shown in Figure 9(a). Peaks depicting diamond crystal planes (111), (200) and (311) (represented as D in graph) were observed together with

peaks showing Mo (used as substrate) and Mo/C alloy. Both the multi-faceted particles and membrane have proved to be diamond.

On the other hand, many spherical particle precipitates were produced under low pressure. This is shown in Figure 9(c). When the hydrogen flow volume was increased, square crystal planes were observed in the spherical particles as depicted in (d). No diamond peaks were observed when specimen (c) was X-ray diffracted. On the other hand, the particles in (d) were confirmed to be diamonds.

Although Raman spectroscopy is necessary for further confirmation, we can conclude that the plasma jet can be applied for diamond synthesis under reduced pressure and not under high pressure through a proper selection of the processing conditions.

4. Conclusion

A processing device consisting of a forced constricted plasma jet generator equipped with an FR for material introduction and extraction was developed. Application of this device in hot plasma processing was investigated by the production of ultrafine particles of materials with high melting points and diamond synthesis. A summary of the results follows.

- (1) The plasma source was unaffected by changes in the pressure vessel, introduction of powdered material or even reactive gas. A stable high temperature plasma jet was maintained.

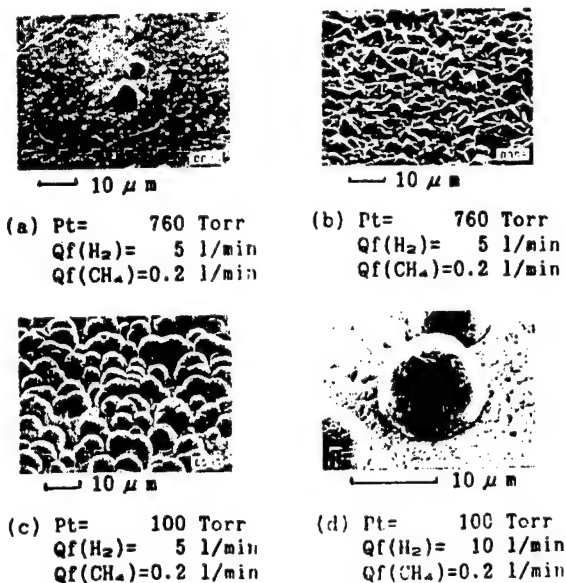


Fig. 9 SEM photographs of the particles and film grown on the molybdenum substrate.

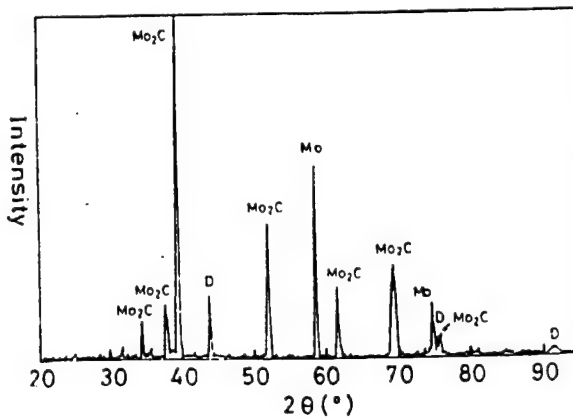


Fig. 10 X-ray diffraction pattern of the particles grown on the molybdenum substrate.

(2) This device can be used to produce ultrafine particles of materials with high melting points. By increasing the length of FR, the number of particles produced can be increased. Production increase under reduced pressure is particularly significant.

(3) Diamond synthesis under both high and low pressure is possible through the proper selection of the production conditions.

The above proves that this device can be applied in processing under reduced pressure.

Magnesia Ceramics—Effect of Microstructure on Bending Strength of Sintered Magnesia

916C0035R Ube CHO KO-ON ZAIRYO KOKUSAI SHINPOJIUMU in Japanese 15 Mar 91 p 155

[English abstract of article by Shinji Fukuda, Akio Nishida, Yasuhiko Toda, and Kouzoh Hirosawa (Ube Industries, Ltd.)]

[Text] To increase bending strength of the sintered magnesia, we controlled its microstructure (relative density and grain size) by changing sintering conditions (sintering temperature and time). Although grain size of sintered magnesia was smaller than 4 μm when its relative density was lower than 97.5 percent, rapid grain growth occurred when it was densified over 97.5 percent. The sintered magnesia which had a relative density of 97.5 percent showed the highest bending strength at room temperature and 1200°C. Bending strength of the sintered magnesia was affected by porosity in a lower density region and grain size in a higher density region.

And 3-point bending deformation of sintered magnesia was carried out at temperatures between R.T. and 1500°C to compare the mechanical properties of Ube's and usual sintered magnesia. Ube's sintered magnesia was deformed at higher temperature than usual sintered magnesia because of higher purity.

Key Words: Magnesia, Bending strength, Grain growth, microstructure

Properties and Application of SiC Produced by Chemical Vapor Deposition

916C0035S Ube CHO KO-ON ZAIRYO KOKUSAI SHINPOJIUMU in Japanese 15 Mar 91 pp 159-162

[Article by Kazuhisa Matsumoto, Fusao Fujita, Yoshiharu Chinone, and Saishiro Ezaki (Mitsui Engineering & Shipbuilding Co., Ltd.)]

[Text] English abstract: Some mechanical properties of CVD-SiC films and sintered SiC coated with CVD-SiC were investigated. It was found that the four-point bend strength of sintered SiC and the Weibull modulus of the bend strength of sintered SiC were considerably increased by CVD-SiC coating. The thermal shock resistance of sintered SiC was also considerably increased by CVD-SiC coating. The CVD-SiC films showed relatively high strength although they had high residual stress.

We developed some components such as a combustion chamber liner, a heat exchanger test element and other high temperature test components. The test results suggest that the CVD-SiC is a promising material for high temperature use.

1. Introduction

We have focused our attention on the Chemical Vapor Deposition (CVD) Method for synthesizing ceramics from gas to investigate the properties of silicon carbide

(SiC) and successfully developed a SiC coating technique. The CVD-SiC we have developed is (1) highly pure with impurities of the order of ppb, (2) able to uniformly coat surfaces of complex shapes, (3) extremely strong. These and many other advantages have resulted in our product finding wide applications in the field of semiconductors as well as a material for structures to be used under extremely high temperatures. The development of production techniques for fabricating objects made only of CVD-SiC is in progress. Some products and trial products will be introduced.

We will describe the results of tensile tests and residual stress tests on CVD-SiC conducted recently. The strength of a sintered SiC object coated with CVD-SiC as well as their applications will be explained.

2. Characteristics of CVD-SiC

2.1 Tensile Strength and Coefficient of Longitudinal Elasticity

2.1.1 Experimental Method

The graphite substrate shown in Figure 1 is removed by atmospheric oxidation after about 0.27 mm CVD-SiC is coated onto it to fabricate the hollow tensile test piece (shown in Figure 2). A metallic rod is attached to each prong of the test piece for fixing those attachments for tensile stress experiments at room temperature. The all-purpose Instron test equipment was loaded with a crosshead speed of 2 mm/min.

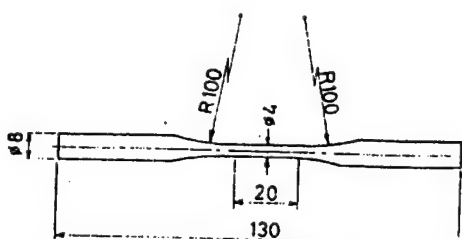


Fig. 1 Graphite substrates used for the production of hollow tensile specimens

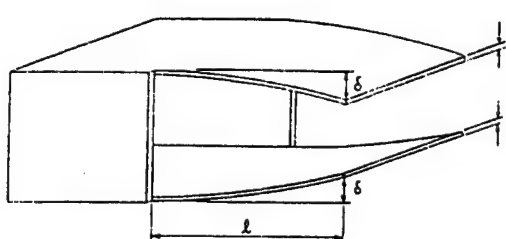


Fig. 2 Residual stress measuring method in a CVD-SiC film

The test piece for measuring longitudinal elastic coefficient was also fabricated in a manner similar to that for making the hollow tensile test piece. A strain meter is attached to the hollow tube of internal diameter 10 mm and thickness of 0.58 mm. The longitudinal elastic coefficient was determined from the stress/distortion gradient.

The thickness of CVD-SiC was measured from observations made on the cross-section of the ruptured plane by an optical microscope.

2.1.2 Experimental Results and Observations

Table 1 shows the results of tensile tests made on CVD-SiC. The mean tensile strength of five test pieces is 460 MPa. However, since residual stress exists in the material fabricated by the CVD method, it is believed that this tensile strength also includes the effects of the residual stress. The residual stress can be roughly classified into thermal stress due to the difference in the linear expansion coefficients of the membrane and the substrate, and intrinsic stress generated within the membrane during CVD process. In the case when the substrate is removed, only the intrinsic stress need be considered. The intrinsic residual stress of CVD-SiC at room temperature was measured by the following method.

Table 1. Tensile Strength of CVD-SiC at Room Temperature (MPa)

Tensile strength	Mean strength
460	
490	
530	460
380	
430	

The amount of deflection δ at each end of the test piece shown in Figure 2 was measured to determine the residual stress σ_R from equation (1) assuming 1) a moment operates on one end of the prong of length of about 13 mm when the other end is fixed; 2) the residual stress changes linearly along the direction of the thickness of the prong plate.

$$\sigma_R = E \times t \times \delta/l^2 \quad (1)$$

E represents the longitudinal elastic coefficient, t the thickness of the plate and l the length of the prong plate. By introducing the experimental values of $t = 0.252$ mm, $l = 12.6$ mm and $\delta = 0.35$ mm into equation (1), the residual stress obtained is $\sigma_R = 260$ MPa. When the substrate was removed, the membrane distorts like in Figure 2. As such, the intrinsic residual stress within the membrane vaporized into the substrate would become the tensile stress on the substrate side while becoming the compressive stress on the upper surface. The deflection in the hollow tubular tensile test piece was suppressed because an intrinsic residual stress equal to that when a coating is vaporized onto the substrate results. If

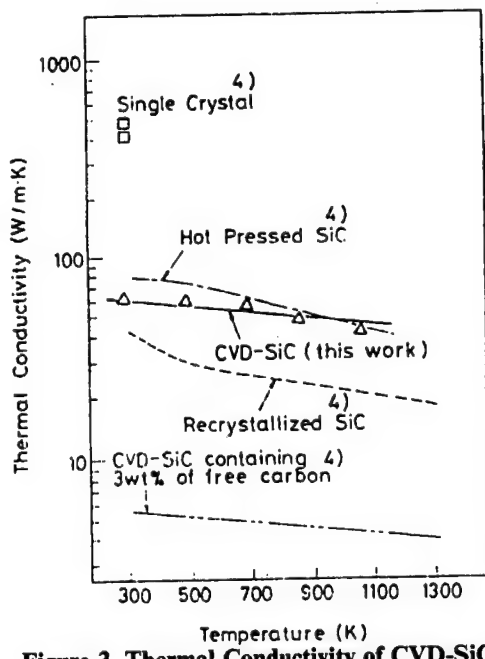


Figure 3. Thermal Conductivity of CVD-SiC

the Poisson ratio was ignored and assuming the test piece was under 460 MPa of tensile stress, the stress generated on the surface of the substrate was estimated to be 720 MPa while that on the outer surface was 200 MPa.

2.2 Other Characteristics

The thermal conductivity of CVD-SiC obtained by the laser flash method on the roughly 2 mm thick circular plate test piece is shown in Figure 3. The thermal conductivities of other SiC determined in other papers are also included for comparison. The thermal conductivity of CVD-SiC is almost equal to hot-pressed SiC.

The purity of our CVD-SiC was measured by neutron analysis of the impurities. The impurity of CVD-SiC was found to be less than that of very pure silica glass.

Photo 1 shows the cross-sections of both CVD-SiC and commercially marketed SiC sintered under normal pressure, oxidized for 148 hours in a 1500°C electric furnace. An oxidized layer of about 8 µm was found on the surface of the SiC sintered under normal pressure and not on the surface of CVD-SiC, thereby proving the superior resistance of CVD-SiC to oxidation under static conditions.

3. Examples of Applications

3.1 As a Coating

3.1.1 Coating for Sintered SiC

The bending strength and thermal shock resistance of SiC sintered under normal pressure can be improved as



(a) CVD-SiC



(b) Sintered SiC

Photo 1. Cross-Sections of Oxidized SiC

previously reported, by coating it with a layer of CVD-SiC. Figure 4 shows Weibull plots of the bending strength and thermal shock resistance at room temperature of sintered SiC coated with CVD-SiC [shown as Figure 4(a)]. Figure 5 [as published] shows Weibull plots of four-point flexural strength of SSC and CVD/SSC at 1250°C [shown as Figure 4(b)]. Next, test results of four-point bend tests and thermal shock resistance tests for two types of sintered Si_3N_4 (SSN-1 and SSN-2) is shown in Table 2. The average four-point bending strength of sintered SiC at 1250°C is 390 MPa as is evident from Table 2, while that at room temperature is 330 MPa. Therefore, it is clear that the strength is 18 percent higher at the higher temperature. On the other hand, as is clear from Table 2, the four-point bending strength of sintered SiC coated with CVD-SiC was 520 MPa at room temperature and 440 MPa at 1250°C, values higher than that in the case of uncoated sintered SiC. Also the Weibull coefficient of the sintered SiC increased from 6.5 to 18 when coated with CVD-SiC when at room temperature. In the case of 1250°C, the coefficient again leaped from 9.7 to 11. Therefore, the CVD-SiC coating not only improved the four-point bending strength but also helped to reduce the fluctuation in the values. Some values in Figures 4 and 5 [as published] are very different from the rest. Observations on rupture plane of SSC with bending strength of 290 MPa and of CVD/SSC with 310 MPa, showed that holes or rough crystals of about 100 µm in size existed in test pieces which are especially weak. These holes or crystals are believed to be the crack origin. If these kinds of test pieces with defects could be removed prior to the experiment, the Weibull coefficients of both SSC and CVD/SSC would become large values and fluctuations could

be reduced. In particular, the Weibull coefficient of sintered SiC coated with CVD-SiC at room temperature was 18 and when the test pieces containing large defects

were removed, the coefficient became 15 at 1250°C, therefore creating a material whose values do not differ much.

Table 2. Test Results of Four-Point Bend Tests and Thermal Shock Tests

Material		Flexural strength at room temperature		Flexural strength at high temperature		Thermal shock resistance (T_c °C)
		Mean value MPa	Weibull parameter	Mean value MPa	Weibull parameter	
Sintered SiC	SSC	340	6.5	390 (1250°C)	9.7 (1250°C)	300
	CVD/SSC	520	18	440 (1250°C)	11 (1250°C)	450
Sintered Si ₃ N ₄	SSN-1	1000	8.6	570 (1250°C)	19 (1250°C)	700-850
	SSN-2	630	15	450 (1120°C)	13 (1120°C)	850<

3.1.2 Coating of Other Materials Besides Sintered SiC

A combustion chamber liner and a combustion gas compressing nozzle made of CVD-SiC coated graphite substrate and a specimen holder made of CVD-SiC coated carbon-ceramic substrate were actually heated in combusted kerosene gas at 1100°C-1400°C. Such experiments proved that CVD-SiC is an appropriate material for use in a high-temperature oxidation environment.

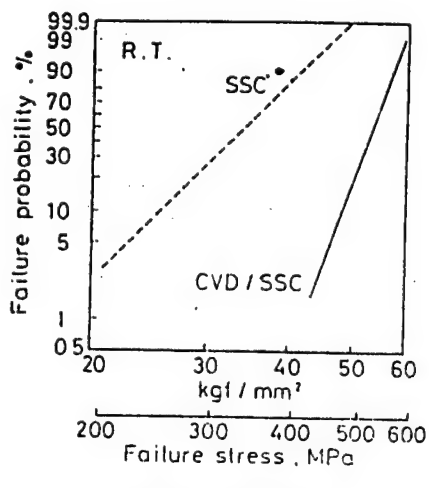
3.2 CVD-SiC Structures

CVD-SiC was not only tested as a coating, techniques to fabricate structures out of it were also investigated. Several products and test products were fabricated. Photo 2 shows a combustion chamber liner while Photo 3 shows the heat exchanger test element. The combustion chamber liner was tested in combustion experiments at the Space and Aeronautical Research Laboratory. It was found to be able to withstand rapid cooling when accidental fires were extinguished. The maximum temperature of the combustion gas was 1300°C while that in the liner was 1100°C and the total test time was several hours. The heat exchanger test element is presently being tested at the Space and Aeronautical Research Laboratory. We and the Space and Aeronautical Research Laboratory are presently in the midst of developing these trial products.

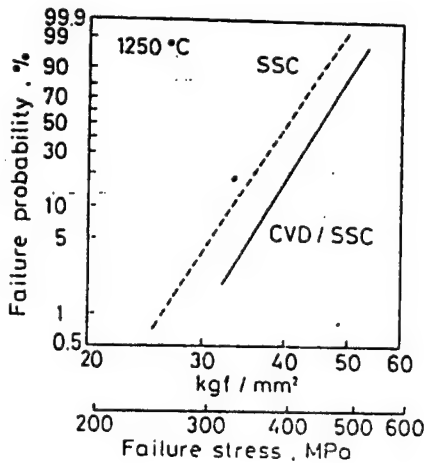
A heat insulator with a low thermal conductivity will not only help conserve energy but its high strength will also allow smaller furnaces with larger capacities to be built by reducing the amount of space required by the insulator within the furnace.

2-3 Purity

The infinitesimal amount of metallic impurities within the heat insulator usually becomes a problem when it is used under clean conditions. Table 2 shows the ash content in isotropic sponge carbon. The ash content of isotropic sponge carbon was less than 100 ppm through strict control of the raw materials and processing method. Consequently, isotropic sponge carbon that is not highly purified can be used for general purposes. The ash content of isotropic sponge carbon changes to less than 20 ppm through purification thereby allowing it to be used in special applications.



(a) Room temperature



(b) 1250 °C

Figure 4. Weibull Plots of Four-Point Flexural Strength of Sintered Silicon Carbide Coated With CVD-SiC

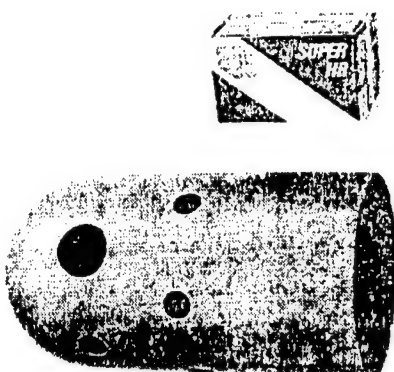


Photo 2 Combustion chamber liner

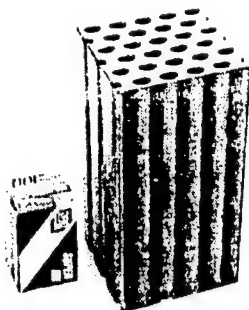


Photo 3 Heat exchanger test element

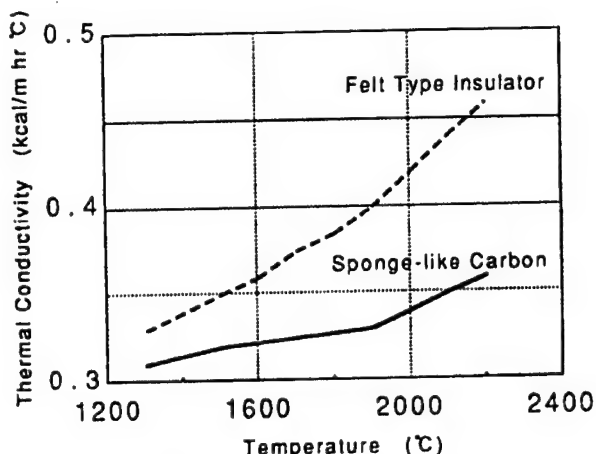


Figure 1. Thermal Conductivity

Table 3 Anisotropy of Sponge-like Carbon
($\rho = 0.13$)

	\perp	\parallel
Flexural Strength (kgf/cm^2)	12	12
Compressive Strength (kgf/cm^2)	17	16
Thermal Conductivity ($\text{kcal/m hr } ^\circ\text{C}$)	0.19 (at Room Temperature)	0.20

2-4 Anisotropy

The anisotropy along the fibers of the carbon fiber felt-type heat insulator results in strong anisotropy in the strength factors and the thermal conductivity. This phenomenon makes it difficult and complex for furnaces to be designed. On the other hand, the anisotropy is extremely small in sponge carbon as shown in Table 3.

2-5 Processability

One of the characteristics of the isotropic sponge carbon is that it can be easily processed. This material can be cut by cutter knife therefore allowing it to be made into complex shapes without special processing or treatment. Its carbon fibers need not be fluffed unlike felt-type insulators. This material can also be glued together with the special glue developed by our company. Coverings like elastic graphite sheets or carbon fiber cloths can be attached onto the surface of the isotropic sponge carbon.

2-6 Other Characteristics

Table 4 shows other characteristics of isotropic sponge carbon. (1) Since isotropic sponge carbon has a high specific electrical resistivity, it is difficult to be heated by induction and thus can be used in induction heating furnaces. (2) Since the material has a low permeability, it has the advantage of preventing heat conduction via gas flow.

Table 4. Properties of Sponge-Like Carbon

C.T.E. (K^{-1})	2.17×10^{-6}
Specific resistance ($\Omega \text{ cm}$)	0.13
Porosity (%)	93.5
Permeability ($(\text{cm}^3/\text{sec})\text{cm} / \text{cm}^2 \text{cmH}_2\text{O}$)	1.04×10^{-3}

3. C/C Composite

The C/C composite (hereafter termed product) developed by Nippon Steel Corp. and Nippon Steel Chemical uses the short carbon fibers and pitch as raw materials in

Table 2. Ash Content of Sponge-Like Carbon

General grade	<100 ppm
Purified grade	20 ppm

Table 5 Properties of Developed C/C

Fiber Volume (%)	40				
Density (g/cm ³)	1.7				
Flexural Strength (kgf/mm ²)	15				
ILSS (kgf/mm ²)	1.7				
Tensile Strength (kgf/mm ²)	7				
Izod (kgcm/cm ²)	<table border="1" style="display: inline-table; vertical-align: middle;"> <tr> <td style="padding: 2px;">⊥</td> <td style="padding: 2px;">13</td> </tr> <tr> <td style="padding: 2px;">//</td> <td style="padding: 2px;">7</td> </tr> </table>	⊥	13	//	7
⊥	13				
//	7				
Compressive Strength (kgf/mm ²)	<table border="1" style="display: inline-table; vertical-align: middle;"> <tr> <td style="padding: 2px;">⊥</td> <td style="padding: 2px;">13</td> </tr> <tr> <td style="padding: 2px;">//</td> <td style="padding: 2px;">15</td> </tr> </table>	⊥	13	//	15
⊥	13				
//	15				
Rockwell Hardness(R Scale)	110				

a special dispersion technique to create a three-dimensional material. The characteristics are described below.

3-1 Strength Characteristics

Table 5 shows the properties of the product. Note that the flexural strength and the interlayer shear strength is high. This is because the fibers are three-dimensional thereby resulting in a 1.5 times higher interlayer shear strength value as compared to conventional products.

3-2 Oxidation Resistivity

Table 6 shows the oxidation of the product and conventional materials under normal atmospheric conditions. Since pitch is used in the matrix of the product, it is superior to oxidation and at 600°C, it only reduces to less than half of its original weight as compared to conventional types in the air.

Table 6. Result of Oxidation Test

Temp.	Weight loss (%)	
	Developed C/C	Conventional C/C
600°C	28	58
800°C	53	63
Flow rate: 500 cc/min		
Oxidation time: 1 hr		
Sample size: 10 mm x 10 mm x 20 mm		

3-3 Processability

Defects do not appear even when the product is processed into uneven structures like nuts and bolts because of its three-dimensional carbon fibers. In other words, this product can be extremely precisely processed. Figure 2 shows a photo of bolts made of the product and



Developed C/C Conventional C/C
Figure 2. Photograph of Bolts

conventional materials. Defects can be observed in the protruding part of the screw made of conventional materials while such defects do not exist in that made of the product.

3-4 Strength Characteristics of Bolt

The tensile strength of a test produced bolt is shown in Table 7. The instrument in Figure 3 was used for the measurements. As is evident from the table, the bolt made from the product is significantly stronger than that made of conventional materials or special carbon materials. This is believed to be the improved interlayer shear strength due to effective alignment of the carbon fiber. A bolt made from this product can have smaller diameters with stronger screwing strength. The product can be used in moving parts because of its superior anti-impact strength.

Table 7. Strength of Bolts (kgf/mm²)

Bolt size	Developed C/C	Conventional C/C	Carbon
M8	6.1	—	1.0
M10	5.8	1.6	1.3
M12	6.2	—	1.1
M16	6.0	1.3	—

4. Conclusion

We have described the isotropic sponge carbon and C/C composite developed by Nippon Steel Chemical and Nippon Steel Corp. The characteristics are summarized as follows:

Isotropic sponge carbon has the following properties as compared to conventional carbon felt-type heat insulators.

- (1) high strength;
- (2) low thermal conductivity;
- (3) low ash content;
- (4) can be easily designed because it is an isotropic material;
- (5) can be assembled or glued together because it can be easily processed.

These characteristics mean that this material will find increased applications in high temperature furnaces.

C/C composite composite, as compared to conventional products.

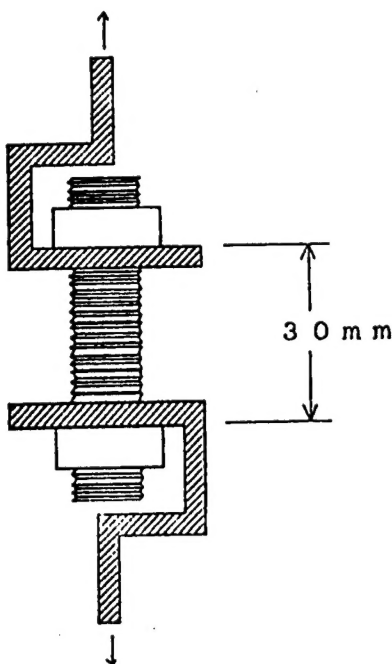


Figure 3. Attachment for Tensile Test of Bolts

- (1) has high interlayer shear strength;
- (2) can be precisely processed;
- (3) has superior anti-oxidative properties.

This product can be used for making high temperature nuts and bolts.

Development of High Performance Carbon-Carbon Composites for Space Vehicles

916C0035U Ube CHO KO-ON ZAIRYO KOKUSAI SHINPOJIUMU in Japanese 15 Mar 91 pp 167-170

[Article by Tadashi Matsushita, Hidehiko Mitsuma, and Tomoyuki Kobayashi of the National Aeronautical Space Development Agency; Hirotoshi Nakayama and Akihito Sakai of Kawasaki Heavy Industries; Nobuo Tsuchiya and Tsuneo Kinjo of Kawasaki Steel]

[Text] English abstract: Carbon-Carbon (C/C) is a lightweight refractory composite, and a prime candidate material for hot sections of space vehicles which are exposed to severe aerodynamic heating during re-entry. A resin char process was chosen for making C/C, and 2D carbon cloth and phenolic resin were selected for the preforming materials, to get high strength and to enable relatively complex shape forming. To prevent oxidation at high temperature, we have established multilayer coating method whose main coating is Chemical Vapor Deposited (CVD) SiC. Preliminary data acquisition tests are conducted, and some trial products such as an integral skin-stringer panel and other shaped components were fabricated to develop forming process and to demonstrate the feasibility of the material system.

1. Introduction

Various projects have been planned by Europe and America as well as Japan for developing space vehicles that can travel to and back from outer space as part of the space transportation systems project. There are several basic technologies in the development of such vehicles but the key technology is the development of a lightweight ultrahigh heat resistant material for use during the space vehicle's re-entry into the earth's atmosphere.

Carbon-carbon (C/C) composite is lightweight and has an incomparable heat resistance thereby becoming a prime candidate for use as a material in the main heat resistant structures and heat protective systems in these kinds of space vehicles. However, the processing and application technology for fabricating this kind of material for use in high performance structures is not yet established. The present situation is that the advanced nations are locked in a heated battle for its development.

With this kind of background, we have been and are now conducting research such that the following objectives will be realized within the next few years.

- (1) Development of very strong materials (specific strength comparable to aluminum alloy).
- (2) Development of a technique for fabricating a 1700°C anti-oxidation coating.
- (3) Development of a method for molding large-sized complex structured parts.

This report summarizes the results of our recent work.

2. Development of High Strength Materials

The following policy was adopted before the beginning of this research.

"The C/C for use in the main structures and heat protective systems in space vehicles must be strong and rigid yet at the same time, must be able to be processed into the large-sized, complex-shaped parts. Further, no matter how strong a material is, laboratory work will not include test pieces or simple structures like plane boards."

Based on the above policy, the optimum constituent material (carbon fiber, matrix or precursor, etc.), fiber reinforcement (uni-directional, bi-directional, three-dimensional) and the processing method (method, treatment conditions) are selected.

High strength type carbon fiber and highly elastic type carbon fiber was mixed with several combinations of precursor resins to make the constituent test material whose properties were then investigated. The mixture of highly elastic type carbon fiber and phenolic resins with a high aromatic content, was finally selected to be the optimum constituent material.

The reinforcements similar to that in fiber reinforced plastics and shown in Table 1 were next considered. The

two directional reinforcement structure was selected from a practical and ease of shaping point of view.

Table 1. Classification of Reinforced Structure

Reinforcement structure	Advantages	Limitations	Total evaluation
UD (Uni-directional)	High fiber volume fraction; Highest in-plane strength; Fiber orientation flexibility (easy to get anisotropic laminate)	Conformability for complex shaping	Fair
2D (Two-directional)	Formability and conformability for complex shaping; High in-plane strength as UD in case of quasi-isotropic stacking	Fiber orientation possibility	Excellent
3D (Three-directional)	High interlaminar shear strength; High fracture toughness	In-plane strength; Preformability and conformability for shaping	Good

The following three methods are usually employed for fabricating C/C.

(1) Resin-char method

The CFRP preform is placed in the furnace for primary carbonization. After that, resin impregnation and then carbonization is repeated.

(2) Hot press/HIP method

Reinforced fiber (weaved materials etc.) and matrix precursor (pitch etc.) is placed in a mold and then carbonized under pressure. It is then impregnated when necessary.

(3) CVD (CVI) method

Hydrogen carbide gas is poured into a pre-heated fiber preform to directly precipitate carbon by heat decomposition.

The simple resin-char process with high conformability for complex shaping was selected. Figure 1 shows the production scheme of the resin-char process.

The mechanical properties obtained when optimum preform FRP conforming conditions, carbonization temperature and length of time and impregnation method was implemented, are depicted in Table 2.

Table 2. Data Acquisition Tests Results

Properties	Data
Tensile strength	(RT) 268 MPa
	(1000°C) 303 MPa
Tensile stiffness	(RT) 88 GPa
	(1000°C) 94 GPa
Compressive strength	(RT) 320 MPa
Compressive stiffness	(RT) 95 GPa
Flexural strength	(RT) 439 MPa
	(1700°C) 551 MPa
Flexural stiffness	(RT) 68 GPa
	(1700°C) 90 GPa
I.L.S.S.	(RT) 18 MPa
Density	1.65

Note: Quasi-isotropic, coated samples were tested.

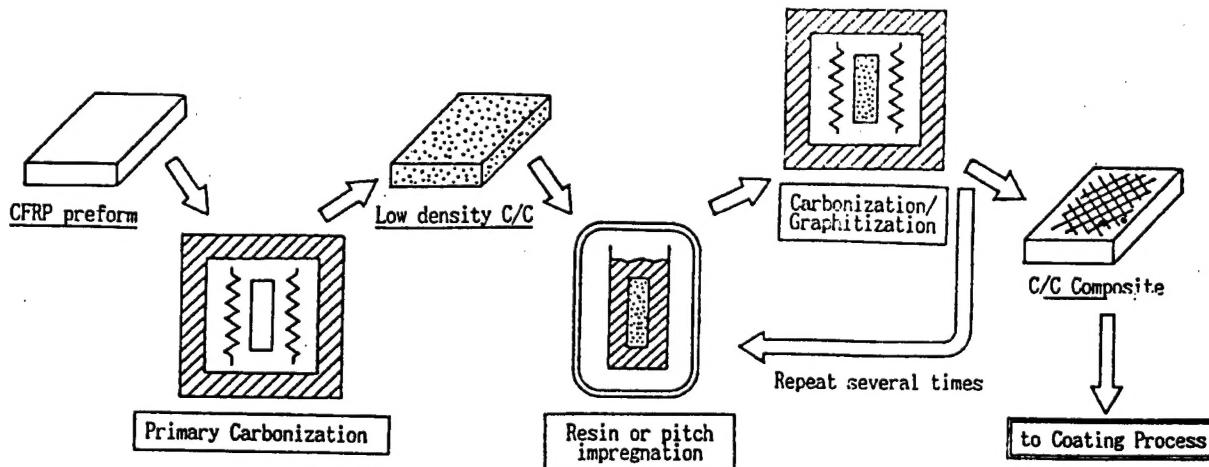


Figure 1. Production Scheme of Resin-Char Process

The results are about five times that of the first generation C/C design data used in the present American space shuttle. This data indicates that even if the safety factors were taken into consideration, we have succeeded in fabricating a significantly high performance material. The relative tensile strength is about 17 km and we have proved that this is similar to that of the aluminum alloy used in space vehicle structures. From results of bending tests made at 1700°C, the strength of C/C at high temperatures was proved to be equivalent to that at room temperature or higher. We have reconfirmed that this material is most appropriate for use as an ultra-high temperature heat resistant material.

3. Development of Anti-Oxidation Technology

C/C has superior heat resistance but the biggest disadvantage is its weakness to oxidation. C/C is severely oxidized at 500-600°C by the oxygen in the atmosphere. As such, the surface of the C/C used in space vehicles requires an anti-oxidation coating. This is one of the most important items that must be developed. As described in the Introduction, the anti-oxidation coating targeted for study this time is 1700°C because this is the maximum predicted temperature at the surface of the currently planned space vehicle during its re-entry into the earth's atmosphere.

First the coating material was considered. The thermal resistance, the strength of the oxygen barrier, physical and chemical compatibility with carbon and the ease of membrane fabrication of different high heat resistant ceramics were compared and finally, SiC was selected as the optimum main constituent.

Next the coating method was selected by comparing the various ceramic coating methods available. The

extremely difficult CVD method for fabricating a well-packed and pure coating was chosen to realize the heat resistance at 1700°C. The C/C thermal expansion was not temperature-dependent and had a value of about 0°C.

In the case when various ceramics with SiC are directly coated onto the C/C surface by even the CVD method, thermal stress peeling would become a problem. Therefore, a different layer was introduced between the SiC coating and the C/C base material for the purpose of neutralizing the stress. Further, pore-sealing treatment by high-melting point glass was implemented to seal-off the micro-cracks which could not be prevented by even the introduction of this stress relaxation intermediate layer.

In this manner, various coating methods with CVD method as the main were established. The introduction of these coating methods has resulted in great improvements in the adhering property and the durability of the coating.

Plasma flame tests were employed in the investigation of the effectiveness of the anti-oxidation coating. A plasma flame coating device was used to blast an air flow at high speed and high temperature onto the surface of the sample. In other words, this is a dynamic anti-oxidation testing method. The normal speed of a plasma flame is about Mach 2, a negligible value when compared to the atmospheric re-entry speed of a space vehicle (Mach 25). However, it is extremely difficult to realize a speed of Mach 25 for tests on earth and as such, the plasma flame test is the most cost effective method at the material developing stage. Three surface temperatures of 1300°C, 1500°C and 1700°C were considered in this study. The surface of the sample was exposed 10 times, each time

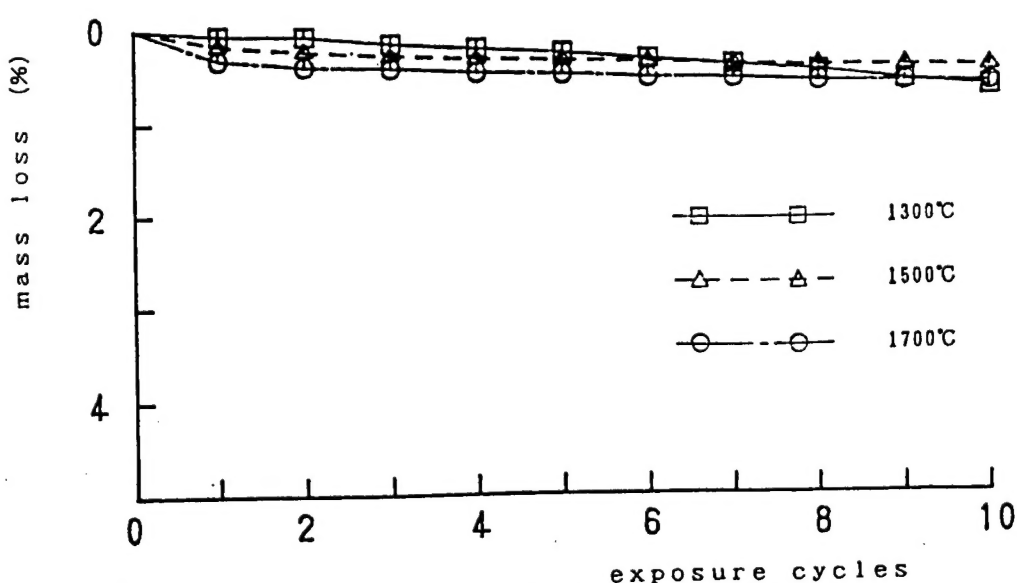


Figure 2. Weight Loss After Plasma Flame Tests

for a total of 6 minutes. The results are shown in Figure 2. The total mass loss of the sample at the respective temperatures were less than 0.6 percent (i.e., about 30 mg of about 5 g sample weight). The anti-oxidation of the test coating at 1700°C was proved to be practical.

4. Development of Structuring Technology for Large-Sized, Complex Shaped Parts

The above-mentioned materials and fabricating processes were developed with the structuring of large and complex-shaped parts in mind but in actual molding, a layering method and a uniform heating method for the mold and large-sized part must first be established. The FRP molding and the graphite annealing expertise accumulated through the years was employed when considering the design of actual large-sized complex parts. Several differently shaped parts were test produced.

The nose cone-like component shown in Figure 3 has a diameter of 380 mm at the opening and a height of 200 mm with a minimum radius of curvature. This structure did not require a layer of reinforced fiber. Deep molding with ease of removal from the mold and a superior 2-D structure was proved.

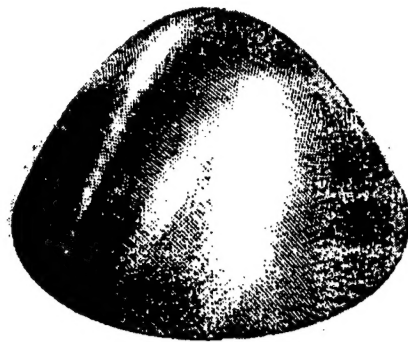


Figure 3. Nose Cone-Like Component

The Figure 4 integral skin-stringer panel was 1000 mm x 500 mm. The panel was reinforced by three stringers along its length. The stringers and the panel had a one-body structure. This structure proves the high degree of freedom in the resin-char molding process. Both structures were confirmed to be well molded in after-molding tests.

References

1. Noda, Sakai: "Development of C/C Composite for Use in HOPE," HOPE-related workshop (Tsukuba city) 1988, [NASDA]
2. Itoh, et al.: "Anti-Oxidative Coatings for C/C Composites," No. 26 Aeronautical Symposium (Sendai city), 1988, 408-411, [Japan Aeronautics and Space Association, Japan Air Lines Technical Association]
3. T. Matsushita, H. Mituma, T. Kobayashi, H. Nakayama, A. Sakai, N. Tsuchiya, T. Kinjo: "Development of High Performance Carbon-Carbon Composites for Space Applications," 10th Tsukuba General Symposium Japan-France Joint Seminar, (Tsukuba, Japan), 1990, 169-174, [The Agency of Industrial Science and Technology, MITI, Japan Industrial Technology Association]

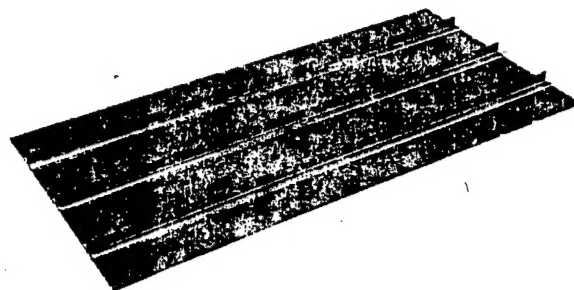


Figure 4. Integral Skin-Stringer Panel